Synthesis and Functionalization of Carbohydrate Capped Silicon Nanoparticles for Targeting Cancer Cells

By

Jayshree Hemant Ahire

UEA
University of East Anglia

School of Chemistry

University of East Anglia

Norwich

U.K.

2014

A thesis submitted in fulfilment of the requirements for the degree of Doctor of Philosophy of the University of East Anglia.

Declaration

I hereby declare that the work described in this thesis, submitted for the degree of Doctor of Philosophy, has been carried out by myself and to the best of my knowledge, except where due reference is made to other authors has not previously been submitted by me for a degree at this or any other universities.

- Jayshree Hemant Ahire

Acknowledgements

In the course on my PhD, there are a lot of people who have helped make this thesis possible and whom I would like to thank. First and foremost I offer my sincerest gratitude to my supervisor Dr. Yimin Chao, for giving me the opportunity to pursue this work and providing me with dedicated support throughout. I would also like to extend my deepest thanks to Dr. Isabelle Chambrier who has been a surrogate supervisor to me and whose assistance has always been on hand and freely given. My thesis wouldn't have been accomplished without her support and valuable criticism throughout this research work. I also acknowledge the help and kindness of Dr. Victoria Sherwood, for providing me with the necessary laboratory facilities to carry out the biomedical research of this work and also for her help to improve my biology perception during this research. Without their expertise, I would never have been able to fully appreciate the wide range of experimental techniques I've been privileged to use nor realize the completion of this work.

I am also thankful to Prof. Andrew Cammidge for his advice as my second supervisor as well as providing me with the necessary laboratory facility to carry out my synthetic chemistry work.

I also thank Dr. Yongping Bao and Mrs Wei Wang for providing me the cell lines to carry out the biomedical research in this work.

My sincere appreciation also goes to my colleagues, Dr. Paul Coxon, Qi Wang and Shane Ashby for their constant help and critical discussions about my research work, especially for their good humour and friendship. Furthermore I would like to take this opportunity to thank all the members from Dr. Yimin Chao's research group, past and present: Mehrnaz Behray, Jason Thomas, Wenchao Zhang, Ruoxi Liu, Frederik Huld, Ting Li and Tiezheng Bian for their hospitality and friendship.

I would also like to thank Carl Webster, for his help in carrying out the biological assays. I am also thankful to the members of Prof. Andrew Cammidge's research group: Alejandro Diaz-Moscoso, Daniel Gonzalez Lucas and Sonia Remiro Buenamanana for their help, support and friendship.

Many friends have helped me stay sane through these difficult years. Their support and care helped me overcome setbacks and stay focused on my study. I greatly value their friendship and I deeply appreciate their belief in me.

This thesis is dedicated to my beloved

husband Hemant Ahire

I love you.

Abstract

Silicon nanoparticles (SiNPs) hold prominent interest in various aspects of biomedical applications. For this purpose, surface functionalization of the NPs is essential to stabilize them. A facile method is reported here to synthesize highly stable and brightly luminescent amine-terminated SiNPs. The diameter of the crystal cores is 4.6 nm. The NPs emit strong blue-green photoluminescence (PL) at peak position 460 nm with quantum yield (QY) 22%. The NPs exhibited an exceptional stability over a wide pH range (4–14) and are resistant to aging over several weeks.

For SiNPs to target specific disease area, and allow them to selectively bind to the cells or the bio-molecules present on the surface of the cells, carbohydrate capped SiNPs were synthesized. However, no such functionalization has been explored with SiNPs. In this study, we report the first synthesis of SiNPs functionalized with carbohydrates (Galactose, Mannose, Glucose and Lactose). The NPs show blue-green luminescence in water and orange luminescence in the dry state with emission of 600nm with the highest QY and exhibit an exceptional stability over weeks.

Further study explores the possibility of using carbohydrate capped SiNPs to detect and outline various cell types on the basis of the more physiologically related carbohydrate-receptor interactions. The NPs prove to be very stable in biological media. The toxicity, which was tested both *in vitro* and *in vivo*, proved that the NPs were non-toxic. The cellular uptake efficiency was quantified by flow cytometry and indicated that the NPs internalize in the cell within 24 hours. The fluorescence uptake was quantified by both cancer and non-cancerous cell lines and the cancerous cells were shown to uptake more NPs than normal cell lines. The cellular uptake of these NPs, which was visualized by fluorescence and confocal microscopy, showed quick accumulation inside cancer cells within cytoplasm.

Publications:

The following list details the papers which have resulted over the duration of this work.

- **Ahire, J. H.**; Wang, Q.; Coxon, P.; Malhotra, G.; Brydson, R.; Chen, R. and Chao, Y., Highly Luminescent and Nontoxic Amine-Capped Nanoparticles from Porous Silicon: Synthesis and Their Use in Biomedical Imaging. *ACS Applied Materials & Interfaces*. 2012, 4 (6), 3285-3292

- **Ahire, J. H.**; Chambrier, I.; Mueller, A.; Bao, Y.; Chao, Y., Synthesis of D-Mannose Capped Silicon Nanoparticles and Their Interactions with MCF-7 Human Breast Cancerous Cells. *ACS Applied Materials & Interfaces* 2013, 5 (15), 7384-7391

- Wang, Q.; Bao, Y.; **Ahire, J. H.**; Chao, Y., Co-encapsulation of Biodegradable Nanoparticles with Silicon Quantum Dots and Quercetin for Monitored Delivery. *Advanced Healthcare Materials* 2013, 2(3), 459-466

- Coxon, P. R.; **Ahire, J. H.**; Ashby, S., P.; Frogley, M., D.; Chao, Y.; Amine-terminated Nanoparticle films: Pattern Deposition by a Simple Nanostencilling Technique and Stability Studies under X-ray Irradiation. *Physical Chemistry Chemical Physics* 2014, 16, 5817-5823

1 Contents

List of Figures:

List of schemes:

List of Tables:

Abbreviations:

AFM	Atomic Force Microscopy
ASGP-R	Asialoglycoprotein Receptor
ATR	Attenuated Total Reflectance
a.u	Abbreviated Units
AuNP	Gold Nanoparticle
CDCl$_3$	Deuterated chloroform
CdSe	Cadmium Selenide
CdTe	Cadmium Telluride
CO$_2$	Carbon Dioxide
Con A	Concanavalin A
CT	Cholera Toxin
DAPI	4',6-diamidino-2-phenylindole
DCC	*N,N'*-Dicyclohexylcarbodiimide
DCM	Dichloromethane
DI	Deionized Water
DLS	Dynamic Light Scattering
DMEM	Dulbecco's Modified Eagle Medium
DMSO	Dimethylsulfoxide
DNA	Deoxyribonucleic acid
ECACC	European Collection of Cell Cultures
EDC	1-Ethyl-3-(3-dimethylaminopropyl)carbodiimide
EDX	Energy Dispersive X-ray Spectroscopy
EMA	Effective Mass Approximation
ESCA	Electron Spectroscopy for Chemical Analysis
EtOAc	Ethyl Acetate
EtOH	Ethanol
FBS	Foetal Bovin Serum
FTIR	Fourier Transform Infrared Spectroscopy
FWHM	Full Width at Half Maximum
HA-QD	Hyaluronic Acid coated Quantum dot
H-terminated	Hydrogen-terminated
H$_2$O	Hydrogen Oxide
HF	Hydrofluoric Acid
HIV	Human Immunodeficiency Virus
HNO$_3$	Nitric Acid
H$_2$PtCl$_6$	Hexachloroplatinic Acid
HRTEM	High Resolution Transmission Electron Microscope
H$_2$SO$_4$	Sulfuric Acid
IC$_{50}$	Half Maximal Inhibitory Concentration
ITC	Isothermal Titration Calorimetry
LEC	Lymphatic Endothelial Cells
LiAlH$_4$	Lithium Aluminium Hydride
LYVE-1	Lymphatic Vessel Endothelial Receptor 1

MGNP	Magnetic Glyco-nanoparticle
MMR	Marc's Modified Ringers
MRI	Magnetic Resonance Imaging
MTT	3-(4,5-dimethylthiazol-2-yl)-2,5-diphenyltetrazolium bromide
NaCl	Sodium Chloride
NF	Nieuwkoop and Faber
NHS	*N*-Hydroxysuccinimide
NaHCO$_3$	Sodium Bicarbonate
NaOH	Sodium Hydroxide
Na$_2$SO$_4$	Sodium Sulfate
nm	Nanometer
NMR	Nuclear Magnetic Resonance Spectroscopy
NP	Nanoparticle
OAc	Acetate
PBS	Phosphate Buffered Saline
PET	Photoinduced Electron Transfer
PL	Photoluminescence
P-Si	Porous Silicon
Pt	Platinum Catalyst
QD	Quantum Dots
QY	Quantum Yield
RES	Reticuloendothelical System
RPMI	Roswell Park Memorial Institute medium
S.D.	Standard Deviation
Si	Silicon
SiCl$_4$	Silicon Tetrachloride
SiNP	Silicon Nanoparticle
SiO$_2$	Silicon Dioxide
SiQD	Silicon Quantum Dot
SPR	Surface Plasmon Resonance
SR-FTIR	Synchrotron Radiation Fourier transform infrared Spectroscopy
TBDMS	*tert*-Butyldimethylsilyl
TEM	Transmission Electron Microscopy
UV	Ultra Violet
UV-vis	Ultra Violet-Visible
Wt	Weight
w/v	Weight to Volume Ratio
XPS	X-ray Photoelectron Spectroscopy
ZnS	Zinc Sulphide

1   Introduction

Nanotechnology will change the world. It will affect almost any aspect of our lives: medicines we use, power of our computers, the energy supplies we require, the food we eat, the cars we drive, the buildings we live in and the clothes we wear."

P. Holister

1.1   Nanotechnology

Nanotechnology is the promising interdisciplinary field, which involves biological, chemical, physical and engineering studies of nano-sized objects (1-100 nm scale, Figure 1.1).[1] The recorded history of nanotechnology is generally understood to have begun in December 1959 when physicist Richard Feynman gave a speech, "There's Plenty of Room at the Bottom" (Feynman 1959), at an American Physical Society meeting at the California Institute of Technology in which he identified the potential of nanotechnology.[2]
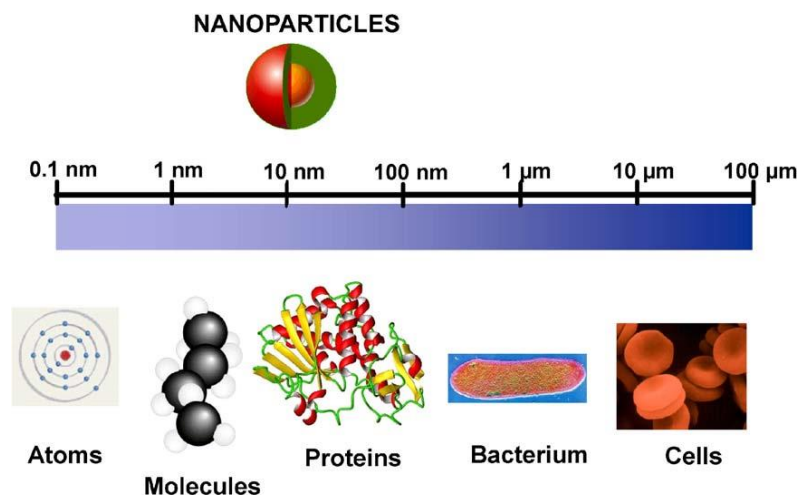
Figure 1.1: The figure depicts the sizes of nanoparticles in relation to other biological objects.

Nanotechnology is a revolutionary new approach towards the construction and use of functional structures designed from atomic or molecular scale with at least one characteristic dimension measured in nanometers. In other words it is concerned with the study of nano-meter sized objects (1-100 nm). As the size of a material decreases from bulk to the range of about 1 to 100 nanometers, the object displays physical attributes substantially different from those displayed by either atoms or bulk materials. One of the most exciting and challenging aspects of the nanomaterial is the role which quantum mechanics plays within it.[3, 4] Quantum phenomena are, of course, the ultimate basis of atoms

and molecules, but are largely hidden behind classical macroscopic matter and structures. The real breakthrough in nanoscience was the invention of the Scanning Tunneling Microscope (STM).[5] This invention allowed an entrance into the nano world by direct observation of nanostructures. Since then, this field is blossoming: knowledge, creativity and futuristic visions of scientists of different profiles gather to create and study new nano-objects, of which many have already found applications in various fields of medicine[6, 7] and technology.[8]

1.1.1 Nanotechnology in Ancient History

Evidence suggests that nanotechnology was present in ancient time. A definitive and remarkable piece of old Roman glasswork, dating to the fifth century shows one of the grandest examples of nanotechnology in the ancient world. The magnificent cup present in the British museum represents King Lycurgus being dragged into the underworld by Ambrosia. When illuminated from outside the cup appears green (Figure 1.2). When illuminated from inside the cup appears crimson red except for the King who looks purple. The dichroic effect of the glass is achieved by making the glass with tiny proportions of nanoparticles of gold and silver dispersed in colloidal form throughout the glass material. The exact process used remains unclear, and it is likely that it was not well understood or controlled by the makers, and was probably discovered by accidental contamination with minutely ground gold and silver dust.

Figure 1.2: The Lycurgus Cup in (a) reflected and (b) transmitted light, Department of Prehistory and Europe, The British Museum.

1.2   Semiconductor Nanoparticles

Semiconductor nanoparticles (NPs), also referred to as Quantum dots (QDs), have attracted a lot of interest from interdisciplinary areas of science due to their unique optical, electronic and mechanical properties that differ from their bulk counterparts. QDs were first fabricated in the 1980s by Louis E. Brus[9] and the unique properties of these special nano-structures attracted interest from many fields.[10-12] Nanoparticles with diameters in the range of 1 nm to 20 nm exhibit unique physical properties that give rise to many potential applications in fields such as nonlinear optics, luminescence, electronics, catalysis, solar energy conversion and optoelectronics. Two essential factors, related to the size of the individual nanocrystal, are responsible for these unique properties. The first is the large surface to volume ratio, and the second is the quantum confinement effect.[3, 9] As the size of the semiconductor material decreases the ratio of the number of surface atoms to those contained within the NP volume increases, which leads to the surface taking a dominant role in the properties of the material.[13] Concurrently the band gap gradually increases due to the quantum confinement effect. Thus the synthetic method, which controls the particle size, determines the physical and electronic properties of the semiconductor NP produced, which gives scientists the unique ability to change and control the electronic and chemical properties of a semiconductor material.

1.2.1   Quantum Confinement Effect

The most striking property of semiconductor NPs is the large change observed in their electronic and optical spectra as their sizes are reduced. This size dependent property is generally called the quantum confinement effect.[14] The word "confinement" refers to the motion of randomly moving electrons as their motion in specific energy levels (discreteness) is restricted and "quantum" reflects the atomic realm of particles. Therefore as the size of a particle decreases up to the nano scale, the decrease in confining dimension makes the energy levels discrete and this increases or widens up the band gap and ultimately the band gap energy also increases. Since the band gap and wavelength are inversely related to each other the wavelength decreases with decrease in size and this gives rise to the blue emission by the particle. This is shown in figure 1.3, as the cluster size of a semiconductor decreases, the gap between valence and conduction band increases.[15-17]
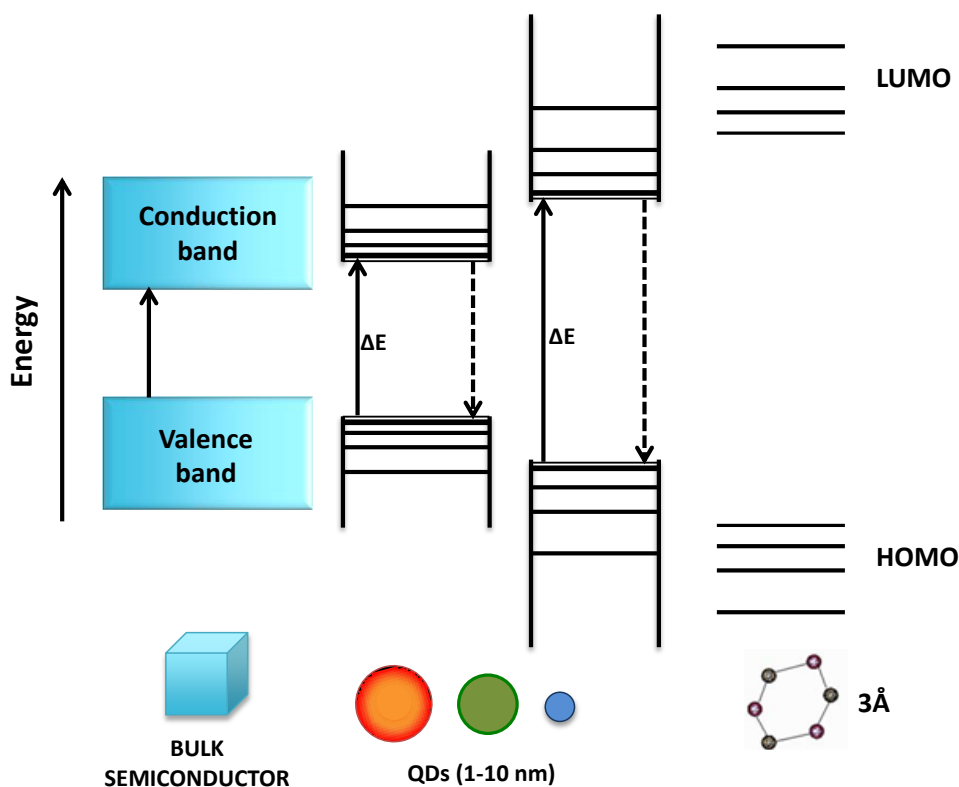
Figure 1.3: Schematic energy diagrams illustrating the state of a NP, in between a molecule and a bulk semiconductor.

This phenomenon can be explained by the relationship between the position and energy of an electron in both free and confined space. The energy or crystal momentum of an electron in a bulk semiconductor can be precisely defined, while the position cannot. However, in the case of a semiconductor NP, the momentum is no longer well defined as the uncertainty in the electron position decreases. In the bulk semiconductor, series of nearby transitions occur at slightly different energies, while in the NP, transitions will be compressed by quantum confinement into a single, intense transition.[15] The electron-hole pair produced by the absorption of a photon is delocalized across the interior of the NP, and recombination of the electron and hole causes emission of the photon. The photoluminescence (PL) of the semiconductor NP is a result of such a phenomenon. Efficient PL is only possible when the size of semiconductor NP is smaller than the exciton Bohr radius of the bulk material.[18] This radius controls how large a crystal must be before its energy bands can be treated as continuous. In general, semiconductor show large size-dependent changes in their spectroscopy below a radius of a few nm; the precise radius is characteristic of the material: these quantum confinement effects set in for particle radii of 5 nm for silicon (Si) and for cadmium selenide (CdSe), a widely employed luminescent label. Absorption of light in the bulk semiconductor promotes an electron to a higher energy

orbital and creates an unoccupied orbital at lower energy (a "hole") which behaves as a mobile positive charge. The lowest excited state of the solid can be pictured as consisting of the electron orbiting the hole in a manner analogous to the hydrogen atom. However, compared with the hydrogen atom, there are two important differences: the effective mass of the hole is much less than that of the proton and the electrostatic interaction between the electron and hole is screened by the intervening atoms in the solid. The radius of the wavefunction describing the electron-hole pair (exciton) is therefore much larger (5 nm) than the Bohr radius of hydrogen (0.053 nm). Therefore, the exciton Bohr radius defines whether a crystal can be called a semiconductor quantum dot, or simply acts like a bulk semiconductor.[19]

1.2.2 Core-shell Semiconductor Quantum Dots

It took nearly 16 years for the QDs to enter their new role as fluorescent probes,[20-23] since the first directed synthesis of QDs.[24] In order to achieve high stability and high-quality QDs, it was essential to develop an efficient synthesis procedure. Following the initial reports,[3, 24] extensive research has been carried out in terms of developing a variety of Group II-VI QDs.[25] The research finally progressed to an advanced and commercial stage, with the development of CdSe/ZnS/silane (Core/shell/coat) QDs. Nowadays, these stable, multifunctional and highly bright QDs are used for a variety of *in vitro* and *in vivo* bioimaging purposes.[26-28] These core shell NPs consist of three segments, the first centre core (heart) is CdSe, the second outer layer is the ZnS shell and the final coating is the silane layer. The CdSe core is responsible for the PL and can be tuned by controlling the size in order to achieve different colors across the visible region of the spectrum.[29] The ZnS shell, is a high band gap material desirable to stabilize the PL of the core and to provide a physical barrier with the surrounding.[30] The ultimate silane layer is necessary to reduce the toxicity of the semiconductor materials and also to provide a hydrophilic interface with aqueous solutions. It increases stability and can be subjected to subsequent functionalization.[28]

Different materials can be used for building core/shell/coat complex structures to specifically adjust the emission wavelength of QDs from UV to IR, such as Group II-VI compounds (ZnSe and CdTe [25, 31-35] or SnTe) and Group II-V materials (InP and GaAs).[36-38]
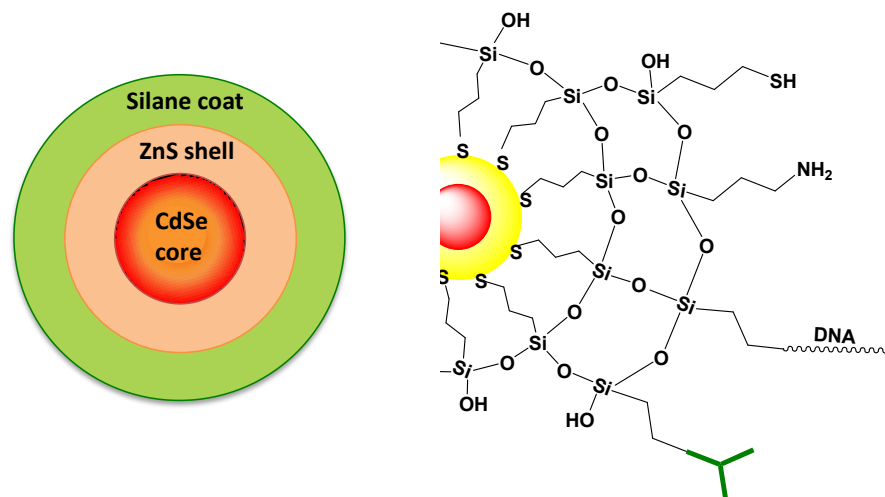
Figure 1.4: Schematic representation of core/shell/coat quantum dot.

However, these core/shell/coat QDs have some limiting factors regarding their potential application range, such as large overall size and not least high elemental toxicity. These properties restrict their use in cellular application, because the internalization (cellular uptake) of small NPs is much more efficient. The intrinsic toxicity of Group II-VI semiconductors is a major concern for application in any biological system.[39, 40] Silane coatings help to reduce this problem, but the porosity thereof is hard to control. Another often used method for the coating of core/shell QDs is the use of various polymers. In this case further specific functionalization is not important but the required reaction conditions may interfere with the stability of the polymer coating. However such stabilized QDs are still highly useful for novel solar cell and light-emitting diode applications.[41, 42]

In addition, long-term toxicity of waste materials after the use of such QDs is also a concern. Considering the above described limiting factors there is certainly a great opportunity (and huge commercial interest) for the development of a smaller, more versatile, and less toxic class of luminescent QDs for use in biological and many other applications.

1.2.3 Silicon Nanoparticles

Silicon (Si) nanoparticles (SiNPs) hold prominent interest, due to their high chemical stability,[43, 44] low inherent toxicity as compared to all Group II-VI nanoparticles,[45] and their potential to make future nano-electronic and nano-photonic devices.[46, 47] Most of all Group II-VI QDs are known to have a direct band-gap transition, while bulk Si is an indirect band-gap semiconductor. In this case the transition from the bottom of the

conduction band to the top of the valence band interrupts conservation of momentum and is electronically forbidden.[48, 49] The transition does occur, but only with phonon (a quantum of lattice vibration) assistance,[50-52] which is an indirect process with a low probability. Thus, SiNPs tend to have a long PL lifetime and low PL efficiencies when compared to direct band-gap semiconductors.[53] PL mechanism in SiNPs can be explained by quantum confinement effects, which was described in the previous section. Besides that, it is also dependent on surface reconstruction[54, 55] and surface termination[56] of SiNPs. The Si atoms on the surface of the NP adopt a significantly different geometry to the bulk lattice structure due to surface reconstruction. These alterations can have a major impact on NP properties, particularly in ultra-small SiNPs (i.e. 1-2 nm).[54] The surface termination also has a big effect on the final photophysical properties of SiNPs. In the case of a monohydride termination, each surface atom has three Si-Si "back-bonds" and one Si-H bond, which gives a different set of bonding constrains, as compared to dihydride termination.[50, 57]

1.2.4 Surface Functionalization of SiNPs

Due to the low stability of Si–H and Si–X (X = Cl, Br) bonds,[58] H or X terminated-NPs are extremely prone to oxidation in air. Further stabilization is a necessity and is usually performed by reaction with alkyl-lithium salts[59] or terminal alkenes,[60] to provide very stable Si-C linkages. In order to form the covalent bonding on planar or porous silicon surfaces hydrosilylation reactions are often employed, in which surface Si-H[61-64] or Si-X (X=halogen)[64,65] bonds add across terminal carbon-carbon double bonds. The reaction can be initiated thermally,[63, 65, 66] photochemically (with UV[67] or visible light[62, 68, 69]) or by a radical initiator,[67, 70] alkyl- or aryl-carbanions[71] and a variety of platinum[72] and triphenylcarbenium-based catalysts.[73] Alkylation with Grignard or alkyl lithium reagents occurs through nucleophilic attack by a carbanion on an electron-deficient Si atom, cleaving Si-Si bonds to form Si-C bonds and silyl anion (Si-) species.[74] The advantage of the hydrosilylation reaction is that it occurs without breaking Si-Si bond which leads to an adverse effect on optical properties and also on particle solubility.[63] A very broad range of compounds can be used to functionalize the surface and provide the desired stability by using hydrosilylation reactions. For example, it has been demonstrated that attaching terminating –COOH[63] or –NH_2 groups[72, 75, 76] (Chapter 3) makes the NPs water soluble, while using nonpolar groups at the end of the alkyl chain makes them soluble in nonpolar solvents.

1.3 Synthetic Strategies for SiNPs

Since the first bottom-up synthesis in 1992 in which SiNPs were prepared via the reduction of SiCl$_4$ and RSiCl$_3$ with sodium,[77] Several methods have been developed and reported that produce stable and monodisperse SiNPs, as well as reproducible surface chemistry, shape and size control, tunable optical properties, etc. Several reviews about the synthesis and optoelectronic properties of SiNPs have been published.[60, 78]

These can be divided into two approaches:

- Top-down, i.e. the reduction of bulk materials to nanometer-sized objects

- Bottom-up, i.e. the assembly of Si atoms up to nanometer size.

In general, the produced Si nanocrystals are hydrogen or halogen-terminated, but require a second surface passivation step to prevent the particle from oxidation and subsequent degradation. The oxidation has a large influence on the optical properties, since the initial luminescence originates from quantum confinements effects in non-oxidized SiNPs, which shifts to luminescence effects originating from surface-state effects in oxidized particles.[53, 79, 80] Each of the individual methods has its own advantages and disadvantages with respect of control of monodispersity, reaction yield, surface chemistry, shape, stability and optical properties and are described below in more detail.

1.3.1 Top Down/ Bulk Reduction method

1.3.1.1 Electrochemical etching and sonication of silicon wafers

Leigh Canham[81] was first to demonstrate that porous Si materials can have large PL efficiency at room temperature. He used electrochemical and chemical dissolution methods to produce mesoporous Si layers of high porosity, which exhibited visible red PL at room temperature. Subsequently a few years later, Heinrich and co-workers[82] electrochemically etched n-type or p-type silicon wafers to form porous silicon by applying an electric potential on a wafer upon soaking in a (1:1) HF:ethanol solution. After etching, the material was ultrasonically dispersed to form suspensions of SiNPs. The resulting material was a polydisperse colloidal solution of SiNPs with size 1 nm to μm and was irregularly shaped. Nayfeh and co-workers used this method to produce SiNPs with a very broad range of sizes that could not be well controlled.[83] In 1999, Wolkin et al.[53] produced hydrogen terminated SiNPs by electrochemical etching followed by photo-assisted stain etching of p-type Si wafers. They demonstrated that depending on the size of the SiNP the PL of such SiNP could

be tuned from the near infrared to the ultraviolet. In the same year, Sweryda-Krawiec et al.[84] produced colloidal solutions of SiNPs by sonicating porous Si wafers. During sonication, NPs leached out from the porous Si network and dissolved in toluene. The SiNPs were then modified by heating with 1-undecanol, 1-hexadecanol, and 1-octanol to obtain alcohol-capped SiNPs of size 1-100 nm. In 2002, Belomoin and co-workers[85] obtained H-capped SiNPs as a family of discrete sizes (1.0, 1.67, 2.15, 2.9, and 3.7nm in diameter) using electrochemical etching. The smallest four exhibited ultra-bright blue, green, yellow, and red luminescence. Lie *et al*. in 2002[86] also produced alkyl-terminated SiNP by refluxing porous Si in toluene solutions of alkenes. A hydrocarbon monolayer was formed at the SiNP surfaces by hydrosilylation of alkene, which protected the SiNPs and solubilized them in organic solvents. The size of the Si core of these particles was about 2.5 nm diameter and could easily be re-dispersed in organic solvents.[87, 88]

1.3.1.2 Etching of Hydrosilsesquioxane/ Thermal decomposition

A relatively new and a straightforward method described by Veinot and co-workers[89-92] for preparing small quantities (ca 0.25g) of nc-Si/SiO$_2$ and Fs-nc-Si that shows luminescence in visible and near IR-regions of the electromagnetic spectrum. The bulk preparation of nanocrystalline Si-SiO$_2$ (nc-Si/SiO$_2$) was carried out via straightforward reductive thermal annealing of a well-defined molecular precursor, hydrogen silsesquioxane. The method provides high yield and excellent purity and optical properties.
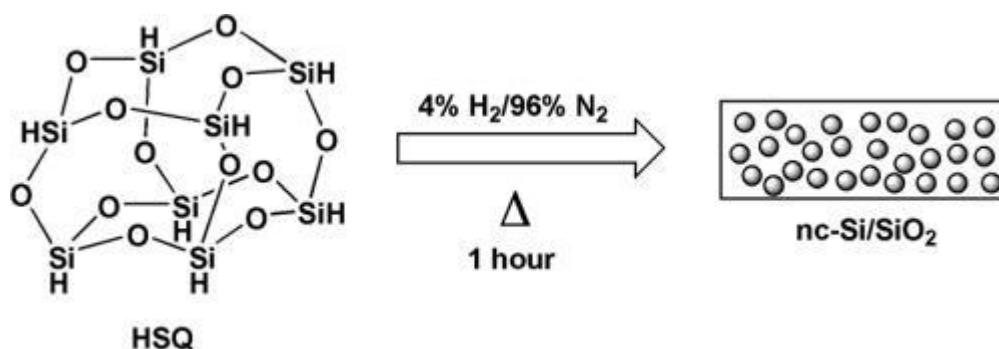
Figure 1.5: Thermal processing of hydrogen silsesquioxane (HSQ) for synthesizing silica NPs /SiO$_2$-like (nc-Si/SiO$_2$) nanocomposites. Reproduced from Veinot's et. al.[89]

1.3.1.3 Annealing of SiO Powders

A relatively new method described by Liu, Kimura and co-workers[93, 94] involves annealing SiO powders at 1000°C under ambient atmosphere, etching the annealed powders with 10% HF and functionalizing the etched particles by common hydrosilylation. The

resulting SiNPs were polydisperse (5.1 ± 1.9 nm) but also had a significant amount of oxygen on their surface. The advantage of this method is its low cost.

1.3.1.4 Laser ablation

Niu and co-workers synthesized SiNPs with a diameter of 4 nm at high rate 400-500 mg/h by using the pulsed laser ablation of a Si (100) wafer in an inert gas.[95] Similarly, Umezu and co-workers prepared SiNPs by laser ablation in He/H_2 gas by pulsing a laser on a Si single crystal. It was found that the higher the H_2 gas pressures the higher the particle crystallinity.[96] Shiharata and co-workers performed a one-pot synthesis with Si wafer by laser ablation in the presence of 1-octene, which effectively capped the NPs resulting in octyl-terminated SiNPs. The diameter of the SiNPs ranged from 1 to 10 nm and the highest fluorescence emission was found around 375 nm.[97]

1.3.1.5 High energy ball milling

Heintz and co-workers synthesized alkyl-capped SiNPs by milling silicon pieces. The resulting particles were 5-10 nm in diameter and showed fluorescence emission around 450 nm.[98] Recently, they developed a method to functionalize SiNPs with acids, aldehydes, and alcohols.[99] However, this functionalization is carried out via the oxygen atoms on the surface, which renders them unavailable for further use and affects both their optical properties and long-term stability.

1.3.1.6 Reactive Sputtering

In 1998 Furukawa and Miyasato[100] successfully synthesized crystalline H-terminated SiNPs materials using a reactive sputtering technique with a low substrate temperature of ~100K. The obtained SiNP had a wide optical band-gap of up to 2.4 eV. The structural analysis showed that the materials consisted of small crystalline Si particles surrounded by hydrogen atoms.

1.3.2 Bottom-up Synthetic Methods / Assembly Methods

1.3.2.1 Laser-Driven Pyrolysis

Swihart and co-workers modified a method in which silane is pyrolyzed (thermally dissociated) by a CO_2 laser beam.[101] A flow of H_2/He gas and temperature is used to tune the reaction. By controlling the flow rate and the laser power the NP sizes can be controlled to a

certain extent and by employing higher temperatures (at least 850°C) helps particle nucleation. These particles required further etching with HF and HNO_3 to remove the surface oxidation layer and to reduce the size. The obtained NPs (up to 20-200 mg/h) have an average diameter of 5 nm with a mixture of hydrogen- and oxygen-terminated Si atoms at the surface. However, the photophysical properties did not remain constant, mainly due to the significant degree of oxidation and the irregularity of the surface.[101] The SiNPs were further etched with 5% HF and thermally hydrosilylated with a series of alkyl- and ester-termination which resulted in a much more stable photoluminescence.[62, 102]

1.3.2.2 Synthesis in supercritical fluids

Among others Korgel and co-workers have used the decomposition of organosilanes (e.g. diphenylsilane) in solvents heated and pressurized above their critical points to build SiNPs.[103, 104] The reaction was performed in a continuous flow reactor, in octanol at 500°C at approximately 250 bar. The obtained SiNPs were monodisperse with an average diameter of 1.5 nm, but the surface coverage of alkoxy termination was only 50%.[105] Adding hexane as a co-solvent, thereby reducing the Si/octanol ratio, could increase the size of the NPs. The same synthesis principle can be used to produce more polydisperse SiNPs with a diameter of 4.7 ± 1.4 nm.[104] The drawback of the decomposition method is the lack of control of the functionalization of the NPs. The same synthetic approach can be employed to produce Si nanowires.[103, 106, 107]

1.3.2.3 Oxidation and Reduction in Solution

Various solution phase oxidation-reduction reactions have been developed and extensively studied. Kauzlarich and co-workers made an extensive effort to synthesize SiNPs using various solution routes. The first solution synthesis method was developed in 1996 by Bley and Kauzlarich.[108] They reacted Zintl compound KSi with silicon tetrachloride ($SiCl_4$) to fabricate crystalline SiNPs at ambient temperature. Conversely in their next paper they reported several problems regarding the Zintle synthesis method, such as low yields and the lack of size control due to the heterogeneous nature of the reaction mixture. In 2002, Liu and Kauzlarich[109] described a new synthetic route for the synthesis of hydrogen-terminated (H-terminated) SiNPs by the initial reaction of the metal silicide with either $SiCl_4$ or bromine and subsequently with lithium aluminium hydride. These reactions produced H-terminated SiNPs, which could be suspended in an organic solvent. A variety of other routes have been investigated: such as oxidation of Mg_2Si with Br_2,[59, 109] reduction of $SiCl_4$ with Na-naphthalenide[110] to give stable SiNPs.

A $x\,Mg_2Si$ + $2.5x\,Br_2$ $\xrightarrow[\text{N}_2\text{ atm, Reflux}]{\text{Octane}}$ Si—Br + $2x\,MgBr_2$

B   R-Si + $SiCl_4$ $\xrightarrow[\text{N}_2\text{ atm, Reflux}]{\text{Glyme, Diglyme Or THF}}$ Si—Cl + Salts

(R = K, Na, Mg)

C $4SiCl_4$ + 15 Na (naphthalide) $\xrightarrow[\text{N}_2\text{ atm, Reflux}]{\text{Octane}}$ Si—Cl + 15 NaCl

D $SiCl_4$ + $LiAlH_4$ $\xrightarrow[\text{Sonication}]{\text{Surfactant}}$ Si—H

E $SiCl_4$ + $RSiCl_3$ + Na $\xrightarrow[\text{Pressure}]{\text{Heat}}$ Si—Cl + NaCl

F $Si(OC_2H_5)_4$ + 4 Na $\xrightarrow{\text{Sonicate}}$ Si—O + $4\,NaOC_2H_5$
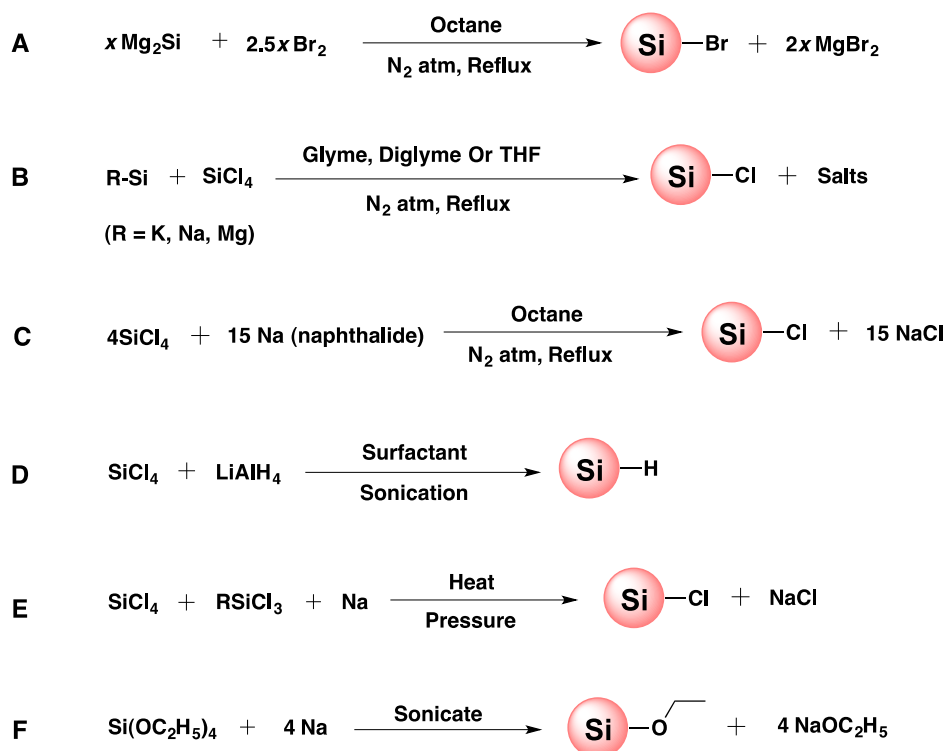
Figure 1.6: Various solution methods to synthesize SiNPs by oxidation and reduction reaction.

The size of the SiNPs can be controlled by changing the balance between growth and nucleation speed through controlling several parameters such as temperature, concentration of precursors and the choice of functionalizing ligands. Similar synthetic methodology and principle can be used to synthesize GeNPs (2 nm size).[111] The advantage of these methods is their versatility, as they can also be used to synthesize doped SiNPs (with Mn[112] or P[113]) or mixed Si-Ge NPs.[114] The obtained NPs initially terminated with halogen atoms (Cl or Br) give an access for further functionalization using alkyllithium (R-Li) compounds,[59, 115] alkoxy groups (via reaction with alcohols)[110, 116] or hydrogen atoms by reduction with $LiAlH_4$.[109]

Out of all these methods a few claim to provide partial control over the NP shape. Particularly sodium naphthalenide has been proven useful for preparing free standing SiNPs of various sizes and surface chemistry.[117] The major drawbacks of this synthesis approach are: the polydispersity of the obtained material (1-20 nm, and in the best case 3-6 nm), time-consuming reaction conditions (~72 h per reaction), and the requirement of an extensive purification protocol. FTIR analysis of isolated NPs shows, besides the characteristic C-H bands, a significant degree of oxidation, which subsequently leads to red-tailed broad emission features.

1.3.2.4 Synthesis in reverse micelles

In order to gain more control over the size and size distribution of SiNPs, Wilcoxon and group developed a method to synthesize SiNPs in reverse micelles.[118] Performing the reaction in nanoreactors limits the size of the resulting SiNPs, and a narrower size distribution is achieved. In this approach, an anhydrous compound (e.g. SiX_4; X = Cl, Br or I) is dissolved in the hydrophilic interior of a solution of micelles and nucleation and growth of SiNPs are restricted to the micelle interior. Control of cluster size can be achieved by variation of the micelles size, inter-micellar interactions and reaction chemistry. The reduction of $SiCl_4$ with $LiAlH_4$ in nanoreactors, was carried out by Wilcoxon and coworkers,[118] resulting in SiNPs with a broad size distribution of 2-10 nm which exhibit a highly structured optical absorption and photoluminescence across the visible range of the spectrum. It was assumed that the obtained NP surfaces were hydride terminated, however, no experimental evidence was provided. HRTEM and selected-area electron diffraction of small samples were consistent with diamond lattice Si. Tilley et al.[119] later used a variation of such solution reduction to prepare very small quantities of small, relatively monodisperse, freestanding SiNPs (d = 1.8 ± 0.2 nm). Recently, Rosso-Vasic et al.[75] synthesized amine-functionalised SiNPs using inverse micelles. The obtained SiNPs were stable over a wide pH range (1–13) and high temperatures (120°C), and were suitable for bioimaging studies as they were readily taken up by BV2 cells.

1.3.2.5 Plasma Processing

In 2005, Mangolini *et al.*[120] presented a single-step continuous flow non-thermal plasma process that produced luminescent SiNPs on time scales of a few milliseconds. The luminescent SiNPs had diameters of 2-8 nm and process yields of 14–52 mg/h. In the same year, Giesen et al.[121] investigated the formation and growth of SiNPs by the addition of silane to plasma gases (i.e. argon/hydrogen) in a microwave reactor. The SiNPs formed by this approach were found to lie in the 5–8 nm range and contained crystalline Si.

1.4   Applications of Silicon Nanoparticles

SiNPs have attracted tremendous interest from the scientific community because of their unique characteristics that differ from those of their bulk counterparts, such as novel optical, catalytic, electronic, and mechanical properties.[15, 122] At nanometer scales, silicon exhibits visible photoluminescence because of the quantum confinement effect that can be exploited for uses in electronic and photonic devices.[47, 123] Indeed, silicon has several

advantages to be an ideal nanoparticle material such as size-dependent tunable light emission,[85, 104, 124] high brightness,[125] and their great stability against photobleaching compared to organic dye molecules used for bioimaging.[72, 126] Moreover, their core consists of non-toxic silicon, which has been further studied for SiNPs in particular,[127, 128] whereas the conventional group II-VI or III-V QDs often consist of the inherently toxic Cd, CdTe ZnSe.[40, 129] In general, group II-VI or III-V QDs are typically stabilized by attachment of non-covalently bound organic molecules such as oleic acid, thiols or phosphine oxide derivatives.[130] This leaves them intolerant to many solvents, since the stability of such a layer is highly dependent on the chemical environment, and these non-covalently attached molecules can thus dissociate from the QDs and thereby cause them to precipitate. Furthermore, a lot of effort has been invested in preventing leakage of the toxic Cd, Zn and Se ions from the core of the group II-VI or III-V QDs by applying organic polymeric coatings, since the small capping molecules are not sufficient.[131] Next to the non-toxicity of the Si core, the covalently attached organic monolayer tolerates a wide range of solvents. So far, fewer applications with SiNPs have been developed than with group II-VI or III-V QDs, which is most likely due to the lack of a method to synthesize well defined, functional SiNPs in large amounts with relatively easy methods. Furthermore, in contrast to group II-VI or III-V QDs, the SiNPs have an indirect bandgap, which is characterized by relatively low luminescence efficiency. The combination of these properties opens a new avenue of applications of SiNPs for optoelectronic and bioimaging purposes.

1.5   Biomedical Applications of Semiconductor Nanoparticles

Significant interest has arisen in the field of NPs during the last decade, in particular towards biomedical applications. The integration of nanotechnology into the field of medical science has opened new possibilities. Working with nanomaterials has allowed a better understanding of molecular biology. As a consequence, there is the potential for providing novel methods for the treatment of diseases which were previously difficult to target due to size restrictions. For biomedical applications, the synthesis of biofunctionalized NPs is very important, and it has recently drawn the attention of numerous research groups, making this area constantly grow. Silicon nanoparticles and structures hold prominent interest in various aspects of biomedical research. Their applications in drug delivery, cancer cell diagnostics and therapeutics have been active fields of research over recent years.[11, 132, 133]

1.5.1 Cytotoxicity

In *vitro* studies have become an essential component in assessing NP toxicity since they are a relatively rapid and cost-effective way of screening[134]; moreover, they restrict animal use, as required by ethical issues. Although a large number of studies have been performed with *in vitro* systems, yet there remain some serious obstacles as data on this topic obtained by several groups are often contradictory. Multiple factors are responsible for the differences found in toxicity studies; some might be related to particles sizes, shapes and physicochemical surface properties, while others may relate to the cell lines used, and finally one should consider differences in methodologies of the test itself. Cytotoxicity of the NPs inside the cells can be determined by different assay.

Bright field microscopy can be used as a simple tool to visualize the cellular and nuclear morphological changes in the cells; the majority of the cytotoxicity assays measure the colorimetric changes upon cell death. These colorimetric methods are divided into two categories including plasma membrane integrity measurements and mitochondrial activity tests.[129] For example, Trypan blue dye exclusion assay provides information of cell death by showing dye staining on cells that were ruptured, while live cells remain colourless, and the amount of cell death can be determined via light microscopy.[135]

Another method to determine the cytotoxicity is the MTT (3-(4,5- dimethylthiazol-2-yl)-2,5-diphenyl tetrazolium bromide) assay, which measures the activity of the mitochondrial dehydrogenase enzyme.[136, 137] This enzyme present in living cells cleaves the tetrazolium ring, which only occurs in living cells.[138] MTT is pale yellow in solution but produces an insoluble purple formazan product within live cells.

Another method to test the cytotoxicity of the cells uses the genotoxicity assay, which tests the toxicity of NPs exposure on the genome by means of the COMET system. This is the most widely used method able to detect both single- and double-stranded breaks of DNA chains. In fact, if any DNA is damaged, the cell would produce a comet tail whose length is proportional to the amount of damaged DNA. A DNA-specific dye such as propidium iodide and 4',6-diamidino-2-phenylindole (DAPI) is used to visualize the comet. The amount of DNA damage is indicated by the amount of DNA found in the tail.[139]

Other factors responsible for toxicity in the cells are the physical and chemical properties of NPs. The overall size of the nanoparticles plays an important role to induced toxicity. NPs sometimes show aggregation and morphological variation when dispersed in water, therefore it is important to check their stability in biological media first. For size

analysis, either dynamic light scattering (DLS) or transmission electron microscopy (TEM) is mostly used. For instance Lin et al.[140] found that it is very important to control the aggregation state in the cell culture medium. They studied two different sizes (15 nm and 46 nm) of NPs and found no difference, the reason being that both nanoparticles reached a similar size due to aggregation in the culture medium. Therefore, NP aggregation state is a critical parameter that needs to be controlled.

Another source of nanoparticle-induced cytotoxicity occurs when the NP is composed of toxic materials that can be gradually released. Some examples of the fluorescent semiconductor NPs that gradually release heavy metal ions such as Cd^{2+} from CdSe or CdSe/ZnS quantum dots are well known.[39, 40] Heavy metal ions are cytotoxic and often show several pathways of cytotoxicity. Indeed, Cd^{2+} may induce hepatotoxicity, immunotoxicity, and nephrotoxicity, apoptosis being a critical part of each toxicity type.[141] Studies concerning Cd-induced hepatotoxicity show, for example, the relevance of direct and indirect cytotoxic pathways.[142] The direct pathway is caused by Cd^{2+} binding to sulfhydryl groups on key mitochondrial molecules, thus damaging the mitochondria. The indirect pathway, though, is assumed to occur via activation of Kupffer cells. Derfus and group reported that the cadmium selenide (CdSe) core causes acute toxicity under certain condition. However they also mention that CdSe NPs did not show cytotoxicity when functionalized with mercaptoacetic acid under standard synthesis condition. The cytotoxicity of green, yellow, and red light emitting mercapto-undecanoic acid-modified QDs was investigated by Shiohara et al., using three types of cells: Vero cell, HeLa cell and primary human hepatocyte. The results showed that the cell viability decreased with increasing concentration of NPs. They proposed that SiNPs could be the new safer QDs[143] to eliminate cytotoxic effect. Kirchner and colleagues[39] investigated the effect of different organic coatings (*i.e.* mercaptopropionic acid) on QD cytotoxicity. Their results showed that the zinc sulphide capping (ZnS) layer of a CdSe core-shell NP reduced the toxicity, which is in agreement with the work of Derfus *et al*.[40] They also found that embedding the particles in a stable ligand shell dramatically reduces the release of Cd^{2+} ions. Thus, the cytotoxicity of semiconductor NPs can be reduced when their cores are protected from degradation given that the added coatings are biocompatible.

The cytotoxicity of group II-VI semiconductor NPs (*e.g* CdSe, Cadmium telluride (CdTe), ZnS) is extensively studied as compared to SiNPs. The long-term cytotoxic effect of porous silicon material on primary hepatocytes was explored by Chin et. al.[144] The attachment and spreading of primary hepatocyte on nanoporous silicon were compared across a variety of culture conditions. He demonstrated that cells in all conditions remained

viable at comparable levels, suggesting that there were no long-term cytotoxic effects of nanoporous silicon on primary hepatocytes. Alsharif et al.[145] investigated the intracellular internalization and toxicity of alkyl-capped silicon nanocrystals in human neoplastic and normal primary cells. Their findings suggested no evidence of *in vitro* cytotoxicity when the cells were exposed to the alkyl-capped nanocrystals. Thus, surface functionalized SiNPs exhibit insignificant cytotoxicity and show great potential over ordinary semiconductor NPs in biomedical research.

One *in vivo* study carried out by Sailor's group demonstrated that porous SiNPs injected intravenously were accumulated mainly in mononuclear phagocytic system organs. Within a few days the SiNPs were degraded *in vivo* into non-toxic products and removed from the body through renal clearance.[146]

Consequently, Si nanoparticles show very low cytotoxicity taking care that all potential sources of cytotoxicity are prevented efficiently.

1.6 Biomedical Applications of SiNPs

In order to employ NPs in biological applications, the particles have to be water soluble, non-toxic, possess high luminescence quantum yield and should have the ability to be labeled with targeting agents to direct the particles to specific tissues or areas inside cells. SiNPs have substantial photoluminescence quantum yields, great stability against photobleaching and low toxicity compared with heavy metals. In order to stabilize SiNPs in water and in biological environment to prevent aggregation and precipitation, they require a desirable surface functionalization.[72] Several methods have been developed to functionalize SiNPs to use them for biological applications. Perez et al.[147] synthesized nanometric particles from porous silicon film to investigate the growth behavior of *B. subtilis* and *K. pneumoniae* bacterial strains. The different and particular behavior that each bacterium presents when grown in a medium containing nanometric silicon particles supports the idea that these particles can work well as a bacteriological sensor. Li and Ruckenstein[87] synthesized poly-acrylic acid terminated SiNPs for cell imaging. The SiNPs are water soluble, exhibited bright fluorescence images and provided higher resistance to photobleaching than the commonly used organic dyes. Warner et al.[72] described a simple room-temperature synthesis for producing water-soluble SiNPs that exhibited strong blue photoluminescence with a rapid rate of recombination. They used these allylamine capped SiNPs to demonstrate bioimaging in HeLa cells. The bright blue fluorescence from the SiNPs is distributed uniformly inside the

cytosol of the HeLa cells and shows the possibility of using these hydrophilic SiNPs as chromophores in biological fluorescence imaging.

1.7 Glyconanoparticles for Biomedical Applications

Since the last decade, there has been an explosion in the synthesis, characterization and applications of nanomaterials, which can potentially revolutionize the diagnosis and treatment of diseases.[148-151] The field is actively progressing towards using more specific and targeted nano-therapies by gaining the knowledge at cellular and molecular level. Tremendous advances have been made in recruiting sugar-functionalized nanocomposites for biological applications by recognizing the important multi-faceted roles that carbohydrates play in many biological systems (figure 1.6).[149, 150, 152] Currently Glyco-nanomaterials have attracted a great deal of attention owing to their multi-faceted carbohydrate functionality, small size, biocompatibility, as well as their unique optical, electronic and magnetic properties.
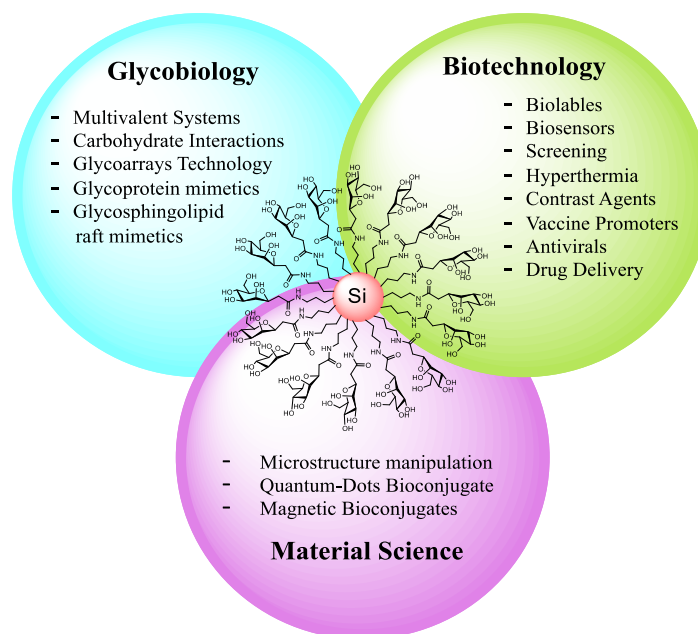
Figure 1.7: The concept of prospective uses of glyconanoparticles in biomedical applications. Reproduced from Penadés et al.[1]

1.7.1 The "GLYCO" Perspective

Carbohydrates play a critical role in the process of cell recognition.[11, 153, 154] Naturally occurring carbohydrates, glycoproteins and glycolipids present at the surface of cells play crucial roles in biological events, acting as recognition sites between cells. They can trigger various phenomena such as cell growth, inflammatory responses to viral infections. Carbohydrate-mediated interactions at the cell surface range from hormones, enzymes and antibodies to bacteria, viruses and toxins. Surface-exposed carbohydrate moieties that are characteristic of a given microbe may serve as key biomarkers for bacteria and pathogen identification, diagnosis and vaccine development. Carbohydrates, as a detection platform, have already demonstrated tremendous potential to achieve superior sensitivity and selectivity.[155, 156] At present, carbohydrate-functionalized glyconanomaterials are finding many important applications in explaining carbohydrate protein interactions and cell-cell communication.[154, 157-160] Identifying, quantifying and imaging the carbohydrates, glycoproteins and glycolipids are critical both for elucidating their biological function and for the evaluation and design of therapeutics.

Despite all the developments, there are still several obstacles, which need to be overcome in order to use the carbohydrates in diagnosing and therapeutics applications. Carbohydrate-based molecular interactions have been shown to be generally weak and of low affinity, but Nature seems to compensate these drawbacks with a multivalent receptor ligand presentation.[160, 161] Thus, a suitable platform is required to display carbohydrates in a polyvalent system to increase the binding strength and selectivity. In the second challenge, unlike the specific receptor interaction, there can be several receptors recognizing the same carbohydrate ligand thus strategies need to be developed to differentiate these receptors. The third challenge is to obtain pure carbohydrates for biological studies. Due to the heterogeneity it is difficult to purify large quantities of oligosaccharides from natural sources. Therefore, to realize the full potential of carbohydrates in biomedical applications requires a multi-disciplinary approach.

1.7.2 The "NANO" Perspective

Nanomaterials can act as promising platforms for displaying carbohydrates for biological recognition. Owing to their small size and large surface to volume ratio NPs can enable higher capacity in receptor binding. Moreover functionalizing the NPs with multiple carbohydrate ligands can potentially enhance the binding affinities of individual ligands to

their binding partners. Glyco-conjugated / bioconjugated nanoparticles have been utilized in various fields of *in vivo* and *in vitro* work.

Penadés and co-worker provided excellent contributions to the field where they investigated carbohydrate-carbohydrate interactions and carbohydrate-mediated cell–cell adhesion processes. In their early report they demonstrated the synthesis of disaccharide lactose (Galβ (1→4)Glcβ_1 - OR) and trisaccharide Lewis^x (Le^x-) Galβ (1→4) [Fucα (1→3)] GlcNAcβ_1-OR) to functionalize Gold NPs (AuNPs) as a multivalent ligand carrier for studying Ca^{2+} mediated carbohydrate-carbohydrate interactions.[162] They used different hydrophobic and hydrophilic linkers to bind the carbohydrates to the gold core. Using TEM they revealed the specific binding between Ca^{2+} and Le^x-AuNPs as it resulted in self-aggregation, while Lacto-AuNPs did not show any clustering. The method proved the importance of the sugar structure in inducing aggregation. Later they studied the adhesion forces between Le^x antigens self-assembled on gold surfaces. They verified this phenomenon using Atomic force microscopy (AFM).[163] Furthermore they showed that Ca^{2+} mediated aggregation of Le^x-AuNPs was a slow but highly exothermic process, while in the case of Lacto-AuNPs the heat evolved was very low and its thermal equilibrium was quickly achieved. They proved this phenomenon by using surface plasmon resonance (SPR) and isothermal titration calorimetry (ITC).[164, 165] El-Boubbou synthesized Mannose capped (Man-) Magnetic glyco-nanoparticles (MGNPs).[166] They incubated Man-MGNPs with *E. coli* and reported that within five minutes 65% of the *E. coli* ORN178 cells were removed from the solution using a hand-held magnet (figure 1.7). Furthermore, in addition to Man-MGNPs, they also synthesized Gal-MGNPs in order to overcome the challenge that different types of bacteria may bind to the same carbohydrate with various affinities. Based on this they used three different *E. coli* strains (ORN178, ORN208 and an environmental strain) and showed that they were easily differentiated. Thus, they demonstrated that MGNPs present a unique approach, which can be used not only for rapid pathogen detection, but also for strain differentiation and efficient pathogen decontamination.
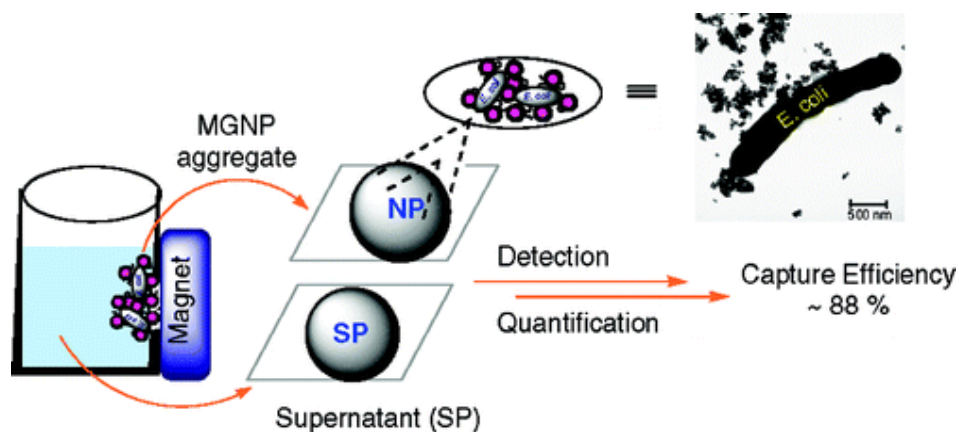
Figure 1.8: Schematic representation of E. coli strain ORN178 incubated with Man-MGNPs followed by magnet mediated separation of detected bacteria, showing up to 88% of the bacteria removed by this procedure.

In addition Syková et al.[167] showed that Mannose-modified iron oxide NPs were efficient probes for labeling stem cells.

The Cho group prepared superparamagnetic NPs coated with a galactose polymer (Gal-SPIONs) (diameter ~ 25 nm)[168] and applied them to target liver cells knowing that liver cells (hepatocyte) contain the galactoside binding asialoglycoprotein receptor (ASGP-R) which selectively binds to galactose. Using confocal microscopy studies they validated the receptor-mediated endocytosis. Later they used these NPs *in Vivo* module by injecting into a rat tail vein; the experiment showed a 75% T2 signal drop for rat liver by MRI, which was more than twice the contrast change (36%) observed using control NPs without any galactose.

Lin and co-workers[169] synthesized polyvalent glyco-NPs (Man-, Glu- or Gal-AuNPs) and proved the high affinity and specificity of multivalent carbohydrate-protein interactions. They quantitatively analyzed the binding affinity with lectin *Concanavalin A* (Con A) using surface plasma resonance. Later they reported the separation of carbohydrate binding proteins from protein mixtures aided by the gold glyco-NPs as affinity probes. Furthermore, using this approach, they determined the identity and the carbohydrate binding epitopes of the proteins by mass spectrometry analysis.[170]

For studying NP-cell interactions, the Penadés groups reported the preparation of gold and gold–iron NPs[171] (Size 1.5-2.5 nm) functionalized with maltose (Malto), Glc (Glucose) and Lactose (Lacto) and evaluated their biological effects.[172] It was shown that Lacto-NPs were taken up by endocytosis in a human fibroblast cell line without provoking

apoptosis, while Malto-NP were endocytosed and promoted cell death. Glc-NPs were not endocytosed and did not affect cell viability either. The study demonstrated the possibility of using Lacto-NPs to image an experimental C6 glioma in mice for *in vivo* applications.

Recently, the same group prepared a small library of multivalent Au-NPs functionalized with different structural fragments of the high mannose undecasaccharide of gp120 in various ligand densities and evaluated their effects on the inhibition of HIV glycoprotein gp120 binding to DC-SIGN expressing cells (figure 1.8).[173]
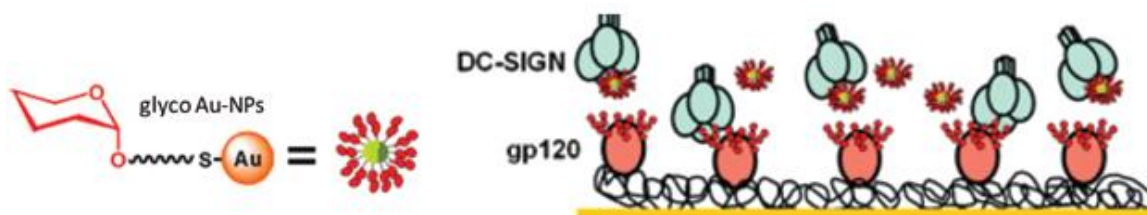
Figure 1.9: Schematic representations of the glyco Au-NPs showing that it can reduce the binding between DC-SIGN and gp120, which have a significant inhibitory effect on HIV infection to cells expressing DC-SIGN.[173]

A simple colorimetric bioassay for the detection and quantification of cholera toxin (CT) was developed by Russell and co-workers.[174] They synthesized lactose-functionalized AuNPs and incubated with the cholera toxin, which formed aggregates within 10 minutes.

For *in vivo* applications, the Penades group developed sugar-coated AuNPs combined with Gd(III) chelates as new paramagnetic probes for MRI.[175] Besides imaging applications they reported the utilization of Lacto-AuNPs as potent inhibitors of tumor metastasis in mice and evaluated their potential as anti-adhesive tools against metastasis progression.[176] The mouse melanoma B16F10 cells are known to bind with lactose due to the presence of galectins on the surface. Pre-incubation of the B16F10 cells with the Lacto-AuNPs prior to injections into mice substantially inhibited the lung metastasis of the tumor (up to 70%) shown in figure 1.9.
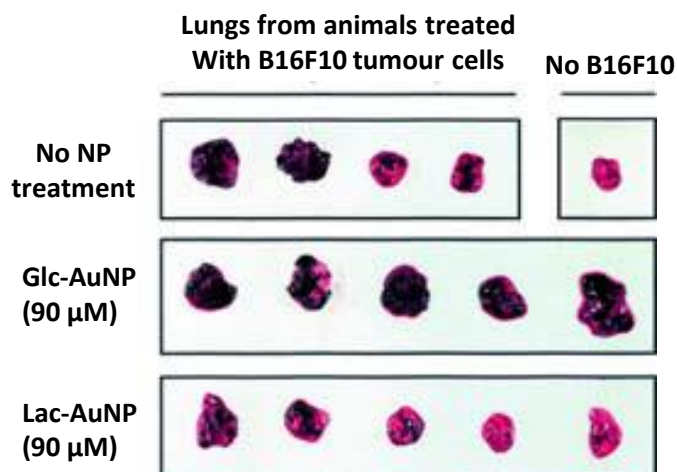
Figure 1.10: The incubation of Lacto-AuNPs with mouse melanoma B16F10 cells prior to intravenous inoculation in C57/Bl6 mice significantly reduced the lung metastasis of the tumour. In comparison, the Glc-AuNPs were ineffective in reducing metastasis.[176]

Later in 2009 Mousa and co-workers reported the synthesis of heparin coated AuNPs (HP-AuNPs).[177] Heparin is a class of naturally occurring polysaccharide, which can inhibit basic fibroblast growth factor-2 induced angiogenesis.[178] They studied HP-AuNPs in a mouse model where they demonstrated that HP-AuNPs have significantly higher anti-angiogenesis efficiency compared with Glc-AuNPs, while control Au was lethal to the animal at the same concentration.

In 2003 the Rosenzweig group reported the QDs protected with polysaccharide.[179] They synthesized carboxymethyldextran and polylysine coated CdSe-ZnS QDs through electrostatic interaction and demonstrated Con A had binding affinities with glycol-QDs.

Subsequently Fang and coworkers prepared CdSe-ZnS QDs terminated with *β-N*-acetylglucosamine (GlcNAc) and Mannose through an in situ reduction and coating procedure. They incubated these glycol-NPs with live sperm from mice, pigs and sea-urchin.[180] Interestingly, their results showed that GlcNAc captured QDs were found to be concentrated at the sea-urchin sperm heads, while Man-coated QDs tended to spread over the whole body of mouse sperm (figure 1.10). This was presumably due to the different distribution of the GlcNAc and Man receptors on the sperm surface. Their work suggested that glycol-NPs could be useful as fluorescent tags for monitoring cellular events.
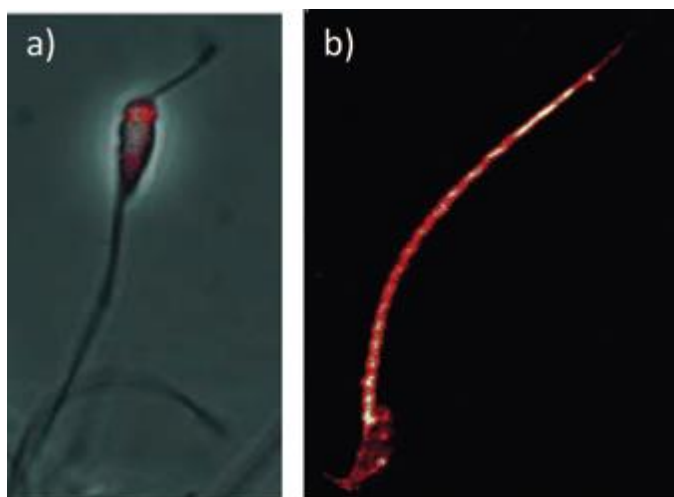
Figure 1.11: Confocal image of glyconanoparticles upon incubation with sperm. (a) GlcNAc-QDs was mainly found on the heads of sea-urchin sperm (scale bar=20 µm), and b) Man-QD labelled the tail of mouse sperm.[180]

Furthermore the glyco- QDs are also used in *in vivo* detection. Kim and co-worker reported the synthesis of hyaluronic acid coated QDs (HA-QDs).[181] They demonstrated that HA-QDs were able to selectively endocytose by lymphatic vessel endothelial receptor 1 (LYVE-1) over-expressing lymphatic endothelial cells (LEC) and HeLa cells, but not by LYVE-1 negative human dermal fibroblasts. The binding between LYVE-1 and HA-QDs in mice was confirmed by immunohistochemistry, where LYVE-1 and HA-QDs were found to co-localize in mouse tissues. Additionally HA-QDs were also used to image liver in cirrhotic mice.[182] Through *in vitro* assay the authors demonstrated that the HA-QDs were taken up more by chronic liver diseased cells such as hepatic stellate cells (HSC-T6) and hepatoma cells (HepG2), than normal hepatocytes (FL83B). They then administrated HA-QDs in cirrhotic mice and observed the enhanced fluorescence from the liver. The clearance of the fluorescence from the cirrhotic mouse liver was much slower than that from the normal mice, allowing detection of the cirrhotic liver.

Later the Seeberger group reported the synthesis of Man, Gal, GalN (Galactosamine) - capped PEGylated QDs to study in vivo liver imaging.[153] They demonstrated that Gal- and GalN-capped QDs were selectively taken up by hepatocellular carcinoma HepG2 cells via the ASGP-R receptor.

By looking at the extensive work done on glyco-NPs it is clear that the affinity between carbohydrates and receptors can be greatly improved through the multivalent display of carbohydrates on nanomaterials. In order to fully appreciate the potential of

glyco-nanotechnology, especially for future clinical applications, better fundamental knowledge of how NPs interact with biological systems is required. This can be achieved by changing the parameters such as size, shape, surface charge, ligand type and ligand density. Moreover, bio-distribution, clearance and long-term side effect/toxicity of glyconanocomposites need to be established.

Silicon nanoparticles and structures hold prominent interest in various aspects of biomedical research. Current fields of interest range from imaging, detection and sensing to drug delivery and new therapeutic uses. This is in addition to the intrinsic electronic and optical properties of the nanostructures. Their fluorescence signatures, high quantum efficiency, size-dependent tunable light emission, high brightness and great stability against photobleaching compared to organic dye molecules make them ideal tools for fluorescence imaging. These properties have helped to establish silicon based nanoparticles in a swathe of diagnostic and assay roles as fluorescent cellular markers.[45, 183] Furthermore, silicon exhibits a low inherent toxicity when compared with the heavy elements of several other types of semiconductor quantum dots, which can pose significant risks to human health. The overall combination of these properties of SiNPs opens up new avenues of applications in optoelectronics and bioimaging.

When considering biomedical applications, surface functionalization of SiNPs is essential in order to target them to specific disease areas and to allow them to selectively interact with cells or biomolecules.[184, 185] When capped with organic molecules SiNPs can take their functionality and display a number of interesting additional properties, such as increasing overall stability of NPs, increased solubility and preventing aggregation and precipitation in a biological environment, all of which are important in biomedical applications. The properties of nanoparticles can be controlled as a result of variation in chemical synthesis methods. The organic shell located on the external part of the SiNPs provides chemical functionality to the nanostructure and is thus responsible for solubility, stability, charge effects and interactions with other molecules. By looking at the potential application and development of SiNPs in biomedical fields, it is worth synthesizing carbohydrate capped SiNPs. However, no such functionalization has been explored with SiNPs.

1.8 Scope of This Thesis

This thesis consists of five chapters; a brief summary of each is given below.

This thesis deals with the development and optimization of a method for the preparation of stable and monodisperse SiNPs, and their photophysical characterization. In addition, it displays possible applications of SiNPs as well as the investigations into their toxicity, specifically in the realm of bioimaging.

Chapter 1 gives a general introduction about semiconductor quantum dots and Si NPs, in particular. It gives an overview about the variety of methods published so far that are used for the production of SiNPs and the description of the origin of Si NPs luminescence. It also gives an overview about the cytotoxicity and applications of the NPs in biomedical field.

Chapter 2 describes the methods for producing and functionalizing SiNPs such as amine-terminated SiNPs and carbohydrate capped SiNPs. Also discussed are various physical and chemical characterization techniques. In addition, the methods and materials used in the biomedical studies of the particles are described.

In ***Chapter 3***, the preparation of water-soluble amine functionalized silicon nanoparticles is described. A facile method to synthesize highly stable amine-terminated SiNPs including their photophysical characterization such as ultra violet-visible (UV-vis) spectroscopy measurements are outlined and discussed. The surface chemical composition of amine-terminated SiNPs was confirmed by Fourier Transform Infrared Spectroscopy (FTIR), Nuclear Magnetic Resonance Spectroscopy (NMR) and X-ray Photoelectron Spectroscopy (XPS). The size of amine-terminated SiNPs was examined using Transmission Electron Microscope (TEM) and Dynamic Light Scattering (DLS) techniques. Moreover photoluminescence (PL) and pH stability of the obtained SiNPs were studied.

The work described in this chapter has led to the following publication:

*__Ahire, J. H__.; Wang, Q.; Coxon, P. R.; Malhotra, G.; Brydson, R.; Chen, R.; Chao, Y., Highly Luminescent and Nontoxic Amine-Capped Nanoparticles from Porous Silicon: Synthesis and Their Use in Biomedical Imaging. ACS Applied Materials & Interfaces **2012**, 4 (6), 3285-3292.*

*Coxon, P. R.; __Ahire, J. H__.; Ashby, S., P.; Frogley, M., D.; Chao, Y.; Amine-terminated Nanoparticle films: Pattern Deposition by a Simple Nanostencilling Technique and Stability Studies under X-ray Irradiation. Physical Chemistry Chemical Physics **2014**, 16, 5817-5823*

Chapter 4 demonstrates the synthesis of highly stable and water-soluble carbohydrate capped SiNPs. A simplified method is described to functionalize SiNPs with various monosaccharide and disaccharide sugar moiety. The surface functionalization of carbohydrate capped SiNPs is confirmed by FTIR, NMR, and energy dispersive X-ray spectroscopy (EDX) studies. The photophysical and optical properties were measured by UV and PL spectroscopy. The size of all NPs was measured by TEM, while the hydrodynamic diameter and Zeta-potential were obtained by DLS. The biochemical activity of carbohydrate capped SiNPs was tested with ConA as a target protein.

<u>The work described in this chapter has led to the following publication:</u>

Ahire, J. H.; *Chambrier, I.; Mueller, A.; Bao, Y.; Chao, Y., Synthesis of d-Mannose Capped Silicon Nanoparticles and Their Interactions with MCF-7 Human Breast Cancerous Cells. ACS Applied Materials & Interfaces **2013**, 5 (15), 7384-7391.*

Chapter 5 deals with the application of carbohydrate capped SiNPs for selectively targeting cancerous cells as well as for bioimaging purposes. All carbohydrate capped SiNPs are studied by using several mammalian cell lines. All carbohydrate capped SiNPs proved to be non-toxic inside normal mammalian cells and cancer cells, moreover they were found to be highly stable in biological media. It was shown that carbohydrate capped SiNPs are taken up selectively by cancerous cells rather than normal cells. All the SiNPs can be successfully used for staining several cancer cell lines, as well as demonstrated receptor mediate endocytosis, which could favor the development of nanomedicine in cancer treatment.

1.9 References

1.   de la Fuente, J. M.; Penadés, S., Glyconanoparticles: Types, synthesis and applications in glycoscience, biomedicine and material science. *Biochimica et Biophysica Acta (BBA) - General Subjects* **2006,** *1760* (4), 636-651.

2.   Feynman, R., "There's plenty of room at the bottom" *Seminar talk* **1959**.

3.   Alivisatos, A. P., Semiconductor Clusters, Nanocrystals, and Quantum Dots. *Science* **1996,** *271* (5251), 933-937.

4.   Whitesides, G. M., Nanoscience, Nanotechnology, and Chemistry. *Small* **2005,** *1* (2), 172-179.

5.   Binnig, G.; Rohrer, H., Scanning tunneling microscopy. *IBM J. Res. Dev.* **2000,** *44* (1-2), 279-293.

6.   Iverson, N.; Plourde, N.; Chnari, E.; Nackman, G.; Moghe, P., Convergence of Nanotechnology and Cardiovascular Medicine. *BioDrugs* **2008,** *22* (1), 1-10.

7.   Nazem, A.; Mansoori, G. A., Nanotechnology Solutions for Alzheimer's Disease: Advances in Research Tools, Diagnostic Methods and Therapeutic Agents. *Journal of Alzheimer's Disease* **2008,** *13* (2), 199-223.

8.   Kaounides, L.; Yu, H.; Harper, T., Nanotechnology innovation and applications in textiles industry: current markets and future growth trends. *Materials Technology* **2007,** *22* (4), 209-237.

9.   Brus, L. E., Electron-electron and electron-hole interactions in small semiconductor crystallites: The size dependence of the lowest excited electronic state. *The Journal of Chemical Physics* **1984,** *80* (9), 4403-4409.

10.   Ntziachristos, V.; Tung, C.-H.; Bremer, C.; Weissleder, R., Fluorescence molecular tomography resolves protease activity in vivo. *Nat Med* **2002,** *8* (7), 757-761.

11.   Michalet, X.; Pinaud, F. F.; Bentolila, L. A.; Tsay, J. M.; Doose, S.; Li, J. J.; Sundaresan, G.; Wu, A. M.; Gambhir, S. S.; Weiss, S., Quantum dots for live cells, in vivo imaging, and diagnostics. *Science* **2005,** *307* (5709), 538-544.

12.   Gao, X.; Cui, Y.; Levenson, R. M.; Chung, L. W. K.; Nie, S., In vivo cancer targeting and imaging with semiconductor quantum dots. *Nat Biotech* **2004,** *22* (8), 969-976.

13.   Pickett, N. L.; O'Brien, P., Syntheses of semiconductor nanoparticles using single-molecular precursors. *The Chemical Record* **2001,** *1* (6), 467-479.

14.   Woggon, U.; Gaponenko, S.; Langbein, W.; Uhrig, A.; Klingshirn, C., Homogeneous linewidth of confined electron-hole-pair states in II-VI quantum dots. *Physical Review B* **1993,** *47* (7), 3684-3689.

15.   Nirmal, M.; Brus, L., Luminescence Photophysics in Semiconductor Nanocrystals. *Accounts of Chemical Research* **1999,** *32* (5), 407-414.

16.   Zorman, B.; Ramakrishna, M. V.; Friesner, R. A., Quantum Confinement Effects in CdSe Quantum Dots. *The Journal of Physical Chemistry* **1995,** *99* (19), 7649-7653.

17.   Rama Krishna, M. V.; Friesner, R. A., Quantum confinement effects in semiconductor clusters. *The Journal of Chemical Physics* **1991,** *95* (11), 8309-8322.

18.   Einevoll, G. T., Confinement of excitons in quantum dots. *Physical Review B* **1992,** *45* (7), 3410-3417.

19.   Kastner, M. A., Artificial Atoms. *Print edition* **1993,** *46* (1), 24-31.

20.   Wang, Y., Luminescent CdTe and CdSe Semiconductor Nanocrystals: Preparation, Optical Properties and Applications. *Journal of Nanoscience and Nanotechnology* **2008,** *8* (3), 1068-1091.

21.   Sharma, P.; Brown, S.; Walter, G.; Santra, S.; Moudgil, B., Nanoparticles for bioimaging. *Advances in Colloid and Interface Science* **2006,** *123,Äì126* (0), 471-485.

22.   Santra, S.; Xu, J.; Wang, K.; Tand, W., Luminescent Nanoparticle Probes for Bioimaging. *Journal of Nanoscience and Nanotechnology* **2004,** *4* (6), 590-599.

23.   Hoshino, A.; Fujioka, K.; Oku, T.; Nakamura, S.; Suga, M.; Yamaguchi, Y.; Suzuki, K.; Yasuhara, M.; Yamamoto, K., Quantum Dots Targeted to the Assigned Organelle in Living Cells. *Microbiology and Immunology* **2004,** *48* (12), 985-994.

24.   Murray, C. B.; Norris, D. J.; Bawendi, M. G., Synthesis and characterization of nearly monodisperse CdE (E = sulfur, selenium, tellurium) semiconductor nanocrystallites. *Journal of the American Chemical Society* **1993,** *115* (19), 8706-8715.

25.   Liu, W.; Choi, H. S.; Zimmer, J. P.; Tanaka, E.; Frangioni, J. V.; Bawendi, M., Compact Cysteine-Coated CdSe(ZnCdS) Quantum Dots for in Vivo Applications. *Journal of the American Chemical Society* **2007,** *129* (47), 14530-14531.

26.   Pinaud, F.; Michalet, X.; Bentolila, L. A.; Tsay, J. M.; Doose, S.; Li, J. J.; Iyer, G.; Weiss, S., Advances in fluorescence imaging with quantum dot bio-probes. *Biomaterials* **2006,** *27* (9), 1679-1687.

27.   Michalet, X.; Pinaud, F.; Lacoste, T. D.; Dahan, M.; Bruchez, M. P.; Alivisatos, A. P.; Weiss, S., Properties of Fluorescent Semiconductor Nanocrystals and their Application to Biological Labeling. *Single Molecules* **2001,** *2* (4), 261-276.

28.   Gerion, D.; Pinaud, F.; Williams, S. C.; Parak, W. J.; Zanchet, D.; Weiss, S.; Alivisatos, A. P., Synthesis and Properties of Biocompatible Water-Soluble Silica-Coated CdSe/ZnS Semiconductor Quantum Dots. *The Journal of Physical Chemistry B* **2001,** *105* (37), 8861-8871.

29.   Dabbousi, B. O.; Rodriguez-Viejo, J.; Mikulec, F. V.; Heine, J. R.; Mattoussi, H.; Ober, R.; Jensen, K. F.; Bawendi, M. G., (CdSe)ZnS Core-Shell Quantum Dots:Synthesis and Characterization of a Size Series of Highly Luminescent Nanocrystallites. *The Journal of Physical Chemistry B* **1997,** *101* (46), 9463-9475.

30.   Little, R. B.; El-Sayed, M. A.; Bryant, G. W.; Burke, S., Formation of quantum-dot quantum-well heteronanostructures with large lattice mismatch: ZnS/CdS/ZnS. *The Journal of Chemical Physics* **2001,** *114* (4), 1813-1822.

31.   Liu, F.-C.; Cheng, T.-L.; Shen, C.-C.; Tseng, W.-L.; Chiang, M. Y., Synthesis of Cysteine-Capped Zn_x Cd_{1-x} Se Alloyed Quantum Dots Emitting in the Blue-Green Spectral Range. *Langmuir* **2008,** *24* (5), 2162-2167.

32.   Yang, C. S.; Wang, J. S.; Lai, Y. J.; Luo, C. W.; Chen, D. S.; Shih, Y. T.; Jian, S. R.; Chou, W. C., Formation of a precursor layer in self-assembled CdTe quantum dots grown on ZnSe by molecular beam epitaxy. *Nanotechnology* **2007,** *18* (38), 385602.

33.   Thuy, U. T. D.; Liem, N. Q.; Thanh, D. X.; Protiere, M.; Reiss, P., Optical transitions in polarized CdSe, CdSe,ZnSe, and CdSe/CdS/ZnS quantum dots dispersed in various polar solvents. *Applied Physics Letters* **2007,** *91* (24), -.

34.	Li, C. L.; Nishikawa, K.; Ando, M.; Enomoto, H.; Murase, N., Highly luminescent water-soluble ZnSe nanocrystals and their incorporation in a glass matrix. *Colloids and Surfaces A: Physicochemical and Engineering Aspects* **2007,** *294* (1-3), 33-39.

35.	Lee, H. S.; Park, H. L.; Kim, T. W., Formation mode of self-assembled CdTe quantum dots directly grown on GaAs substrates. *Journal of Crystal Growth* **2006,** *291* (2), 442-447.

36.	Ulloa, J. M.; Anantathanasarn, S.; van Veldhoven, P. J.; Koenraad, P. M.; Nötzel, R., Influence of an ultrathin GaAs interlayer on the structural properties of InAs/InGaAsP/InP (001) quantum dots investigated by cross-sectional scanning tunneling microscopy. *Applied Physics Letters* **2008,** *92* (8), -.

37.	Gong, M.; Duan, K.; Li, C.-F.; Magri, R.; Narvaez, G. A.; He, L., Electronic structure of self-assembled InAs / InP quantum dots: Comparison with self-assembled InAs/GaAs quantum dots. *Physical Review B* **2008,** *77* (4), 045326.

38.	Anantathanasarn, S.; Barbarin, Y.; Cade, N. I.; van Veldhoven, P. J.; Bente, E. A. J. M.; Oei, Y. S.; Kamada, H.; Smit, M. K.; Nötzel, R., Wavelength tunable InAs/InP(10 0) quantum dots in 1.55-μm telecom devices. *Materials Science and Engineering: B* **2008,** *147* (2-3), 124-130.

39.	Kirchner, C.; Liedl, T.; Kudera, S.; Pellegrino, T.; Muñoz Javier, A.; Gaub, H. E.; Stölzle, S.; Fertig, N.; Parak, W. J., Cytotoxicity of Colloidal CdSe and CdSe/ZnS Nanoparticles. *Nano Letters* **2004,** *5* (2), 331-338.

40.	Derfus, A. M.; Chan, W. C. W.; Bhatia, S. N., Probing the Cytotoxicity of Semiconductor Quantum Dots. *Nano Letters* **2003,** *4* (1), 11-18.

41.	Li, Y.; Rizzo, A.; Cingolani, R.; Gigli, G., White-light-emitting diodes using semiconductor nanocrystals. *Microchim Acta* **2007,** *159* (3-4), 207-215.

42.	Chaudhary, S.; Ozkan, M.; Chan, W. C. W., Trilayer hybrid polymer-quantum dot light-emitting diodes. *Applied Physics Letters* **2004,** *84* (15), 2925-2927.

43.	Canham, L., A glowing future for silicon. *New Scientist* **1993,** *138*, 23-37.

44.	Brus, L., Squeezing light from silicon. *Nature* **1991,** *353* (6342), 301-302.

45.	Mayne, A. H.; Bayliss, S. C.; Barr, P.; Tobin, M.; Buckberry, L. D., Biologically Interfaced Porous Silicon Devices. *physica status solidi (a)* **2000,** *182* (1), 505-513.

46.	Chao, Y.; Houlton, A.; Horrocks, B. R.; Hunt, M. R. C.; Poolton, N. R. J.; Yang, J.; Šiller, L., Optical luminescence from alkyl-passivated Si nanocrystals under vacuum ultraviolet excitation: Origin and temperature dependence of the blue and orange emissions. *Applied Physics Letters* **2006,** *88* (26), -.

47.	Froner, E.; Adamo, R.; Gaburro, Z.; Margesin, B.; Pavesi, L.; Rigo, A.; Scarpa, M., Luminescence of porous silicon derived nanocrystals dispersed in water: dependence on initial porous silicon oxidation. *Journal of Nanoparticle Research* **2006,** *8* (6), 1071-1074.

48.	Kovalev, D.; Heckler, H.; Polisski, G.; Koch, F., Optical Properties of Si Nanocrystals. *physica status solidi (b)* **1999,** *215* (2), 871-932.

49.	Kovalev, D.; Diener, J.; Heckler, H.; Polisski, G.; Künzner, N.; Koch, F., Optical absorption cross sections of Si nanocrystals. *Physical Review B* **2000,** *61* (7), 4485-4487.

50.	Allan, G.; Delerue, C.; Lannoo, M., Excitons in silicon nanostructures. *Journal of Luminescence* **1993,** *57* (1-6), 239-242.

51.   Allan, G.; Delerue, C.; Lannoo, M., Nature of Luminescent Surface States of Semiconductor Nanocrystallites. *Physical Review Letters* **1996,** *76* (16), 2961-2964.

52.   Delerue, C.; Allan, G.; Lannoo, M., Optical band gap of Si nanoclusters. *Journal of Luminescence* **1998,** *80* (1-4), 65-73.

53.   Wolkin, M. V.; Jorne, J.; Fauchet, P. M.; Allan, G.; Delerue, C., Electronic States and Luminescence in Porous Silicon Quantum Dots: The Role of Oxygen. *Physical Review Letters* **1999,** *82* (1), 197-200.

54.   Mitas, L.; Therrien, J.; Twesten, R.; Belomoin, G.; Nayfeh, M. H., Effect of surface reconstruction on the structural prototypes of ultrasmall ultrabright Si29 nanoparticles. *Applied Physics Letters* **2001,** *78* (13), 1918-1920.

55.   Puzder, A.; Williamson, A. J.; Reboredo, F. A.; Galli, G., Structural Stability and Optical Properties of Nanomaterials with Reconstructed Surfaces. *Physical Review Letters* **2003,** *91* (15), 157405.

56.   Belomoin, G.; Rogozhina, E.; Therrien, J.; Braun, P. V.; Abuhassan, L.; Nayfeh, M. H.; Wagner, L.; Mitas, L., Effects of surface termination on the band gap of ultrabright Si29 nanoparticles: Experiments and computational models. *Physical Review B* **2002,** *65* (19), 193406.

57.   Nayfeh, M. H.; Rigakis, N.; Yamani, Z., Photoexcitation of Si-Si surface states in nanocrystallites. *Physical Review B* **1997,** *56* (4), 2079-2084.

58.   David R. Lide, *Handbook of Chemistry and Physics.* 81 ed ed.; 2000.

59.   Pettigrew, K. A.; Liu, Q.; Power, P. P.; Kauzlarich, S. M., Solution Synthesis of Alkyl- and Alkyl/Alkoxy-Capped Silicon Nanoparticles via Oxidation of Mg2Si. *Chemistry of Materials* **2003,** *15* (21), 4005-4011.

60.   Veinot, J. G. C., Synthesis, surface functionalization, and properties of freestanding silicon nanocrystals. *Chemical Communications* **2006,** (40), 4160-4168.

61.   Hua, F.; Erogbogbo, F.; Swihart, M. T.; Ruckenstein, E., Organically Capped Silicon Nanoparticles with Blue Photoluminescence Prepared by Hydrosilylation Followed by Oxidation. *Langmuir* **2006,** *22* (9), 4363-4370.

62.   Hua, F. J.; Swihart, M. T.; Ruckenstein, E., Efficient surface grafting of luminescent silicon quantum dots by photoinitiated hydrosilylation. *Langmuir* **2005,** *21* (13), 6054-6062.

63.   Rogozhina, E. V.; Eckhoff, D. A.; Gratton, E.; Braun, P. V., Carboxyl functionalization of ultrasmall luminescent silicon nanoparticles through thermal hydrosilylation. *Journal of Materials Chemistry* **2006,** *16* (15), 1421-1430.

64.   Sato, S.; Swihart, M. T., Propionic-Acid-Terminated Silicon Nanoparticles:Synthesis and Optical Characterization. *Chemistry of Materials* **2006,** *18* (17), 4083-4088.

65.   Scheres, L.; Arafat, A.; Zuilhof, H., Self-Assembly of High-Quality Covalently Bound Organic Monolayers onto Silicon. *Langmuir* **2007,** *23* (16), 8343-8346.

66.   Sieval, A. B.; Vleeming, V.; Zuilhof, H.; Sudhölter, E. J. R., An Improved Method for the Preparation of Organic Monolayers of 1-Alkenes on Hydrogen-Terminated Silicon Surfaces. *Langmuir* **1999,** *15* (23), 8288-8291.

67.   Linford, M. R.; Fenter, P.; Eisenberger, P. M.; Chidsey, C. E. D., Alkyl Monolayers on Silicon Prepared from 1-Alkenes and Hydrogen-Terminated Silicon. *Journal of the American Chemical Society* **1995,** *117* (11), 3145-3155.

68.   Stewart, M. P.; Buriak, J. M., Exciton-Mediated Hydrosilylation on Photoluminescent Nanocrystalline Silicon. *Journal of the American Chemical Society* **2001,** *123* (32), 7821-7830.

69.   Sun, Q.-Y.; de Smet, L. C. P. M.; van Lagen, B.; Giesbers, M.; Thüne, P. C.; van Engelenburg, J.; de Wolf, F. A.; Zuilhof, H.; Sudhölter, E. J. R., Covalently Attached Monolayers on Crystalline Hydrogen-Terminated Silicon:‚Extremely Mild Attachment by Visible Light. *Journal of the American Chemical Society* **2005,** *127* (8), 2514-2523.

70.   de Smet, L. C. P. M.; Zuilhof, H.; Sudhölter, E. J. R.; Lie, L. H.; Houlton, A.; Horrocks, B. R., Mechanism of the Hydrosilylation Reaction of Alkenes at Porous Silicon: Experimental and Computational Deuterium Labeling Studies. *The Journal of Physical Chemistry B* **2005,** *109* (24), 12020-12031.

71.   Buriak, J. M., Organometallic Chemistry on Silicon and Germanium Surfaces. *Chemical Reviews* **2002,** *102* (5), 1271-1308.

72.   Warner, J. H.; Hoshino, A.; Yamamoto, K.; Tilley, R. D., Water-Soluble Photoluminescent Silicon Quantum Dots. *Angewandte Chemie International Edition* **2005,** *44* (29), 4550-4554.

73.   Nelles, J. r.; Sendor, D.; Ebbers, A.; Petrat, F.; Wiggers, H.; Schulz, C.; Simon, U., Functionalization of silicon nanoparticles via hydrosilylation with 1-alkenes. *Colloid Polym Sci* **2007,** *285* (7), 729-736.

74.   Buriak, J. M., Silicon-Carbon Bonds on Porous Silicon Surfaces. *Advanced Materials* **1999,** *11* (3), 265-267.

75.   Rosso-Vasic, M.; Spruijt, E.; Popovic, Z.; Overgaag, K.; van Lagen, B.; Grandidier, B.; Vanmaekelbergh, D.; Dominguez-Gutierrez, D.; De Cola, L.; Zuilhof, H., Amine-terminated silicon nanoparticles: synthesis, optical properties and their use in bioimaging. *Journal of Materials Chemistry* **2009,** *19* (33), 5926-5933.

76.   Ahire, J. H.; Wang, Q.; Coxon, P. R.; Malhotra, G.; Brydson, R.; Chen, R.; Chao, Y., Highly Luminescent and Nontoxic Amine-Capped Nanoparticles from Porous Silicon: Synthesis and Their Use in Biomedical Imaging. *ACS Applied Materials & Interfaces* **2012,** *4* (6), 3285-3292.

77.   Heath, J. R., A Liquid-Solution-Phase Synthesis of Crystalline Silicon. *Science* **1992,** *258* (5085), 1131-1133.

78.   Shirahata, N., Colloidal Si nanocrystals: a controlled organic-inorganic interface and its implications of color-tuning and chemical design toward sophisticated architectures. *Physical Chemistry Chemical Physics* **2011,** *13* (16), 7284-7294.

79.   Fan, J.; Chu, P. K., Group IV Nanoparticles: Synthesis, Properties, and Biological Applications. *Small* **2010,** *6* (19), 2080-2098.

80.   Zhou, Z.; Brus, L.; Friesner, R., Electronic Structure and Luminescence of 1.1- and 1.4-nm Silicon Nanocrystals:‚Äâ Oxide Shell versus Hydrogen Passivation. *Nano Letters* **2003,** *3* (2), 163-167.

81.   Canham, L. T., Silicon quantum wire array fabrication by electrochemical and chemical dissolution of wafers. *journal article* **1990,** *57* (10), 1046-1048.

82.   Henrich, J. L.; Curtis, C. L.; Credo, G. M.; Sailor, M. J.; Kavanagh, K. L., Luminescent Colloidal Silicon Suspensions from Porous Silicon. *Science* **1992,** *255* (5040), 66-68.

83.   Yamani, Z.; Ashhab, S.; Nayfeh, A.; Thompson, W. H.; Nayfeh, M., Red to green rainbow photoluminescence from unoxidized silicon nanocrystallites. *Journal of Applied Physics* **1998,** *83* (7), 3929-3931.

84.   Sweryda-Krawiec, B.; Cassagneau, T.; Fendler, J. H., Surface Modification of Silicon Nanocrystallites by Alcohols. *The Journal of Physical Chemistry B* **1999,** *103* (44), 9524-9529.

85.   Belomoin, G.; Therrien, J.; Smith, A.; Rao, S.; Twesten, R.; Chaieb, S.; Nayfeh, M. H.; Wagner, L.; Mitas, L., Observation of a magic discrete family of ultrabright Si nanoparticles. *journal article* **2002,** *80* (5), 841-843.

86.   Lie, L. H.; Duerdin, M.; Tuite, E. M.; Houlton, A.; Horrocks, B. R., Preparation and characterisation of luminescent alkylated-silicon quantum dots. *Journal of Electroanalytical Chemistry* **2002,** *538-539*, 183-190.

87.   Li, Z. F.; Ruckenstein, E., Water-Soluble Poly(acrylic acid) Grafted Luminescent Silicon Nanoparticles and Their Use as Fluorescent Biological Staining Labels. *Nano Letters* **2004,** *4* (8), 1463-1467.

88.   Chao, Y.; Krishnamurthy, S.; Montalti, M.; Šiller, L.; Lie, L. H.; Houlton, A.; Horrocks, B. R.; Kjeldgaard, L.; Dhanak, V. R.; Hunt, M. R. C., Reactions and luminescence in passivated Si nanocrystallites induced by vacuum ultraviolet and soft-x-ray photons. *Journal of Applied Physics* **2005,** *98* (4), 044316.

89.   Hessel, C. M.; Henderson, E. J.; Veinot, J. G. C., Hydrogen Silsesquioxane: A Molecular Precursor for Nanocrystalline Si–SiO2 Composites and Freestanding Hydride-Surface-Terminated Silicon Nanoparticles. *Chemistry of Materials* **2006,** *18* (26), 6139-6146.

90.   Kelly, J. A.; Veinot, J. G. C., An Investigation into Near-UV Hydrosilylation of Freestanding Silicon Nanocrystals. *ACS Nano* **2010,** *4* (8), 4645-4656.

91.   Regli, S.; Kelly, J. A.; Shukaliak, A. M.; Veinot, J. G. C., Photothermal Response of Photoluminescent Silicon Nanocrystals. *The Journal of Physical Chemistry Letters* **2012,** *3* (13), 1793-1797.

92.   Dasog, M.; Yang, Z.; Regli, S.; Atkins, T. M.; Faramus, A.; Singh, M. P.; Muthuswamy, E.; Kauzlarich, S. M.; Tilley, R. D.; Veinot, J. G. C., Chemical Insight into the Origin of Red and Blue Photoluminescence Arising from Freestanding Silicon Nanocrystals. *ACS Nano* **2013,** *7* (3), 2676-2685.

93.   Liu, S.-M.; Yang; Sato, S.; Kimura, K., Enhanced Photoluminescence from Si Nano-organosols by Functionalization with Alkenes and Their Size Evolution. *Chemistry of Materials* **2006,** *18* (3), 637-642.

94.   Liu, S.-m.; Sato, S.; Kimura, K., Synthesis of Luminescent Silicon Nanopowders Redispersible to Various Solvents. *Langmuir* **2005,** *21* (14), 6324-6329.

95.   Niu, H.-j.; Zhang, L.; Zhu, J.-y.; Zhang, M.-l.; Bai, X.-d., High-yield synthesis of silicon nanoparticles via the perpendicular pulsed laser ablation in the inert gas. *Optoelectron. Lett.* **2010,** *6* (2), 81-84.

96.   Umezu, I.; Kondo, I.; Sugimura, A., Formation of surface stabilized Si nanocrystal by pulsed laser ablation in hydrogen gas. *Appl. Phys. A* **2008,** *93* (3), 717-720.

97.   Shirahata, N.; Linford, M. R.; Furumi, S.; Pei, L.; Sakka, Y.; Gates, R. J.; Asplund, M. C., Laser-derived one-pot synthesis of silicon nanocrystals terminated with organic monolayers. *Chemical Communications* **2009,** (31), 4684-4686.

98.   Heintz, A. S.; Fink, M. J.; Mitchell, B. S., Mechanochemical Synthesis of Blue Luminescent Alkyl/Alkenyl-Passivated Silicon Nanoparticles. *Advanced Materials* **2007,** *19* (22), 3984-3988.

99. Heintz, A. S.; Fink, M. J.; Mitchell, B. S., Silicon nanoparticles with chemically tailored surfaces. *Applied Organometallic Chemistry* **2010,** *24* (3), 236-240.

100. Furukawa, S.; Miyasato, T., Quantum size effects on the optical band gap of microcrystalline Si:H. *Physical Review B* **1988,** *38* (8), 5726-5729.

101. Li, X.; He, Y.; Talukdar, S. S.; Swihart, M. T., Process for Preparing Macroscopic Quantities of Brightly Photoluminescent Silicon Nanoparticles with Emission Spanning the Visible Spectrum. *Langmuir* **2003,** *19* (20), 8490-8496.

102. Li, X.; He, Y.; Swihart, M. T., Surface Functionalization of Silicon Nanoparticles Produced by Laser-Driven Pyrolysis of Silane followed by HF-HNO$_3$ Etching. *Langmuir* **2004,** *20* (11), 4720-4727.

103. Shah, P. S.; Hanrath, T.; Johnston, K. P.; Korgel, B. A., Nanocrystal and Nanowire Synthesis and Dispersibility in Supercritical Fluids. *The Journal of Physical Chemistry B* **2004,** *108* (28), 9574-9587.

104. English, D. S.; Pell, L. E.; Yu, Z.; Barbara, P. F.; Korgel, B. A., Size Tunable Visible Luminescence from Individual Organic Monolayer Stabilized Silicon Nanocrystal Quantum Dots. *Nano Letters* **2002,** *2* (7), 681-685.

105. Holmes, J. D.; Ziegler, K. J.; Doty, R. C.; Pell, L. E.; Johnston, K. P.; Korgel, B. A., Highly Luminescent Silicon Nanocrystals with Discrete Optical Transitions. *Journal of the American Chemical Society* **2001,** *123* (16), 3743-3748.

106. Lee, D. C.; Hanrath, T.; Korgel, B. A., The Role of Precursor-Decomposition Kinetics in Silicon-Nanowire Synthesis in Organic Solvents. *Angewandte Chemie International Edition* **2005,** *44* (23), 3573-3577.

107. Holmes, J. D.; Johnston, K. P.; Doty, R. C.; Korgel, B. A., Control of Thickness and Orientation of Solution-Grown Silicon Nanowires. *Science* **2000,** *287* (5457), 1471-1473.

108. Bley, R. A.; Kauzlarich, S. M., A Low-Temperature Solution Phase Route for the Synthesis of Silicon Nanoclusters. *Journal of the American Chemical Society* **1996,** *118* (49), 12461-12462.

109. Liu, Q.; Kauzlarich, S. M., A new synthetic route for the synthesis of hydrogen terminated silicon nanoparticles. *Materials Science and Engineering: B* **2002,** *96* (2), 72-75.

110. Baldwin, R. K.; Pettigrew, K. A.; Ratai, E.; Augustine, M. P.; Kauzlarich, S. M., Solution reduction synthesis of surface stabilized silicon nanoparticles. *Chemical Communications* **2002,** (17), 1822-1823.

111. Tanke, R. S.; Kauzlarich, S. M.; Patten, T. E.; Pettigrew, K. A.; Murphy, D. L.; Thompson, M. E.; Lee, H. W. H., Synthesis of Germanium Nanoclusters with Irreversibly Attached Functional Groups: Acetals, Alcohols, Esters, and Polymers. *Chemistry of Materials* **2003,** *15* (8), 1682-1689.

112. Zhang, X.; Brynda, M.; Britt, R. D.; Carroll, E. C.; Larsen, D. S.; Louie, A. Y.; Kauzlarich, S. M., Synthesis and Characterization of Manganese-Doped Silicon Nanoparticles: Bifunctional Paramagnetic-Optical Nanomaterial. *Journal of the American Chemical Society* **2007,** *129* (35), 10668-10669.

113. Baldwin, R. K.; Zou, J.; Pettigrew, K. A.; Yeagle, G. J.; Britt, R. D.; Kauzlarich, S. M., The preparation of a phosphorus doped silicon film from phosphorus containing silicon nanoparticles. *Chemical Communications* **2006,** (6), 658-660.

114.	Yang, C.-S.; Kauzlarich, S. M.; Wang, Y. C., Synthesis and Characterization of Germanium/Si-Alkyl and Germanium/Silica Core-Shell Quantum Dots. *Chemistry of Materials* **1999,** *11* (12), 3666-3670.

115.	Mayeri, D.; Phillips, B. L.; Augustine, M. P.; Kauzlarich, S. M., NMR Study of the Synthesis of Alkyl-Terminated Silicon Nanoparticles from the Reaction of SiCl4 with the Zintl Salt, NaSi. *Chemistry of Materials* **2001,** *13* (3), 765-770.

116.	Zou, J.; Baldwin, R. K.; Pettigrew, K. A.; Kauzlarich, S. M., Solution Synthesis of Ultrastable Luminescent Siloxane-Coated Silicon Nanoparticles. *Nano Letters* **2004,** *4* (7), 1181-1186.

117.	Baldwin, R. K.; Pettigrew, K. A.; Garno, J. C.; Power, P. P.; Liu, G.-y.; Kauzlarich, S. M., Room Temperature Solution Synthesis of Alkyl-Capped Tetrahedral Shaped Silicon Nanocrystals. *Journal of the American Chemical Society* **2002,** *124* (7), 1150-1151.

118.	Wilcoxon, J. P.; Samara, G. A., Tailorable, visible light emission from silicon nanocrystals. *journal article* **1999,** *74* (21), 3164-3166.

119.	Tilley, R. D.; Warner, J. H.; Yamamoto, K.; Matsui, I.; Fujimori, H., Micro-emulsion synthesis of monodisperse surface stabilized silicon nanocrystals. *Chemical Communications* **2005,** (14), 1833-1835.

120.	Mangolini, L.; Thimsen, E.; Kortshagen, U., High-Yield Plasma Synthesis of Luminescent Silicon Nanocrystals. *Nano Letters* **2005,** *5* (4), 655-659.

121.	Giesen, B.; Wiggers, H.; Kowalik, A.; Roth*, P., Formation of Si-nanoparticles in a microwave reactor: Comparison between experiments and modelling. *Journal of Nanoparticle Research* **2005,** *7* (1), 29-41.

122.	Zhu, X.; Yukawa, T.; Kishi, T.; Hirai, M.; Suematsu, H.; Jiang, W.; Yatsui, K., Synthesis of Light-emitting Silicon Nanoparticles by Intense Pulsed ion-beam Esvaporation. *Journal of Nanoparticle Research* **2005,** *7* (6), 669-673.

123.	Chao, Y.; Siller, L.; Krishnamurthy, S.; Coxon, P. R.; Bangert, U.; Gass, M.; Kjeldaard, L.; Patole, S. N.; Lie, L. H.; O' Farrell, N.; Alsop, T. A.; Houlton, A.; Horrocks, B. R., Evaporation and deposition of alkyl-capped silicon nanocrystals in ultrahigh vacuum. *Nat Nano* **2007,** *2* (8), 486-489.

124.	Schuppler, S.; Friedman, S. L.; Marcus, M. A.; Adler, D. L.; Xie, Y. H.; Ross, F. M.; Chabal, Y. J.; Harris, T. D.; Brus, L. E.; Brown, W. L.; Chaban, E. E.; Szajowski, P. F.; Christman, S. B.; Citrin, P. H., Size, shape, and composition of luminescent species in oxidized Si nanocrystals and H-passivated porous Si. *Physical Review B* **1995,** *52* (7), 4910.

125.	Rogozhina, E.; Belomoin, G.; Smith, A.; Abuhassan, L.; Barry, N.; Akcakir, O.; Braun, P. V.; Nayfeh, M. H., Si-N linkage in ultrabright, ultrasmall Si nanoparticles. *journal article* **2001,** *78* (23), 3711-3713.

126.	Rosso-Vasic, M.; Spruijt, E.; van Lagen, B.; De Cola, L.; Zuilhof, H., Alkyl-Functionalized Oxide-Free Silicon Nanoparticles: Synthesis and Optical Properties. *Small* **2008,** *4* (10), 1835-1841.

127.	Ruizendaal, L.; Bhattacharjee, S.; Pournazari, K.; Rosso-Vasic, M.; de Haan, L. H. J.; Alink, G. M.; Marcelis, A. T. M.; Zuilhof, H., Synthesis and cytotoxicity of silicon nanoparticles with covalently attached organic monolayers. *Nanotoxicology* **2009,** *3* (4), 339-347.

128.	Bhattacharjee, S.; de Haan, L.; Evers, N.; Jiang, X.; Marcelis, A.; Zuilhof, H.; Rietjens, I.; Alink, G., Role of surface charge and oxidative stress in cytotoxicity of organic monolayer-

coated silicon nanoparticles towards macrophage NR8383 cells. *Particle and Fibre Toxicology* **2010,** *7* (1), 25.

129.   Lewinski, N.; Colvin, V.; Drezek, R., Cytotoxicity of Nanoparticles. *Small* **2008,** *4* (1), 26-49.

130.   Chan, W. C. W.; Nie, S., Quantum Dot Bioconjugates for Ultrasensitive Nonisotopic Detection. *Science* **1998,** *281* (5385), 2016-2018.

131.   Selvan, S. T.; Tan, T. T.; Ying, J. Y., Robust, Non-Cytotoxic, Silica-Coated CdSe Quantum Dots with Efficient Photoluminescence. *Advanced Materials* **2005,** *17* (13), 1620-1625.

132.   Salata, O., Applications of nanoparticles in biology and medicine. *Journal of Nanobiotechnology* **2004,** *2* (1), 3.

133.   Ghaderi, S.; Ramesh, B.; Seifalian, A. M., Fluorescence nanoparticles "quantum dots" as drug delivery system and their toxicity: a review. *Journal of Drug Targeting* **2011,** *19* (7), 475-486.

134.   Sayes, C. M.; Reed, K. L.; Warheit, D. B., Assessing Toxicity of Fine and Nanoparticles: Comparing In Vitro Measurements to In Vivo Pulmonary Toxicity Profiles. *Toxicological Sciences* **2007,** *97* (1), 163-180.

135.   Altman, S. A.; Randers, L.; Rao, G., Comparison of Trypan Blue Dye Exclusion and Fluorometric Assays for Mammalian Cell Viability Determinations. *Biotechnology Progress* **1993,** *9* (6), 671-674.

136.   Takahashi, H.; Niidome, Y.; Niidome, T.; Kaneko, K.; Kawasaki, H.; Yamada, S., Modification of Gold Nanorods Using Phosphatidylcholine to Reduce Cytotoxicity. *Langmuir* **2005,** *22* (1), 2-5.

137.   Magrez, A.; Kasas, S.; Salicio, V.; Pasquier, N.; Seo, J. W.; Celio, M.; Catsicas, S.; Schwaller, B.; Forró, L., Cellular Toxicity of Carbon-Based Nanomaterials. *Nano Letters* **2006,** *6* (6), 1121-1125.

138.   Mosmann, T., Rapid colorimetric assay for cellular growth and survival: Application to proliferation and cytotoxicity assays. *J. Immunol. Methods* **1983,** *65* (1-2), 55-63.

139.   Fairbairn, D. W.; Olive, P. L.; O'Neill, K. L., The comet assay: a comprehensive review. *Mutation Research/Reviews in Genetic Toxicology* **1995,** *339* (1), 37-59.

140.   Lin, W.; Huang, Y.-w.; Zhou, X.-D.; Ma, Y., In vitro toxicity of silica nanoparticles in human lung cancer cells. *Toxicology and Applied Pharmacology* **2006,** *217* (3), 252-259.

141.   Kondoh, M.; Araragi, S.; Sato, K.; Higashimoto, M.; Takiguchi, M.; Sato, M., Cadmium induces apoptosis partly via caspase-9 activation in HL-60 cells. *Toxicology* **2002,** *170* (1-2), 111-117.

142.   Rikans, L. E.; Yamano, T., Mechanisms of cadmium-mediated acute hepatotoxicity. *Journal of Biochemical and Molecular Toxicology* **2000,** *14* (2), 110-117.

143.   Shiohara, A.; Hoshino, A.; Hanaki, K.-i.; Suzuki, K.; Yamamoto, K., On the Cyto-Toxicity Caused by Quantum Dots. *Microbiology and Immunology* **2004,** *48* (9), 669-675.

144.   Chin, V.; Collins, B. E.; Sailor, M. J.; Bhatia, S. N., Compatibility of Primary Hepatocytes with Oxidized Nanoporous Silicon. *Advanced Materials* **2001,** *13* (24), 1877-1880.

145.   Alsharif, N. H.; Berger, C. E. M.; Varanasi, S. S.; Chao, Y.; Horrocks, B. R.; Datta, H. K., Alkyl-Capped Silicon Nanocrystals Lack Cytotoxicity and have Enhanced Intracellular

Accumulation in Malignant Cells via Cholesterol-Dependent Endocytosis. *Small* **2009,** *5* (2), 221-228.

146.   Park, J.-H.; Gu, L.; von Maltzahn, G.; Ruoslahti, E.; Bhatia, S. N.; Sailor, M. J., Biodegradable luminescent porous silicon nanoparticles for in vivo applications. *Nat Mater* **2009,** *8* (4), 331-336.

147.   Perez, L.; Flores, M.; Avalos, J.; San Miguel, L.; Resto, O.; Fonseca, L., *In Comparative study of the growth curves of B. Subtilis, K. Pneumoniae, C. Xerosis and E. Coli bacteria in medium containing nanometric silicon particles*. Materials Research Society Symposium Proceedings, Materials Research Society: 2003.

148.   Pankhurst, Q. A.; Thanh, N. T. K.; Jones, S. K.; Dobson, J., Progress in applications of magnetic nanoparticles in biomedicine. *Journal of Physics D: Applied Physics* **2009,** *42* (22), 224001.

149.   Huang, X.; Neretina, S.; El-Sayed, M. A., Gold Nanorods: From Synthesis and Properties to Biological and Biomedical Applications. *Advanced Materials* **2009,** *21* (48), 4880-4910.

150.   Peer, D.; Karp, J. M.; Hong, S.; Farokhzad, O. C.; Margalit, R.; Langer, R., Nanocarriers as an emerging platform for cancer therapy. *Nat Nano* **2007,** *2* (12), 751-760.

151.   Ferrari, M., Cancer nanotechnology: opportunities and challenges. *Nat Rev Cancer* **2005,** *5* (3), 161-171.

152.   Pankhurst, Q. A.; Connolly, J.; Jones, S. K.; Dobson, J., Applications of magnetic nanoparticles in biomedicine. *Journal of Physics D: Applied Physics* **2003,** *36* (13), R167.

153.   Kikkeri, R.; Lepenies, B.; Adibekian, A.; Laurino, P.; Seeberger, P. H., In Vitro Imaging and in Vivo Liver Targeting with Carbohydrate Capped Quantum Dots. *Journal of the American Chemical Society* **2009,** *131* (6), 2110-2012.

154.   Lis, H.; Sharon, N., Lectins: Carbohydrate-Specific Proteins That Mediate Cellular Recognition. *Chemical Reviews* **1998,** *98* (2), 637-674.

155.   Babu, P.; Sinha, S.; Surolia, A., Sugar–Quantum Dot Conjugates for a Selective and Sensitive Detection of Lectins. *Bioconjugate Chemistry* **2006,** *18* (1), 146-151.

156.   Dam, T. K.; Brewer, C. F., Thermodynamic Studies of Lectin–Carbohydrate Interactions by Isothermal Titration Calorimetry. *Chemical Reviews* **2002,** *102* (2), 387-430.

157.   Ratner, D. M.; Adams, E. W.; Disney, M. D.; Seeberger, P. H., Tools for Glycomics: Mapping Interactions of Carbohydrates in Biological Systems. *ChemBioChem* **2004,** *5* (10), 1375-1383.

158.   Oh, E.; Lee, D.; Kim, Y.-P.; Cha, S. Y.; Oh, D.-B.; Kang, H. A.; Kim, J.; Kim, H.-S., Nanoparticle-Based Energy Transfer for Rapid and Simple Detection of Protein Glycosylation. *Angewandte Chemie International Edition* **2006,** *45* (47), 7959-7963.

159.   Lindhorst, T. K., *Essentials of carbohydrate chemistry and biochemistry*. Wiley-VCH: Weinheim, 2003.

160.   Lee, Y. C.; Lee, R. T., Carbohydrate-Protein Interactions: Basis of Glycobiology. *Accounts of Chemical Research* **1995,** *28* (8), 321-327.

161.   Mammen, M.; Choi, S.-K.; Whitesides, G. M., Polyvalent Interactions in Biological Systems: Implications for Design and Use of Multivalent Ligands and Inhibitors. *Angewandte Chemie International Edition* **1998,** *37* (20), 2754-2794.

162.   de la Fuente, J. M.; Barrientos, A. G.; Rojas, T. C.; Rojo, J.; Cañada, J.; Fernández, A.; Penadés, S., Gold Glyconanoparticles as Water-Soluble Polyvalent Models To Study Carbohydrate Interactions. *Angewandte Chemie International Edition* **2001,** *40* (12), 2257-2261.

163.   Tromas, C.; Rojo, J.; de la Fuente, J. M.; Barrientos, A. G.; García, R.; Penadés, S., Adhesion Forces between LewisX Determinant Antigens as Measured by Atomic Force Microscopy. *Angewandte Chemie International Edition* **2001,** *40* (16), 3052-3055.

164.   Hernáiz, M. J.; de la Fuente, J. M.; Barrientos, Á. G.; Penadés, S., A Model System Mimicking Glycosphingolipid Clusters to Quantify Carbohydrate Self-Interactions by Surface Plasmon Resonance. *Angewandte Chemie International Edition* **2002,** *41* (9), 1554-1557.

165.   de la Fuente, J. M.; Eaton, P.; Barrientos, A. G.; Menéndez, M.; Penadés, S., Thermodynamic Evidence for Ca2+-Mediated Self-Aggregation of Lewis X Gold Glyconanoparticles. A Model for Cell Adhesion via Carbohydrate–Carbohydrate Interaction. *Journal of the American Chemical Society* **2005,** *127* (17), 6192-6197.

166.   El-Boubbou, K.; Gruden, C.; Huang, X., Magnetic Glyco-nanoparticles: A Unique Tool for Rapid Pathogen Detection, Decontamination, and Strain Differentiation. *Journal of the American Chemical Society* **2007,** *129* (44), 13392-13393.

167.   Horák, D.; Babič, M.; Jendelová, P.; Herynek, V.; Trchová, M.; Pientka, Z.; Pollert, E.; Hájek, M.; Syková, E., d-Mannose-Modified Iron Oxide Nanoparticles for Stem Cell Labeling. *Bioconjugate Chemistry* **2007,** *18* (3), 635-644.

168.   Yoo, M. K.; Kim, I. Y.; Kim, E. M.; Jeong, H.-J.; Lee, C.-M.; Jeong, Y. Y.; Akaike, T.; Cho, C. S., Superparamagnetic Iron Oxide Nanoparticles Coated with Galactose-Carrying Polymer for Hepatocyte Targeting. *Journal of Biomedicine and Biotechnology* **2007,** *2007*.

169.   Lin, C.-C.; Yeh, Y.-C.; Yang, C.-Y.; Chen, G.-F.; Chen, Y.-C.; Wu, Y.-C.; Chen, C.-C., Quantitative analysis of multivalent interactions of carbohydrate-encapsulated gold nanoparticles with concanavalin A. *Chemical Communications* **2003,** (23), 2920-2921.

170.   Chen, Y.-J.; Chen, S.-H.; Chien, Y.-Y.; Chang, Y.-W.; Liao, H.-K.; Chang, C.-Y.; Jan, M.-D.; Wang, K.-T.; Lin, C.-C., Carbohydrate-Encapsulated Gold Nanoparticles for Rapid Target-Protein Identification and Binding-Epitope Mapping. *ChemBioChem* **2005,** *6* (7), 1169-1173.

171.   de la Fuente, J. M.; Alcántara, D.; Eaton, P.; Crespo, P.; Rojas, T. C.; Fernández, A.; Hernando, A.; Penadés, S., Gold and Gold–Iron Oxide Magnetic Glyconanoparticles: Synthesis, Characterization and Magnetic Properties. *The Journal of Physical Chemistry B* **2006,** *110* (26), 13021-13028.

172.   De la Fuente, J. M.; Alcantara, D.; Penades, S., Cell Response to Magnetic Glyconanoparticles: Does the Carbohydrate Matter? *NanoBioscience, IEEE Transactions on* **2007,** *6* (4), 275-281.

173.   Martínez-Ávila, O.; Hijazi, K.; Marradi, M.; Clavel, C.; Campion, C.; Kelly, C.; Penadés, S., Gold Manno-Glyconanoparticles: Multivalent Systems to Block HIV-1 gp120 Binding to the Lectin DC-SIGN. *Chemistry – A European Journal* **2009,** *15* (38), 9874-9888.

174.   Schofield, C. L.; Field, R. A.; Russell, D. A., Glyconanoparticles for the Colorimetric Detection of Cholera Toxin. *Analytical Chemistry* **2007,** *79* (4), 1356-1361.

175.   Marradi, M.; Alcantara, D.; de la Fuente, J. M.; Garcia-Martin, M. L.; Cerdan, S.; Penades, S., Paramagnetic Gd-based gold glyconanoparticles as probes for MRI: tuning relaxivities with sugars. *Chemical Communications* **2009,** (26), 3922-3924.

176.   Rojo, J.; Díaz, V.; de la Fuente, J. M.; Segura, I.; Barrientos, A. G.; Riese, H. H.; Bernad, A.; Penadés, S., Gold Glyconanoparticles as New Tools in Antiadhesive Therapy. *ChemBioChem* **2004,** *5* (3), 291-297.

177.   Kemp, M. M.; Kumar, A.; Mousa, S.; Dyskin, E.; Yalcin, M.; Ajayan, P.; Linhardt, R. J.; Mousa, S. A., Gold and silver nanoparticles conjugated with heparin derivative possess anti-angiogenesis properties. *Nanotechnology* **2009,** *20* (45), 455104.

178.   Wang, Z.; Xu, Y.; Yang, B.; Tiruchinapally, G.; Sun, B.; Liu, R.; Dulaney, S.; Liu, J.; Huang, X., Preactivation-Based, One-Pot Combinatorial Synthesis of Heparin-like Hexasaccharides for the Analysis of Heparin–Protein Interactions. *Chemistry – A European Journal* **2010,** *16* (28), 8365-8375.

179.   Chen, Y.; Ji, T.; Rosenzweig, Z., Synthesis of Glyconanospheres Containing Luminescent CdSe–ZnS Quantum Dots. *Nano Letters* **2003,** *3* (5), 581-584.

180.   Robinson, A.; Fang, J.-M.; Chou, P.-T.; Liao, K.-W.; Chu, R.-M.; Lee, S.-J., Probing Lectin and Sperm with Carbohydrate-Modified Quantum Dots. *ChemBioChem* **2005,** *6* (10), 1899-1905.

181.   Bhang, S. H.; Won, N.; Lee, T.-J.; Jin, H.; Nam, J.; Park, J.; Chung, H.; Park, H.-S.; Sung, Y.-E.; Hahn, S. K.; Kim, B.-S.; Kim, S., Hyaluronic Acid-Quantum Dot Conjugates for In Vivo Lymphatic Vessel Imaging. *ACS NANO* **2009,** *3* (6), 1389-1398.

182.   Kim, K. S.; Hur, W.; Park, S.-J.; Hong, S. W.; Choi, J. E.; Goh, E. J.; Yoon, S. K.; Hahn, S. K., Bioimaging for Targeted Delivery of Hyaluronic Acid Derivatives to the Livers in Cirrhotic Mice Using Quantum Dots. *ACS NANO* **2010,** *4* (6), 3005-3014.

183.   Erogbogbo, F.; Yong, K.-T.; Roy, I.; Xu, G.; Prasad, P. N.; Swihart, M. T., Biocompatible Luminescent Silicon Quantum Dots for Imaging of Cancer Cells. *ACS Nano* **2008,** *2* (5), 873-878.

184.   Erogbogbo, F.; Tien, C.-A.; Chang, C.-W.; Yong, K.-T.; Law, W.-C.; Ding, H.; Roy, I.; Swihart, M. T.; Prasad, P. N., Bioconjugation of Luminescent Silicon Quantum Dots for Selective Uptake by Cancer Cells. *Bioconjugate Chemistry* **2011,** *22* (6), 1081-1088.

185.   Sailor, M. J.; Park, J.-H., Hybrid Nanoparticles for Detection and Treatment of Cancer. *Advanced Materials* **2012,** *24* (28), 3779-3802.

2 Silicon Nanoparticle Synthesis and Characterization Techniques

The following chapter describes the synthesis, methods to functionalize the nanoparticles, experimental apparatus, and chemicals used in the work presented in this thesis. An overview of the preparation methods used in the synthesis of amine terminated silicon nanoparticles, different types of carbohydrates capped silicon nanoparticles, and the biological methods and materials used to implicate the NPs inside the cells. All chemical analyses of the compounds, optical measurements, size determinations for the entire samples are also described in detail, followed by the techniques used in the biomedical applications.

All chemicals used were purchased from Sigma-Aldrich or Fisher Scientific and employed without further purification unless specified differently.

2.1 Synthesis of Hydrogen terminated Porous Silicon NPs

2.1.1 Porous Silicon

As mentioned in the introductory chapter 1, there are two major strategies to synthesize silicon nanoparticles: bulk reduction (top down) and self-assembly (bottom up). The silicon nanoparticles studied and synthesized throughout this work are derived from the nanostructures found within the surface layers of porous silicon by bulk reduction (top down) method. The formation of porous silicon can be carried out in several ways. In this work porous silicon was obtained by electrochemical etching (anodisation) of crystalline silicon. Many nanoparticle production methods involve elaborate and expensive techniques with relatively low yields and low purity. Fabrication of porous silicon is, by contrast, a cheap and simple procedure based upon the electrochemical dissolution of crystalline silicon.

2.1.2 Brief History of Porous Silicon

Porous Silicon (p-Si) was accidentally discovered in 1956 by the husband and wife team Arthur and Ingeborg Uhlir working at Bell Laboratories in the United States.[1] They were trying to develop an electrochemical method to machine silicon wafers for use in

microelectronic circuits. They observed that under appropriate electrochemical conditions, the silicon wafer did not dissolve uniformly as expected, but instead the surfaces appeared to be covered in dark red-brown stains. These deposits were dismissed as a suboxide of silicon and no further research was carried out on it for over a decade. However, in the 1970s and 1980s a significant level of interest in this obscure material grew because its large internal surface area offered a model of the crystalline silicon surface in IR spectroscopic studies[2, 3], as a precursor to generate thick oxide layers on silicon, and as a dielectric layer in capacitance-based chemical sensors[4]. In 1990, Leigh Canham[5] discovered its visible luminescence properties. Researchers started studying its nonlinear optical, electric and mechanical properties. These academic and technological efforts have enabled the fabrication of uniform porous layers with size as small as one nanometer, permitting an enormous inner surface area, which is useful for biosensing applications.

2.1.3   Synthesis of Porous Silicon

Porous silicon samples were made by anodisation (electrochemical 'etching') of bulk silicon in a hydrofluoric acid (HF) based electrolyte (1:1 98 wt.% ethanol: 48 wt.% HF volumetric ratio). HF is typically used since it is known to dissolve bulk silicon in an efficient manner.[6] The addition of ethanol is useful for several reasons; owing to the hydrophobic nature of the clean silicon surface, access to the fine pores by the pure electrolyte is severely restricted. Ethanol increases the surface wettability, aiding pore penetration, which improves the lateral homogeneity and leads to a more uniform porous layer. In addition to this, the presence of ethanol helps with the removal of hydrogen gas (see equation 2.1), which form during the dissolution reaction from the surface of silicon and allows a more uniform current density to be maintained. The dissolution process is based upon the presence of holes (h^+) at the Si:HF solution interface

$$Si + 4HF_2^- + 2H^+ \rightarrow SiF_6^{2-} + 2HF + 2H_2 \qquad \text{Equation: 2.1}$$
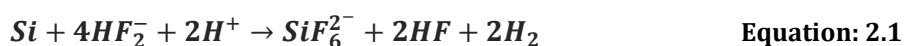
In the dissolution process, a vacancy is formed in the silicon valence band. A vacancy is also called a hole. In other words, an electron is removed from near one of the Si–H bonds. This activates the previously passivated Si–H bond, making it susceptible to attack by the fluoride solution. After initiation, the etching of one silicon atom proceeds very rapidly according to the mechanism outlined in Scheme 2.1.

	1. In the absence of electron holes, a hydrogen saturated silicon surface is virtually free from attack by flouride ions in the HF based electrolyte. The induced polarisation between the hydrogen and silicon atoms is low because the electron affinity of hydrogen is about that of silicon.
	2. When a hole reaches the surface, nucleophilic attack on an Si-H bond by a fluoride ion can occur and a Si-F bond is formed
	3. The Si-F bond causes a polarisation effect allowing a second fluorine ion to attack and replace the remaining hydrogen bond. Two hydrogen atoms can then combine, injecting an electron into the substrate.
	4. The polarisation induced by the Si-F bonds reduces the electron density of the remaining Si-Si backbonds making them susceptible to attack by the HF in a manner such that the remaining silicon surface atoms are bonded to the hydrogen atoms.
	5. The silicon tetrafluoride molecule reacts with the HF to form the highly stable SiF_6^{2-} fluoroanion. The surface returns to it's 'neutral' state until another hole is made available.

Scheme 2.1: Reaction mechanism of H-terminated porous SiNPs formed by electrochemical etching reproduced from Lehmann & Gösele (1991).[7]

The anodisation was carried out in a PTFE (Teflon) cell where the silicon wafer acts as anode and HF-resistant electrode (Tungsten wire) serves as the cathode. The PTFE (Teflon) cell is used in order to withstand the aggressive nature of hydrofluoric acid used during the etching process. The cell chamber consists of an upper and lower plate, and the silicon chip is positioned between two plates. The upper plate contains an open cavity in the center to hold the etchant or electrolyte solution and is fitted with a VitonTM O-ring (Polymax LT) to prevent the etching solution from leaking. The p-Si (100) wafer (10 cm

resistivity, Compart Technology, Peterborough, UK) was first cut into 1.25cm x1.25cm square chips to fit the anodisation cell (circular in cross-section). The wafers were cut into the chips by using a diamond-tipped scribe. After cutting, the chips were rinsed in absolute ethanol (EtOH, 98 wt.% Sigma-Aldrich) and distilled water, in order to eliminate impurities from the surface, and dried under nitrogen flow.
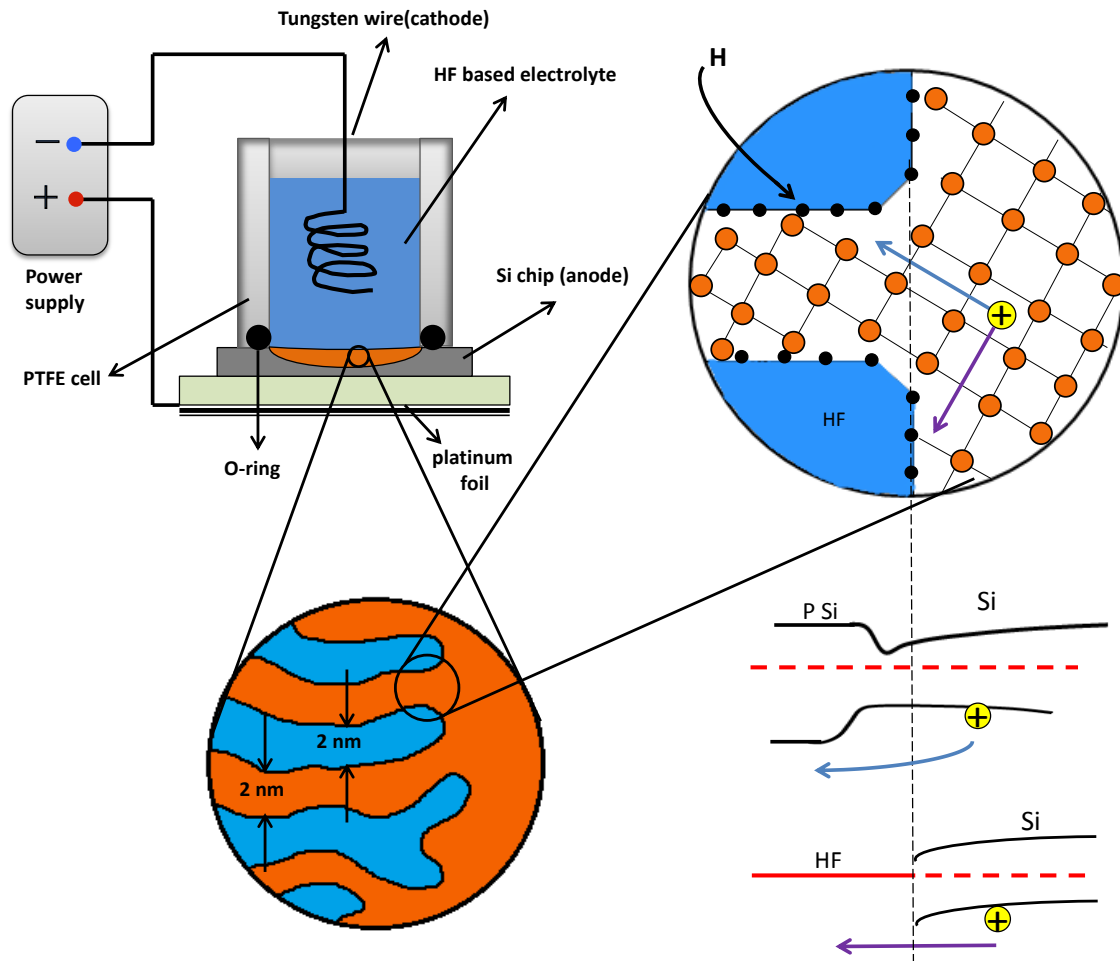
Figure 2.1: Schematic diagram of formation of porous silicon - Top left shows a two-electrode electrochemical cell used to make porous silicon. Lower left, enlarged cross-section of the Psi-Si interface. Top right, silicon wall isolated by two pores with possible routes for a hole to cross the silicon highlighted (blue and purple arrows). Lower right, energy barriers for the hole penetrating into a wall (blue arrow) and a pore base (purple arrow). Reproduced from Lehmann et al. (1993).

Prior to the etching process, the chip was dipped rapidly (approximately 30 sec) in 48 wt.% HF (VWR International Ltd.) then rinsed gently with distilled water and dried under nitrogen flow. After drying the chip was placed into the cell in such a way that only the polished side of the chip is exposed to the electrolyte solution. The upper plate of the cell

with an O-ring is fastened to the lower plate and the cell is filled with the electrolyte solution (1:1 98 wt.% ethanol: 48 wt.% HF). The counter electrode is a piece of tungsten wire (0.5 mm in diameter, Goodfellow UK) coiled into a loop to improve the uniformity of the current distribution, which is suspended from an insulated arm above the cell and submerged in the electrolyte solution. A constant current source (Keithley Source Meter 2061) is then connected across the cathode and anode in order to transmit current through the electrolyte solution and the surface of the Si chip. The direction of current flow is important; if the connections are switched, no pore formation takes place.

In this work porous silicon layers were formed by 5 min etching at a current of 400mA with a maximum driving potential of 40 V. After the process was complete the solution is decanted and the H-terminated porous silicon chips were dried under vacuum.

2.2   Synthesis of Amine-terminated SiNPs

Amine terminated silicon nanoparticles were synthesized using a hydrosilylation reaction method, i.e. the addition across a carbon-carbon multiple bond under catalysis by transition metal complexes. Hydrogen terminated porous SiNPs produced from the electrochemical etching were reacted with allylamine using a platinum catalyst (Pt).

2.2.1   Hydrosilylation

The first reports of the covalent attachment of alkenes and alkynes onto hydrogen-terminated silicon by hydrosilylation of the unsaturated molecules in the early 1990s marked an important development. The early work by Matthew Linford at Stanford University successfully demonstrated Si-C bonded organic monolayers prepared by hydrosilylation of the unsaturated molecules which remained robust, even at elevated temperatures or under highly acidic conditions[8] [9] and the field has continued to attract attention ever since.

Several methods for the formation of Si-C bonded monolayers at hydrogen-terminated silicon surfaces have been proposed.[10-13] The hydrosilylation reaction of 1-alkenes with the hydrogen-terminated silicon surfaces is somewhat flexible, and may be induced by photochemical[14-16] or thermal[17-19] means, UV irradiation[20] or by employing catalysts (typically $EtAlCl_2$ or H_2PtCl_6) on porous silicon and single-crystal surfaces.[21-23]

In order to properly understand the physical and chemical properties of these monolayers, it is crucial to understand the mechanism, which governs their formation. The

conventional hydrosilylation of alkenes catalyzed by chloroplatinic acid (H_2PtCl_6, Speier's catalysts)[24] in the presence of iso-propanol is generally assumed to proceed by the Chalk-Harrod mechanism (Scheme 2.2).[25]

The catalytic cycle is considered to involve two steps as depicted in Scheme 2. The oxidative addition of a hydrosilane gives a hydridosilyl complex (I), which is coordinated with the substrate allylamine. The complex I undergoes migratory insertion of the allylamine into the Pt-H bond (hydrometallation) to give the propylamine-silyl species (II). Reductive elimination of the propylamine and silyl ligands from (II) forms the hydrosilylation product. An alternative mechanism has been proposed which is usually termed as "Modified-Chalk-Harrod" mechanism.[26, 27] With the Modified-Chalk-Harrod mechanism, the allylamine inserts into the Pt-Si (silylmetallation) bond instead of the Pt-H bond as in the Chalk-Harrod mechanism. Following allylamine insertion, C-H reductive elimination yields a hydrosilylation product.
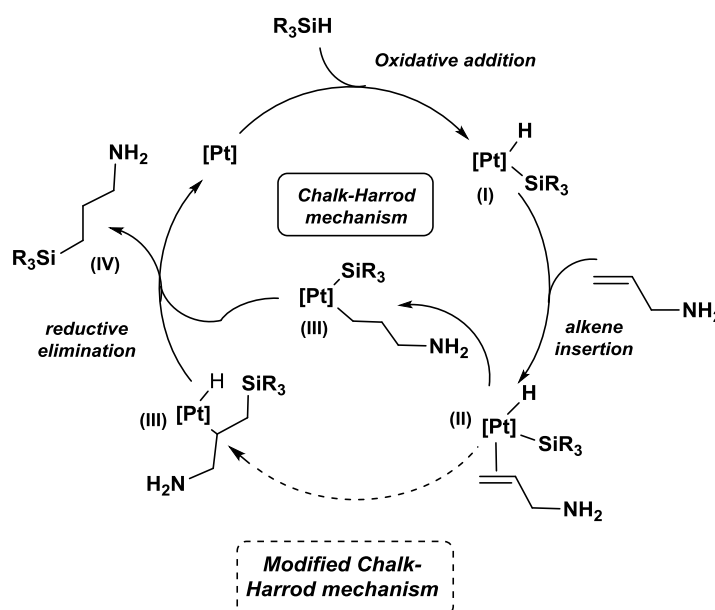
Scheme 2.2: Hydrosilylation reaction by Chalk-Harrod and Modified-Chalk-Harrod mechanisms.

2.2.2 Procedure to Synthesize Amine-Capped SiNPs

The porous silicon nanoparticle surfaces formed by the electrochemical etching method are passivated by an organic monolayer coating. The amine-terminated SiNPs were synthesized from H-terminated porous silicon in a two-step procedure, which involves the breakup of the nanostructured porous silicon layer followed by the functionalization of the

silicon particles surface by covalently bonded propylamine. In order to minimize the opportunity for sample contamination by adventitious hydrocarbons, all reactions took place under grease free Young's Schlenk line under nitrogen atmosphere.

After electrochemical etching, the obtained H-terminated porous silicon chips (4 chips) were dried under vacuum for 2 hours. Chloroplatinic acid solution (H_2PtCl_6 8 wt. % in H_2O, 160μL) catalyst was added to the Schlenk flask in the presence of iso-propanol (10 mL) under nitrogen (N_2) followed by allylamine (2 mL, >99% Sigma-Aldrich). The Schlenk flask was then subjected to 30 min of sonication at room temperature (RT). The resulting reaction mixture was then filtered and dried under reduced pressure at 60°C to remove any unreacted allylamine and Pt catalyst. The obtained amine-terminated SiNPs were also washed three times with dichloromethane (CH_2Cl_2) in order to remove any impurities and dried under vacuum. A solid brown powder of the amine-terminated SiNPs was obtained. About thirty milligrams of dry powder was obtained from each reaction. This powder was re-dissolved in water for further characterization. After the catalytic hydrosilylation reaction the obtained amine-terminated SiNPs become soluble and highly stable in water and show blue-green visible photoluminescence when exposed to ultraviolet light.

2.3   Synthesis of Carbohydrates capped SiNPs

2.3.1   Synthesis of Carboxylic Acid Functionalized Carbohydrates

The procedure used to synthesize the carboxylic acid functionalized carbohydrates was described by Deming and Kramer.[28] Galactose and glucose pentaacetate were commercially available from Sigma-Aldrich UK.

2.3.2   General Procedure to Synthesize Mannose and Lactose pentaacetate (2a and 4a)

Acetic anhydride (16 mL) was added to a solution of *β*-D-mannose (3.06 g, 17.0 mmol) in pyridine (15mL, 186 mmol, 11 equiv) at 0°C under nitrogen. The reaction mixture was sealed and kept at -20°C for 17 hours. The reaction mixture was slowly poured into ice-cold water (100 mL) and extracted with ethyl acetate (3 × 150 mL). The organic layer was washed with saturated $NaHCO_3$ until the evolution of gases ceased (3 × 150 mL), and then washed with water (2 × 100 mL), then once with brine (1 × 100 mL). The organic layer was then dried over Na_2SO_4 and the solvent was evaporated under vacuum to yield 97% as a glassy solid.
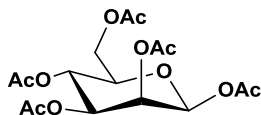
Mannose pentaacetate (2a)

^{1}H NMR (500 MHz, CDCl$_3$) δ = 6.07 (1H, d, J=1.5 Hz), 5.33 (1H, dd, J=2.5, 3.5 Hz), 5.24 (1H, t, J= 2Hz), 4.26 (1H, dd, J=5, 12.5 Hz), 4.09 (1H, dd, J=2, 2.5 Hz), 4.02-4.05 (1H,m), 2.16 (3H, s), 2.15 (3H, s), 2.08 (3H, s), 2.04 (3H, s), 1.99 (3H, s) ppm; ^{13}C NMR (126 MHz, CDCl$_3$) δ 170.75, 170.10, 169.85, 169.64, 168.17, 90.72, 73.42, 70.73, 68.85, 68.45, 65.66, 62.22, 20.97, 20.88, 20.82, 20.77, 20.75, 20.65 ppm.

$β$-D-lactose was synthesized following the same route:

$β$-D-lactose (2g), Acetic anhydride (12.8 mL), pyridine (24 mL), reaction was kept at -20°C for 48 hours.
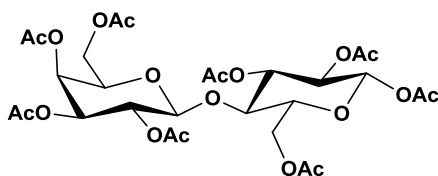
Lactose octaacetate (4a)

^{1}H NMR (500 MHz, CDCl$_3$) δ = 5.66 (1H, d, J=8.5 Hz), 5.34 (1H, d, J= 3.5 Hz), 5.23 (1H, t, J=9 Hz), 5.1 (1H, t, J=10.5 Hz), 5.03 (1H, t, J=8 Hz), 4.43-4.48 (2H, m), 4.05-4.16 (4H, m), 3.81-3.89 (2H, m), 2.14 (3H, s), 2.11 (3H, s), 2.09 (3H, s), 2.06 (3H, s), 2.04 (3H, s), 2.03 (3H, s), 2.02 (3H, s), 1.95 (3H, s) ppm; ^{13}C NMR (126 MHz, CDCl$_3$) δ 170.49, 170.44, 170.27, 170.19, 169.75, 169.69, 169.14, 168.99, 101.10, 91.67, 75.81, 73.64, 72.77, 71.10, 70.88, 70.65, 69.14, 66.73, 61.88, 60.97, 60.52, 21.18, 20.97, 20.94, 20.89, 20.77, 20.73, 20.64, 14.33 ppm.

2.3.3   General Procedure for Allylation of Galactose, Glucose and Mannose Pentaacetate

To a solution of pentaacetate **1a** (7.50 g, 19.2 mmol) in dry acetonitrile (40 mL) at 0°C under N$_2$ was added allyltrimethylsilane (9.20 mL, 57.6 mmol, 3 equiv). Boron trifluoride etherate (13.6 mL, 96.1 mmol, 5 equiv) was then added dropwise over fifteen minutes. The reaction mixture was stirred for 2 hours at 0°C and then allowed to warm to room temperature as stirring continued for an additional 14 hours. The reaction was slowly poured into saturated NaHCO$_3$ (150 mL) and stirred until the evolution of gases ceased. The

mixture was extracted with CH_2Cl_2 (3 x 100 mL), washed with brine and dried over Na_2SO_4. Following evaporation of the solvent under reduced pressure, the crude residue was purified by flash chromatography on silica (eluent 35-45% EtOAc in hexanes) to give the product as a clear oil (55-75% yield).
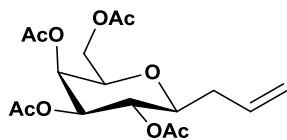
1-Allyl-2,3,4,6-tetra-*O*-acetyl-*β*-D-galactopyranoside (1b)

^{1}H NMR (500MHz, CDCl$_3$) δ = 5.69-5.79 (1H, m), 5.39-5.41 (1H, m), 5.23 (1H, dq, *J*= 6, 11.5 Hz), 5.13-5.14 (1H, m), 5.06-5.11 (1H, m), 4.28 (1H, p, *J*=6, 12.5 Hz), 4.14-4.22 (1H, m), 4.04-4.13 (2H, m), 2.41-2.49 (1H, m), 2.22-2.32 (1H, m), 2.10 (3H, s), 2.05 (3H, s), 2.02 (3H,s), 2.01 (3H, s) ppm; ^{13}C NMR (126 MHz, CDCl$_3$) δ 170.57, 170.10, 169.95, 169.83, 133.33, 117.67, 71.44, 68.27, 67.93, 67.60, 61.46, 60.38, 30.93, 20.78, 20.72, 20.66, 14.19 ppm.

Compound **2b** was prepared as above.
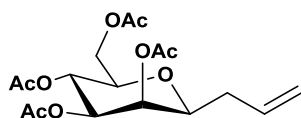
1-Allyl-2,3,4,6-tetra-*O*-acetyl-*β*-D-mannopyranoside (2b)

Yield 65 %. ^{1}H NMR (500MHz, CDCl$_3$) δ = 5.71-5.79 (1H, m), 5.25 (1H, dd, *J*= 3, 8.5 Hz), 5.17-5.19 (2H, m), 5.13-5.15 (1H, m), 5.10-5.12 (1H, m), 4.09 (1H, dd, *J*= 2.5,3 Hz), 4.0-4.04 (1H, m), 3.86-3.90 (1H, m), 3.60-3.63 (1H, m), 2.46-2.54 (1H, m), 2.37-2.42 (1H, m), 2.10 (3H, s), 2.07 (3H, s), 2.0 (3H, s), 2.01 (3H, s) ppm. ^{13}C NMR (126 MHz, CDCl$_3$) δ = 170.79, 170.31, 170.07, 169.79, 132.64, 118.44, 74.24, 70.75, 70.11, 68.89, 67.11, 62.50, 33.67, 21.05, 20.86, 20.80, 14.30 ppm.

Compound **3b** was prepared as above but was stirred at room temperature for 72 hrs.
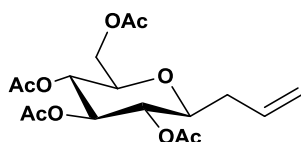
1-Allyl-2,3,4,6-tetra-*O*-acetyl-*β*-D-glucopyranoside (3b)

Yield 54 %. ¹H NMR (500MHz, CDCl₃) δ =5.69-5.77 (1H, m), 5.31 (1H, dd, *J* = 9, 18 Hz), 5.0-5.18 (2H, m), 4.87-4.98 (1H, m), 4.24-4.28 (1H, m), 4.19 (1H, dd, *J*=5.5, 12.5 Hz), 4.04-4.12 (1H, m), 3.83-3.86 (1H, m), 2.50-2.57 (1H, m), 2.29-2.34 (1H, m), 2.05 (3H, s), 2.03 (3H, s), 2.02 (3H, s), 2.01 (3H, s) ppm; ¹³C NMR (126 MHz, CDCl₃) δ 170.79, 170.32, 169.81, 169.54, 133.10, 117.98, 72.06, 70.51, 69.96, 68.95, 68.03, 62.38, 61.60, 31.07, 30.70, 20.86, 20.80, 20.71, 20.59 ppm.

Compound **4b** was prepared as above:

Lactose octaacetate **2b** (3g), allyltrimethylsilane (1.5 equiv, 12ml), Boron trifluoride etherate (14.9 mL, 2.5 equiv) and was stirred at room temperature for 72 hrs.
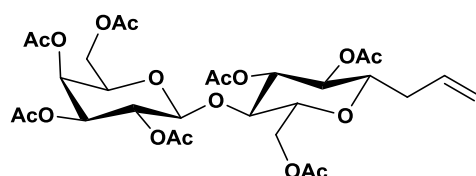
Allyl Lactose (4b)

Yield 55 %. ¹H NMR (500 MHz, CDCl₃) δ = 5.61-5.70 (1H, m), 5.24-5.29 (2H, m), 5.01-5.07 (2H, m), 4.88-4.91 (2H, m), 4.45 (1H, d, *J*=8 Hz), 4.27 (1H, dd, *J*= 2.5, 11.5 Hz), 4.00-4.11 (5H, m), 3.84 (1H, t, *J*=7), 3.72-3.75 (1H, m), 2.07 (3H, s), 2.01 (3H, s), 1.99 (3H, s), 1.98 (3H, s), 1.96 (3H, s), 1.95 (3H, s), 1.88 (3H, s) ppm; ¹³C NMR (126 MHz, CDCl₃) δ 170.37, 170.31, 170.07, 169.98, 169.86, 169.55, 169.13, 133.10, 117.69, 101.26, 76.52, 71.44, 70.97, 70.70, 70.05, 70.00, 69.75, 69.09, 66.75, 62.26, 60.91, 60.30, 30.99, 20.96, 20.82, 20.75, 20.70, 20.58, 20.57, 20.45, 14.14 ppm.

2.3.4 General Procedure for Oxidation of 1-Allyl-2,3,4,6-tetra-O-acetyl-*β*-D-galacto-, gluco-, and manno-pyranosides

To a solution of **1b** (0.755 g, 2.03 mmol) in acetonitrile (8 mL), carbon tetrachloride (8 mL), and water (12 mL) was added first NaIO₄ (1.95 g, 9.13 mmol, 4.5 equiv) followed by RuCl₃ (21.2 mg, 0.08 mmol, 4 mol %,). The reaction was stirred at room temperature for 3 hours then transferred to a separating funnel. After the addition of water (50 mL) the mixture was extracted with CH₂Cl₂ (3 x 50mL), and the combined organic phase was washed with brine (50 mL) and dried over Na₂SO₄. Following evaporation of the solvent under reduced pressure, the crude dark brown oil was passed through a silica plug (eluent 100% EtOAc) to give 1b as white solids. (72-92% yield).

Compound **1c** was prepared as above.
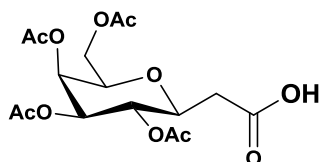
2,3,4,6-tetra-*O*-acetyl-*β*-D-galactopyranosyl acid (1c)

Yield 91% : ^{1}H NMR (500MHz, CDCl$_3$) δ =5.42 (1H, t, *J*=4 Hz), 5.32 (1H, q, *J*=6.5, 11 Hz), 5.17 (1H, dd, *J*=4, 11 Hz), 4.67-4.72 (1H, m), 4.21-4.25 (1H, m), 4.05-4.16 (2H, m), 3.88-3.93 (1H, m), 2.60-2.74 (2H, m), 2.11 (3H, s), 2.06 (3H, s), 2.03 (3H, s), 2.01 (3H, s) ppm; ^{13}C NMR (126 MHz, CDCl$_3$) δ 175.16, 170.82, 170.16, 170.02, 169.75, 69.59, 68.94, 67.95, 67.73, 67.23, 61.21, 33.20, 20.84, 20.78, 14.32 ppm.

Compound **2c** was prepared as above.
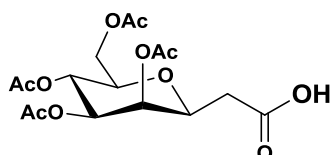
2,3,4,6-tetra-*O*-acetyl-*β*-D-mannopyranosyl acid (2c)

Yield 80% : ^{1}H NMR (500 MHz, CDCl$_3$) δ = 5.25 (1H, q, *J*=3, 7 Hz), 5.13 (1H, q, *J*=3, 5.5 Hz), 5.09 (1H, t, *J*=6.5 Hz), 4.41-4.45 (2H, m), 4.06-4.16 (2H, m), 3.97-4.0 (1H, m), 2.63-2.75 (2H, m), 2.08 (6H, s), 2.067 (3H, s), 2.063 (3H, s) ppm; ^{13}C NMR (126 MHz, CDCl$_3$) δ 174.74, 170.90, 170.03, 169.84, 169.74, 72.17, 69.37, 69.27, 68.09, 67.45, 61.55, 35.53, 20.90, 20.88, 20.81, 20.78 ppm.

Compound **3c** was prepared as above.
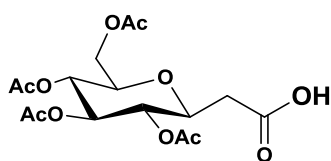
2,3,4,6-tetra-*O*-acetyl-*β*-D-glucopyranosyl acid (3c)

Yield 72% : ^{1}H NMR (500MHz, CDCl$_3$) δ= 5.46 (1H, t, *J*=9.5 Hz), 5.25 (1H, 1, *J*= 9, 16 Hz), 5.09 (1H, dd, *J*=4, 10.5 Hz), 5.0 (1H, t, *J*=8.5 Hz), 4.66-4.70 (1H, m), 4.23 (1H, dd, *J*= 4, 11 Hz), 4.07-4.13 (2H, m), 3.92-3.95 (1H, m), 2.82-2.77 (1H, m), 2.71-2.67 (1H, m), 2.08 (3H, s), 2.07 (3H, s), 2.03 (3H, s), 2.01 (3H, s) ppm; ^{13}C NMR (126 MHz, CDCl$_3$) δ 174.27, 170.86, 170.16, 169.52, 168.92, 72.94, 69.96, 69.33, 68.34, 68.03, 67.89, 61.61, 32.86, 21.18, 21.01, 20.83, 20.81, 20.77, 20.70, 20.58, 14.33 ppm.

Compound **4c** was prepared as above.
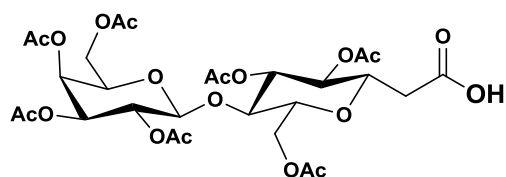
Acid Lactose (4c)

Yield 81% : ^{1}H NMR (500 MHz, CDCl$_3$) δ = 5.34 (1H, d, *J*=3.5 Hz), 5.31 (1H, t, *J*=7 Hz), 5.10-5.13 (1H, m), 5.02 (1H, q, *J*=5, 7.5 Hz), 4.97 (1H, dd, *J*=3.5, 10.5 Hz), 4.58 (1H, p, *J*=5, 9.5), 4.51 (1H, d, *J*=8), 4.34 (1H, dd, *J*=3.5, 12 Hz), 4.07-4.17 (6H, m), 3.86-3.91 (2H, m), 3.68 (1H, t, *J*=7 Hz), 2.76 (1H, q, *J*=9, 16 Hz), 2.64 (1H, dd, *J*=5, 15.5 Hz), 2.16 (3H, s), 2.14 (3H, s), 2.09 (3H, s), 2.05 (6H, s), 2.03 (3H, s), 1.96 (3H, s) ppm.

2.3.5 General Procedure to Synthesize Carbohydrate capped SiNPs Using DCC Coupling Reagent

A corresponding pyranosyl acid (30 mg, 0.078 mmol) and DCC (18 mg, 1.1 equiv, 0.085 mmol) were dissolved in dichloromethane (5 ml) and left, with stirring, for 2 hr at room temperature. Freshly prepared amine-terminated SiNPs (10 mg) were added into the reaction mixture and stirred overnight at room temperature. The reaction mixture was washed with water (3 × 10 mL) and extracted into CH$_2$Cl$_2$. The mixture was dried with Na$_2$SO$_4$, and solvent was removed under vacuum.

2.3.6 General Procedure to Synthesize Carbohydrate capped SiNPs Using EDC Coupling Reagent

A corresponding pyranosyl acid (30 mg, 0.078 mmol) and EDC (14 mg, 1 equiv, 0.085 mmol) were dissolved in dichloromethane (5 ml) and left, with stirring, for 2 hr at room temperature. After 2 hour *N*-hydroxysuccinimide (NHS) (7 mg, 1 equiv) and freshly prepared amine terminated SiNPs (10 mg) were dissolved in methanol and added into the reaction mixture and stirred overnight at room temperature. The reaction mixture was washed with water (3 × 10 mL) and extracted into CH$_2$Cl$_2$. The mixture was dried with Na$_2$SO$_4$, and solvent was removed under vacuum.

2.3.7 General Procedure for Deacetylation of *β*-D-galactose mannose, glucose and lactose capped SiNPs

To a solution of carbohydrate capped SiNPs (30 mg) in methanol (5 mL) was added 0.5 M sodium methoxide in methanol (0.015 mL, 0.0076mmol). The reaction was stirred for 4 hours at room temperature. The reaction mixture was neutralized by stirring with Dowex 50W-X8 [H+] resin for 30 min, filtered, and concentrated to yield a brownish sticky solid of carbohydrate capped SiNPs (93-98% yield). The obtained SiNPs were characterized by ^{13}C NMR and FTIR.

2.4 Characterization of Amine terminated SiNPs and Carbohydrate capped SiNPs

Characterization of the functionalized NPs is essential to address the validity of the synthetic procedure. A variety of different experimental techniques have been used to explore the characteristics of the amine terminated and carbohydrate capped SiNPs in an attempt to understand their influences on properties.

2.5 Optical measurements

All measurements have been performed at standard pressure and room temperature, unless stated differently.

2.5.1 Photoluminescence Spectroscopy (PL)

Photoluminescence spectroscopy is a non-contact, non-destructive method of probing the electronic structure of materials. In essence, light is directed onto a sample, where it is absorbed and where a process called photo-excitation can occur (figure 2.2). The photo-excitation causes the electrons in a material to jump to a higher electronic state. As it relaxes, the electrons return to a lower energy level through the release of energy (photons). The emission of light or luminescence through this process is photoluminescence, PL.
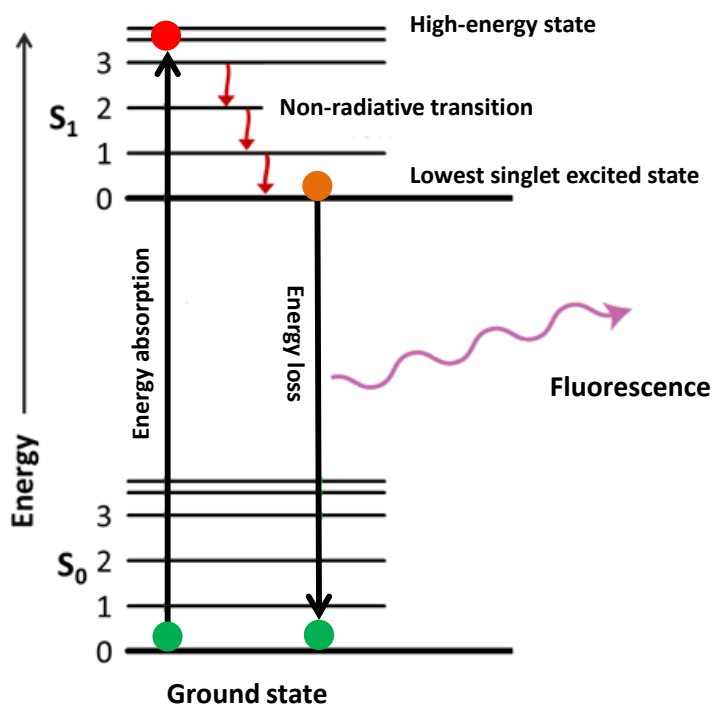
Figure 2.2: Schematic representation of an energy diagram (Jablonski diagram) shows the process of fluorescence. The colored circles represent the energy state of the fluorophore, where green depicts the normal energy level and red the maximum energy level.

Photoluminescence spectra were collected in a quartz cuvette with a PerkinElmer LS55 spectrophotometer, with an excitation slit width of 10 nm and an emission slit width set at 5 nm. The excitation wavelength was fixed at 360 nm. The emission spectra were corrected using the solvent emission as background.

2.5.2 Ultraviolet-visible Spectroscopy (UV-vis)

The absorbance of UV-vis light is related to the concentration through the Beer-Lambert Law, which is described as follows:

$$A = \varepsilon\, l\, c \qquad\qquad \text{Equation: 2.2}$$

Here, A is absorbance; ε is the molar absorptivity, l is the path length of the sample, and c is the concentration of the sample.

Absorption spectra were recorded in a quartz cuvette (path length 10 mm), using a Perkin-Elmer 35 UV-vis double-beam spectrophotometer. The scan range was 300-700 nm

with a 900 nm/min rate. Absorption spectra are corrected for solvent absorption, by subtracting the contribution from solvent from the recorded spectrum.

2.5.3   Quantum Yield Measurement

The fluorescence quantum yield is the ratio of the number of photons absorbed to the number of photons emitted through fluorescence. There are two ways of measuring quantum yields, called "absolute" and "relative". While measurements of the absolute quantum yield require sophisticated instrumentation, it is easier to determine the relative quantum yield of a fluorophore by comparison to a reference fluorophore with a well-known quantum yield. There are two methods for relative quantum yield measurements: a single-point and a comparative method.[29] Using the single-point method the quantum yield is calculated using the integrated emission intensities from a single sample and reference pair at identical concentrations. The quantum yield of the unknown sample is calculated using equation 2.3:

$$Q = Q_R \frac{I}{I_R} \frac{A_R}{A} \frac{\eta^2}{\eta_R^2} \qquad \text{Equation: 2.3}$$

Where Q is the quantum yield, I is the integrated intensity, η is the refractive index of the solvent, A is the absorbance. The subscript R refers to the standard fluorophore of a known quantum yield.

Although this method is fast and easy, it is not always reliable due to the inaccurate measurement of the fluorophore's absorbance. The second is the comparative method of Williams et al., which involves the use of multiple well-characterized references with known fluorescence quantum yields.[30] It is more time consuming but provides much higher accuracy. In this case, solutions with absorbance between 0.1 and 0.01 were prepared and the quantum yield is obtained by calculating the slope of the line generated by plotting the integrated fluorescence intensity against the absorption for multiple concentrations of fluorophore. The quantum yield can be calculated, using equation 2.4.

$$Q = Q_R \left(\frac{Grad}{Grad_R} \right) \left(\frac{\eta^2}{\eta_R^2} \right) \qquad \text{Equation: 2.4}$$

Where Q is the quantum yield, and η is the refractive index of the solvent. Grad is the gradient from the plot of integrated fluorescence intensity vs. absorbance. The subscript R refers to the reference fluorophore of a known quantum yield. Quinine sulphate (Q_R =0.546 in 0.5M H_2SO_4)[31] was used as reference in this study.

2.6 Size and Dispersity Measurements

2.6.1 Transmission Electron Microscopy (TEM)

Transmission Electron Microscopy (TEM) is an electron-based technique used to study materials. TEM probes the internal structure of samples to give an access to morphological fine structural details.
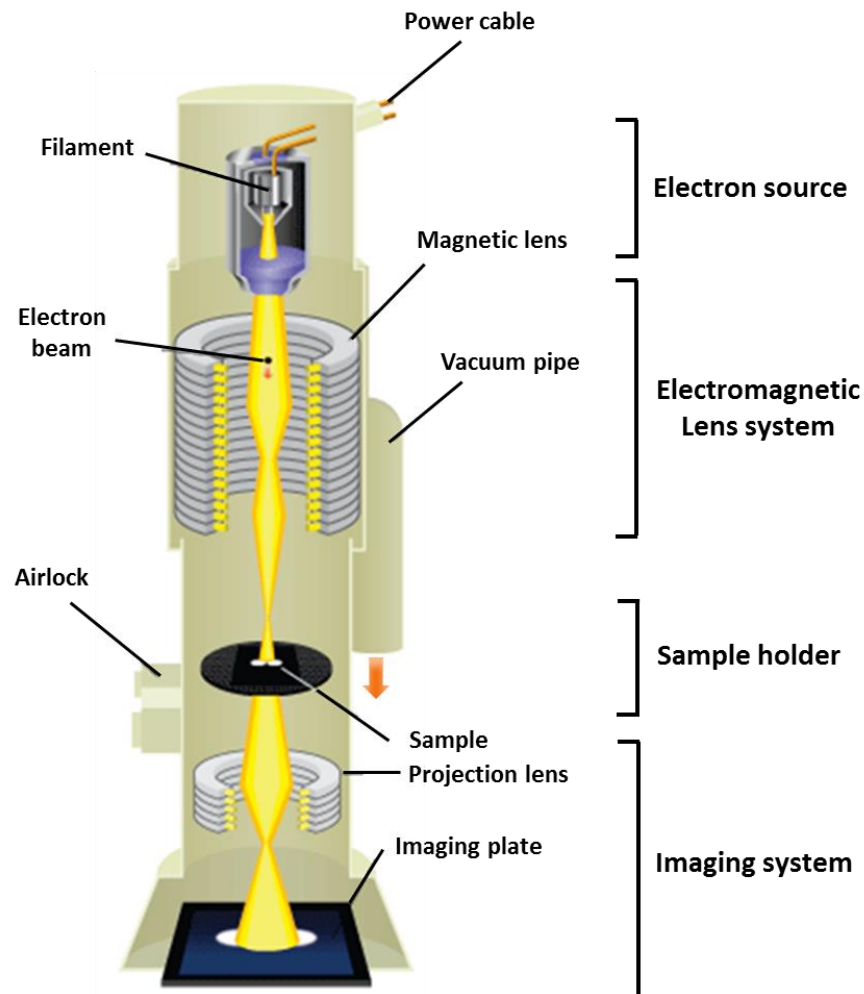
Figure 2.3: Schematic representation of Transition electron microscopy

The instrument is operated under high level of vacuum to avoid scattering of electrons from the air molecules. TEM uses a beam of electrons that transmit through a thin sample and are detected on the other side (figure 2.3). Electrons interact very strongly with matter, giving rise to the ability to use contrast for detection. Dark areas in the image

represent regions where electrons do not transmit through, while lighter areas are those that are more electron transparent.[32]

In this work, the samples were visualized on a JOEL 2000EX instrument with the accelerating voltage at 200kV. Dilute suspensions of amine-terminated SiNPs and all carbohydrate capped SiNPs were prepared in distilled water. Drops of suspension were placed on carbon-coated 300-mesh copper grid (Agar Scientific). The excess liquid was wiped away with filter paper, and the grid was dried in air. At least 100 particles were counted from each sample, and five different regions were scanned to assure representative results. ImageJ software was used to view and analyze the micrographs.

The High resolution transmission electron microscope images (HRTEM) of amine-terminated SiNPs were acquired with a Philips CM200 FEGTEM microscope at Leeds University (Leeds, UK) in collaboration with Prof. Rik Brydson and group.

2.6.2   Dynamic Light Scattering (DLS)

Dynamic Light Scattering (DLS) is also known as Photon Correlation Spectroscopy. This is an alternative technique for measuring the size of particles, which is typically in the sub-micron region. Shining a monochromatic light beam, such as a laser, onto a solution with spherical particles in Brownian motion causes a Doppler Shift when the light hits the moving particle, changing the wavelength of the incoming light. This change is related to the size of the particle. The velocity of the Brownian motion is defined by the translational diffusion coefficient. So the size of a particle can be calculated from the translational diffusion coefficient by using the Stokes- Einstein equation 2.5;

$$D_h = \frac{k_B T}{3\pi\eta D_t}$$

Equation: 2.5

Where D_h is the hydrodynamic diameter, D_t is translational diffusion coefficient, k_B is the Boltzmann's constant, T is the absolute temperature, and η is the dynamic viscosity. The diameter that is measured in DLS is a value that refers to how a particle diffuses within a fluid so it is referred to as a hydrodynamic diameter. Measurements of the hydrodynamic diameter of amine-terminated SiNPs and carbohydrate capped SiNPs were performed in a variety of solvents including distilled water, absolute ethanol, dichloromethane, including biological solvents like phosphate buffer saline (PBS) and in biological media such as DMEM (Dulbecco's modified essential medium), RPMI (Roswell Park Memorial Institute medium) and MMR (Marc's Modified Ringers) using a Zetasizer Nano ZS (Malvern Instruments,

Malvern, UK). The scattered photons were detected under an angle of 173°, and the relative number distribution was obtained. In order to obtain accurate measurements ultrasonication (2 min) and filtration (Whatman Anotop 25 0.2μm 25mm Syringe Filters) were applied before any measurement.

2.7   Chemical Analysis

2.7.1   Nuclear Magnetic Resonance Spectroscopy (NMR)

The selective absorption of electromagnetic radiation by the nuclei of atoms placed in the presence of strong magnetic field is called as NMR spectroscopy. The nuclei of different atoms absorb unique frequencies of radiation depending on their environment, thus by analyzing these frequencies which are absorbed by a sample placed in a strong magnetic field, the sample is analyzed. NMR spectroscopy is widely used to get the molecular information of the compounds and to understand the structure of the compounds.

^{1}H and ^{13}C NMR (500 MHz) spectra of samples in D_2O and $CDCl_3$ were recorded on a Bruker 500 MHz spectrometer. The fresh sample was dried under vacuum and re-dissolved in D_2O and $CDCl_3$, respectively.

2.7.2   Fourier Transform Infrared Spectroscopy (FTIR)

Fourier Transform Infrared Spectroscopy (FTIR) most commonly deals with an infrared radiation range of 4500 cm^{-1} to 500 cm^{-1}. The molecules or parts of the molecules absorb the radiation at specific frequencies and give structural information. It is a very powerful tool for identifying types of chemical bonds in a molecule. In the case of nanoparticles surface functionalization is necessary to stabilize them and therefore changing the functionalization from one group to another could be confirmed by the appearance of the new group and disappearance of the reacted group. Solution spectra gave weak signals, so it was better to measure powder samples using Attenuated Total Reflection (ATR) Fourier Transform-Infra-Red (FT-IR) spectroscopy. The instrument used was a Perkin-Elmer 65 FTIR spectrometer with a SensIR single pass diamond ATR attachment. The solid sample of NPs was placed directly on the ATR crystal and the spectra corrected by the background signal.

In this work Synchrotron radiation FTIR microscopy was also used to analyze the samples by mapping the interesting area and to obtain the structural information of carbohydrate capped SiNPs. The crystals of carbohydrate capped SiNPs were mainly

characterized with 3D Synchrotron radiation FTIR by mapping the crystal. The carbohydrate capped SiNPs were also analyzed–inside the biological cells. Using synchrotron radiation (SR) IR microscopy gives a high spatial resolution and signal-to-noise ratio for cell study. The principle of FTIR microscopy is to couple an FTIR spectrometer with a microscope using the synchrotron emission in the infrared domain as a source of light. It enables on one hand to visualize the sample and to choose specifically the region for analysis and on the other hand to carry out two-dimensional acquisitions by raster scanning the sample. Infrared spectra are acquired at each pixel of 1D or 2D maps, and chemical maps can thus be derived. Compared to classical laboratory sources, the synchrotron radiation brightness is far greater and enables the beam size to be reduced below 10μm without a significant loss of photons.

The measurements were performed with a Bruker IFS66V FTIR Microscope: Bruker Hyperion 3000, Detector: 100x100 mikron MCT (MIR) at beam line D7 in MAX-lab at Lund, Sweden.

The biological cell samples were analyzed with a Bruker Vertex 80 V Fourier Transform IR Interferometer Microscope: Hyperion 3000 microscope, Detector: 100x100 MCT broadband at beam line B22 of Diamond at Oxfordshire, UK.

2.7.3   X-ray Photoelectron Spectroscopy (XPS)

X-ray photoelectron spectroscopy is one of the surface analytical techniques that bombard the sample with photons, electrons or ions in order to excite the emission of photons, electrons or ions. It is also known as ESCA (electron spectroscopy for chemical analysis) and was developed by the group of Siegbahn at the University of Uppsala in Sweden.

The sample is irradiated with photons of energy hν which interact with the sample by exchanging enough energy (see figure 2.4). The electrons from the inner orbital near the surface of the material gets excited and result in ejection of electrons. Depending upon the photon energy the electrons will jump from the solid state and get detected. Ejected core electrons have a specific kinetic energy (**E$_k$**) that is related to the energy of the exciting photon (**hν**), the binding energy of the electron to the atom (**E$_b$**) and the characteristic work function of the material (**Φ**) by the relation shown in equation 2.6:

$$E_k = h\nu - E_b - \phi$$ **Equation: 2.6**

Every element has a specific binding energy associated with each atomic orbital, such that each element will give rise to a characteristic set of peaks in the photoelectron

spectrum at kinetic energies determined by the photon energy and the respective binding energies.
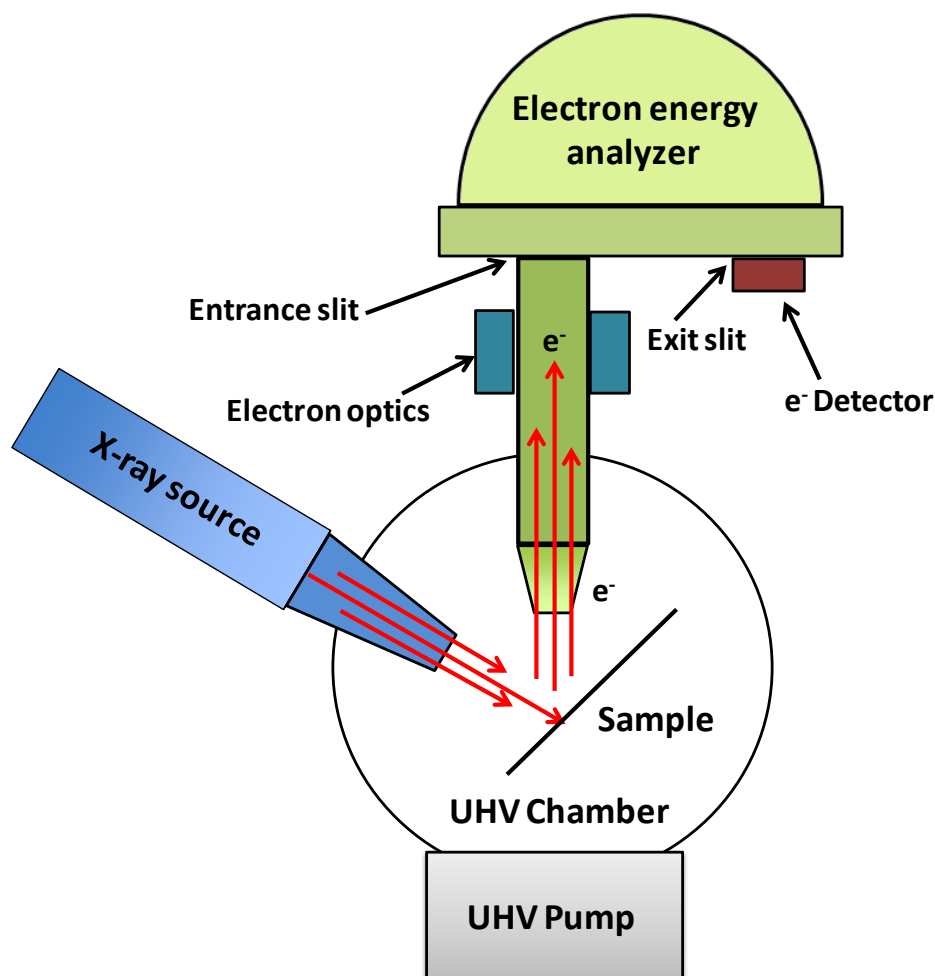
Figure 2.4: Schematic representation of X-ray Photoelectron spectrometer equipped with an x-ray source and a hemispherical analyzer

The measurements were performed with a SCIENTA ESCA300 XPS analyzer at the National Centre for Electron Spectroscopy and Surface Analysis (NCESS), Daresbury Laboratory, U.K. A few drops of the suspension of SiNPs sonicated in dichloromethane were cast onto a freshly cleaned gold substrate. The sample was introduced immediately into a nitrogen-filled locked chamber and allowed to dry before being transferred into the instrument chamber where the base pressure was kept below 1×10^{-8} mbar. All spectra were acquired at room temperature in normal emission, and the energy resolution was kept under 0.4 eV. In all photoemission spectra, binding energies (E_b) were referenced to the Au4f7/2 line measured on a gold foil in direct electrical contact with the sample, which was found at E_b of 83 eV.

2.8 Biological Studies

2.8.1 Culture of Cell Lines

Six mammalian cell lines including MCF-7 (human breast adenocarcinoma), HHL-5 (immortalized human hepatocytes), HepG2 (human liver hepatocellular carcinoma), A549 (Human lung adenocarcinoma epithelial cell line), MDCK (Madin Darby canine kidney cells), SK-Mel (Human Melanoma cell line) were used in the study. The cell culture facilities and cells were kindly provided by Dr. Victoria Sherwood (School of Pharmacy, UEA). Some of the cell lines such as MCF-7, HHL5 and HepG2 were generously supplied by Dr.Yongping Bao (Biomedical Research Centre, UEA). All cell lines are adherent cell lines, which grow in *vitro* until they have covered the available surface area or the medium nutrients are depleted. At this point the cell lines should be subcultured in order to prevent cell death.

In general, cells were subcultured when they reached 80% confluence. The old cell medium was removed by 10 mL pipette then cells were washed with pre-warmed (37°C) Phosphate Buffered Saline (PBS). This approach was done by carefully pipetting PBS into the flask, gently mixing by tilting the flask from side to side twice. Cells were detached by adding 1mL Trypsin/EDTA (0.25%, Invitrogen, Carlsbad, CA), and incubated at 37°C for 5-10 min. Trypsin was deactivated by adding 5 mL fresh media. Cells were maintained at 37°C in a humidified 5% CO_2 atmosphere. The medium was changed every two-three days and the cells often checked under the microscope.

All cell lines were incubated with required medium supplements according to the European Collection of Cell Cultures (ECACC) recommendation. MCF-7, HepG2, HHL-5, MDCK, SK-Mel were cultured in Dulbecco's modified essential medium (DMEM, Invitrogen, Carlsbad, CA) supplemented with 10% Fetal Bovine Serum (FBS, biosera). A549 was cultured in Roswell Park Memorial Institute medium (RPMI, Invitrogen, Carlsbad, CA) supplemented with 10% Fetal Bovine Serum (FBS, biosera). All media contained 1% Penicillin/ Streptomycin (P/S, 5000u) (Invitrogen, Carlsbad, CA) and 1% L-Glutamine (200mM) (Invitrogen, Carlsbad, CA).

2.9   Cytotoxicity Studies

2.9.1   *In Vivo* Toxicity Assay in *Xenopus laevis*

2.9.1.1 Obtaining Embryos

The *Xenopus* embryos were kindly supplied by Dr. Grant N. Wheeler (Biological science, UEA) in collaboration with Dr. Victoria Sherwood (School of Pharmacy, UEA)

Female *Xenopus laevis* were primed by injection of 100 units of pregnant mare serum gonadotrophin (PMSG) into the dorsal lymph sac 5-7 days before the eggs were required. Ovulation was then induced by injection of 250µl of human chorionic gonadotrophin (hCG) into each dorsal lymph sac. After 14–16 hrs at 18°C, the eggs were liberated into a petri dish from the female by manual squeezing of the abdomen. Eggs can be collected once every hour, 6 times a day per frog. Testis were removed from a sacrificed male Xenopus and stored in testes buffer. A portion of the testis was rubbed on the isolated eggs. The eggs were then covered, for 5 min at 18°C, by testes that have been homogenized in MMR. Concentration of the salt solution was reduced to 0.1 x MMR and the eggs were left for 20 min at 18°C for fertilization. The eggs were placed in a beaker containing 2% cysteine pH 8.0 dissolved in MMR and gently stirred to remove the jelly coat the eggs are encased in. Cysteine was removed by washing in MMR followed by a wash of 0.1 x MMR. Embryos were left at different temperatures to control the rate of development until they were at the required stage according to Nieuwkoop and Faber (NF) (Nieuwkoop and Faber, 1956). The eggs were cleaned once every hour in 0.1 x MMR and gentamycin until they reached the necessary stage. Any dead embryos were removed.

Reagents: 2% cysteine (pH 8) in MMR, MMR (pH 7.5) (100mM NaCl, 5nM HEPES, 2mM KCl, 2nM $CaCl_2$, 1mM $MgCl_2$), 0.1 x MMR (pH 7.5) (10mM NaCl, 0.5 mM HEPES, 0.2mM KCl, 0.2mM $CaCl_2$, 0.1mM $MgCl_2$), Testes buffer (pH 7.5) (100% FCS, MMR (4:1), 1:1000 gentamycin).

2.9.1.2 Exposure to Silicon Nanoparticles

Live embryos were collected for exposure to SiNPs at NF stages 4, 15, and 38, as described in 2.9.1.1. The stages of *Xenopus* were selected to assess NP toxicity during key stages of the development of an organism. These stages correlate to pre-gastrulation (NF stage 4), pre-neuralation (NF stage 15), and pre-tadpole (NF stage 38). Concentrations of NPs were made up using serial dilutions in 0.1 x MMR, total volume 500µl per well. In a 24-

well plate, 5 embryos per well were collected in 500µl of 0.1 x MMR and added to the NPs, total volume 1000 µl per well.

Embryos were incubated, exposed to NPs, at 18°C until the required NF stage. Embryos exposed to NPs at NF stages 4 and 15 were fixed, as described in 2.9.1.3, at NF stage 38. Those that were exposed to NPs at NF stage 38 were fixed at NF stage 45.

2.9.1.3 Fixing Embryos

Once the embryos reached the required stage they were washed in 0.1 x MMR and fixed in MEMFA. The embryos were left in MEMFA for 1hr at room temperature or overnight at 4°C. After 2 washes in PBS all embryos were ranked by phenotypic abnormalities. Once ranked, the embryos were dehydrated in increasing concentrations of methanol, 25%, 50%, and 75%, before being stored at -20°C in 100% MeOH.

The embryos were rehydrated using decreasing concentrations of MeOH, 75%, 50%, and 25% and 2 washes of PBST, before imaging.

Reagents: MEMFA (3.7% formaldehyde, MEM salts, MQW (1:1:8)), PBST (pH 7.2) (8g NaCl, 0.2g KCl, 1.44g Na_2HPO_4, 0.24g KH_2PO_4, 2 ml Tween- 20, 800 ml MQW), MeOH.

2.9.2 Colourimetric MTT Assay (*In Vitro*)

To evaluate the influence of cell proliferation by carbohydrates capped SiNPs and amine terminated SiNPs, an MTT (3-(4,5-dimethylthiazol-2-yl)-2,5 diphenyltetrazolium bromide) assay was performed to determine cell viability. MTT measures mitochondrial activity using tetrazolium salts as mitochondrial dehydrogenase enzymes cleave the tetrazolium ring, which only occurs in living cells.[33] HHL-5, HepG2, MDCK and A549 cells were seeded in a 96- wells plate (Applied Biosystems) for 72 hours. Then, the cells were stimulated with samples at various concentrations (50, 300, 500, 700 and 1000µg /mL) for 72 hours. After incubation for specified times, the medium was removed. 10µL of MTT (Sigma-Aldrich) solution (5mg/mL in sterile water) mixed with 100µL fresh medium was added to each well, including controls. After four hours incubation at 37°C, the medium was removed, and formazan was solubilized in dimethylsulfoxide (DMSO, Sigma-Aldrich). The absorbance was recorded on a microplate reader at the wavelength of 560 nm, blanking on control wells. The percentage of viable cells was estimated by comparison with the untreated control cells. All experiments were repeated at least on three different occasions.

2.10 Bioimaging Studies

2.10.1 Microscope Slide Preparation

Cells were grown on cover slips (VWR international, size 18 mm, thickness 0.16 mm) which were each set in 35 mm not TC- treated culture dish (Corning®). Approx. 1mL fresh medium was added in each pre-marked culture dishes. Cells were grown on cover slips until approx. 50% confluent. The growth medium was then removed and 50, 150 and 300 μg /mL of sample were added on top of the cells (Control was also made at the same time). Various incubation times (24 hrs, 48 hrs and 72 hrs) at 37°C were used. The cells were then rinsed in PBS and fixed either by a Methanol or Paraformaldehyde solution for 10 min. Then, a drop (approximately 2μL) of fluorescent mounting medium (VECTASHIELD® hard, Vector Labs) was added on top of the microscope slide. The cover slip in which cells were grown was turned upside down on top of the mounting medium. The slide was then dried in the fridge for approx. 30 min before use.

2.10.2 Cell Staining

The glass cover slips were taken out from the well plate and carefully placed on parafilm (small plastic box covered with parafilm) surrounded by a damp cloth or wet tissue (to prevent the cells from dehydration). The cells were fixed with paraformaldehyde solution (approx. 300 μl) to envelop all the glass cover slip, for 10 min. After that time the solution was taken out carefully using a small suction pump, then permeablise buffer solution was mounted on the cover slip and left for 5 min. The solution was then removed by suction and the cells were washed with wash buffer (4 × 300 μL). Texas Red®-X Phalloidin (6 μM) or LysoTracker® Red (50 nM) in PBS solution was mounted on the cover slips (making sure all the cell area was covered) and left for 20 min in the dark. After that time, the solution was removed by suction and DAPI (300 nM in PBS) was added on the cover slips to stain the nuclei. After 5 min the DAPI solution was removed and cells were washed once with permeablise buffer and with wash buffer (6 × 300 μL). The cells were fixed with paraformaldehyde solution (300 μL) for 10 min and washed with wash buffer (3 × 300 μL). Then, a drop (approximately 2μL) of fluorescent mounting medium (VECTASHIELD® hard, Vector Labs) was added on top of the microscope slide. The cover slip which cells were grown in was dipped into water, tapped on tissue paper and turned upside down on top of the mounting medium. The slide was then dried in the fridge for approx. 30 min before use.

Permeablise buffer: PBS, 1% fetal calf serum, 0.1% sodium azide, 0.1 % saponin (pH 7.4-7.6, adjusted by adding drops of NaOH)

2.10.3 Fluorescence Microscopy

The Fluorescence microscope uses a much higher intensity light source, which excites a fluorescent species in a sample. In most cases the sample is labeled with a fluorescent substance known as a fluorophore and then illuminated through the lens with the higher energy source. The illumination light is absorbed by the fluorophores and causes them to emit a longer wavelength (lower energy) light that produces the magnified image instead of the original light source by a special dichroic mirror, which reflects light shorter than a certain wavelength, and passes light longer than that wavelength. The fluorescent microscopy analysis for bioimaging was performed using a Leica TCS inverted fluorescence microscope with green/blue (carbohydrates capped SiNP) and red (LysoTracker® Red or Texas Red®-X Phalloidin) filters.

2.10.4 Confocal Laser Scanning Microscopy

Compared to fluorescent microscopy, confocal microscopy has an additional pinhole, which is efficient at rejecting out of focus fluorescent light. The pinhole is conjugated to the focal point of the lens, thus it is a confocal pinhole.[34] Figure 2.5 shows the internal workings of a confocal microscope. By scanning many thin sections through a sample, a very clean three-dimensional image of the sample can be built up. In this study, cells were observed using a laser scanning confocal microscope Zeiss 510 LSM through a 40 x 1.30 NA oil immersion objective lens. The pinhole was set to one Airy. Carbohydrates capped SiNPs were excited using a 488 nm laser. LysoTrcker-Red was excited using 577 nm laser and Texas Red®-X phalloidin red (Life technologies Ltd) was excited using 591 nm laser.
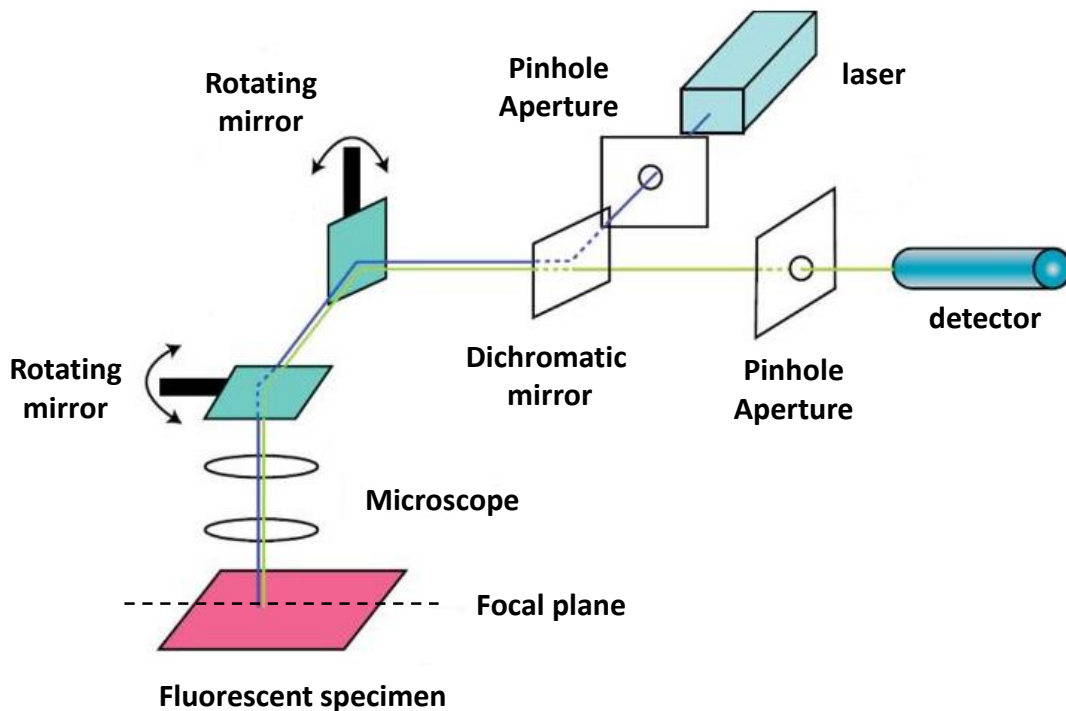
Figure 2.5: Internal workings of a confocal microscope-reproduced from Prasad et al.[34]

First, the laser light is directed by a dichroic mirror towards a pair of rotating mirrors that scan the light in x and y axis. Then, the light passes through the microscope objective and excites the sample. The fluoresced light from the sample passes back through the objective, followed by the same set of rotating mirrors used to scan the sample. After that, the light passes through the dichroic mirror through a pinhole placed in the confocal plane of the sample. The pinhole thus rejects all out-of-focus light arriving from the sample. Finally the light that emerges from the pinhole is measured by a detector.

2.11 Cellular Uptake

Cells were selected to investigate in *vitro* uptake of amine capped SiNPs and carbohydrates capped SiNPs. Cells were seeded on 12-well plates with cover slips at a density of 10^4 cells per well and exposed to 50, 150 or 300 μg /mL of SiNPs for 1–24 hours. The cells were then washed twice by PBS (Gibco®) and fixed by ice-cold methanol (Fisher Chemical) or Paraformaldehyde. Cover slips with intact cells were inverted and mounted on a microscope slide using mounting gel. The images were taken under a confocal microscope (Zeiss LSM510 META system) using a 40 × oil immersion objective lens. DAPI produced a blue fluorescence with an excitation wavelength 380 nm and emission at 460 nm. The SiNPs

were excited at GFP region 488 nm, whereas the LysoTrcker-Red was excited using 577 nm laser and Texas Red®-X phalloidin red was excited using 591 nm laser.

2.12 Flow Cytometry

Flow cytometers have been used in many biological applications to measure both light scattering and fluorescence from particles or biological cells.[35] It is able to characterize individual cells with fluorophore labels, which provide semi quantitative information of cellular uptake of the NPs. It supplies excitation energy with lasers and detects fluorescent emissions with a range of filters and detectors. It can also measure the size of a cell using forward scatter, and the granularity of a cell using side scatter.[36]

In our experiments, cells were seeded on 24-wells plate at a density of 3×10^4 cells per well and incubated at 37°C overnight. After treatment with 50, 100, 200, 300 μg /mL of SiNPs at different time point from 1–72 hrs cells were harvested by trypsinisation and suspended in the medium (300 μL). Then the cells were immediately taken to perform Flow cytometry. Flow cytometry was performed with an Accuri C6 Flow Cytometer System using 380 nm excitation with 10,000 events from each sample, and analysis was performed using FlowJo software.

2.13 Statistics

All data are representative of at least three independent experiments. Data are presented as means ± standard deviation (S.D). Statistical significance was determined using a one-way analysis of variance between the two groups.

2.14 References

1.   A Uhlir, Electrolytic shaping of germanium and silicon. The Bell System Technical Journal 1956, 35, 333-347.

2.   Dillon, A.; Robinson, M.; Han, M.; George, S., Diethylsilane decomposition on silicon surfaces studied using transmission FTIR spectroscopy. Journal of the Electrochemical Society 1992, 139, 537-543.

3.   Gupta, P.; Dillon, A.; Bracker, A.; George, S., FTIR studies of H2O and D2O decomposition on porous silicon surfaces. Surface Science 1991, 243, 360-372.

4.   Anderson, R. C.; Muller, R. S.; Tobias, C. W., Investigations of porous silicon for vapor sensing. Sensors and Actuators. A: Physical 1990, 23, 835 – 839.

5.   Cullis, A. G.; Canham, L. T.; Calcott, P. D. J., The structural and luminescence properties of porous silicon. Journal of Applied Physics 1997, 82 (3), 909-965.

6.   Hamilton, B., Porous silicon. Semiconductor Science and Technology. 1995, 10, 1187 – 1207.

7.   Lehmann, V.; Gösele, U., Porous silicon formation: A quantum wire effect. Applied Physics Letters 1991, 58 (8), 856-858.

8.   Linford, M.; Chidsey, C., Alkyl monolayers covalently bonded to silicon surfaces. Journal of the American Chemical Society 1993, 115, 12631 – 12632.

9.   Linford, M.; Fenter, P.; Eisenberger, P.; Chidsey, C., Alkyl monolayers on silicon prepared from 1-alkenes and hydrogen-terminated silicon. Journal of the American Chemical Society 1995, 117, 3145 – 3155.

10.   Linford, M. R.; Chidsey, C. E. D., Alkyl monolayers covalently bonded to silicon surfaces. Journal of the American Chemical Society 1993, 115 (26), 12631-12632.

11.   Linford, M. R.; Fenter, P.; Eisenberger, P. M.; Chidsey, C. E. D., Alkyl Monolayers on Silicon Prepared from 1-Alkenes and Hydrogen-Terminated Silicon. Journal of the American Chemical Society 1995, 117 (11), 3145-3155.

12.   Bateman, J.; Eagling, R.; Worrall, D.; Horrocks, B.; Houlton, A., Alky- lation of porous silicon by direct reaction with alkenes and alkynes. Angewandte Chemie- International Edition 1998, 37, 2683-2685.

13.   Gurtner, C.; Wun, A.; Sailor, M., Surface modification of porous silicon by electrochemical reduction of organo halides. Angewandte Chemie-International Edition 1999, 38, 1966-1968.

14.   Effenberger, F.; Götz, G.; Bidlingmaier, B.; Wezstein, M., Photoactivated Preparation and Patterning of Self-Assembled Monolayers with 1-Alkenes and Aldehydes on Silicon Hydride Surfaces. Angewandte Chemie International Edition 1998, 37 (18), 2462-2464.

15.   Cicero, R. L.; Linford, M. R.; Chidsey, C. E. D., Photoreactivity of Unsaturated Compounds with Hydrogen-Terminated Silicon(111). Langmuir 2000, 16 (13), 5688-5695.

16.   Stewart, M. P.; Buriak, J. M., Exciton-Mediated Hydrosilylation on Photoluminescent Nanocrystalline Silicon. Journal of the American Chemical Society 2001, 123 (32), 7821-7830.

17.   Sung, M. M.; Kluth, G. J.; Yauw, O. W.; Maboudian, R., Thermal Behavior of Alkyl Monolayers on Silicon Surfaces. Langmuir 1997, 13 (23), 6164-6168.

18.   Bateman, J. E.; Eagling, R. D.; Worrall, D. R.; Horrocks, B. R.; Houlton, A., Alkylation of Porous Silicon by Direct Reaction with Alkenes and Alkynes. Angewandte Chemie International Edition 1998, 37 (19), 2683-2685.

19.   Boukherroub, R.; Wojtyk, J. T. C.; Wayner, D. D. M.; Lockwood, D. J., Thermal Hydrosilylation of Undecylenic Acid with Porous Silicon. Journal of The Electrochemical Society 2002, 149 (2), H59-H63.

20.   Wayner, D. D. M.; Wolkow, R. A., Organic modification of hydrogen terminated silicon surfaces1. Journal of the Chemical Society, Perkin Transactions 2 2002, (1), 23-34.

21.   Zazzera, L. A.; Evans, J. F.; Deruelle, M.; Tirrell, M.; Kessel, C. R.; Mckeown, P., Bonding Organic Molecules to Hydrogen‚ÄêTerminated Silicon Wafers. Journal of The Electrochemical Society 1997, 144 (6), 2184-2189.

22.   M. Buriak, J., Organometallic chemistry on silicon surfaces: formation of functional monolayers bound through Si-C bonds. Chemical Communications 1999, (12), 1051-1060.

23.   Schmeltzer, J. M.; Porter, L. A.; Stewart, M. P.; Buriak, J. M., Hydride Abstraction Initiated Hydrosilylation of Terminal Alkenes and Alkynes on Porous Silicon. Langmuir 2002, 18 (8), 2971-2974.

24.   Speier, J. L., Homogeneous Catalysis of Hydrosilation by Transition Metals. In Advances in Organometallic Chemistry, Stone, F. G. A.; Robert, W., Eds. Academic Press: 1979; Vol. Volume 17, pp 407-447.

25.   Chalk, A. J.; Harrod, J. F., Homogeneous Catalysis. II. The Mechanism of the Hydrosilation of Olefins Catalyzed by Group VIII Metal Complexes1. Journal of the American Chemical Society 1965, 87 (1), 16-21.

26.   Tilley, T. D., Transition-Metal Silyl Derivatives. In Organic Silicon Compounds (1989), John Wiley & Sons, Ltd: 2004; pp 1415-1477.

27.   Harrod, J. F.; Chalk, A. J., In Organic Synthesis via Metal Carbonyls. Eds.: John Wiley & Sons Ltd.: New York, 1977; Vol. 2.

28.   Kramer, J. R.; Deming, T. J., Glycopolypeptides via Living Polymerization of Glycosylated-l-lysine N-Carboxyanhydrides. Journal of the American Chemical Society 2010, 132 (42), 15068-15071.

29.   Lakowicz, J. R., Principles of Fluorescence Spectroscopy. Kluwer Acad./Plenum Publ.: 1999.

30.   Williams, A. T. R.; Winfield, S. A.; Miller, J. N., Relative fluorescence quantum yields using a computer-controlled luminescence spectrometer. Analyst 1983, 108 (1290), 1067-1071.

31.   Eaton, D. F., Reference materials for fluorescence measurement. Pure Applied Chemistyr 1988, 60, 1107-1114.

32.   Keyse, R. J.; Garratt-Reed, A. J.; Goodhew, P. J.; Lorimer, G. W., Introduction To Scanning Transmission Electron Microscopy. Spinger-Verlag: New York, 1998.

33.   Sayes, C. M.; Fortner, J. D.; Guo, W.; Lyon, D.; Boyd, A. M.; Ausman, K. D.; Tao, Y. J.; Sitharaman, B.; Wilson, L. J.; Hughes, J. B.; West, J. L.; Colvin, V. L., The Differential Cytotoxicity of Water-Soluble Fullerenes. Nano Letters 2004, 4 (10), 1881-1887.

34.   Prasad, V.; Semwogerere, D.; Weeks, E. R., Confocal microscopy of colloids. Journal of Physics: Condensed Matter 2007, 19 (11), 113102.

35.   Kumar, A.; Pandey, A. K.; Singh, S. S.; Shanker, R.; Dhawan, A., A flow cytometric method to assess nanoparticle uptake in bacteria. Cytometry Part A 2011, 79A (9), 707-712.

36.   Zucker, R. M.; Massaro, E. J.; Sanders, K. M.; Degn, L. L.; Boyes, W. K., Detection of TiO2 nanoparticles in cells by flow cytometry. Cytometry Part A 2010, 77A (7), 677-685.

3 Highly Luminescent and Nontoxic Amine-Capped silicon Nanoparticles from Porous Silicon: Synthesis and Their Use in Biomedical Imaging
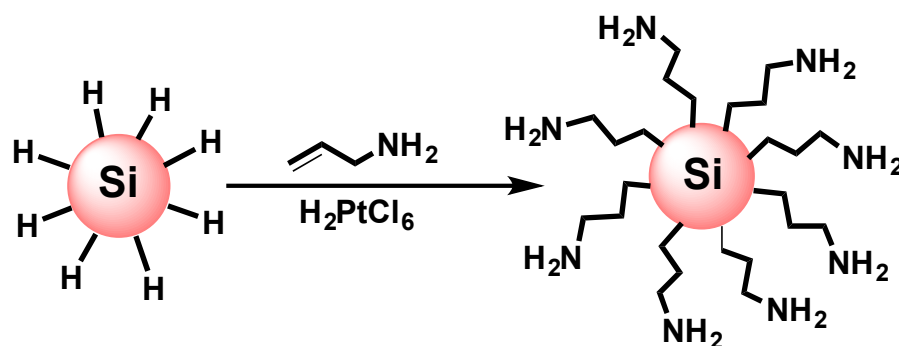
Part of this chapter is published as:

3.1 Introduction and Motivation

Silicon nanoparticles (SiNPs), or "quantum dots" (QDs), have attracted tremendous interest from the scientific community because of their unique characteristics that differ from those of their bulk counterparts, such as novel optical, catalytic, electronic, and mechanical properties.[1, 2] At nanometer scales, silicon exhibits visible photoluminescence (PL) because of the quantum confinement effect that can be exploited for uses in electronic and photonic devices.[3, 4] Furthermore, SiNPs have several advantages in biological applications such as size-dependant tuneable light emission,[5-7] high brightness,[8] great stability against photobleaching compared to organic dye molecules[9, 10] and also SiNPs exhibit a low inherent toxicity in comparison with other types of semiconductor quantum dots, which can pose significant risks to human health.[11-14] The combination of these properties opens a new avenue of SiNPs for optoelectronic and bioimaging purposes.

For SiNPs to be employed within biomedical applications, it is essential that they are water-soluble and hydrophilic to prevent aggregation and precipitation in a biological environment, have a substantial photoluminescence quantum yield in the visible region and a fast radiative recombination rate. The chemical processes used to terminate the surfaces of the SiNPs change the internal electronic structure and thus play an important role in the resultant emission wavelength, radiative lifetime, and ultimately determine the solubility.[15]

As mentioned in Chapter 1 silicon nanoparticles can be synthesized by a wide range of chemical or physical methods, including solution routes using a variety of reducing agents,[16, 17] micro-emulsion techniques,[18, 19] ultrasonic dispersion of electrochemically etched silicon,[3, 20, 21] laser-induced pyrolysis of silane,[22, 23] and synthesis in inverse micelles[10].

The H-terminated SiNPs obtained by electrochemical etching are very prone to oxidation therefore surface functionalization is necessary in order to stabilise them in a biological environment. A good surface functionalization increases the stability and dispersity in a wide range of solvents, helps to increase the brightness of photoluminescence (Quantum yield) and stabilises through a wide range of pHs.

For instance Warner *et al*. in 2005 synthesized amine-terminated SiNPs by using Lithium aluminium hydride (LiAlH₄) as a reducing agent to reduce micelles of silicon tetrachloride (SiCl₄) within inverse micelles. The obtained H-capped SiNPs were functionalized with allylamine using a platinum catalysed hydrosilylation reaction. They demonstrated the application of amine-terminated SiNPs in bioimaging using HeLa cells.[10] In a subsequent contribution, M Rosso-Vasic *et al* in 2009 synthesized amine-terminated SiNPs

again by the reduction of inverse micelles by capping with different amine linkers using platinum catalysed hydrosilylation.[24] They demonstrated the influence of amine groups and linker lengths on the optical properties of alkylamine-functionalized SiNPs they also determined their band gap and examined their cellular uptake by regulating their location inside the cell and the behaviour of cells after labelling.
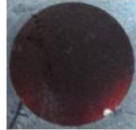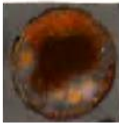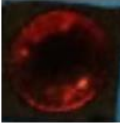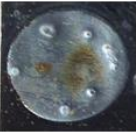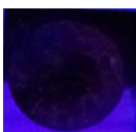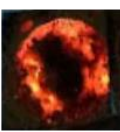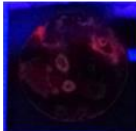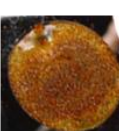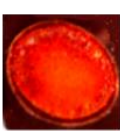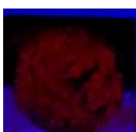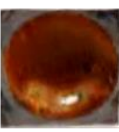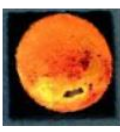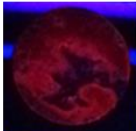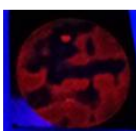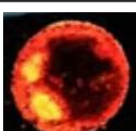
In this chapter we have demonstrated a simple room-temperature synthesis of amine-terminated SiNPs, which are soluble in water and exhibit strong blue photoluminescence. These amine-terminated SiNPs are made from H-terminated SiNPs, a common starting material ideally suited for further functionalization. The H-terminated SiNPs are cleaved from a porous layer of an electrochemically etched silicon wafer in hydrofluoric acid (HF) and ethanol in a simple and short reaction step. This is a key difference from other reported syntheses of amine-terminated SiNPs, which typically involve an intermediate step before the final capping layer which is time consuming; the chemical synthesis route leaves multiple starting material impurities in the final product which are often toxic to cells. Moreover, due to the impurities, the functionalised SiNPs lose stability in solvents and are responsible for decreasing the quantum yield of the SiNPs.

Here, a dried powder of nanoparticles can be obtained in under 4 h, at room temperature, and uses a simple metallic catalyst which is easily removed and ensures a pure final product. The advantages of using H-terminated porous SiNPs as a starting material lie in the relative simplicity of its preparation and excluding the necessary etching fluids, is a relatively environmentally friendly process. Nanoparticles are widely anticipated to be used in a growing number of commercial and clinical products and devices,[25] and so health and environmental impact of the synthesis, handling procedures and the nanoparticles themselves are likely to come under increasing scrutiny.

3.2   Synthesis of H-terminated Porous Silicon NPs

A hydrogen-terminated layer of porous silicon was formed by electrochemical etching of a boron-doped p-Si (100) as described previously in Chapter 2. In order to obtain highly luminescent H-terminated SiNPs with a good surface coverage we performed several experiments by changing the current density and time as summarized in Table 3.1.

Table 3.1: Surface morphology of Si chips etched at various current and time setting

5 min etching duration with various current setting (mA)			400mA etching with various duration (min)		
Current (mA)	Under visible light	Under UV-365 nm	Time (min)	Under visible light	Under UV-365 nm
60mA			1 min		
100mA			2.5 min		
150mA			5 min		
200mA			10 min		
250mA					
300mA					
500mA					

A layer of dark brownish luminescent porous silicon powder was obtained after cleaving the porous silicon layer from the surface of the silicon wafer by electrochemical etching using high current density (>200 mA, Table 3.1). As the current density was increased, the fluorescence of SiNPs powder changed from red to orange, as observed under illumination from a handheld mercury lamp (λ= 365 nm). These results are in agreement with other studies of porous silicon.[16, 19] At 400 mA, the amount of H-terminated SiNPs yield was increased along with increasing current density and etching time (Table 3.1). Thus, for

the best result, safety and convenience, the electrochemical etching parameter was set at 400 mA/5min throughout this work.

The obtained H-terminated SiNPs are unstable as they undergo oxidation in air; to stabilize them surface functionalization is necessary. Functionalization of SiNPs using allylamine makes them stable to oxidation and soluble in polar solvents such as water and alcohols.[7, 14]

3.3 Synthesis of Amine-terminated SiNPs Using Thermally Induced Hydrosilylation Reaction.

An attempt was made to synthesize amine terminated SiNPs using thermally induced hydrosilylation reaction. The hydrosilylation reaction mechanism was originally suggested as a radical reaction[26] in which the surface Si-H bonds add across the carbon-carbon double bonds (Briefly explained in Chapter 2). In this way the Si-C bond is formed by a silyl radical attacking the alkene causing a radical centre on the β-carbon atom to be formed. The chain then propagates over by abstraction of an H atom from the nearest-neighbour Si atom by the carbon-centred radical. The monolayer grows by addition of 1-alkenes surface to the end of a kinetic chain, which walks over the surface. This methodology has been used for synthesising alkyl capped SiNPs.[27, 28]
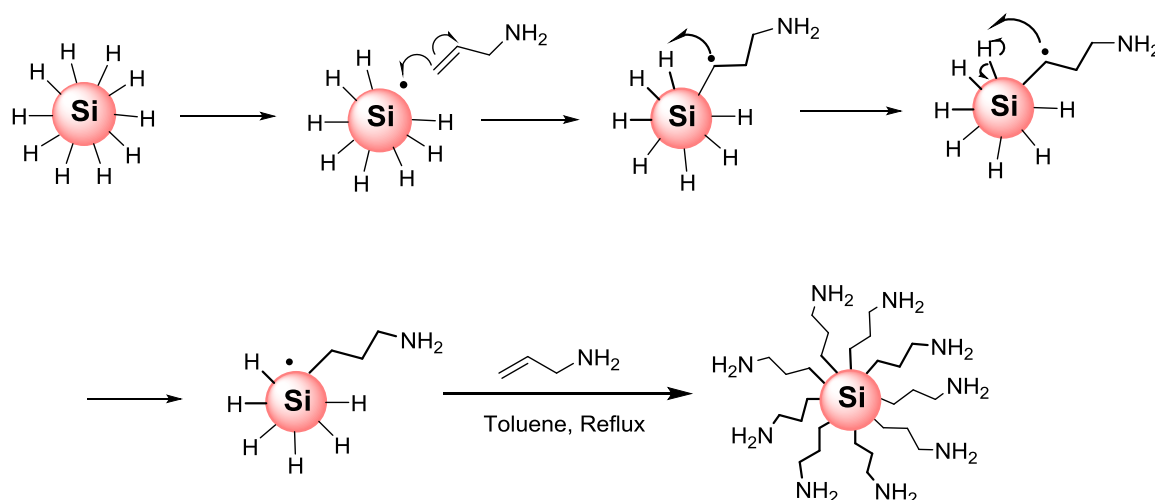
Scheme 3.1: Synthesis of Amine-terminated SiNPs using thermally induced hydrosilylation.

The H-terminated SiNPs were reacted with allylamine in refluxing toluene for 6 hr. The obtained solution was filtered and the solvent was removed under vacuum. The resulting dark brown powder was characterized by FTIR; the spectra did not show any Si-C

bonding. The time of reaction was increased from 6 hr to overnight till to up to 3 days but there was no sign of improvement.

3.4 Synthesis of Amine-terminated SiNPs Using UV Induced Hydrosilylation Reaction.

The next attempt was made to synthesize amine-terminated SiNPs using UV irradiation as described by Wayner *et al.*[29] The H-terminated porous silicon chips were introduced into allylamine diluted in ethanol in a 1% volumetric ratio. Prior to reaction, the ethanol mixture was bubbled with N_2 for one hour to remove the dissolved oxygen that could inhibit the radical-initiated reaction. The whole solution was then subjected to ultrasonic dispersion for 50 min at 40°C. The whole mixture was then kept with magnetic stirring under UV irradiation for five hours to overnight for the allylamine to react with the Si-H sites of the surface. A homemade photochemical reactor equipped with two 48 watt UV tubes was used. The temperature of the reactor chamber was kept at room temperature. After UV irradiation, the solvent of the reaction mixture was removed under vacuum and a dry sample was obtained. The resulting powder was characterized by FTIR and NMR, confirming that no reaction took place. Further attempts were made, changing solvents and temperatures but the reaction did not show any sign of improvement.

3.5 Synthesis of Amine-terminated SiNPs Using Pt catalysed Hydrosilylation

After attempting several ways to synthesize amine-terminated SiNPs, the decision was made to perform catalytic hydrosilylation reaction using Platinum catalyst (Pt). The mechanism of the hydrosilylation reaction in which the surface Si-H bond adds across the unsaturated carbon-carbon bonds, by using a metal catalyst is briefly explained in Chapter 2. The hydrosilylation of allylamine when catalysed by chloroplatinic acid (H_2PtCl_6, Speier's catalysts) in the presence of Iso-propanol is generally assumed to proceed by the Chalk-Harrod mechanism (Chapter 2).
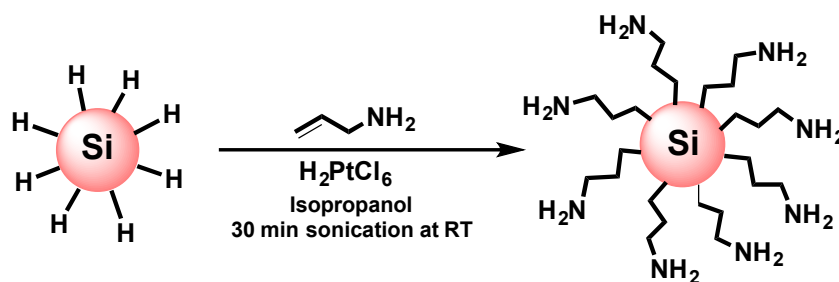
Scheme 3.2: Functionalization of H-terminated SiNPs with allylamine using Pt Catalyst.

Several reaction parameters were changed (Table 3.2) in order to obtain fully functionalized and pure amine-terminated SiNPs. Initially, after drying the H-terminated porous silicon chips, iso-propanol was added followed by H_2PtCl_6. Then allylamine was added to the Schlenk flask under N_2 and evolution of gas was immediately observed. After 2 hr of sonication, the H-terminated SiNPs dissolved and the mixture became slightly cloudy. The reaction mixture was later filtered and dried under vacuum. A dark brownish powder was obtained and characterized by FTIR. The product showed the presence of Si-C bond and proved the functionalization of amine on the surface. The reaction was improved by changing several parameters as shown in Table 3.2. It was observed that sonication time and temperature did not play any role in the reaction, unlike the sonication step applied to remove the NPs from the surface of the chips and to break them into nm size. It was also observed that using higher amounts of allylamine and catalyst did not improve the reaction. Moreover it made the purification of the final reaction mixture difficult. The best parameters were chosen to use 0.5 mL of allylamine and 40 μL of catalyst for 2 chips

Table 3.2: Synthesis of amine-terminated SiNPs by changing reaction parameters

Parameters	Si chips	Allylamine (mL)	Pt catalyst (μL)	Sonication time (min)	Temperature (°C)
Pt catalyst	1	2	80	60	RT
	1	2	40	60	RT
Allylamine	1	1.5	40	60	RT
	1	1	40	60	RT
	1	0.5	40	60	RT
Temp.	1	0.5	40	60	30
	1	0.5	40	60	45
Sonication Time	1	0.5	40	160	RT
	1	0.5	40	120	RT
	1	0.5	40	30	RT

Amine-terminated SiNPs were obtained by reacting the H-terminated SiNPs with allylamine (0.5 mL) within a Schlenk flask under N_2, in the presence of 0.05 M H_2PtCl_6 (40 μL) catalyst in iso-propanol. After 30 min of sonication, the resulting reaction mixture was filtered and dried. The obtained amine-terminated SiNPs were washed three times with dichloromethane in order to remove impurities and dried under vacuum. A solid brown powder of the amine-terminated SiNP product was obtained (Scheme 3.2). About thirty milligrams of dry powder was obtained from each reaction. This powder was re-dissolved in water for further characterization. After attachment of the amines onto the SiNPs, the surface functionalized particles become highly soluble and stable in water and also show blue-green visible photoluminescence when exposed to ultraviolet light.

3.6 Purification of Amine-terminated SiNPs

In order to achieve purity, the obtained amine-terminated SiNPs were washed with various organic solvents such as petroleum ether, diethyl ether, dichloromethane, chloroform, iso-propanol etc. The washing experiment was monitored by PL, shown in figure 3.1. It was observed that washing of the resulting product using dichloromethane successfully removed all the starting material and impurities from the products and left pure amine-capped SiNPs, which showed photoluminescence spectra under an excitation wavelength of 360 nm.
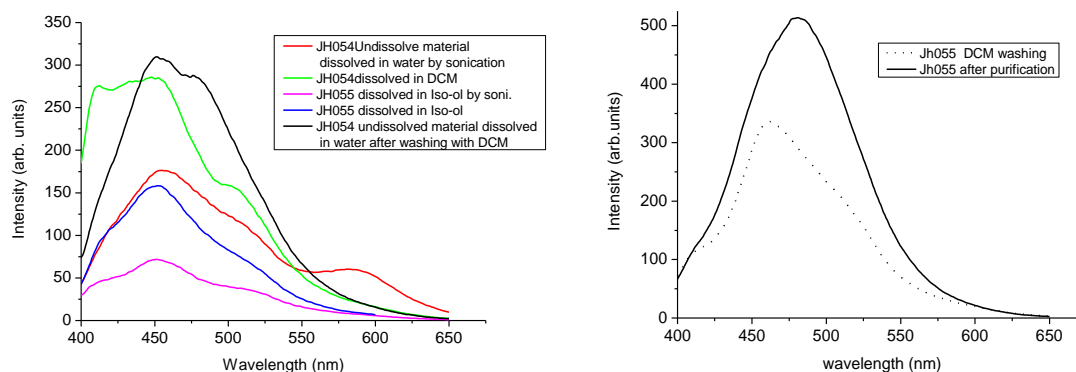
Figure 3.1: Washing experiment of amine-terminated Si NPs using various solvents.

However in later stage we noticed that all volatile starting materials could also be removed successfully under vacuum at 60°C, as the boiling points of allylamine is 53°C. After removing the starting material at 60°C, proton NMR was processed. ^{1}H NMR confirmed that all observed peaks were from the surface functionality of the SiNPs and not from free capping molecules as they have low boiling points.

3.7   Characterization of Amine-terminated SiNPs

3.7.1   Size Measurement

Following synthesis and purification, the nanoparticles were first characterized by TEM (see Chapter 2). Figure 3.1 shows the TEM and HRTEM images of amine-terminated SiNPs. All the TEM images in figure 3.2 are from similar samples but performed at different times. The TEM images show the diameter of the amine terminated NPs is around 2 nm to 8 nm. The HRTEM images show the highly crystalline structure of the atomic lattices. The lattice spacing of 0.31 nm is consistent with the Si (111) plane. Figure 3.3 shows the histogram size distribution of amine-terminated SiNPs. A mean size and size distribution of 4.6 ± 1.9 nm was obtained by analyzing 100 nanoparticles from different regions of the grid. This value is close to that of the exciton Bohr radius of silicon (4.3 nm).
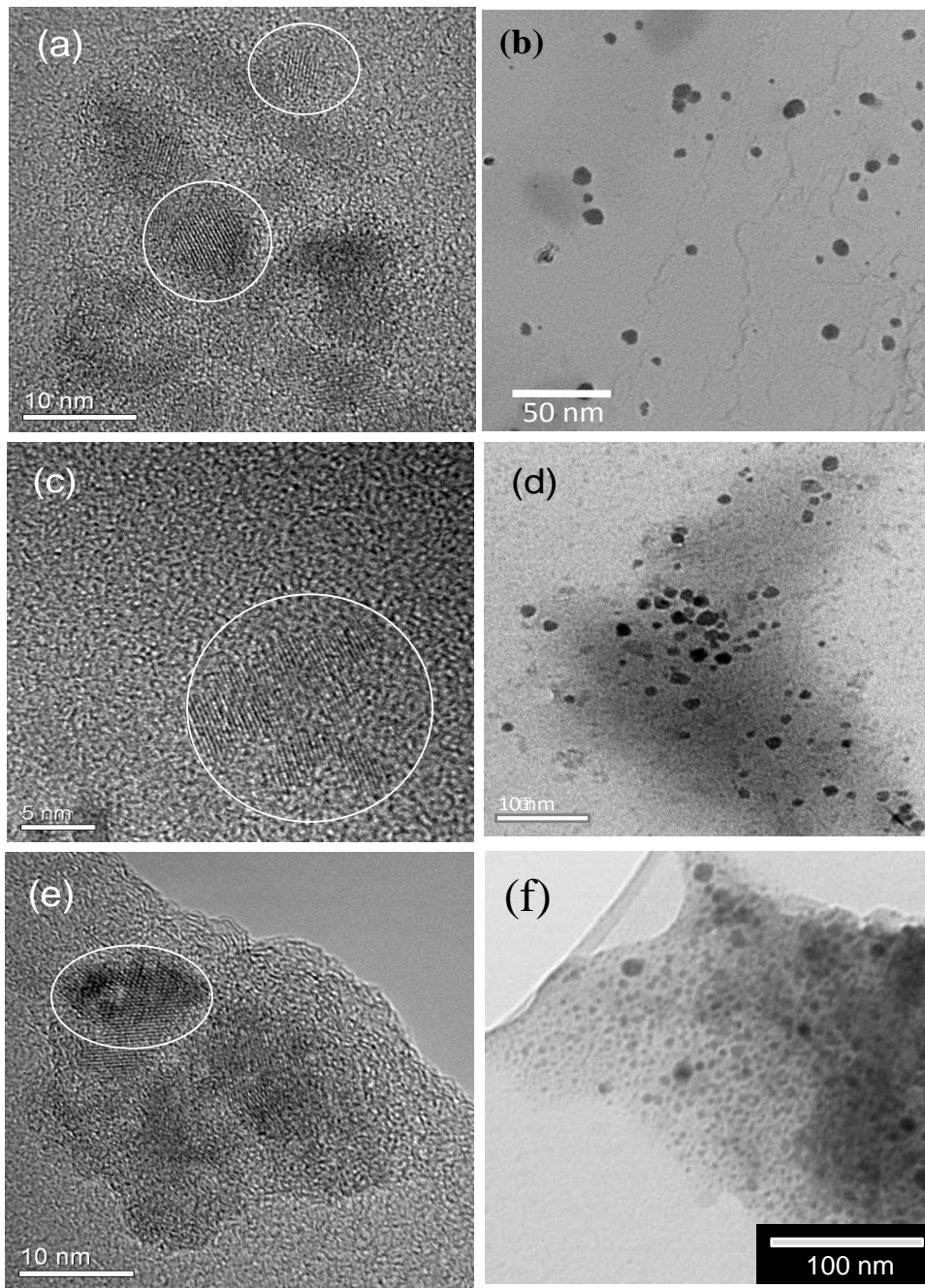
Figure 3.2: (a, c, e) shows HRTEM images of amine-terminated SiNPs. (b, d, f) shows TEM images of amine-terminated SiNPs, the white circle showing an individual silicon nanocrystal and the crystal lattice planes.
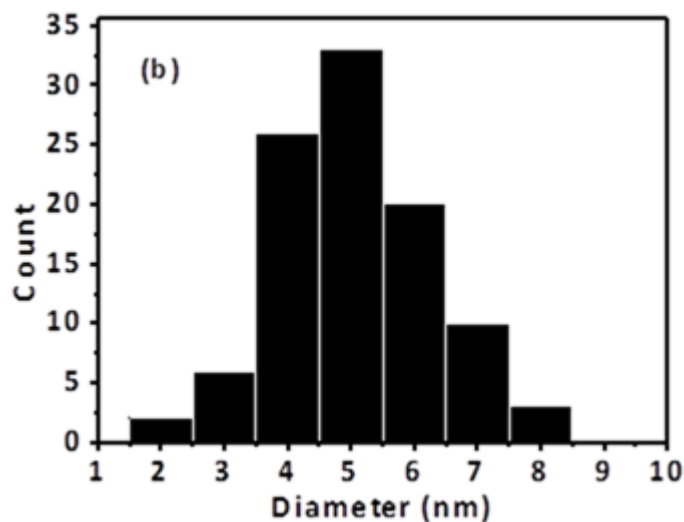
Figure 3.3: Histogram showing the size distribution of amine-terminated SiNPs.

3.7.2 DLS Measurement

Dynamic light scattering (DLS) is one of the principal characterizing techniques used to calculate the diameter of the nanoparticles in a variety of solvents (see Chapter 2). It is important to remember that DLS size distributions are a measurement of the hydrodynamic diameter of the particle and not the physical radius of the particle. Consequently, interpretation of the DLS size distributions (figure 3.4) results in measurements that appear as an overestimate of the size when compared to the data obtained by TEM. Secondly, the solvation properties of the solvent will affect the overall size. The purified NPs were dissolved in water and the effective diameters were measured at room temperature. The DLS measurements were also performed in solvents like methanol, ethanol and iso-propanol. In all solvents the SiNPs show good size distribution and do not show any sign of aggregation.
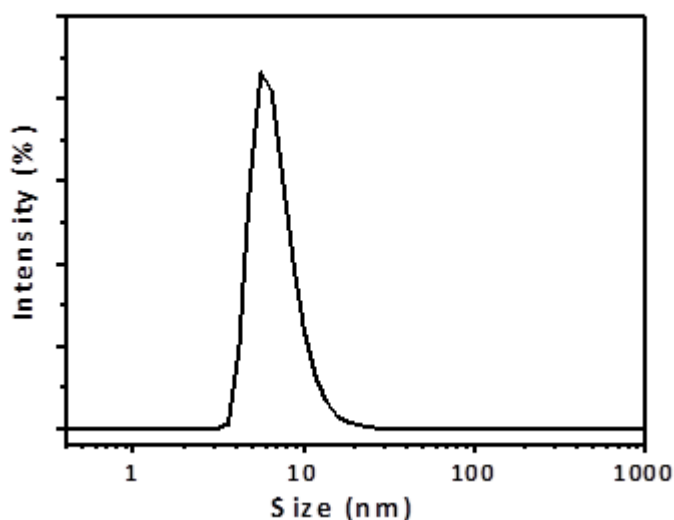
Figure 3.4: Dynamic light scattering spectrum displays the overall diameter and distribution of amine-capped SiNPs in water.

In Figure 3.4, the DLS spectrum confirms that the mean size of the amine-terminated SiNPs is 7.5 ± 1.0 nm (± is the repeatability). The mean diameter obtained from DLS is slightly larger than the one gained from TEM measurements, because the amine groups render SiNPs hydrophilicity and form a hydration shell.[30]

3.8 Chemical bonding and elemental analysis

3.8.1 IR Spectroscopy

As explained in Chapter 2 FTIR is an important technique to obtain the information of molecular bonding on the surface of the NPs. To confirm that the surface of SiNPs is covered with Si–C bonded amine moieties, it was important to perform FTIR spectra in normal transmission alignment. The aim was to carry out FTIR in both solution and solid states, to obtain clear surface bonding information of amine-terminated SiNPs. Samples were first dried under high vacuum. For FTIR in solution the dry powder was dissolved in chloroform using sonication for a few minutes (Figure 3.5) and the spectrum was obtained by subtracting chloroform background. For solid FTIR the dry powder was directly placed on the diamond crystal of the instrument and the spectrum was obtained (Figure 3.6).
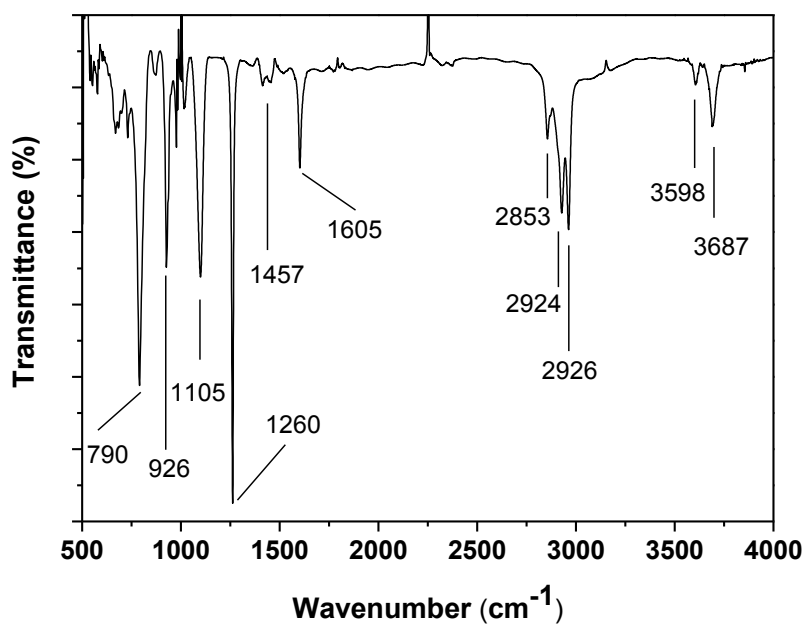
Figure 3.5: FTIR spectrum of amine-capped SiNPs in chloroform (32 scans, 4 cm⁻¹ resolution).
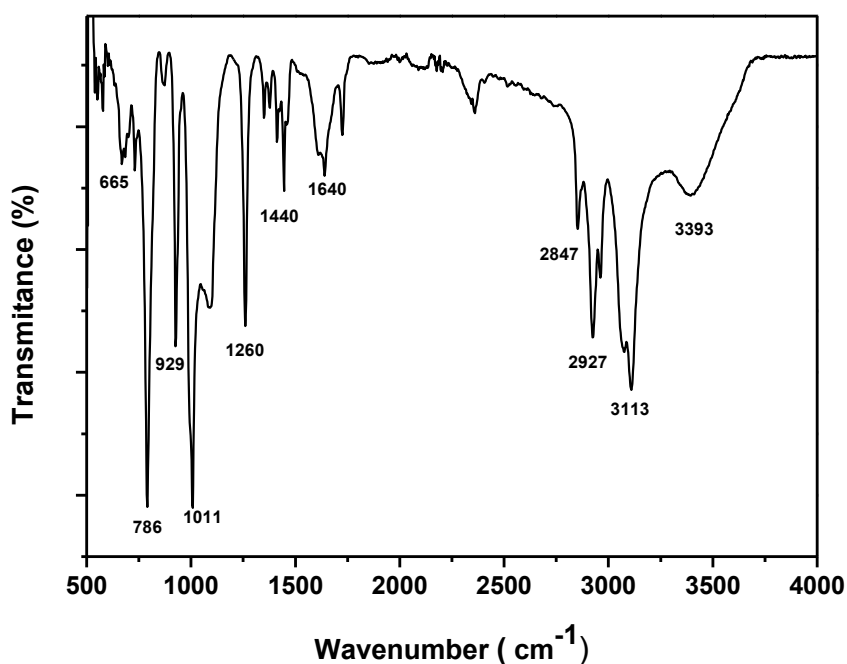
Figure 3.6: FTIR spectra of amine-terminated SiNPs in solid state (32 scans, 4 cm⁻¹ resolution).

The above FTIR spectra of amine-terminated SiNPs in solution and in the solid state are similar in terms of features. In this case the FTIR spectrum in solution showed better features of Si-C bonding at 1260 cm⁻¹ and 1457 cm⁻¹, but mostly the FTIR spectrum of amine-

terminated SiNPs in solvent shows lot of noise and background due to the solvent vaporisation in the cell. In the solid state the FTIR spectrum of amine-terminated SiNPs is always good and shows the best features.

Table 3.3: shows the molecular bonding information of amine-terminated SiNPs.

Structural Feature	Vibrational Motion	Wavenumber / cm^{-1}
Amine	N-H stretching	3500 to 3690
-CH$_2$-	C-H stretch	2853-2926
Amine	N-H scissoring	1650
Si-OR	Vibrational stretching	920-1110
Si-CH$_2$	Vibrational scissoring	1457
Si-C	Symmetric bending	1260
Amine	N-H wagging	790

From the FTIR spectrum, the observed bands at 1457 and 1260 cm^{-1} are attributed to Si-CH$_2$ vibrational scissoring and symmetric bending.[31] The features observed around 2853 to 2926 cm^{-1} are attributed to the C−H stretching of alkane. The transmittance between 3500 to 3690 cm^{-1} is assigned to the N−H stretching of an amine.[32] The band at 1605 cm^{-1} is attributed to allylamine N-H scissoring. The features between 920 and 1110 cm^{-1} are attributed to the vibrational stretching of Si-OR. The band at 790 cm^{-1} is N−H wagging. The data are summarized in table 3.3. These features highlight the strength and stability of the Si−C bond formed between the SiNPs and the allylamine as well as the minimal number of Si-OR surface bonds present.[10]

3.8.2 NMR Spectroscopy

NMR spectroscopy (see Chapter 2) is an important technique to obtain accurate information on the chemical bonding from the sample. The surface coverage with amines was also confirmed by ^{1}H NMR spectroscopy. Figure 3.7 shows the NMR spectra of amine-terminated SiNPs in D$_2$O and Figure 3.8 in chloroform. In order to perform the NMR in chloroform the sample was dried and re-dissolved in chloroform by sonication for 5 min, as it is poorly soluble in organic solvents.

A doublet of triplet (dt) peak in Figure 3.7 found between 3.38 and 3.42 ppm is attributed to the protons adjacent to the amine group.[32] The sharp singlet at 4.6 ppm corresponds to the dispersing solvent.
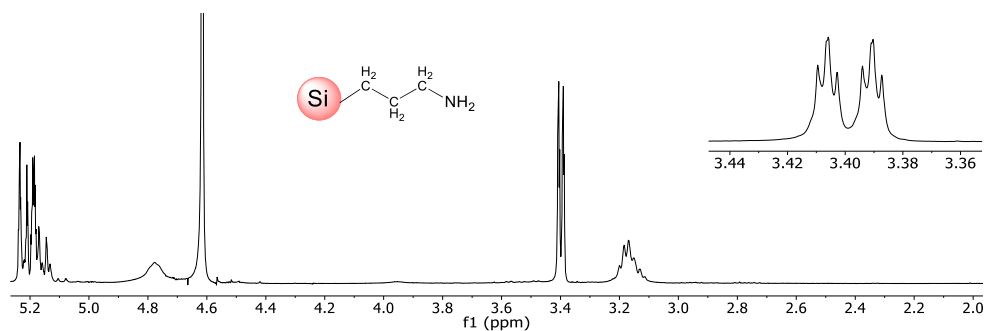
Figure 3.7: ¹H NMR spectrum of amine-terminated SiNPs in D₂O.

Similarly, the doublet of triplet (dt) peak at 3.57 ppm in Figure 3.8 arises from the protons next to the amine group, the broadening of the peak may have occurred due to the poor solubility of the amine-terminated SiNPs in chloroform. The sharp peak at 1.18 ppm is from the two protons of the amine moiety.
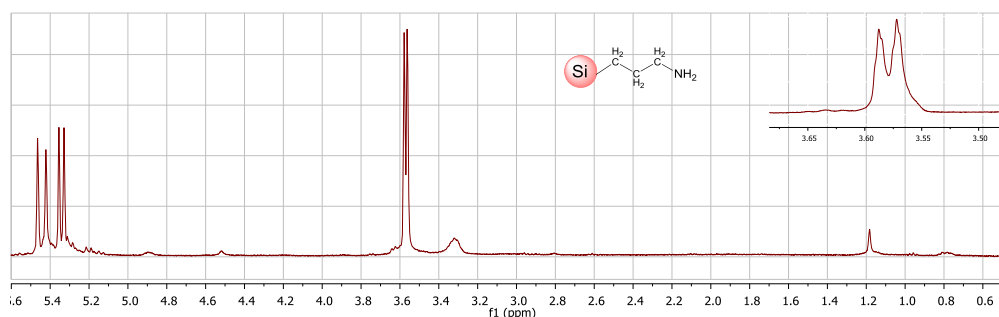
Figure 3.8: ¹H NMR spectra of amine-terminated SiNPs in CDCl₃

3.8.3 X-ray Photoelectron Spectroscopy

X-ray photoelectron spectroscopy (XPS) is an important technique for gathering information on the elements present on the surface of the SiNPs (see Chapter 2). XPS can also indicate the environment in which these elements exist. The process of analysis and identification strongly depends on the fitting of the observed peaks with Gaussians and requires care. A full survey of the photoelectron spectrum is shown in Figure 3.9.
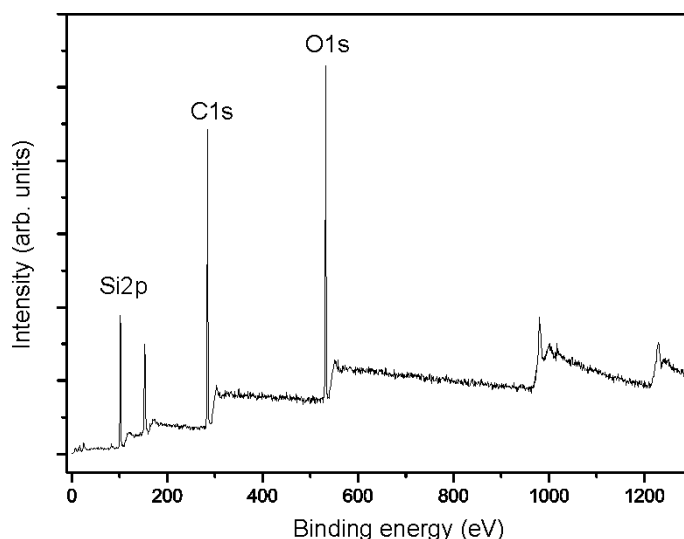
Figure 3.9: XPS survey spectrum from the film of amine-terminated SiNPs deposited on a gold substrate.

The silicon, carbon and oxygen contributions are clearly seen. The N1s peak at 399 eV (Figure 3.9) is too weak to be revealed by the single sweep of the survey scan but is resolved after multiple sweeps of the N1s energy window with small (0.02 eV) sized steps.

The surface chemical bonding was further studied using high resolution XPS spectroscopy. Figure 3.10 shows high-resolution XPS spectra of Si2p, C1s, O1s, and N1s regions of a thin film of amine-terminated SiNPs.

The O1s spectrum presented in the Figure 3.10a is fitted with two components and a Shirley background. The two components are at binding energy 532.68 and 534.23 eV respectively. The first distinct O1s peak at 532.68 eV is from Si–O group of the oxidized surface of SiNPs. The second component is possibly from hydroxide O–H group.[33]

The C1*s* spectrum present in the Figure 3.10b is fitted with three components and a Shirley background. The three peaks are at 285.13, 286.45, and 284.45 eV, respectively. The first C1s peak at binding energy 285.13 eV is assigned to C–C or C–H bonding.[34, 35] The second broad peak at 286.45 eV is ascribed to C–N bonding,[36] and the third distinct peak at binding energy 284.45 eV is attributed to the C–Si bonding.[33] The existence of a C–Si component implies that the surface of the silicon nanoparticle changed from hydrogen to amine termination.
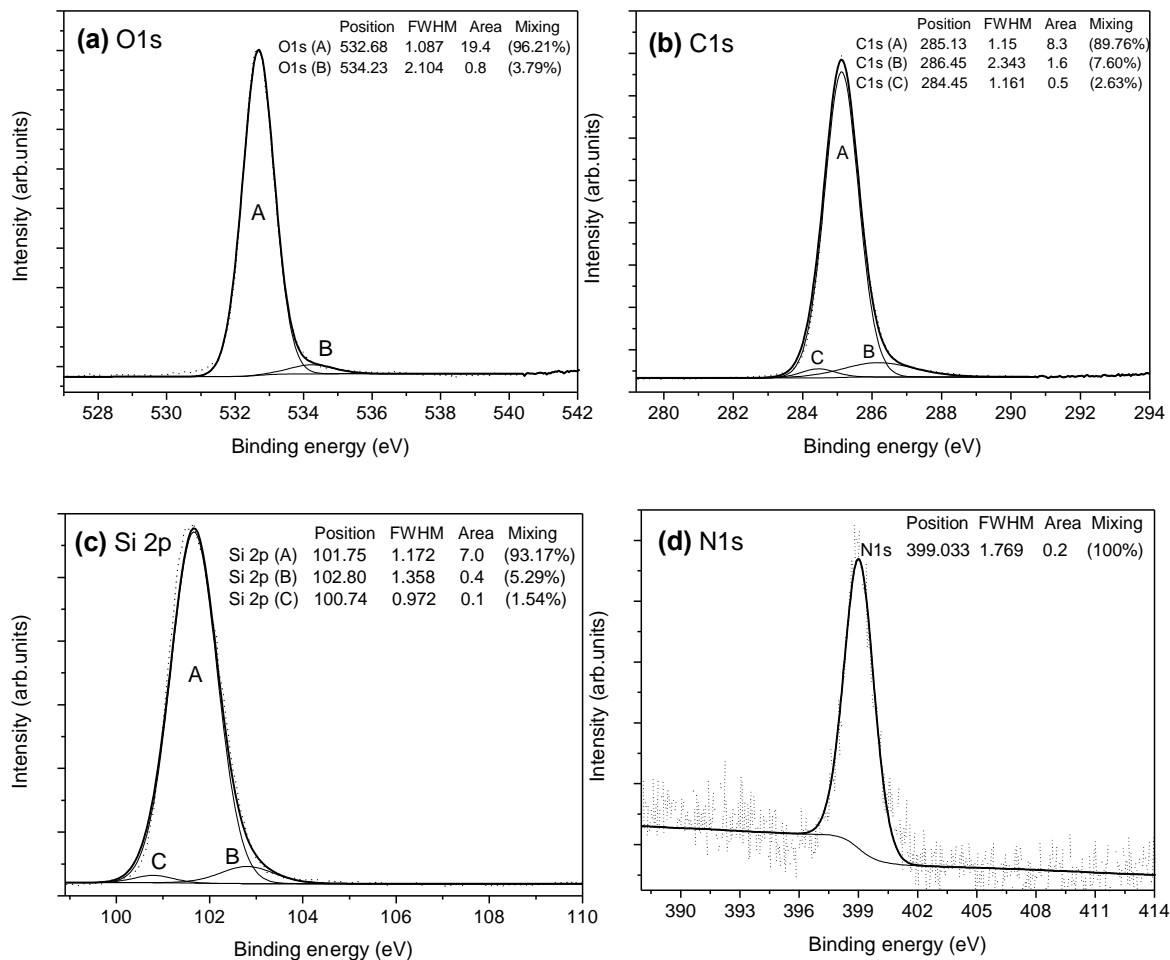
Figure 3.10: XPS core-level spectra of Si-NPs obtained at 20°C to normal emission: the dotted line is experimental data that is fitted with various mixed components. (a) O1s, photon energy 588 eV, (b) C1s, photon energy 347 eV, (c) Si2p, photon energy 150 eV, and (d) N1s, photon energy 400 eV.

The Si2p spectrum present in the Figure 3.10c is fitted with three peaks and a Shirley background. The three peaks are at 101.75, 102.80, and 100.74 eV. The first component is attributed to Si−C indicating that the surface of the SiNP is terminated with amine by replacing the hydrogen with amine. The second component is assigned to Si−O, which is indicative of the sample surface oxidation under ambient conditions. The third peak at 100.74 eV is attributed to Si−Si within the silicon core of the SiNPs.[33, 37]

The N1s spectrum presented in Figure 3.10d is fitted with a single Gaussian and a Shirley background. The broad distinct peak is at 399.03 eV is attributed to the C−N bonding of the amine-terminated SiNPs.[36]

All data presented in the above section of surface chemical bonding analysis suggest that all features appeared in FTIR, NMR and XPS are from amine-capped SiNPs, because "uncapped" SiNPs as such do not exist. Without any capping, bare SiNPs are very quickly oxidized under ambient conditions and are not biocompatible. The propensity of nanoscale structures derived from bulk silicon through electrochemical etching to undergo surface oxidation in ambient conditions is a well-known effect that has been studied with both theoretical and experimental approaches.[38-40] Given the small size of nanoparticles studied here, once they are fully oxidized, they may no longer be described as SiNPs, and should properly be described as silica NPs. For the SiNPs described here, the initial hydrogen termination layer on the etched wafer serves a dual role: first as a convenient molecular anchor point at which surface modification may be performed and second as an interim guard against oxidation in order to preserve the chemical character of the silicon core prior to subsequent functionalization steps.

3.9 Optical properties

3.9.1 Absorption and Emission Spectra

The absorption and emission spectra of amine-terminated SiNPs in water are presented in Figure 3.11. The inset shows a photograph of the amine-capped SiNPs in water under UV illumination at 254 nm.
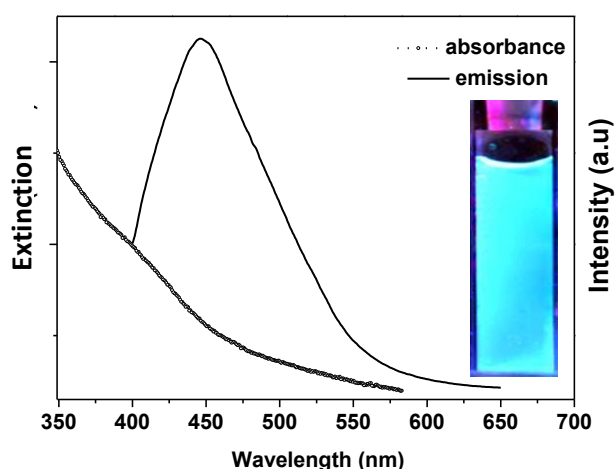
Figure 3.11: The dotted line shows the absorption spectrum of amine-capped SiNPs in water: the solid line shows the photoluminescence spectrum of amine-capped SiNPs in water at an excitation at 360 nm. The inset image shows the luminescence from a vial of amine-capped SiNPs in water when excited with a UV lamp.

The gradual increase in the absorbance with decreasing excitation wavelength from the onset wavelength of 450 nm, corresponding to the absorption edge of 2.75 eV, is characteristic of absorption across the indirect band gap of silicon.[41] The solid line shows the photoluminescence spectrum of amine-capped SiNPs in water at room temperature with the maximum emission peak centred at approximately 450 nm with a full width at half-maximum height of 107 nm under an excitation wavelength of 360 nm.

3.9.2 Quantum Yield Measurement

The luminescence quantum yield is defined as the ratio of the number of photons emitted to the number of photons absorbed by the sample. In terms of NPs it is important to know the overall fluorescence emitted by the sample. (see Chapter 2) Here, it is measured by a comparative method described by Williams *et al*.[42] The standard samples should be chosen to ensure they absorb at the excitation wavelength of choice for the test sample, as well as being well characterized in literature and suitable for such use. Photoluminescence quantum yields of the amine-capped SiNPs in water (Figure 3.12) were obtained using quinine sulfate (Figures 3.13) as a reference emitter which has the quantum yield 54.6% when dissolved in 0.5 M H_2SO_4.[43] Solutions with absorbance (also called optical densities) within 0.1 and 0.01 were prepared. The obtained gradients from the plot of the integrated fluorescence intensity *vs*. absorbance were determined for both the sample and the reference.

The quantum yield of our amine-terminated SiNPs was found to be at approximately 22 % with an excitation wavelength at 360 nm.
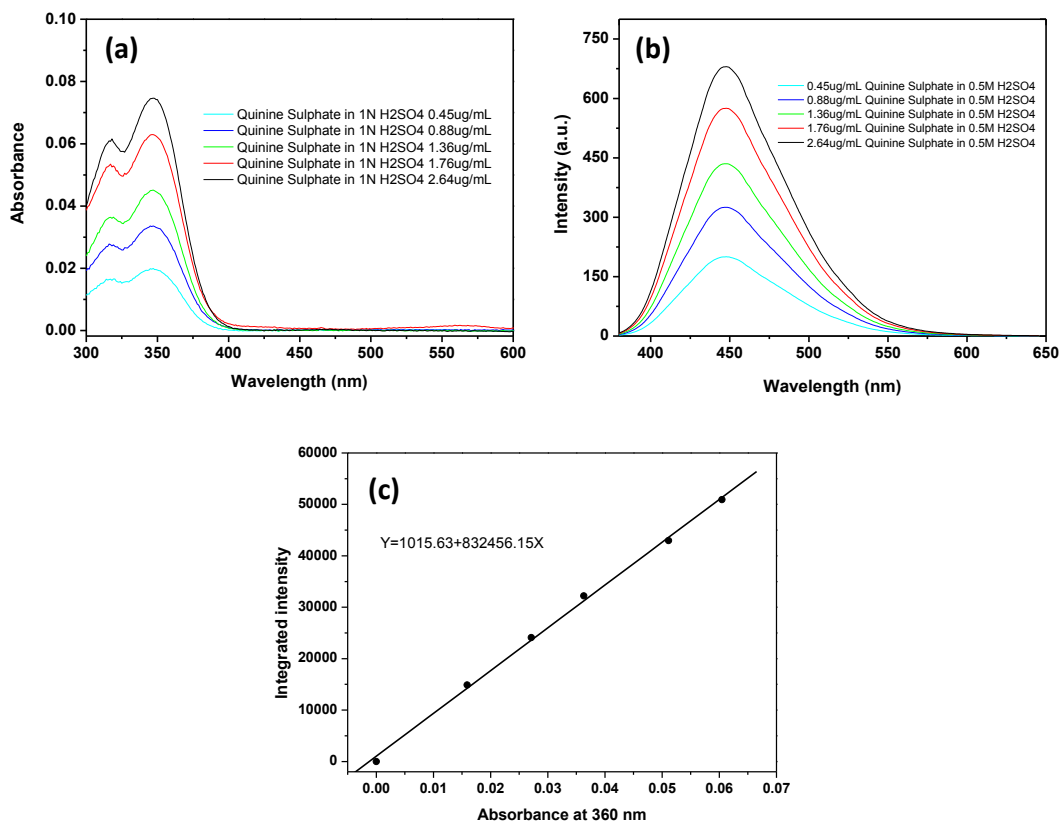
Figure 3.12: Quantum yield measurement of quinine sulphate: (a) Absorption and (b) emission spectra obtained for different concentrations of quinine sulphate, (c) Scatter plot of integrated intensity (area under emission spectrum) against absorbance at 310 nm.
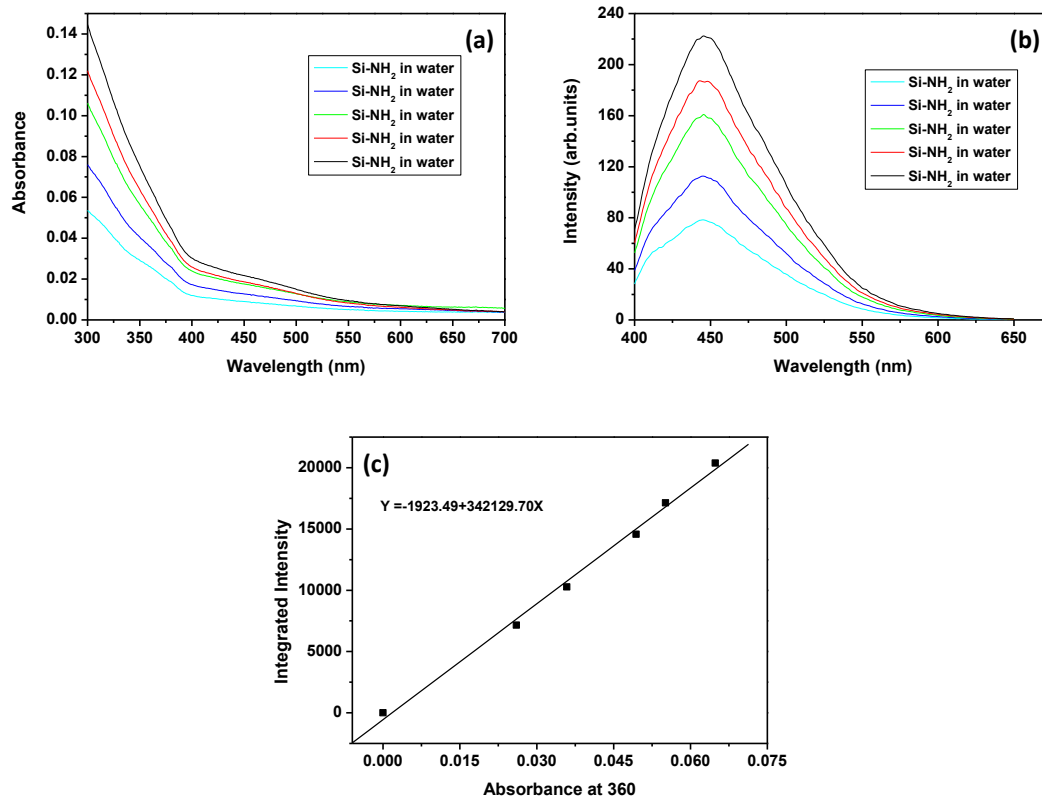
Figure 3.13: Quantum yield measurement of amine-terminated SiNPs: (a) Absorption and (b) emission spectra obtained for different concentrations of amine-terminated SiNPs, (c) Scatter plot of integrated intensity (area under emission spectrum) against absorbance at 360 nm.

The quantum yield of water soluble amine-terminated SiNPs was calculated from the following equation:

$$Q = Q_R \left(\frac{Grad}{Grad_R}\right)\left(\frac{\eta^2}{\eta_R^2}\right)$$ **Equation: 3.1**

Where **Q** is the quantum yield, **Grad** is the gradient from the plot of integrated fluorescence intensity *vs* absorbance, **η** is the refractive index of the solvent. The subscript **R** refers to the reference fluorophore of known quantum yield.

The gradient of quinine sulphate and amine-terminated SiNPs was obtained as 832456 and 342129 respectively (Figures 3.12c and 3.13c). The refractive index of both solvents were known, thus the quantum yield of the amine-terminated SiNPs can be calculated as follows:

$$Q = 54.6\% \left(\frac{342129}{832456}\right) \times \left(\frac{1.33^2}{1.346^2}\right) = 21.9\%$$

The calculated quantum yield of the amine-terminated SiNPs is about 22% with an excitation wavelength at 360 nm. The observed QY value in water is comparable to values of QY for SiNPs reported in the literature, which range from 2-18% in water.[44, 45]

3.9.3 pH effect

It is well known that the amine moiety can strongly quench the emission of semiconductor quantum dots under certain pH values,[46] so it is interesting to investigate this phenomenon to determine the effect of pH upon the emission characteristics of our amine-terminated SiNPs. With this aim, we obtained PL spectra from amine-terminated SiNPs over a range of pH environments (4 to 14) (Figure 3.14). Different pH buffer solutions were prepared using pH 4, 7 and 9 tablet and values were set up to pH 14 by adding stock solutions of 0.1M citric acid (19.2g/L) and 0.2M sodium citrate (28.4g/L). The pH of solutions was tested using pH electrode. For PL measurements, the SiNP particles were left at each pH for 2 days prior to measurement. We observed that the maximum emission peak position is independent of the pH.
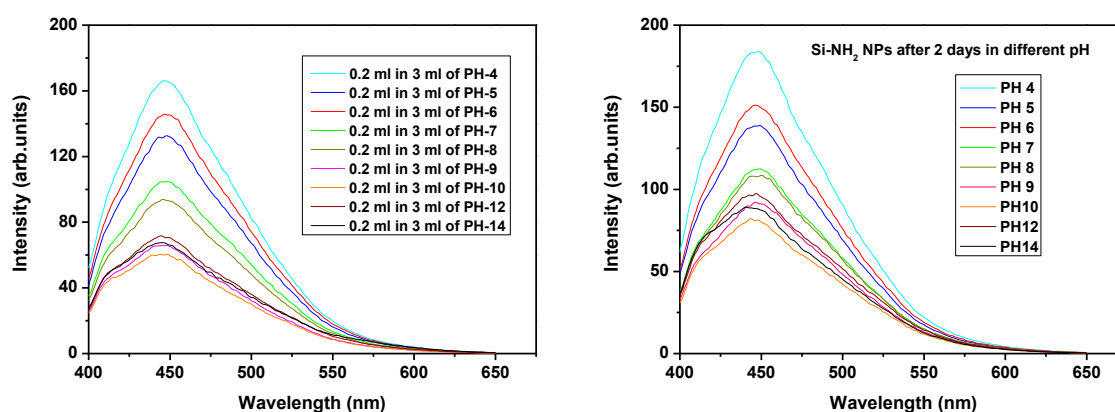
Figure 3.14 : Initial and after 2 days effect of pH onto the emission of the amine-terminated SiNPs

Figure 3.14 shows that increase in pH decreases the luminescence of amine-capped SiNPs while decreasing the pH increases the luminescence of particle. This implies that the SiNPs remain stable in extremely acidic or in basic conditions and that the emission with protonated (non-quencher) and non-protonated (quencher) amine groups originates from the same state. At low pH the amine group is protonated, and electron transfer between the amine moieties and the Si core is prohibited, yielding higher emission intensity.[24] At higher

pH protonation is either incomplete or absent, which allows involvement of the nitrogen lone pair in relaxation processes and yields a reduced emission.[24] It was consequently deemed interesting to investigate the quantum yield of amine-terminated SiNPs in acidic, basic and neutral pH. At low pH, if the fluorescence of the NPs increases then the quantum yield should also increase and at higher pH it should decrease. The quantum yield of amine-terminated SiNPs was calculated in different pH and PBS. A solution of amine-terminated SiNPs was prepared at pH-4, pH-7, pH-9 and PBS with absorbances between 0.1 and 0.01 and the gradient of the plot of integrated fluorescence intensity against absorbance was found. The quantum yield of amine-terminated SiNPs in different pH and PBS is shown in Table 3.4. As expected the quantum yield of amine-terminated SiNPs was found to decrease at higher pH (pH-9) and increase at low pH (pH-4). At low pH the quantum yield increases slightly, however decreasing pH further may perhaps increases the quantum yield of amine-terminated SiNPs and vise-versa.

Table 3.4: Quantum yields of amine-capped SiNPs in water solutions of different pH values and PBS expressed as the percentage of photons emitted per photon absorbed, using quinine sulphate as standard reference

Solvent (pH)	Quantum yield (%)
Water (4)	23±3
Water (7)	22±2
Water (9)	16±5
PBS (7)	18±5

3.9.4 Stability of amine-terminated SiNPs by PL

The lack of PL stability of nanostructured silicon is one of the major barriers to commercial applications.[45] To investigate the PL stability at different pH values, PBS and water further, time dependent PL spectra of amine-terminated SiNPs were measured by monitoring the emission using an excitation wavelength of 360 nm, Figure 3.15 and Figure 3.16.
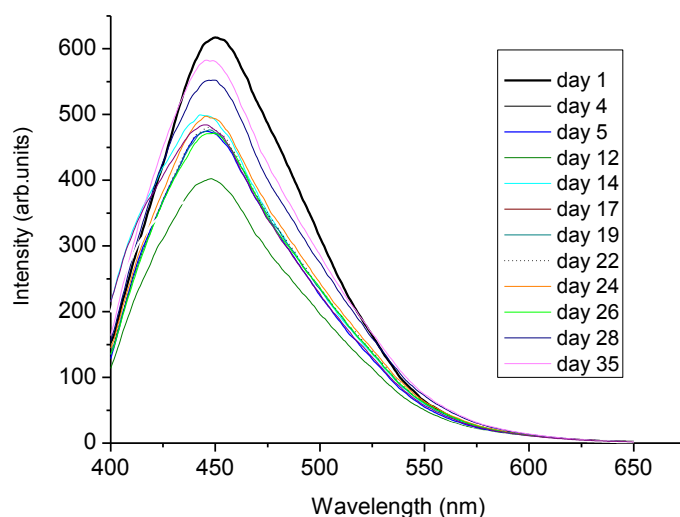
Figure 3.15: PL stability results of the amine-terminated SiNPs in water.

The photoluminescence spectrum in Figure 3.15 shows that the amine-capped SiNPs are moderately stable over a month. The above PL spectra of amine-terminated SiNPs do not show any sign of oxidation of the emission peak. The overall PL intensity slightly decreases with time but it still substantial.
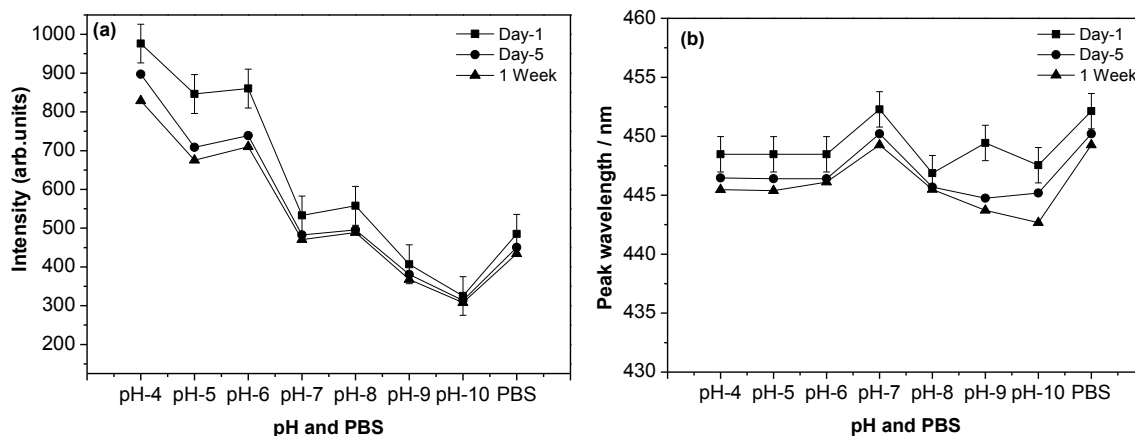
Figure 3.16: Ageing effect on luminescence spectra for amine-capped SiNPs in water at different pH values and in PBS (excitation wavelength = 360 nm): (a) peak intensity; (b) peak wavelength. The samples were stored in glass vials in the dark under ambient conditions and no attempt was made to purge the suspensions of oxygen.

The results shown in Figure 3.15 and Figure 3.16, show that the PL from amine-capped SiNPs decays over a month, but is still strong (about two thirds of initial PL intensity). This is much better than that shown by many other semiconductor QDs. Although

the monolayers formed on single crystal silicon surfaces are robust towards oxidation over long periods, it is likely that the monolayers on these small particles contain more defects or are less ordered and therefore water can penetrate to the underlying Si atoms. For SiNPs of 4-5 nm in diameter, red luminescence is common, although there remains some dispute concerning its origin. The blue shifting of the emission to blue-green observed in the NPs studied here might be indicative of surface oxidation taking place, leading to a reduction in the particle size. Similar shifting has been recently reported in small NPs (<10 nm) after treatment by laser ablation was attributed to the same reason, with PL maxima shifting from 490 nm (blue) to 425 nm.[47]

3.10 Bioimaging Studies of Amine-terminated SiNPs

Due to their visible photoluminescence, SiNPs are useful for bioimaging purposes. Amine-terminated SiNPs have a photoluminescence in the blue-green range (around 470 nm), which is useful for biological imaging. The biological experiments performed here to test the ability of amine-terminated SiNPs to permeate inside the cell were kindly performed by third year PhD student Qi Wang from our group.

Confocal microscope images are shown in Figure 3.17. The nuclei were stained with DAPI and are shown in Figure 3.17 (a). Bright fluorescence has arisen from the emission of SiNPs, see Figure 3.17 (b).
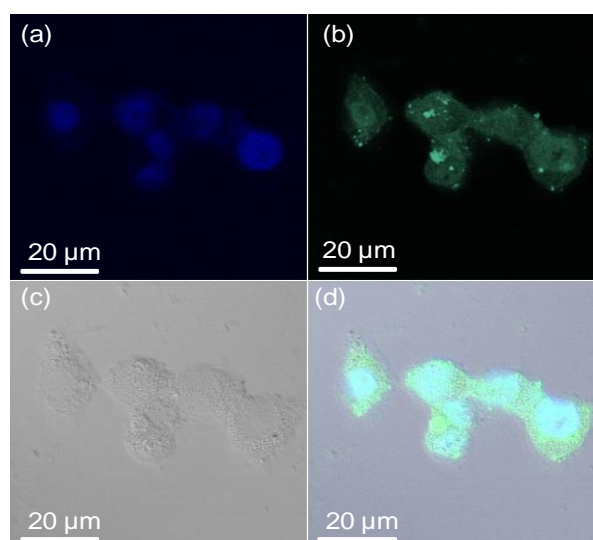
Figure 3.17: HepG2 cells observed under a confocal microscope, (a) nuclei staining with DAPI; (b) fluorescence from the amine-capped SiNPs; (c) the bright field; and (d) the combination of all three.

The image observed in bright field and merged results are also shown in Figure 3.17 (c) and (d). The fluorescence is almost evenly distributed throughout the cells. However, higher concentrations can be observed in the nuclei, where fluorescence overlaps with the DAPI stain. Importantly, no signs of morphological damage to cells were observed upon treatment with the amine-capped SiNPs in de-ionized (DI) water. Such a result is in contrast to recent studies, which suggest the positive charge of the amine-terminated surface can lead to an increase in cytotoxicity. This is a significant advance in the biological applications of SiNPs. Otherwise choosing a suitable solvent would be critical.[48, 49]

3.10.1 *In vitro* Cytotoxicity Assay

Different types of nanoparticles possess their own particular physicochemical properties, which in turn determine their potential toxicity or lack thereof. Amine capping has been applied to a variety of nanoparticles in order to render them compatible with biological media.[50] To evaluate the cytotoxicity of our synthesized nanoparticles, we performed an MTT [3-(4,5-dimethylthiazol-2-yl)-2,5-diphenyltetrazolium bromide] assay to determine cell proliferation. MTT measures mitochondrial activity within cells using tetrazolium salts as mitochondrial dehydrogenase enzymes cleave the tetrazolium ring, which occurs only in living cells. Briefly, HepG2 (human liver hepatocellular carcinoma) cells were seeded in a 96-well plate for 24 h. Then the cells were treated with amine-capped SiNPs at various concentrations (0, 1, 5, 10, 50, 100, and 200 $\mu g\ mL^{-1}$) for a period of 48 h. All experiments were repeated at least three times. After incubation the medium was removed and followed by washing the cells with phosphate buffered saline (PBS). Then, the medium was changed and incubated with the MTT solution (5 mg mL^{-1}) for 2 h. The medium was removed, and formazan was solubilized in dimethylsulfoxide (DMSO). The absorbance was recorded on a microplate reader at the wavelength of 540 nm. The percentage of viable cells was estimated by direct comparison against the untreated control cells.

There was no evidence of morphology change when the cells were observed under a phase-contrast microscope. The values of cytotoxicity induced by exposure to amine-capped SiNPs are given in Figure 3.18.
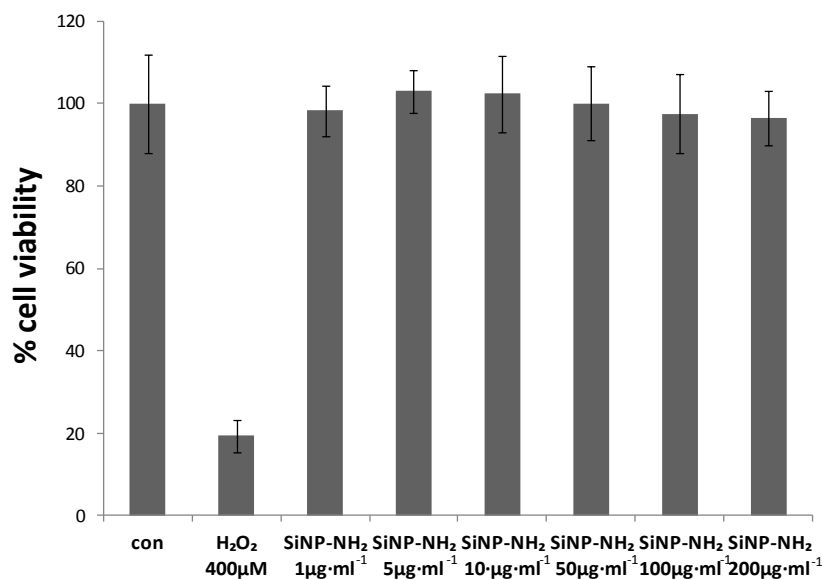
Figure 3.18: MTT assay of amine-capped SiNPs in HepG2 cells

As shown in Figure 3.18, treatment with amine-terminated SiNPs (0-200μg/mL^{-1}) did not remarkably affect the proliferation of HepG2 cells. Amine-terminated SiNPs treatment (0-200 μg/mL^{-1}) did not result in a dose-dependent inhibition of cell growth, as compared to vehicle-treated controls.

3.11 Conclusion

In conclusion, a facile method has been demonstrated to synthesize highly stable amine-terminated SiNPs by using electrochemically etched porous silicon. The surface of silicon quantum dots was effectively modified by using allylamine which conferred the silicon surface hydrophilicity. The obtained nanoparticles have a narrow size distribution and a very high mobility in water exposed by high-resolution TEM images and DLS and show strong blue photoluminescence under UV excitation with a luminescent quantum yield of 22%. These surface functionalized nanoparticles have remarkable photostability against degradation; they are stable for several weeks and demonstrate a great chemical stability over a wide pH range. The FTIR, NMR and XPS displayed the surface chemistry and confirmed that the surface is effectively modified with amine group.

Furthermore MTT assays show that amine- capped SiNPs are nontoxic to HepG2 cells. The synthesized amine-terminated SiNPs not only serve as a great tool for biomedical application but also opens a new door for further surface chemistry.

3.12 References

1.	Zhu, X.; Yukawa, T.; Kishi, T.; Hirai, M.; Suematsu, H.; Jiang, W.; Yatsui, K., Synthesis of Light-emitting Silicon Nanoparticles by Intense Pulsed ion-beam Esvaporation. *Journal of Nanoparticle Research* **2005,** *7* (6), 669-673.

2.	Nirmal, M.; Brus, L., Luminescence Photophysics in Semiconductor Nanocrystals. *Accounts of Chemical Research* **1999,** *32* (5), 407-414.

3.	Chao, Y.; Šiller, L.; Krishnamurthy, S.; Coxon, P. R.; Bangert, U.; Gass, M.; Kjeldgaard, L.; Patoleo, S. N.; Lie, L. H.; O'Farrell, N.; Alsop, T. A.; Houlton, A.; Horrocks, B. R., Evaporation and deposition of alkyl-capped silicon nanocrystals in ultrahigh vacuum. *Nature Nanotechnology* **2007,** *2* (8), 486-489.

4.	Froner, E.; Adamo, R.; Gaburro, Z.; Margesin, B.; Pavesi, L.; Rigo, A.; Scarpa, M., Luminescence of porous silicon derived nanocrystals dispersed in water: dependence on initial porous silicon oxidation. *Journal of Nanoparticle Research* **2006,** *8* (6), 1071-1074.

5.	English, D. S.; Pell, L. E.; Yu, Z.; Barbara, P. F.; Korgel, B. A., Size Tunable Visible Luminescence from Individual Organic Monolayer Stabilized Silicon Nanocrystal Quantum Dots. *Nano Letters* **2002,** *2* (7), 681-685.

6.	Belomoin, G.; Therrien, J.; Smith, A.; Rao, S.; Twesten, R.; Chaieb, S.; Nayfeh, M. H.; Wagner, L.; Mitas, L., Observation of a magic discrete family of ultrabright Si nanoparticles. *journal article* **2002,** *80* (5), 841-843.

7.	Schuppler, S.; Friedman, S. L.; Marcus, M. A.; Adler, D. L.; Xie, Y. H.; Ross, F. M.; Chabal, Y. J.; Harris, T. D.; Brus, L. E.; Brown, W. L.; Chaban, E. E.; Szajowski, P. F.; Christman, S. B.; Citrin, P. H., Size, shape, and composition of luminescent species in oxidized Si nanocrystals and H-passivated porous Si. *Physical Review B* **1995,** *52* (7), 4910.

8.	Rogozhina, E.; Belomoin, G.; Smith, A.; Abuhassan, L.; Barry, N.; Akcakir, O.; Braun, P. V.; Nayfeh, M. H., Si-N linkage in ultrabright, ultrasmall Si nanoparticles. *journal article* **2001,** *78* (23), 3711-3713.

9.	Rosso-Vasic, M.; Spruijt, E.; van Lagen, B.; De Cola, L.; Zuilhof, H., Alkyl-Functionalized Oxide-Free Silicon Nanoparticles: Synthesis and Optical Properties. *Small* **2008,** *4* (10), 1835-1841.

10.	Warner, J. H.; Hoshino, A.; Yamamoto, K.; Tilley, R. D., Water-Soluble Photoluminescent Silicon Quantum Dots. *Angewandte Chemie International Edition* **2005,** *44* (29), 4550-4554.

11.	Pelley, J. L.; Daar, A. S.; Saner, M. A., State of Academic Knowledge on Toxicity and Biological Fate of Quantum Dots. *Toxicological Sciences* **2009,** *112* (2), 276-296.

12.	Kirchner, C.; Liedl, T.; Kudera, S.; Pellegrino, T.; Muñoz Javier, A.; Gaub, H. E.; Stölzle, S.; Fertig, N.; Parak, W. J., Cytotoxicity of Colloidal CdSe and CdSe/ZnS Nanoparticles. *Nano Letters* **2004,** *5* (2), 331-338.

13.	Nilsson, J. R., How Cytotoxic is Zinc? A Study on Effects of Zinc on Cell Proliferation, Endocytosis, and Fine Structure of the Ciliate Tetrahymena. *Acta Protozool* **2003,** *42*, 19-29.

14.	Mayne, A. H.; Bayliss, S. C.; Barr, P.; Tobin, M.; Buckberry, L. D., Biologically Interfaced Porous Silicon Devices. *physica status solidi (a)* **2000,** *182* (1), 505-513.

15.   Zhou, Z.; Brus, L.; Friesner, R., Electronic Structure and Luminescence of 1.1- and 1.4-nm Silicon Nanocrystals: Oxide Shell versus Hydrogen Passivation. *Nano Letters* **2003,** *3* (2), 163-167.

16.   Zhang, X.; Neiner, D.; Wang, S.; Louie, A. Y.; Kauzlarich, S. M., A new solution route to hydrogen-terminated silicon nanoparticles: synthesis, functionalization and water stability. *Nanotechnology* **2007,** *18* (9).

17.   Neiner, D.; Chiu, H. W.; Kauzlarich, S. M., Low-temperature solution route to macroscopic amounts of hydrogen terminated silicon nanoparticles. *Journal of the American Chemical Society* **2006,** *128* (34), 11016-11017.

18.   Tilley, R. D.; Yamamoto, K., The Microemulsion Synthesis of Hydrophobic and Hydrophilic Silicon Nanocrystals. *Advanced Materials* **2006,** *18* (15), 2053-2056.

19.   Yu, Z. R.; Aceves-Mijares, M.; Cabrera, M. A. I., Single electron charging and transport in silicon rich oxide. *Nanotechnology* **2006,** *17* (15), 3962-3967.

20.   Lie, L. H.; Duerdin, M.; Tuite, E. M.; Houlton, A.; Horrocks, B. R., Preparation and characterisation of luminescent alkylated-silicon quantum dots. *Journal of Electroanalytical Chemistry* **2002,** *538-539*, 183-190.

21.   Chao, Y.; Krishnamurthy, S.; Montalti, M.; Šiller, L.; Lie, L. H.; Houlton, A.; Horrocks, B. R.; Kjeldgaard, L.; Dhanak, V. R.; Hunt, M. R. C., Reactions and luminescence in passivated Si nanocrystallites induced by vacuum ultraviolet and soft-x-ray photons. *Journal of Applied Physics* **2005,** *98* (4), 044316.

22.   Hua, F. J.; Swihart, M. T.; Ruckenstein, E., Efficient surface grafting of luminescent silicon quantum dots by photoinitiated hydrosilylation. *Langmuir* **2005,** *21* (13), 6054-6062.

23.   Hua, F.; Erogbogbo, F.; Swihart, M. T.; Ruckenstein, E., Organically Capped Silicon Nanoparticles with Blue Photoluminescence Prepared by Hydrosilylation Followed by Oxidation. *Langmuir* **2006,** *22* (9), 4363-4370.

24.   Rosso-Vasic, M.; Spruijt, E.; Popovic, Z.; Overgaag, K.; van Lagen, B.; Grandidier, B.; Vanmaekelbergh, D.; Dominguez-Gutierrez, D.; De Cola, L.; Zuilhof, H., Amine-terminated silicon nanoparticles: synthesis, optical properties and their use in bioimaging. *J. Mater. Chem.* **2009,** *19* (33), 5926-5933.

25.   Azzazy, H. M. E.; Mansour, M. M. H.; Kazmierczak, S. C., From diagnostics to therapy: Prospects of quantum dots. *Clinical Biochemistry* **2007,** *40* (13–14), 917-927.

26.   de Smet, L. C. P. M.; Zuilhof, H.; Sudhölter, E. J. R.; Lie, L. H.; Houlton, A.; Horrocks, B. R., Mechanism of the Hydrosilylation Reaction of Alkenes at Porous Silicon: Experimental and Computational Deuterium Labeling Studies. *The Journal of Physical Chemistry B* **2005,** *109* (24), 12020-12031.

27.   Coxon, P. R., Studies of Silicon and Carbon Nanomaterials by Electron and X-ray Spectroscopies. *Ph.D. thesis, Newcastle University* **2010**.

28.   de Smet, L. C., Covalently Bound Organic Monolayers on Silicon Surfaces. *Ph.D. thesis, Wageningen Universiteit.* **2006**.

29.   Wayner, D. D. M.; Wolkow, R. A., Organic modification of hydrogen terminated silicon surfaces1. *Journal of the Chemical Society, Perkin Transactions 2* **2002,** (1), 23-34.

30.   Wang, Q.; Bao, Y.; Zhang, X.; Coxon, P. R.; Jayasooriya, U. A.; Chao, Y., Uptake and Toxicity Studies of Poly-Acrylic Acid Functionalized Silicon Nanoparticles in Cultured Mammalian Cells. *Advanced Healthcare Materials* **2012,** *1*, 189-198.

31.	Wang, J.; Sun, S.; Peng, F.; Cao, L.; Sun, L., Efficient one-pot synthesis of highly photoluminescent alkyl-functionalised silicon nanocrystals. *Chemical Communications* **2011,** *47* (17), 4941-4943.

32.	Shiohara, A.; Hanada, S.; Prabakar, S.; Fujioka, K.; Lim, T. H.; Yamamoto, K.; Northcote, P. T.; Tilley, R. D., Chemical Reactions on Surface Molecules Attached to Silicon Quantum Dots. *Journal of the American Chemical Society* **2009,** *132* (1), 248-253.

33.	Chao, Y.; Wang, Q.; Pietzsch, A.; Hennies, F.; Ni, H., Soft X-ray induced oxidation on acrylic acid grafted luminescent silicon quantum dots in ultrahigh vacuum. *Physica Status Solidi a-Applications and Materials Science* **2011,** *208* (10), 2424-2429.

34.	Wagner, C.; Riggs, W.; Davis, L.; Moulder, J., Handbook of X-ray photoelectron spectroscopy. In *Handbook of X-ray photoelectron spectroscopy*, Muilenberg, G. E., Ed. Perkin Elmer Corporation: Eden Prairie, Minnesota, 1997.

35.	*X-ray data booklet.* Lawrence Berkeley National Lab: Berkeley, 2001.

36.	Dementjev, A. P.; de Graaf, A.; van de Sanden, M. C. M.; Maslakov, K. I.; Naumkin, A. V.; Serov, A. A., X-Ray photoelectron spectroscopy reference data for identification of the C3N4 phase in carbon-nitrogen films. *Diamond and Related Materials* **2000,** *9* (11), 1904-1907.

37.	Wang, Q.; Ni, H.; Pietzsch, A.; Hennies, F.; Bao, Y.; Chao, Y., Synthesis of water-dispersible photoluminescent silicon nanoparticles and their use in biological fluorescent imaging. *Journal of Nanoparticle Research* **2011,** *13* (1), 405-413.

38.	Wolkin, M. V.; Jorne, J.; Fauchet, P. M.; Allan, G.; Delerue, C., Electronic States and Luminescence in Porous Silicon Quantum Dots: The Role of Oxygen. *Physical Review Letters* **1999,** *82* (1), 197-200.

39.	Šiller, L.; Krishnamurthy, S.; Kjeldgaard, L.; Horrocks, B. R.; Chao, Y.; Houlton, A.; Chakraborty, A. K.; Hunt, M. R. C., Core and valence exciton formation in x-ray absorption, x-ray emission and x-ray excited optical luminescence from passivated Si nanocrystals at the Si L-2,L-3 edge. *Journal of Physics-Condensed Matter* **2009,** *21* (9), 095005.

40.	Coxon, P. R.; Wang, Q.; Chao, Y., An abrupt switch between the two photoluminescence bands within alkylated silicon nanocrystals. *Journal of Physics D: Applied Physics* **2011,** *44* (49), 495301.

41.	Sato, S.; Swihart, M. T., Propionic-Acid-Terminated Silicon Nanoparticles: Synthesis and Optical Characterization. *Chemistry of Materials* **2006,** *18* (17), 4083-4088.

42.	Williams, A. T. R.; Winfield, S. A.; Miller, J. N., Relative fluorescence quantum yields using a computer-controlled luminescence spectrometer. *Analyst* **1983,** *108* (1290), 1067-1071.

43.	Xiong, H. M.; Wang, Z. D.; Xia, Y. Y., Polymerization Initiated by Inherent Free Radicals on Nanoparticle Surfaces: A Simple Method of Obtaining Ultrastable (ZnO)Polymer Core–Shell Nanoparticles with Strong Blue Fluorescence. *Advanced Materials* **2006,** *18* (6), 748-751.

44.	Erogbogbo, F.; Yong, K.-T.; Roy, I.; Xu, G.; Prasad, P. N.; Swihart, M. T., Biocompatible Luminescent Silicon Quantum Dots for Imaging of Cancer Cells. *ACS Nano* **2008,** *2* (5), 873-878.

45.	Warner, J. H.; Hoshino, A.; Yamamoto, K.; Tilley, R. D., Water-soluble photoluminescent silicon quantum dots. *Angewandte Chemie-International Edition* **2005,** *44* (29), 4550-4554.

46.   Landes, C. F.; Braun, M.; El-Sayed, M. A., On the nanoparticle to molecular size transition: Fluorescence quenching studies. *Journal of Physical Chemistry B* **2001,** *105* (43), 10554-10558.

47.   Alkis, S.; Okyay, A. K.; Ortac, B., Post-Treatment of Silicon Nanocrystals Produced by Ultra-Short Pulsed Laser Ablation in Liquid: Toward Blue Luminescent Nanocrystal Generation. *Journal of Physical Chemistry C* **2012,** *116* (5), 3432-3436.

48.   Alsharif, N. H.; Berger, C. E. M.; Varanasi, S. S.; Chao, Y.; Horrocks, B. R.; Datta, H. K., Alkyl-Capped Silicon Nanocrystals Lack Cytotoxicity and have Enhanced Intracellular Accumulation in Malignant Cells via Cholesterol-Dependent Endocytosis. *Small* **2009,** *5* (2), 221-228.

49.   Dickinson, F. M.; Alsop, T. A.; Al-Sharif, N.; Berger, C. E. M.; Datta, H. K.; Siller, L.; Chao, Y.; Tuite, E. M.; Houlton, A.; Horrocks, B. R., Dispersions of alkyl-capped silicon nanocrystals in aqueous media: photoluminescence and ageing. *Analyst* **2008,** *133* (11), 1573-1580.

50.   Lee, S. H.; Bae, K. H.; Kim, S. H.; Lee, K. R.; Park, T. G., Amine-functionalized gold nanoparticles as non-cytotoxic and efficient intracellular siRNA delivery carriers. *International Journal of Pharmaceutics* **2008,** *364* (1), 94-101.

4 Synthesis of Carbohydrate Capped Silicon Nanoparticles

for selective targeting of cancer cells
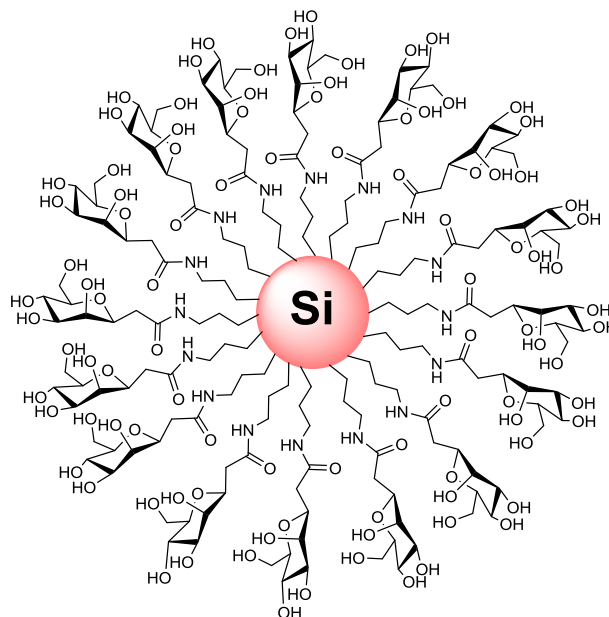
Part of this chapter is published as:

4.1 Introduction and Motivation

Over the past decade, there has been a great deal of interest in the fabrication, characterization and application of nanomaterials, which show potential development in the diagnosis and treatments of diseases.[1-4] Improved understanding at the cellular and molecular level has led us towards using more specific and targeted nano-therapies. Recently tremendous advances have been made in recruiting sugar-functionalized nanocomposites for biological applications following the recognition of the important and multi-faced role carbohydrates play in many biological systems.[5-7] Naturally occurring carbohydrates, glycoproteins and glycolipids present at the surface of cells play crucial roles in biological events, acting as recognition sites between cells. As mentioned in the Introductory Chapter 1, carbohydrates can trigger various phenomena such as cell growth, inflammatory responses or viral infections. Surface-exposed carbohydrate moieties that are characteristic of a given microbe may serve as key biomarkers for bacteria and pathogen identification, diagnosis, and vaccine development. Carbohydrates, as a detection platform, have already demonstrated tremendous potential to achieve superior sensitivity and selectivity.[8, 9] At present, carbohydrate-functionalized glyconanomaterials are finding many important applications in explaining carbohydrate protein interactions and cell-cell communication.[10-14]

Identifying, quantifying and imaging the carbohydrates, glycoproteins and glycolipids are critical both for elucidating their biological function and for the evaluation and design of therapeutics. In order to understand the potential of carbohydrates in diagnostics and therapeutic applications, several obstacles need to be overcome.

The interaction between a single carbohydrate and its receptor is usually weak, however nature solves this problem by simultaneously engaging multiple ligands for binding,[14, 15] leading to enhanced affinity through the multivalency effect.[16] Thus, a suitable platform is required to display carbohydrates in a polyvalent format in order to improve the binding strength and selectivity. The second challenge is that unlike the lock-and-key type of specific molecular recognition common in antigen and antibody binding,[17] there can be several types of receptors recognizing the same carbohydrate ligand. Strategies need to be developed to differentiate these receptors. The third challenge relates to the availability of pure carbohydrates for biological studies. It is difficult to purify large quantities of complex oligosaccharides from natural sources due to the heterogeneity of carbohydrates on cell surfaces and proteins. Although chemical and enzymatic synthesis of oligosaccharides and glyco-conjugates has undergone tremendous progress,[18] it is still restricted to specialized

laboratories. Therefore, to realize the full potential of carbohydrates in biomedical applications requires a multi-disciplinary approach bringing together glyco-biologists, material chemists and synthetic chemists.

Over the past decade, nanotechnology has played an important role in cancer research and advances in nanoresearch have led to the development of novel nanoparticles (NPs) where size, geometry, and surface functionality can be controlled at the nanoscale.[19, 20] Using antibody-immobilized nanoparticles, various types of cancer cells were detected both *in Vitro* and *in Vivo*. For instance Lin *et al*. fabricated mannose-coated gold NPs and studied the selective binding to type 1 pili in *Escherichia coli*,[21] which presented a novel method of labelling specific proteins on the cell surface.[22] Syková et al. showed that mannose-modified iron oxide NPs were efficient probes for labelling stem cells.[23] The Penadés group prepared a small library of multivalent Au-NPs functionalized with different structural fragments of the high mannose undecasaccharide of gp120 in various ligand densities and evaluated their effects on the inhibition of HIV glycoprotein gp120 binding to DC-SIGN expressing cells.[24] Besides imaging applications, the Penadés group reported the utilization of Lacto-AuNPs as potent inhibitors of tumor metastasis in mice and evaluated their potential as anti-adhesive tools against metastasis progression.[25] The mouse melanoma B16F10 cells are known to bind with lactose, presumably due to the presence of cell surface lectins such as galectins. Pre-incubation of the B16F10 cells with the Lacto-AuNPs prior to injections into mice substantially inhibited the lung metastasis of the tumor (up to 70%).

Silicon nanoparticles hold prominent interest in various aspects of biomedical research. For instance current fields of interest range from imaging, detection, drug delivery and new therapeutic uses.[26, 27] Their fluorescence signatures,[28-30] high quantum efficiency,[31] size-dependent tunable light emission,[29, 30, 32] high brightness[33] and stability against photobleaching compared to organic dye molecules make them ideal tools for fluorescence imaging.[34, 35] These properties have helped to establish silicon based nanoparticles in a swathe of diagnostic and assay roles as fluorescent cellular markers.[36, 37] Furthermore, silicon exhibits a low inherent toxicity when compared with the heavy elements of several other types of semiconductor quantum dots, which can pose significant risks to human health.[36, 38-40] The overall combination of these properties of SiNPs opens up new avenues of applications in optoelectronics and bioimaging.[41-43]

In this chapter the first synthesis of stable and brightly luminescent carbohydrates capped SiNPs is demonstrated. Various types of carbohydrate capped SiNPs such as β-D-Mannose (Man), β-D-Galactose (Gal), β-D-Glucose (Glu) and β-D-Lactose (Lac) capped SiNPs

were synthesized from amine-terminated SiNPs and the corresponding pyranosyl acid. The surface functionalization was confirmed by FTIR, NMR XPS and energy dispersive x-ray spectroscopy (EDX) studies. The mean diameter of the crystal core was measured by TEM, while the hydrodynamic diameter was obtained by dynamic light scattering (DLS). The variety of these carbohydrate capped SiNPs constitute a good bio-mimetic model for carbohydrate presentation on the cell surface, and may prove to be an excellent tool for further glycobiology, biomedicine and material science investigations. Proof-of-principle experiments are carried out using Concanavalin A (Con A) as the target protein. Furthermore the Man functionalized SiNPs were verified inside MCF-7 (human breast cancer cells) cells.

4.2 Carbohydrate capped SiNPs NPs from Hydrosilylation

Initially the carbohydrate capped SiNPs were designed to synthesized using a hydrosilylation reaction (scheme 4.1).

Gal: R_1,R_4 = H; R_2,R_3 = OAc
Man: R_2,R_3 = H; R_1,R_4 = OAc
Glu: R_1,R_3 = H; R_2,R_4 = OAc

Hydrogen capped SiNPs

Gal: R_1,R_4 = H; R_2,R_3 = OAc
Man: R_2,R_3 = H; R_1,R_4 = OAc
Glu: R_1,R_3 = H; R_2,R_4 = OAc
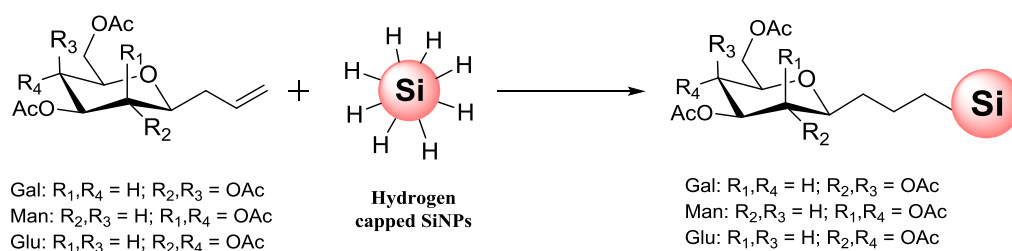
Scheme 4.1: Schematic representation to synthesize carbohydrate capped SiNPs from hydrosilylation reaction.

As explained in chapter 3 the hydrosilylation reaction can be carried out in several ways such as thermally induced, UV induced or using metal catalyst, in which the surface of Si-H bonds add across the carbon-carbon double bond. To proceed for a hydrosilylation reaction it was necessary to synthesize and functionalize carbohydrate derivatives with allyl groups.

4.2.1 Acetylation Reaction

All allyl functionalized carbohydrate synthesis was carried out using a method published by Deming and Kramer.[44]

Formation of both α-and β-anomers are common in glycopeptides and glycoproteins.[45] Although the purification methodology allows using of either anomer, we chose to use the β-anomers as they were easily obtained in high purity.

Gal: $R_1, R_4 = H$; $R_2, R_3 = OH$
Man: $R_2, R_3 = H$; $R_1, R_4 = OH$
Glu: $R_1, R_3 = H$; $R_2, R_4 = OH$

1a: Gal: $R_1, R_4 = H$; $R_2, R_3 = OAc$
2a: Man: $R_2, R_3 = H$; $R_1, R_4 = OAc$
3a: Glu: $R_1, R_3 = H$; $R_2, R_4 = OAc$
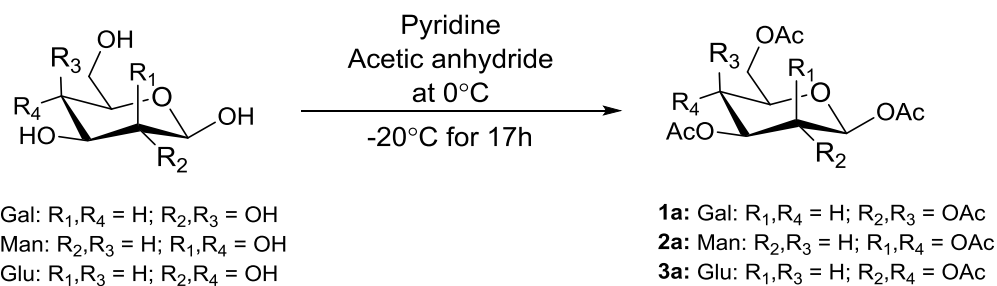
Scheme 4.2: Acetylation of carbohydrates derivatives.

4a
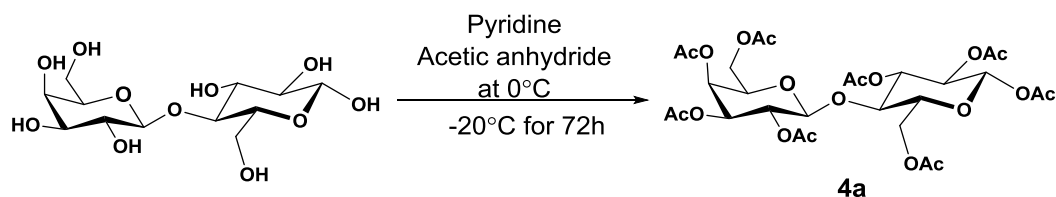
Scheme 4.3: Acetylation of Lactose sugar.

In order to functionalize the sugar with allyl group it is important to protect the hydroxyl group of the sugar. Different types of protecting groups can be used to protect the carbohydrate, such as alkyl ether type, benzoyl (Bz), trimethylacetyl type (Piv), trifluoroacetyl (TFA), silyl based etc. depending on the reaction and reaction conditions chosen. The acetate protection reaction for mannose, glucose and galactose was fast as compared with lactose. The overall yield for all monosaccharide was high (96% yield) compared to lactose (<50%).

4.2.2 Allylation Reaction

1a: Gal: $R_1, R_4 = H$; $R_2, R_3 = OAc$
2a: Man: $R_2, R_3 = H$; $R_1, R_4 = OAc$
3a: Glu: $R_1, R_3 = H$; $R_2, R_4 = OAc$

1b: Gal 75 %
2b: Man 65 %
3b: Glu 54%
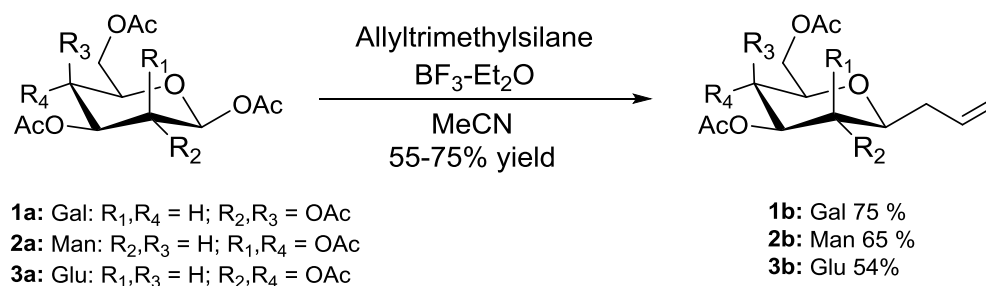
Scheme 4.4: Allylation reaction of carbohydrates derivatives
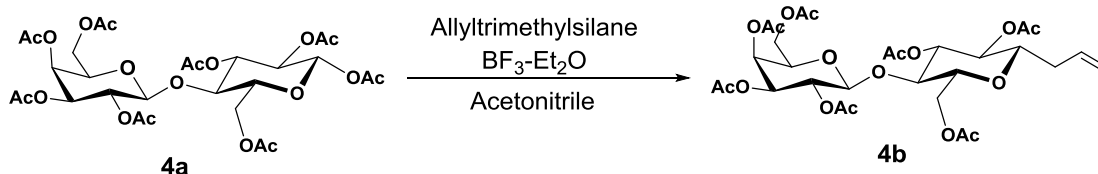
Scheme 4.5: Allylation reaction of Lactose heptaacetate.

Allylation of glu, man, gal pentaacetate and lac heptaacetates was accomplished according to literature procedures and the pure *β*-anomers (Chapter 2) were isolated.[44] Purification of the anomers at this stage in the synthesis is crucial for the ultimate preparation of optically pure, glyco monomers. The anomers were purified by column chromatography (see Chapter 2). Mixtures of anomers would lead to SiNPs containing different sugar configurations, which could make analysis of their properties difficult.

4.2.3   Attempted Thermally induced Hydrosilylation reaction

The hydrosilylation reaction mechanism in which the surface of Si-H bond adds across the carbon-carbon double bonds was mentioned in Chapter 3 (section 3.3). The reaction was first attempted using allyl galactose synthesized as per scheme 4.4
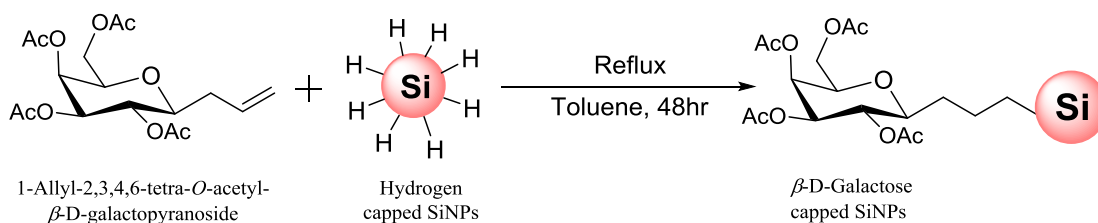
Scheme 4.6: Attempted Hydrosilylation reaction of carbohydrates derivatives.

The allyl galactose was reacted with H-terminated SiNPs under a nitrogen atmosphere by heating at reflux in dry toluene. The resulting reaction mixture did not show any evidence of product characterized by FTIR. Moreover the FTIR showed disappearance of acetate (OAc) peaks and appearance of hydroxy (-OH) peaks at around 3400 cm^{-1} which suggested using different protection group for carbohydrate.

It was decided to use *tert*-butyldimethylsilyl (TBDMS) group. Scheme 4.7 shows the protection of carbohydrate derivative with TBDMS group.
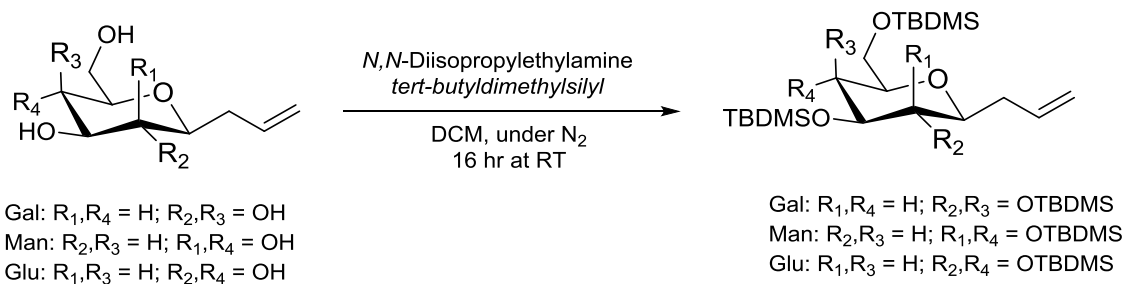
Scheme 4.7: TBDMS protection to carbohydrate derivative.

The allyl galactose was protected with *tert*-butyldimethylsilyl (TBDMS) groups (scheme 4.7). TBDMS protecting groups are particularly useful because they can be installed and removed selectively under mild reaction conditions.
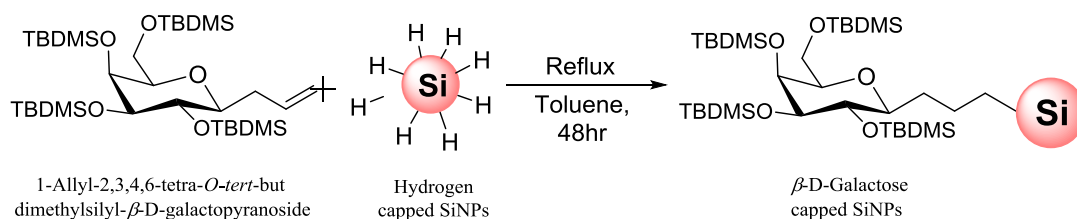
Scheme 4.8: Attempted synthesis of gal capped SiNPs by protecting with TBDMS

The reaction was repeated using TBDMS protecting groups but unfortunately did not show any evidence of the expected product.

4.2.4 Attempted Hydrosilylation reaction using Pt catalyst
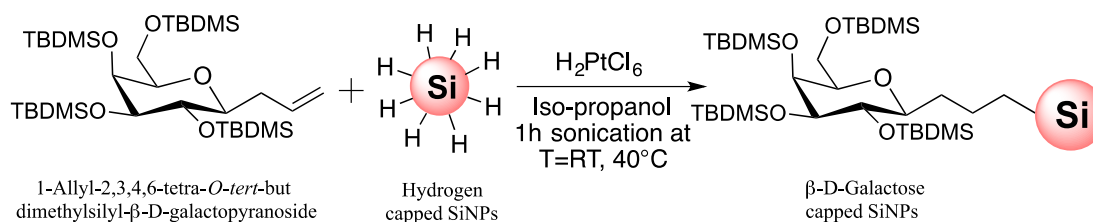
Scheme 4.9: Synthesis of Galactose capped SiNPs using Pt catalyst

The hydrosilylation was attempted using a metal catalyst, chloroplatinic acid (H_2PtCl_6), in the presence of iso-propanol for 1 hour sonication (Scheme 4.9). Initially the reaction was carried out at room temperature and sonication for 1 hour, unfortunately the

resulting reaction mixture did not show any improvement. Additionally it was noticed that the red luminescence from the H-terminated SiNPs was disappearing after the addition of the Pt catalyst. After increasing the temperature, the reaction mixture turned black with complete loss of the red luminescence. FTIR indicated that the desired reaction had not occurred.

4.3   Carbohydrates capped SiNPs Using Amine-terminated SiNPs

After several unsuccessful attempts, it was decided to make use of previously synthesized amine-terminated SiNPs and perform an amidation reaction. For that purpose the carbohydrates were functionalized with carboxylic acid and reacted with amine-terminated SiNPs using various coupling reagents (Scheme 4.10). Scheme 4.10 represents the synthetic route to carbohydrates capped SiNPs from amine-terminated SiNPs and corresponding pyranosyl acid.
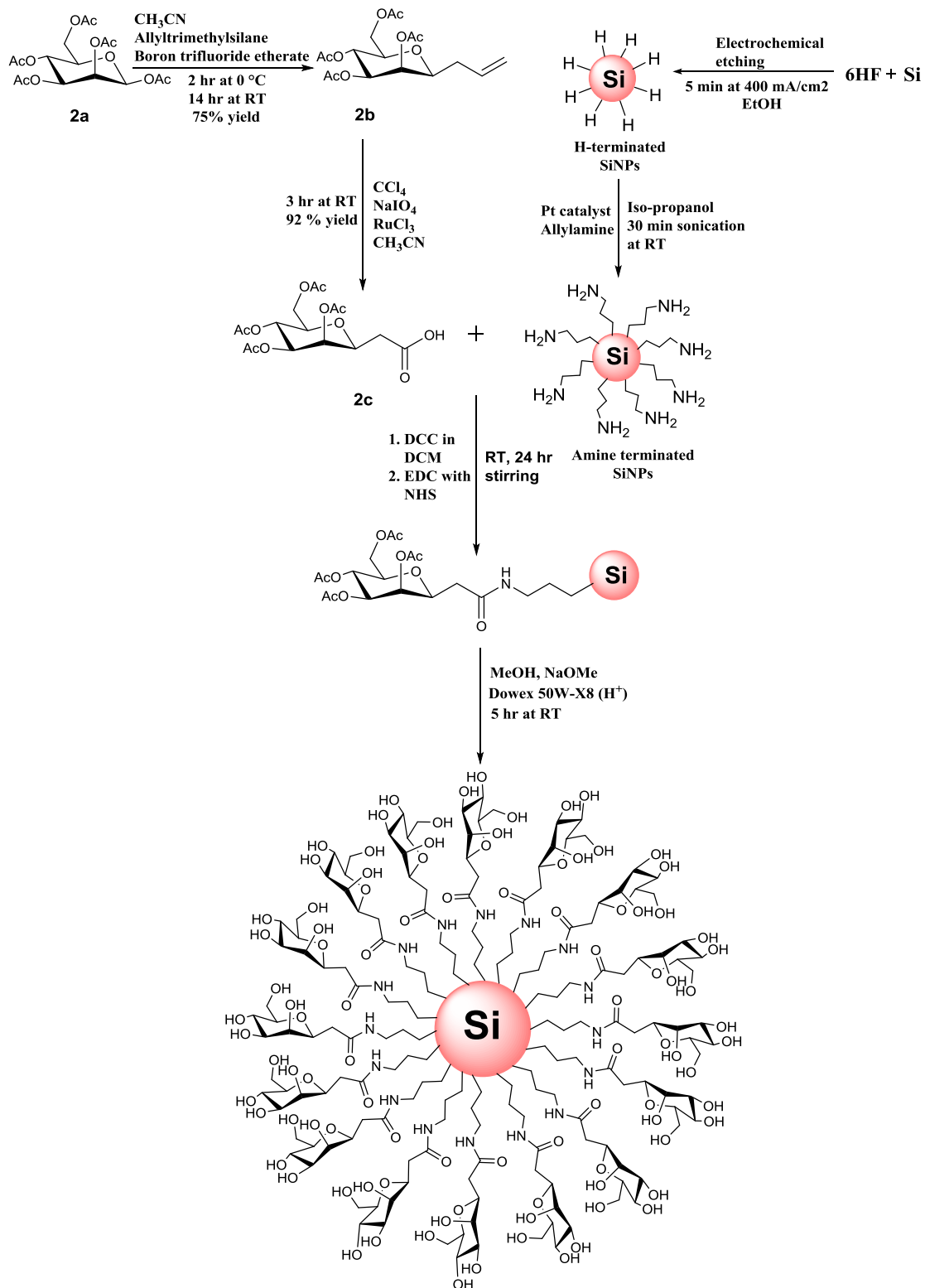
Scheme 4.10: Schematic Representation of Synthesis of D-Mannose Capped SiNPs
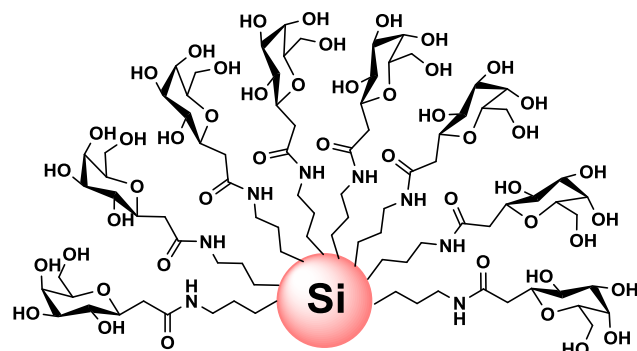
Galactose capped SiNPs
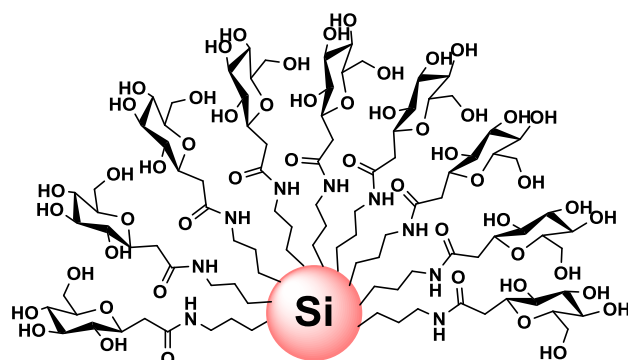
Glucose capped SiNPs
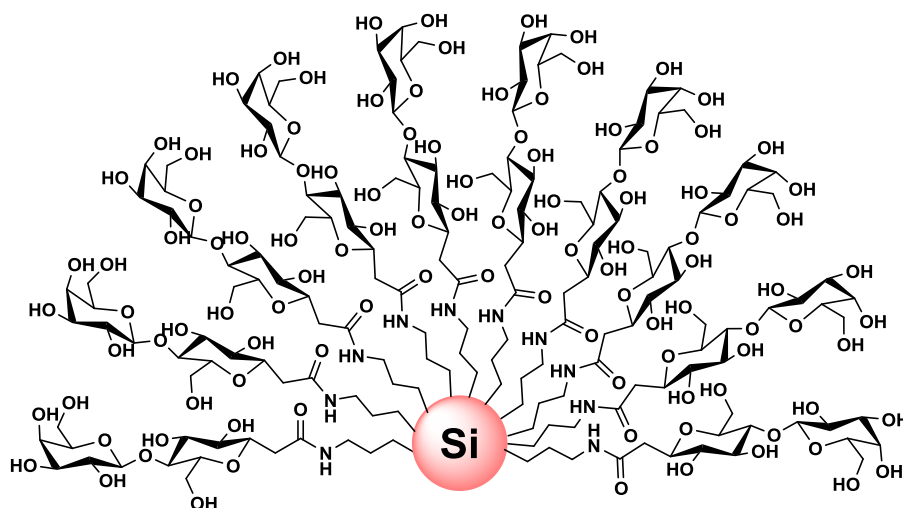
Lactose capped SiNPs

Scheme 4.11: Schematic representation of Galactose, Glucose and Lactose capped SiNPs synthesized in this work.

All acid functionalized carbohydrate synthesis was carried out using a method published by Deming and Kramer.[44]

4.3.1 Oxidation Reaction

1b: Gal: R_1, R_4 = H; R_2, R_3 = OAc
2b: Man: R_2, R_3 = H; R_1, R_4 = OAc
3b: Glu: R_1, R_3 = H; R_2, R_4 = OAc

1c: Gal 91 %
2c: Man 80 %
3c: Glu 72 %
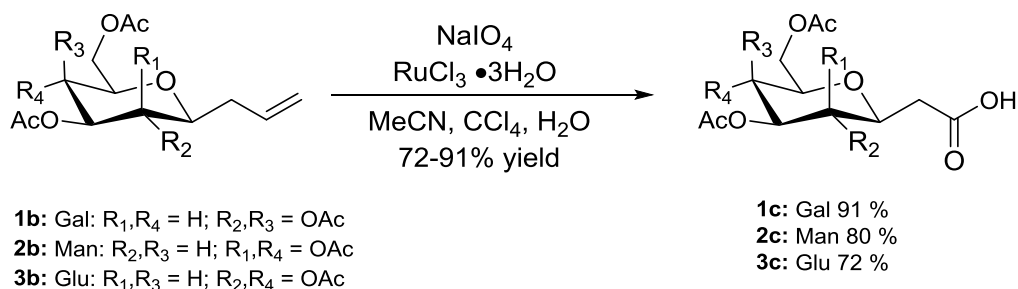
Scheme 4.12: Oxidation of carbohydrate derivatives
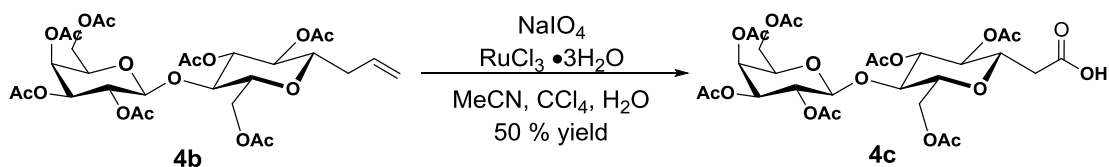
Scheme 4.13: Oxidation of Lactose derivative

The allyl carbohydrate derivatives were functionalized with carboxylic acids by oxidation reaction using sodium periodate ($NaIO_4$) and Ruthenium chloride catalyst ($RuCl_3$) in the presence of carbon tetrachloride (CCl_4) and water. The carboxylate functionalized sugar was purified and coupled with amine-terminated SiNPs to give the desired conjugates.

4.3.2 Using *N,N′*-dicyclohexylcarbodiimide Coupling Reagent (DCC)

A pyranosyl acid and *N,N′*-dicyclohexylcarbodiimide (DCC) were dissolved in dichloromethane (10 ml) and left to stir for 1 h at room temperature. Freshly prepared amine terminated SiNPs (10 mg) were then added into the reaction mixture and stirred for 3 days at room temperature. The reaction mixture was washed with water (3 × 10 mL) and extracted into CH_2Cl_2. The mixture was dried with Na_2SO_4, and the solvent was removed under vacuum. The by-product of the reaction, dicyclohexylurea, proved difficult to remove which could only be achieved by multiple filtrations. Furthermore the reaction was slow and took at least 3 days to completion. Deacetylation of carbohydrate-capped SiNPs was performed using sodium methoxide in methanol and then stirred 30 min with cation exchange [H⁺] resin

4.3.3 Using 1-Ethyl-3-(3-dimethylaminopropyl) Carbodiimide Coupling Reagent (EDC or EDAC)

Because of the purification issue mentioned above, the carbohydrate capped SiNPs were also synthesized using EDC (1-Ethyl-3-(3-dimethylaminopropyl) carbodiimide) as the coupling reagent as it is easy to handle, has a high solubility in water and in organic solvents. The by-product urea formed during the reaction is readily soluble in water and can easily be removed by extraction.

A corresponding pyranosyl acid and EDC were dissolved in dichloromethane and left stirring for 2 hr at room temperature. After 2 hours *N*-hydroxysuccinimide (NHS) and freshly prepared amine terminated SiNPs were added into the reaction mixture and stirred overnight at room temperature (see Chapter 2). The product was isolated and purified (see chapter 2) followed by deacetylation using sodium methoxide in methanol, then neutralized by adding cation exchange [H+] resin. Using EDC as a coupling reagent the reaction was completed overnight with an overall higher yield as compared with DCC.

4.4 Carbodiimide Coupling Reaction Mechanism

The reaction of carbodiimide is more complicated than described above (scheme 4.10) however Nakajima and Ikada unraveled the mechanism of the coupling reaction and it is widely accepted.[46] Scheme 4.14 shows the brief mechanism of formation of carbohydrate capped SiNPs using amine-terminated SiNPs and EDC coupling reagent.
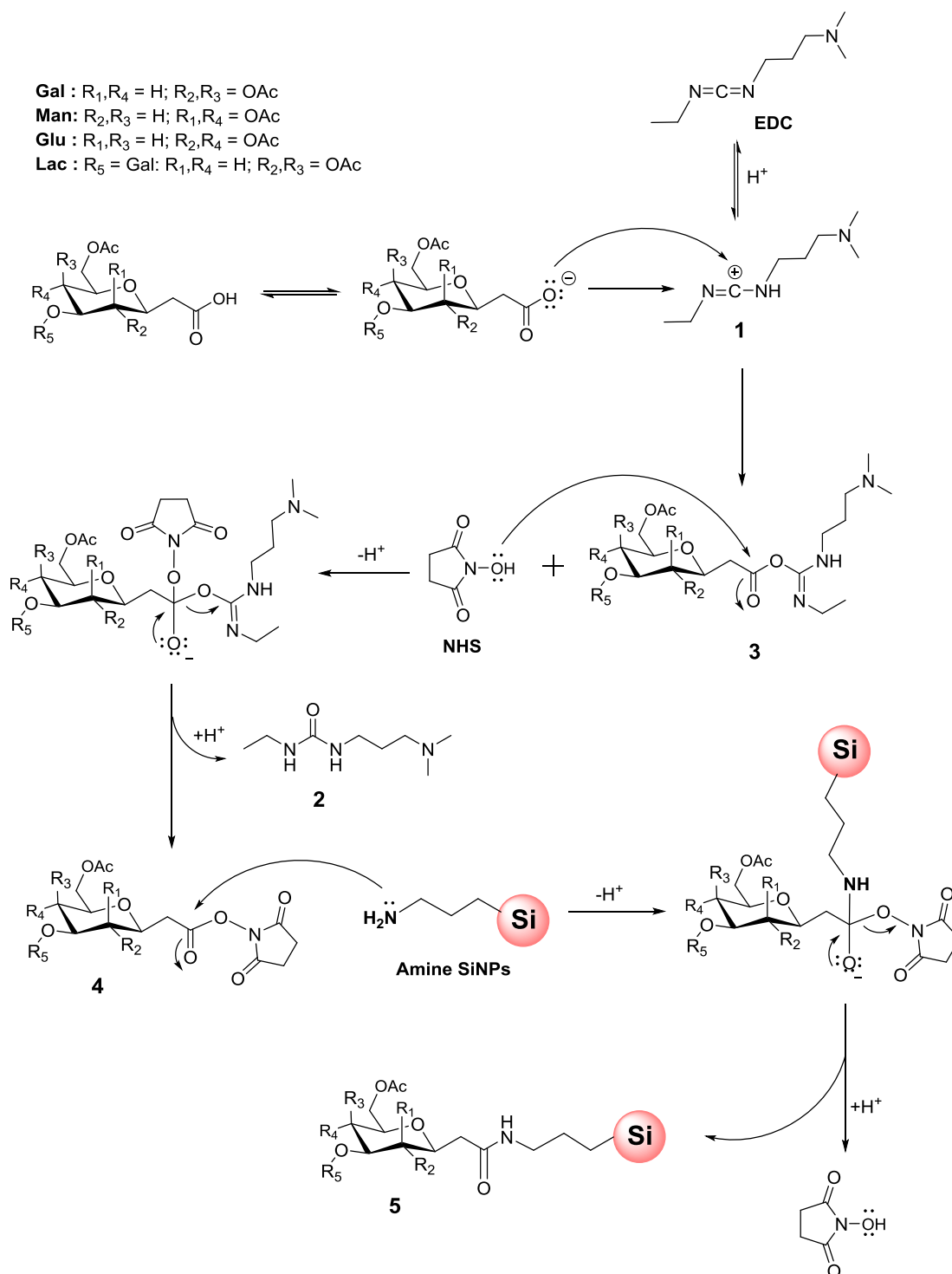
Scheme 4.14: Reaction mechanism of formation of carbohydrate capped SiNPs using EDC, NHS coupling reagent and amine-terminated SiNPs.

The first step in the reaction is the protonation of carbodiimide EDC giving a carbocation **1**. In the presence of carboxylate, carbocation **1** is attacked giving *O*-acylisourea **3**. Amide formation is possible by two routes, the first being when a non-dissociated

nucleophile *i.e.* amine-terminated SiNPs attacks **3** giving the product amide **5** and the urea derivative **2**. On the other hand, a carboxylate, which is a strong nucleophile, can attack **3**, giving an acid anhydride, which a non-dissociated primary amine attack giving the desired amide coupling product **5**. In the absence of nucleophile water can hydrolyze **3** into urea derivative **2**. Since the amount of water is much higher than that of amine SiNPs, the hydrolysis of **3** is most likely to happen than the formation of amide product. The advantage of using *N*-hydroxysuccinimide (NHS) is that it helps to form a less hydro-sensitive compound that is more reactive towards amine SiNPs. The active *O*-acylisourea **3** intermediate reacts with NHS to form succinimidyl ester that is more stable towards the oxidation. The dissociated hydroxyl group of NHS makes a nucleophilic attack on *O*-acylisourea **3**, giving urea derivative and succinimidyl ester **4**, which can then be attacked by amine-terminated SiNPs, resulting in the amide product **5** (sugar capped SiNPs) and regenerating NHS.

4.5   Size Measurement with TEM and DLS

The size and size distribution in diameter of carbohydrate-capped SiNPs were examined by TEM and DLS. Prior to the measurements the sticky solid of pure carbohydrate-capped SiNPs was dissolved in water. Figure 4.1a shows a TEM image of gal-capped SiNPs and figure 4.2 shows the TEM images (along with DLS data) for all carbohydrate capped SiNPs on a carbon coated copper grid.

The histogram in Figure 4.1b shows the size distribution of carbohydrate-capped SiNPs. The TEM measurement displayed the mean diameter and size distribution in diameter of carbohydrate-capped SiNPs is 5.5 ± 2.4 nm after analyzing 195 NPs from different regions of the grid. As all the carbohydrate-capped SiNPs are synthesized from amine-terminated SiNPs, hence the core size of all gal, man, glu and lac-capped SiNPs remain similar. The inset in Figure 4.1a shows the highly crystalline structure of the atomic lattices. The lattice spacing of 0.31 nm is consistent with the Si (111) plane.
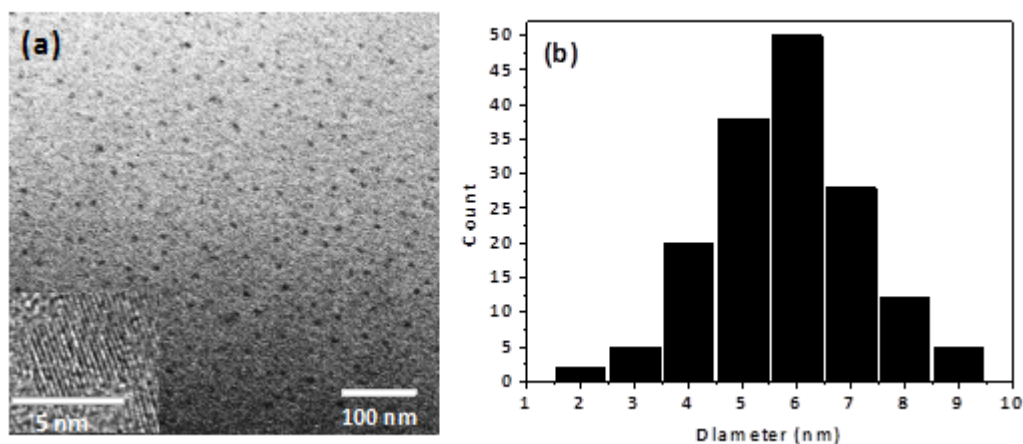
Figure 4.1: (a) TEM image of Gal-capped SiNPs and inset showing a high-resolution TEM image of an individual silicon nanocrystal screening the crystal lattice planes (b) Histogram showing size distribution (in diameter) of Gal capped SiNPs.

The DLS result of all carbohydrate-capped SiNPs is shown in Table 4.1 and in figure 4.2. As mentioned in the previous chapter the DLS measures the hydrodynamic diameter of the NPs and it is dependent on the functionality present on the surface of the NPs, the larger the capping functionality the bigger is the hydrodynamic diameter of the NPs. The diameter of carbohydrate capped SiNPs in water is larger than the one obtained from TEM measurements because the carbohydrate ligands around the SiNPs form a hydration shell, whereas DLS measures the hydrodynamic diameter of the carbohydrates-capped SiNPs in water.[8, 47-49]

Table 4.1: DLS data of carbohydrates capped SiNPs in water (± is repeatability)

Functionalize SiNPs	Diameter measure by DLS
Amine terminated SiNPs	7.5 ± 1.0 nm
Gal capped SiNPs	11 ± 1.0 nm
Man capped SiNPs	15 ± 1.0 nm
Glu capped SiNPs	19 ± 2.0 nm
Lac capped SiNPs	24 ± 1.0 nm
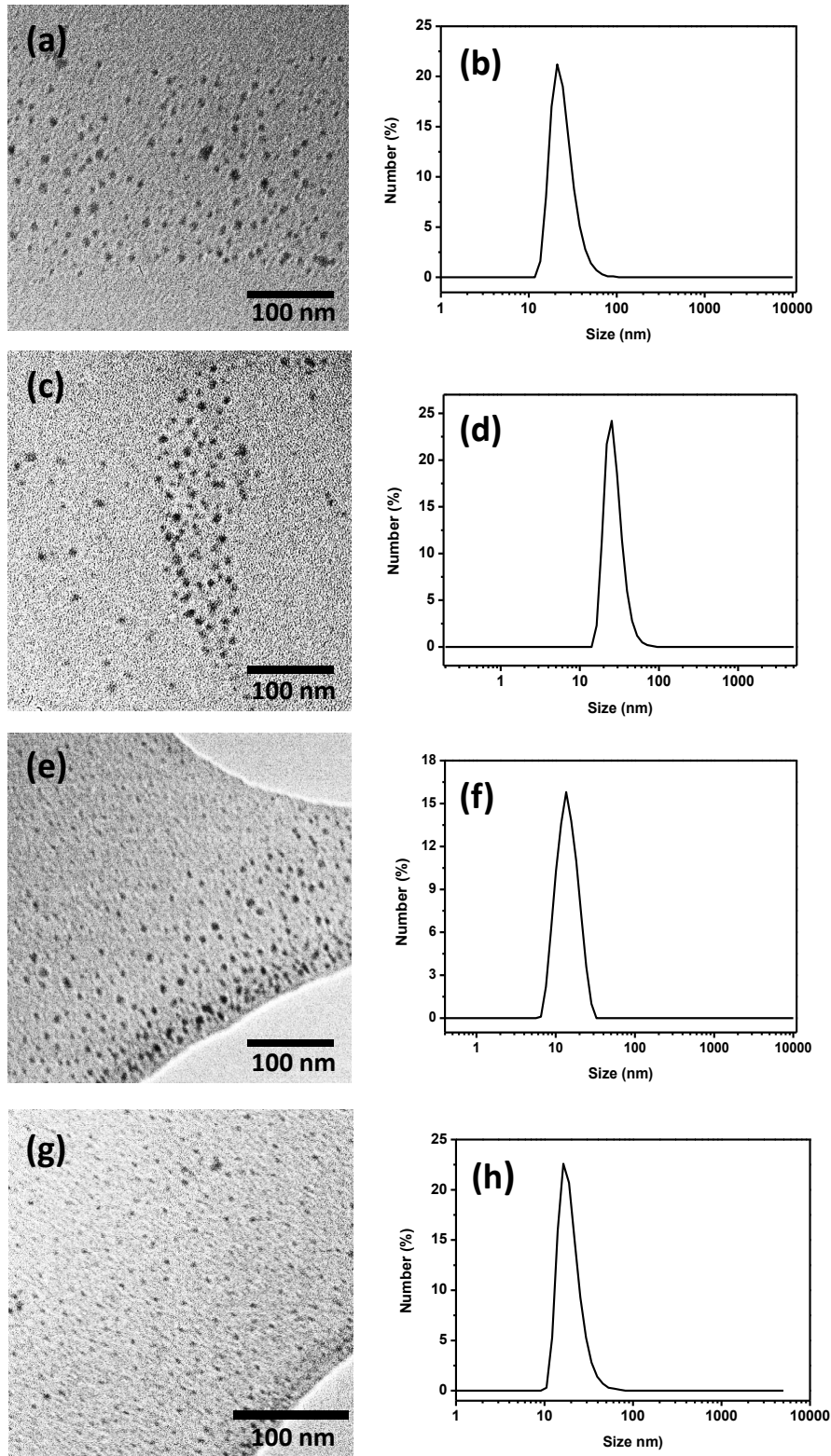
Figure 4.2: TEM images of Gal (a), Lac (c) Glu (e) and Man (g) capped SiNPs. Dynamic light scattering spectrum displays the size and size distribution (in diameter) of Gal (b), Lac (d) Glu (f) and Man (h) capped SiNPs in water.

The hydrodynamic diameter of all carbohydrates capped SiNPs are almost similar, except the lac-capped SiNPs. The galactose, mannose and glucose are monosaccharide moieties, they differ from each other due to their conformational arrangement however Lactose is a disaccharide therefore the size of the ligand is larger than those of monosaccharide which results in a larger hydrodynamic diameter compared with gal, man and glu-capped SiNPs.

4.6 Zeta-potential

In an ionic solution, nanoparticles with a net charge will have a layer of ions with opposite charge, strongly bound to their surface; this layer is referred to as the Stern layer. A second layer is called a diffuse outer layer, which is comprised of loosely associated ions. These two layers are collectively called the electrical double layer. As the particle moves in the solution due to Brownian diffusion or applied force, a distinction is created between ions in the diffuse layer that move with the nanoparticle and ions that remain with the bulk dispersant. The electrostatic potential at this "slipping plane" boundary is called the zeta potential and is related to the surface charge of the nanoparticle.

In zeta potential measurements, an electrical field is applied across the sample and the movement of the nanoparticles (electrophoretic mobility) is measured by laser doppler velocimetry (LDV). The Henry equation is then used to calculate the zeta potential,

$$U_e = \frac{2\varepsilon \, zf(ka)}{3\eta}$$
<div align="right">**Equation: 4.1**</div>

Where, U_e is the electrophoretic mobility, ε is the dielectric constant, η is the absolute zero-shear viscosity of the medium, $f(ka)$ is the Henry function, and ka is a measure of the ratio of the particle radius to the Debye length. Nanoparticles with a zeta potential between −10 and +10 mV are considered approximately neutral, while nanoparticles with zeta potentials of greater than +30 mV or less than −30 mV are considered strongly cationic and anionic, respectively.

Table 4.2: Zeta-potential of carbohydrates capped SiNPs in water

SiNPs in water	SiNPs ζ-potential (mV)
Amine terminated SiNPs	0 ± 3.0
Gal capped SiNPs	-19 ±1.0
Man capped SiNPs	-15 ± 1.0
Glu capped SiNPs	-9 ± 1.5
Lac capped SiNPs	-12 ± 0.5

The zeta-potential of amine-terminated SiNPs is measured as ±3 mV. In contrast, the various functionalized carbohydrate capped SiNPs showed a negatively charged ζ-potential ranging from -20 to +3 mV. The expected zeta-potential value for amine capped particles is in the region of +30 mV as the amines ionize in the water but the zeta value obtained in water was neutral ± 3.0mV. The relative zeta values obtained for sugar capped SiNPs comparing with amine-terminated SiNPs are as expected (i.e. they were less positive since some of the amines were converted to amides) but the absolute values remained unexplained. The relative zeta values for sugar capped SiNPs can also be explained on the basis of steric hindrances and poor capping. Due to the conformational arrangement of sugars on the surface of SiNPs, some area remains uncapped. Surface oxidation might also have occurred due to the reaction conditions or the carry forward surface oxidation (SiO_x) from amine-terminated SiNPs, which could have resulted from the strongly oxidising Pt (IV) hydrosilylation catalyst. The zeta potential of oxidised SiNPs is around -37mV which helps to explain the relative values of sugar capped SiNPs. The more negative value obtained for gal capped SiNPs suggest that the SiNP is poorly capped with galactose sugar, which leaves some areas uncapped and possibly some surface oxidation resulting in the negatively charged zeta potential. This hypothesis also helps to explain the high QY and bright luminescence obtained for lactose and glucose capped SiNPs compared to that of gal capped SiNPs. Therefore the more the zeta potential shifts to the neutral, the better is the capping and thus superior fluorescence QY is observed.

4.7   Chemical Bonding and Elemental Analysis

4.7.1   Energy-dispersive X-ray Measurements (EDX)

EDX analysis was performed on a dry sample; prior to measurement the sample was coated with gold (Au), which was used as a reference. In Figure 4.3, the EDX analysis shows all the elements in the expected functionalities in their expected ratios. The SiNPs surface is

coated with a large number of carbon and oxygen atoms in agreement with this analysis, where the highest peak was carbon and the second highest peak oxygen, which are present in the carbohydrates groups as well as in the Si−O bonding. In addition, there is a sharp peak of silicon, which is indicative of the core. Overall, the analysis proves that not only is the surface functionalized with carbohydrates moiety but also the silicon core nanoparticles are present in the sample.
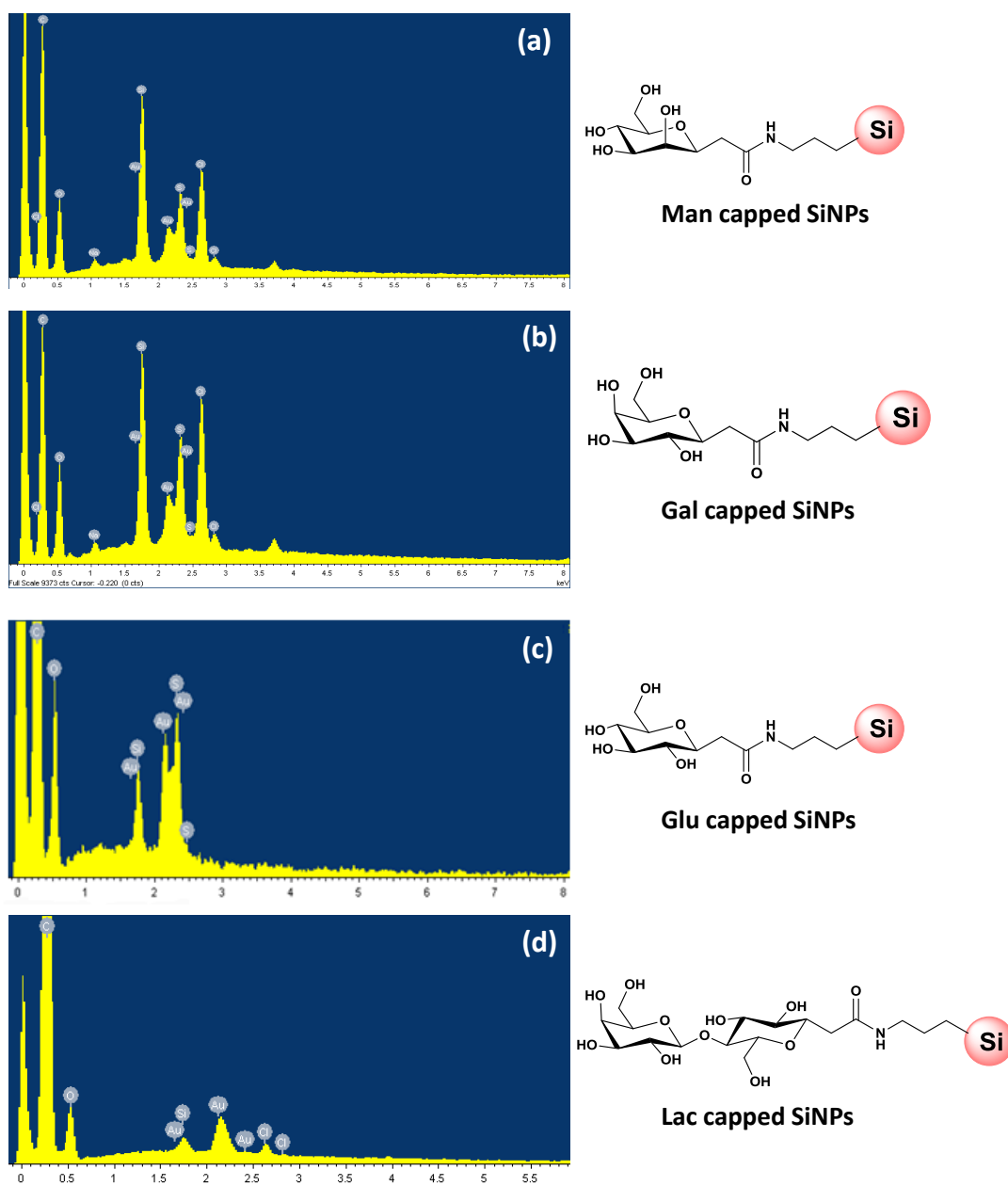
Figure 4.3: EDX spectroscopy of (a) man, (b) Gal, (c) Glu, and (d) Lac capped SiNPs

In Figure 4.3 it is observed that the monosaccharides show higher intensity of Si peak compared with lactose. Since Lactose is a disaccharide so the amount of carbon and oxygen molecule will be higher compared with the monosaccharides.

4.7.2 Fourier Transform Infrared Spectroscopy (FTIR)

In order to confirm the SiNPs surface is covered with carbohydrate groups through an amide bond FTIR spectra were acquired in normal transmission alignment. Figure 4.4 compares the FTIR spectra of the carbohydrate capped SiNPs produced in this work (Figure 4.4.d) with those obtained for the starting amine terminated SiNPs (Figure 4.4a) and D-man pyranosyl acid **2c** (Figure 4.4b) as well as that of the intermediate OAc protected carbohydrate-capped SiNPs (Figure 4.4.c). All spectra were obtained from dry solid samples. At this point it is worth reminding that all carbohydrates (Gal, Man, Glu and Lac) have a similar functionality and bonding, they differ from each other due to their conformational behavior. Although Lactose is a disaccharide and has two sugar molecules bound to each other, the ratio of some bonding features will be more intense but it will still show similar features at similar positions. The FTIR spectra of carbohydrate capped SiNPs are presented in Figure 4.4 and their detailed analysis is shown in Table 4.3.
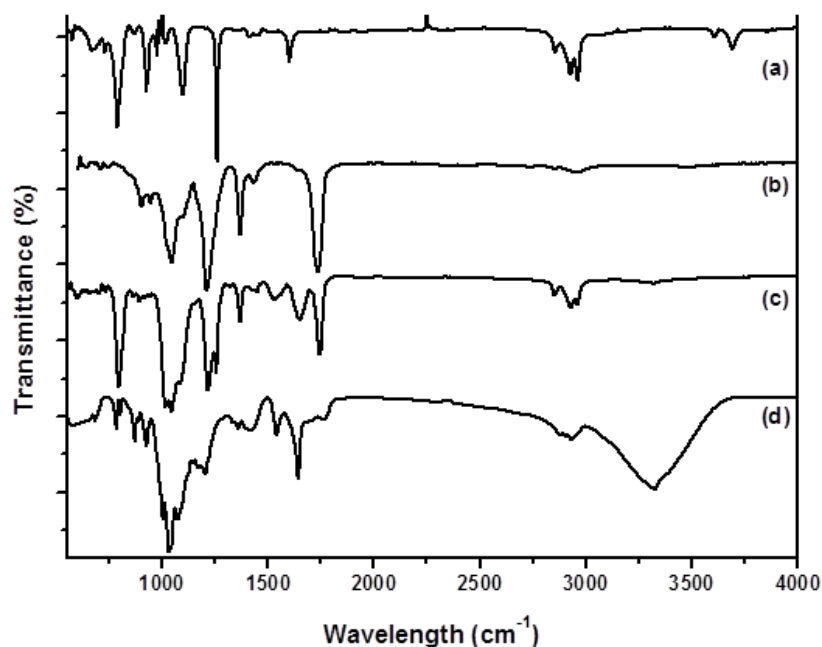
Figure 4.4: FTIR spectra of (a) Amine-terminated SiNPs, (b) Starting material acid sugar c, (c) Intermediate OAc-carbohydrate capped SiNPs, and (d) Pure carbohydrate capped SiNPs in the solid state (32 scans, 2 cm $^{-1}$ resolution).

Table 4.3: Infra-red band analysis of carbohydrates capped SiNPs

Structural Feature	Vibrational Motion	Wavenumber / cm^{-1}
OH	OH stretch	3300-3625
-CH$_2$-	C-H stretch	2929
Amide	C=O stretch	1654
Amide	C-N stretch	1551
Carboxylic acid	C=O	1725
Si-CH$_2$	Vibrational scissoring	1450
Si-C	Symmetric bending	1258
C-O-C	C-O stretching	1369
Si-O	Asymmetric stretching	1030
C-OH	Out of plane bending	999
C-0	stretching	1100
Amide	N-H wagging	737
Amide	N-H stretching	3311

The FTIR spectrum of carbohydrate capped SiNPs (d) shows a broad peak at 3300-3625 cm^{-1} attributed to vibrations of the four –OH groups of the mannose sugar. The N-H stretching of the amide function observed in the spectrum of the intermediate OAc-protected carbohydrate capped SiNPs (c) at 3311 cm^{-1} is evidently not visible in the same region in (d) due to overlap. However, the peak at 1551 cm^{-1} is attributed to the C-N stretching and N-H bending from the amide group, and this is only observed in the intermediate OAc-carbohydrate capped SiNPs (c) and the product (d) spectra. The broad amide N-H wagging band is observed at 737 cm^{-1}. Further evidence for the amide link arises from the presence of a sharp band at 1654 cm^{-1} which is attributed to the C=O stretching of the amide carbonyl, and this is not seen in the starting material sugar 1c (b) whose C=O acid vibration exhibits a peak at 1725 cm^{-1}. Further features observed around 2853-2961 cm^{-1} are attributed to the C-H stretching of the alkane chains. These peaks lose some of their intensity in the product (d) relative to the intermediate (c) due to the removal of the acetate protecting groups (OAc). The bands in the spectrum (c) at 1450 cm^{-1} and 1258 cm^{-1} are attributed to Si-CH$_2$ vibrational scissoring and symmetric bending respectively. These are less visible in (d) due to the effect of an oxide peak at 1100 cm^{-1} and loss of OAc peaks. Spectrum (c) shows two peaks at 1258 cm^{-1} and 1217 cm^{-1} which corresponds to Si-CH$_2$ symmetric bending and C-O bond of the carbohydrate respectively which is also apparent in the starting material (b). The peak observed at 1369 cm^{-1} is assigned to the C-O-C group of

the sugar which can also be observed in spectra (b), (c) and (d). The broad band observed at 999-1100 cm^{-1} is attributed to Si-O, C-O and C-OH. The broadening and the high intensity of this peak is due to the four hydroxyl OH groups of the sugar and not to the Si-O bond, which can be clearly seen in both spectra (c) and (d).

All these observed features confirm that the SiNPs are capped with sugar molecules. Also, these characteristics highlight the strength and stability of the Si–C bond formed between the SiNPs and the carbohydrates, as well as the minimal level of Si-O due to oxidation.

4.7.3 Nuclear Magnetic Resonance Spectroscopy (NMR)

The surface chemical bonding of carbohydrate capped SiNPs was also confirmed by ^{13}C NMR spectroscopy. In the case of NPs it is difficult to analyze the proton NMR due to background noise. In the case of ^{13}C NMR the appearance of the amide carbon at 169.76 ppm and disappearance of the acid carbon peak at 175.79 ppm was clearly observed. For instance, Figure 4.5 compares the ^{13}C NMR spectra of acidic Man sugar 1c (starting material) in $CDCl_3$, intermediate OAc protected Man capped SiNPs in $CDCl_3$ and Man capped SiNPs in D_2O. Figure 4.6 shows the ^{13}C NMR spectra expanded from the interesting amide bonding region, from 167 ppm-176ppm. Unfortunately, it was not possible to obtain all three spectra in the same solvent due to the differing solubilities of the various compounds. It is important to remember at this point that all the monosaccharides differ from each other due to their conformational arrangement so the ^{13}C NMR for all monosaccharides are similar except for Lactose that is a disaccharide, although the amide peak is still at a similar position to that of the monosaccharides.
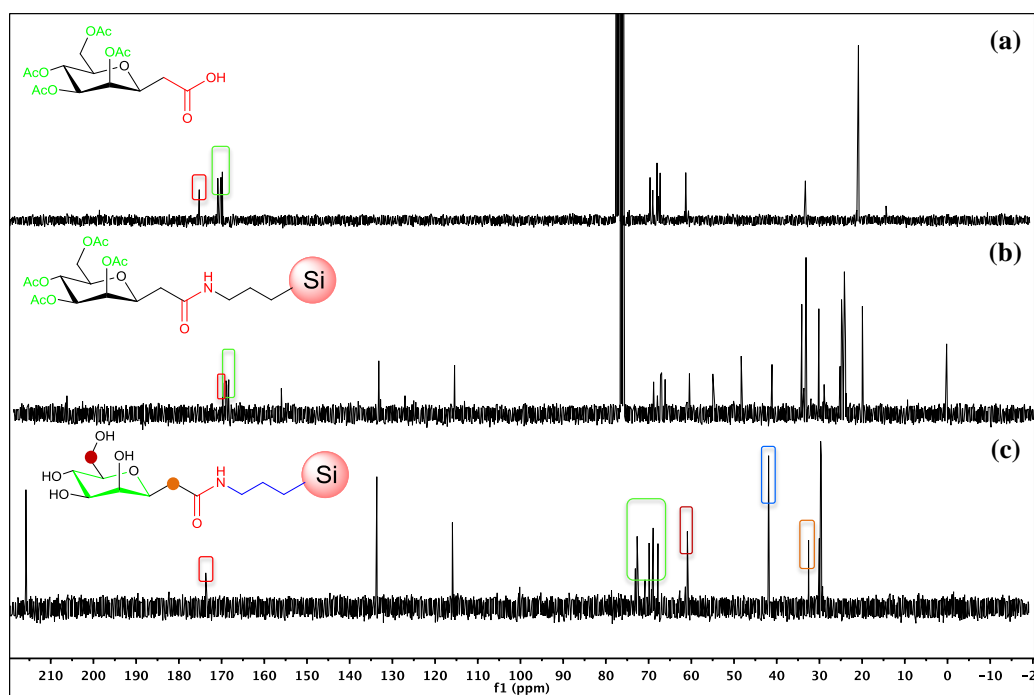
Figure 4.5: ^{13}C NMR spectra of (a) starting material 2c in CDCl$_3$, (b) Intermediate OAc-man capped SiNPs in CDCl$_3$, and (c) Pure man capped SiNPs in D$_2$O.
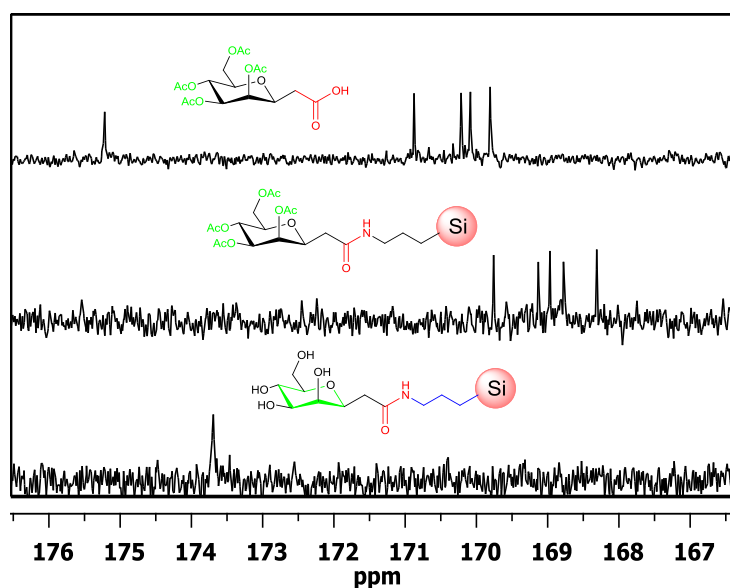
Figure 4.6: ^{13}C NMR spectra of starting material 2c, Intermediate OAc-man capped SiNPs and pure man capped SiNPs, expanded from the region of 167-176 pmm.

The spectrum of the starting material acid sugar 2c (a) shows a peak at 175.79 ppm, which is attributed to the carbonyl carbon (-C=O) of the acid function of man sugar. The four

peaks between 169.6 ppm and 170.6 ppm are attributed to the four OAc protecting groups of man sugar. The five carbon atoms making up the carbohydrate ring have peaks located between 67 ppm and 69.4 ppm. The peaks at 61 ppm and 33 ppm are attributed to the two –CH$_2$ groups of man sugar. The formation of the amide bond is clearly observable in the intermediate OAc-man capped SiNPs (b) through the disappearance of the acid carbon peak at 175.79 ppm and the appearance of a new peak at 169.76 ppm, attributed to the amide carbonyl carbon (see figure 4.6). The spectrum (b) is that of a crude sample due to the complexity of isolation (see experimental) and shows peaks in the aliphatic region belonging to reagents and side-products. Following the removal of the acetate groups, the spectrum of man capped SiNPs (c) shows only a single peak in the carbonyl region at 173 ppm attributed to the amide carbonyl carbon. The peaks at 115.72 ppm and 133.4 ppm belong to the amine-capped nanoparticles. The peaks at 215 ppm and 29 ppm originate from acetone-d^6, which was added as a reference for the sample in D$_2$O.

4.7.4 X-ray Photoelectron Spectroscopy (XPS)

As explained in a previous chapter, XPS is an important technique for characterizing the surface of the SiNPs (see Chapter 2). Furthermore the chemical bonding of carbohydrate capped SiNPs was also investigated with high resolution XPS over the Si2*p*, C1*s,* O1*s* and N1*s*. A full survey of the photoelectron spectrum of gal capped SiNPs is shown in Figure 4.7.
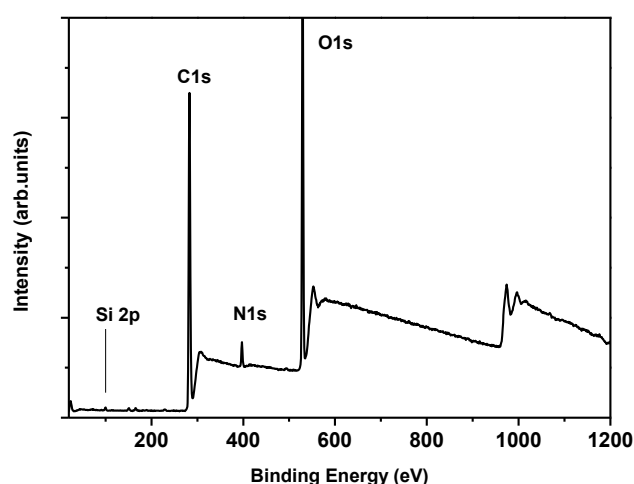
Figure 4.7: XPS survey spectrum from the film of gal capped SiNPs deposited on a gold substrate

The contribution of silicon, oxygen, carbon and nitrogen are clearly seen. The Si2*s* peak shown to be weak, whereas the C1*s* and O1*s* are shown to be strong, which suggest that

the SiNPs are highly coated with carbohydrate functionality (Galactose). Figure 4.8 shows high-resolution XPS spectra of Si$2p$, C1s, O1s and N1s regions of a thin film of gal capped SiNPs.

The Si2p spectrum was fitted with three peaks and a Shirley background. The three peaks are at 101.07, 103.20 and 100.98 eV. The first component is attributed to Si−C indicating that the surface of the SiNP is capped with galactose sugar through the amine moiety. The second component is assigned to Si−O, which is indicative of the sample surface oxidation under ambient conditions. The third peak at 100.98 eV is attributed to Si−Si within the silicon core of the SiNPs.[27, 50]
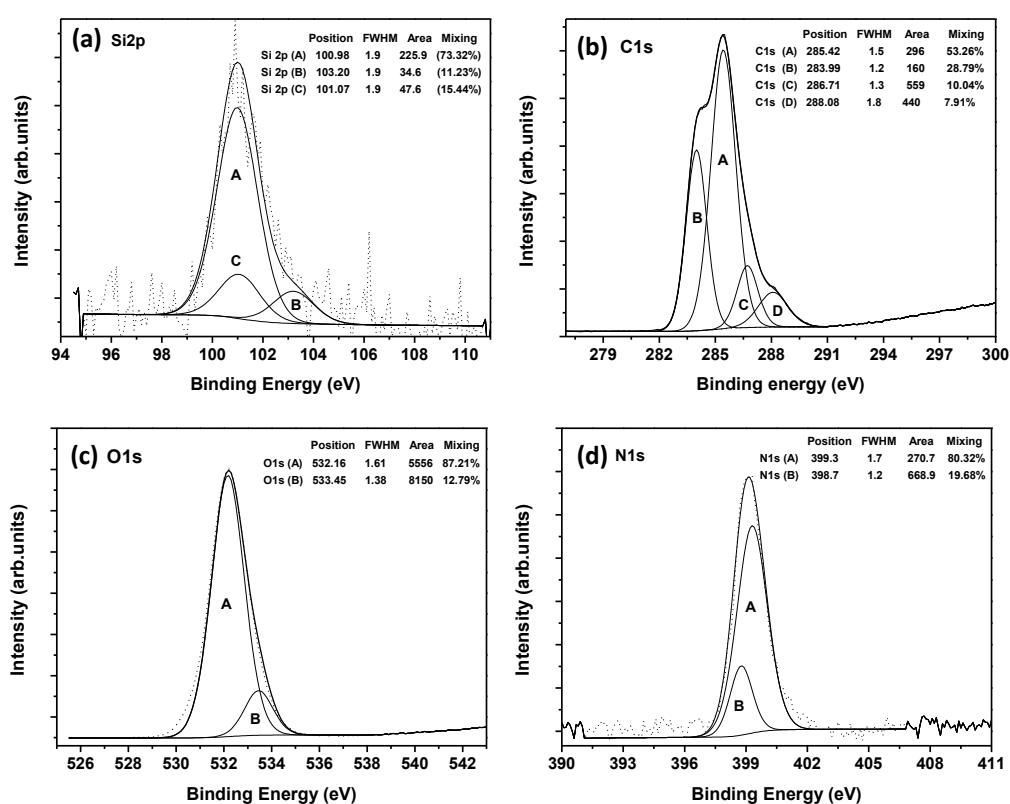
Figure 4.8: XPS core-level spectra of carbohydrate capped SiNPs obtained at 20°C to normal emission: the dotted line is experimental data that is fitted with various mixed components (a) Si2p, (b) C1s, (c) O1s, and (d) N1s at 400 eV.

The C1s spectrum is fitted with four mixed singlet and one Shirley background. The four components were at 285.42, 283.9, 286.71 and 288.08eV respectively. The first C1s peak at binding energy 285.42 eV is assigned to C−C or C−H bonding.[51, 52] The second broad peak at binding energy 283.99 eV is attributed to the C−Si bonding.[50] and the third distinct

125

peak 286.71 eV is ascribed to C−N bonding and C-OH bonding.[53] The fourth peak at binding energy 288.08 eV is assigned to C=O (amide) bonding.[54, 55] The existence of a C−Si and C=O amide bonding component implies that the surface of the silicon nanoparticle was capped with galactose moiety.

The O1s spectrum presented in Figure 4.8c is fitted with two components and a Shirley background. The two components are at binding energy 532.68 and 534.23 eV respectively. The first distinct O1s peak at 532.68 eV is from a Si−O group of the oxidized surface of SiNPs. The second component is possibly from hydroxide O−H group.[50]

The N1s spectrum presented in Figure 4.8d is fitted with two components and a Shirley background. The broad distinct peak is at 399.34 eV is attributed to the NHC=O amide bonding of the galactose capped SiNPs.[54] The second peak at binding energy of 398.9 is attributed to the C-N bonding of amine functionality.[53] This is due to the bulky galactose molecule on the surface, steric hindrance is present which leaves some space uncapped.

4.8 Optical Properties of Carbohydrate capped SiNPs

4.8.1 Photoluminescence Spectroscopy (PL)

The absorption and emission spectra of carbohydrate capped SiNPs in water are presented in Figure 4.9 and Figure 4.10.
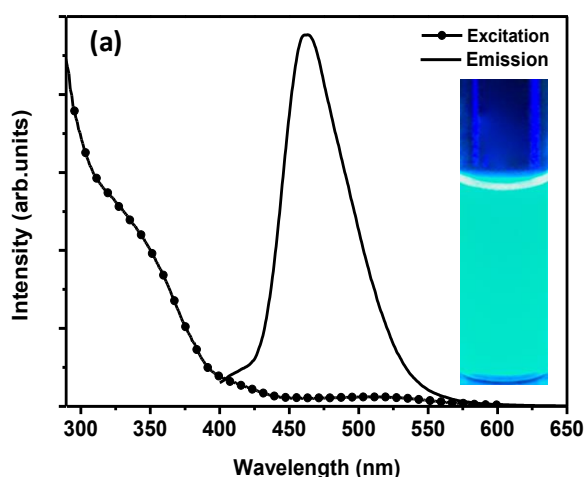
Figure 4.9: The dotted line shows the absorption spectrum of man capped SiNPs in water; the solid line shows the photoluminescence spectrum of man capped SiNPs in water under an excitation of 360 nm. The inset photo shows the fluorescence from Man capped SiNPs in water under a UV lamp.

The inset photograph in Figure 4.9 shows the man capped SiNPs in water under UV illumination at 364 nm. The gradual increase in the absorbance of all carbohydrate capped SiNPs with decreasing excitation wavelength from the onset wavelength of 450 nm, corresponding to the absorption edge of 2.75 eV, is characteristic of absorption across the indirect band gap of silicon.[28] The PL spectrum of all carbohydrate capped SiNPs in water at room temperature is shown as a solid line. The maximum emission peak is centered at 468 nm with a full width at half maximum (FWHM) of 58 nm under an excitation wavelength of 360 nm
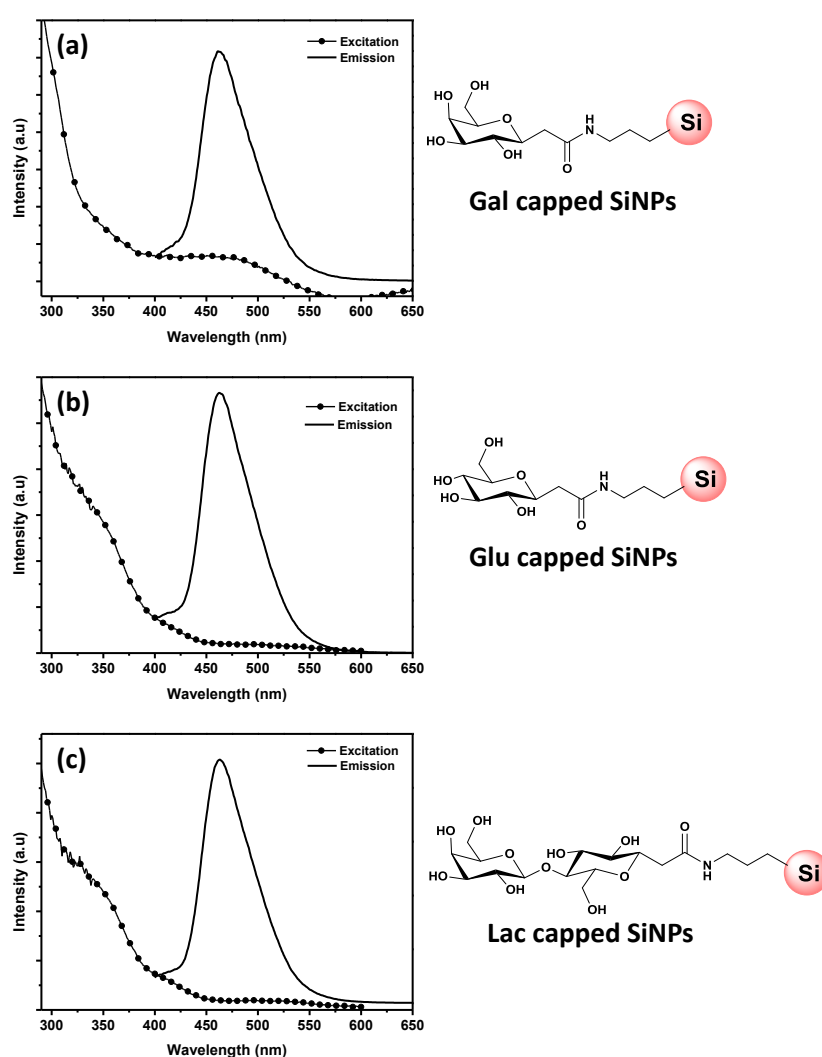
Figure 4.10: The dotted line shows the absorption spectrum in water; the solid line shows the photoluminescence spectrum of (a) gal capped SiNPs, (b) glu capped SiNPs and (c) lac capped SiNPs in water under an excitation of 360 nm

Interestingly the PL of these carbohydrates capped SiNPs in the solid phase, where the sample was drop cast onto a glass coverslip and dried in vacuum, shows a strong orange luminescence under UV light. The PL emission spectrum of Man capped SiNPs in the solid phase is presented in Figure 4.11, with an inset showing a photograph of the man capped SiNPs under UV illumination of 254 nm. The maximum emission peak, under an excitation wavelength of 360 nm, is centred at 600 nm and the second peak is centred at 476 nm, with a FWHM of 51 nm and 56 nm respectively. In Figure 4.9 and Figure 4.11 the peak centred at around 468 nm is characteristic of absorption across the band gap of silicon and is thus responsible for blue emission. Moreover the blue luminescence may be due to the oxidation of silicon (Si-O), nevertheless it is mainly the characteristic of silicon binding to nitrogen which causes a blue-green luminescence recently studied by Veinot *et al.*[56] In Figure 4.11 the peak centred at 600 nm shows orange emission, could also be a consequence of surface states and defects due to surface functionality. In the solid phase, both components are observable, unlike in the solution where the orange emission peak centered at 600 nm is not present. This suggests there is a quenching effect of the solvent around the surface functionality of SiNPs. It is believed that the surface functionality causes this change in luminescence. The hydroxyl –OH groups on the sugar molecule form hydrogen bonds with the solvent and this causes the quenching of the orange emission.
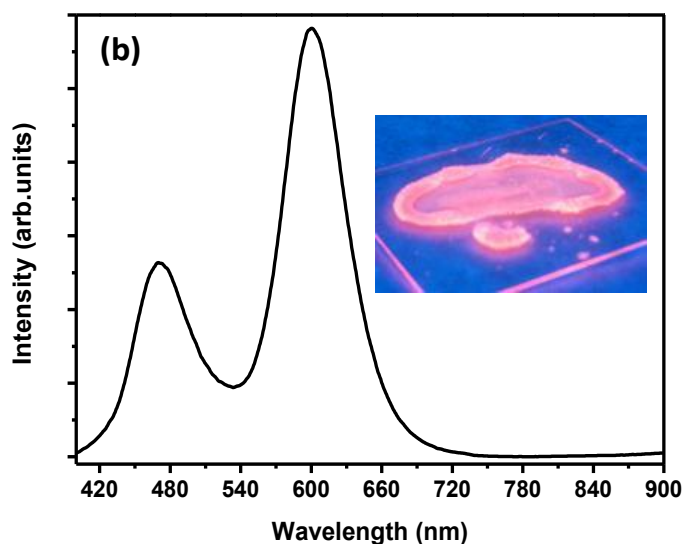
Figure 4.11: The photoluminescence spectrum of man capped SiNPs in the dry state under an excitation of 360 nm. The inset photo shows the fluorescence from a solid sample of man capped SiNPs under a UV lamp.

This phenomenon can also be explained on the basis of previous studies carried out by Chao et al.[57] where it is suggested that the blue PL in alkylated SiNPs prepared by electrochemical etching method and subsequently oxidized, was determined to originate

from excitation of oxidized Si atoms.[58] The observed orange PL is also consistent with the size predicted by the Effective Mass Approximation (EMA) of the SiNPs, as the size of the nanoparticle remained unchanged after the functionalization. Furthermore it is quite common for oxidation of SiNPs to cause a shift from red to blue.

4.8.2 Quantum Yield (QY)

Quantum yield (QY) of carbohydrate capped SiNPs in water were obtained using quinine sulfate (QY = 54.6%) as a reference emitter,[59] see Figure 3.12. A solution of all carbohydrates capped SiNPs in water with absorbance between 0.1 and 0.01 were prepared and the gradient of the integrated fluorescence intensities against absorbance was found. The observed QY of man capped SiNPs (figure 4.12), gal capped SiNPs (figure 4.13), glu capped SiNPs (figure 4.14) and lac capped SiNPs (figure 4.15) in water are presented and are much higher than the values of QY for SiNPs reported in the literature,[34, 37] which range from 2 to 18% in water. The QY of sugar capped SiNPs were found to be much higher than reported previously for SiNPs.

Table 4.4: Quantum Yields of carbohydrate Capped SiNPs in Water as the Percentage of Photons Emitted per Photon Absorbed, Using Quinine Sulphate as Standard Reference

Carbohydrate capped SiNPs	Quantum Yield (%)
Galactose SiNPs	16 ± 3
Mannose SiNPs	27 ± 5
Glucose SiNPs	30 ± 5
Lactose SiNPs	39 ± 5

The QY of all carbohydrate capped SiNPs is significantly higher than that of amine-terminated SiNPs. This phenomenon can be explained on the basis of the pH effect showed by amine-terminated SiNPs.[60] In amine-terminated SiNPs at low pH the $-NH_2$ group is protonated, and electron transfer between the amine moieties and the Si core is prohibited or in other words there are fewer electrons to quench the fluorescence which originates from the Si core yielding higher emission intensity. At higher pH, protonation is either incomplete or absent, which allows involvement of the nitrogen lone pair in relaxation processes and yields a reduced emission. When the amine ($-NH_2$) reacts with an acid sugar it donates a pair of electrons to form an amide bond, the carbonyl group from the amide bond pulls up the electrons from the nitrogen which decreases the electron density on the nitrogen atom resulting in less electronic involvement in quenching the fluorescence than

that of amine-terminated SiNPs and ultimately increases the fluorescence QY of carbohydrate capped SiNPs.

4.8.2.1 QY of mannose capped SiNPs in water
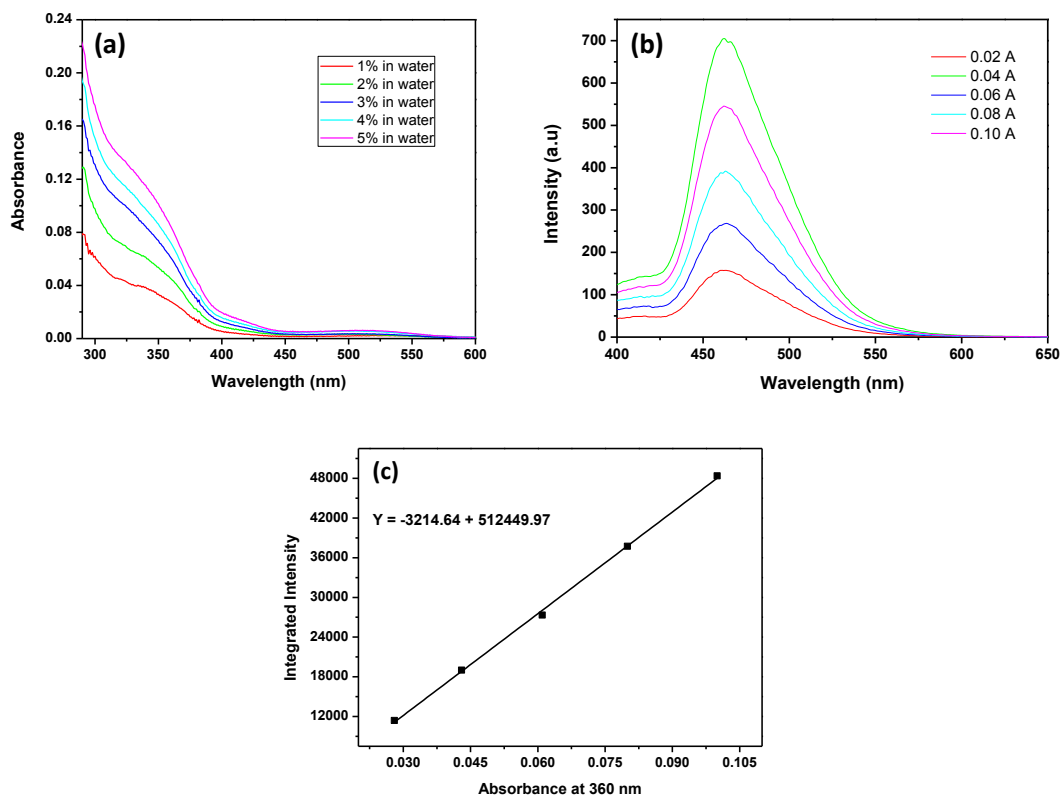
Figure 4.12: Quantum yield measurement of mannose capped SiNPs: (a) Absorption and (b) emission spectra obtained for different concentrations of man capped SiNPs, (c) Scatter plot of integrated intensity (area under emission spectrum) against absorbance at 360 nm.

The gradient of quinine sulphate and man capped SiNPs was obtained as 832456 and 512449.9 respectively (figure 3.12c) and (figure 4.12c). The refractive indices of both solvents were known, thus the quantum yield of the man capped SiNPs can be calculated as follows:

$$Q = 54.6\% \left(\frac{512449}{832456}\right) \times \left(\frac{1.33^2}{1.346^2}\right) = 32.81\%$$

The calculated quantum yield of man capped SiNPs by comparing the integrated PL intensities of the man capped SiNPs and quinine sulphate is about 32.81 % with excitation wavelength at 360 nm.

4.8.2.2 QY of Gal capped SiNPs in water
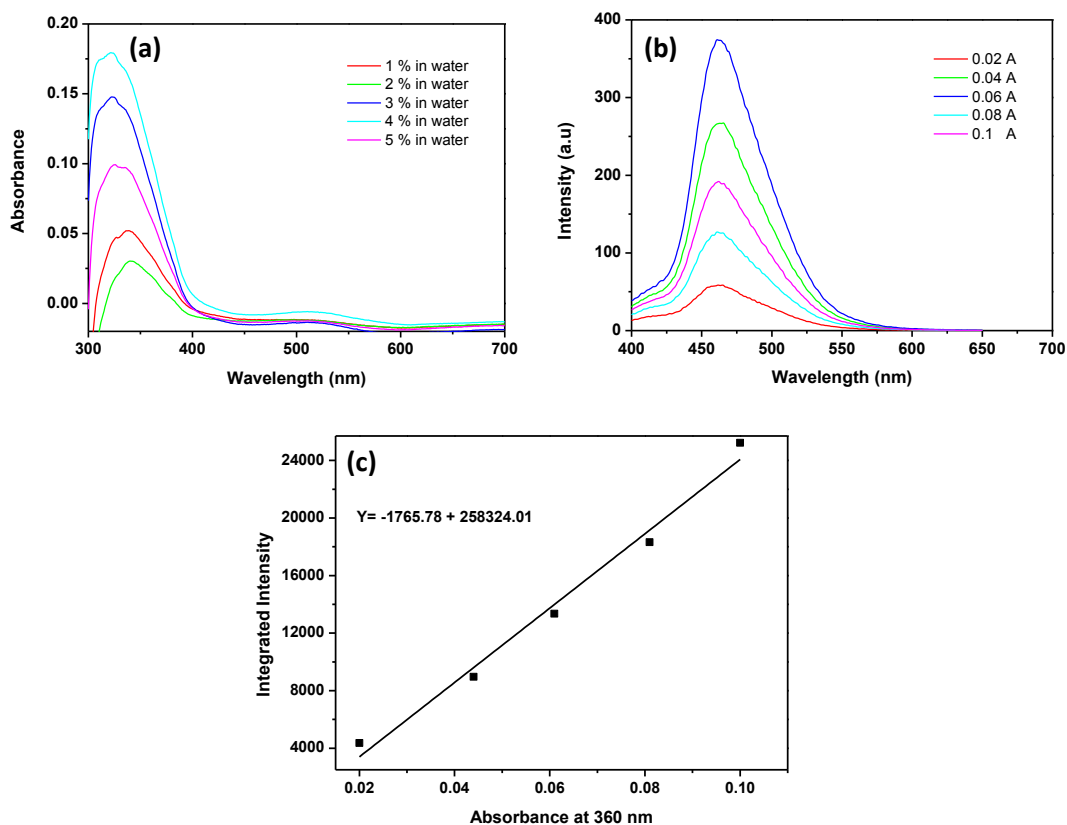
Figure 4.13: Quantum yield measurement of galactose capped SiNPs: (a) Absorption and (b) emission spectra obtained for different concentrations of gal capped SiNPs, (c) Scatter plot of integrated intensity (area under emission spectrum) against absorbance at 360 nm.

The gradient of quinine sulphate and gal capped SiNPs was obtained as 832456 and 258324 respectively (figure 3.12c) and (figure 4.13c). The refractive indexes of both solvents were known, thus the quantum yield of the gal capped SiNPs can be calculated as follows:

$$Q = 54.6\% \left(\frac{258324}{832456}\right) \times \left(\frac{1.33^2}{1.346^2}\right) = 16.54\%$$

The calculated quantum yield of gal capped SiNPs by comparing the integrated PL intensities of the gal capped SiNPs and quinine sulphate is about 16.54% with and excitation wavelength at 360nm.

4.8.2.3 QY of Glucose capped SiNPs in water
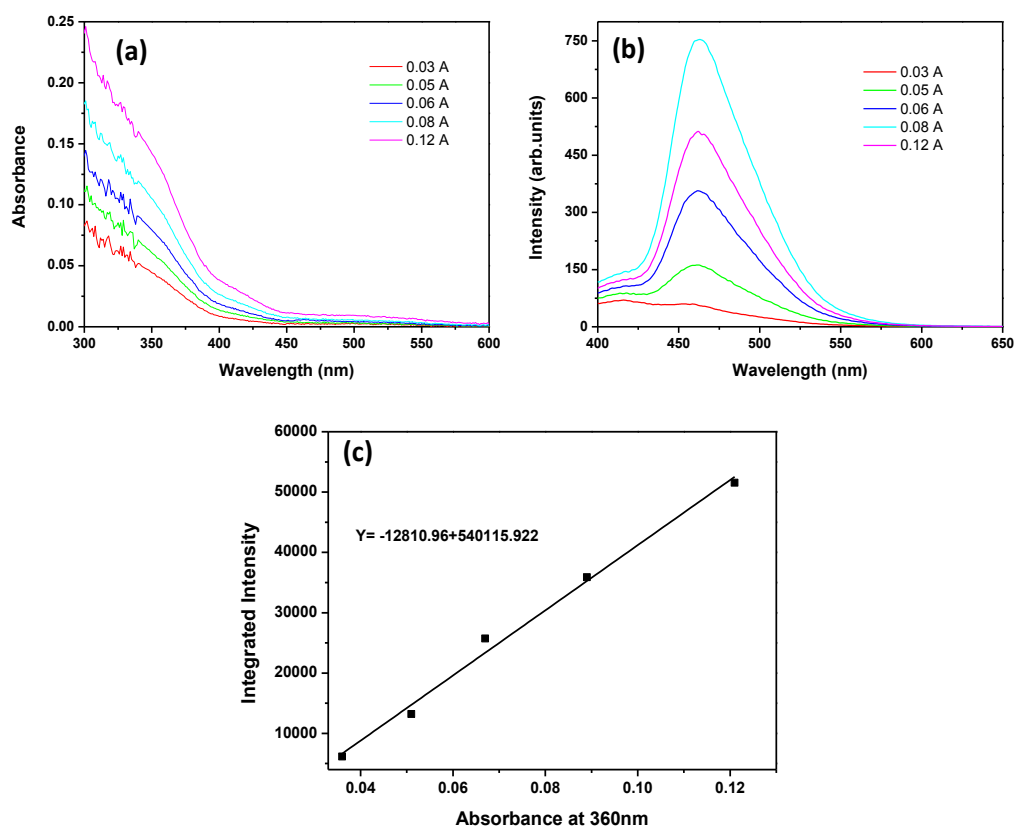
Figure 4.14: Quantum yield measurement of glucose capped SiNPs: (a) Absorption and (b) emission spectra obtained for different concentrations of glu capped SiNPs, (c) Scatter plot of integrated intensity (area under emission spectrum) against absorbance at 360 nm.

The gradient of quinine sulphate and glu capped SiNPs was obtained as 832456 and 540115.9 respectively (figure 3.12c) and (figure 4.14c). The refractive indexes of both solvents were known, thus the quantum yield of the glu capped SiNPs can be calculated as follows:

$$Q = 54.6\% \left(\frac{540115.9}{832456}\right) \times \left(\frac{1.33^2}{1.346^2}\right) = 34.58\%$$

The calculated quantum yield of glu capped SiNPs by comparing the integrated PL intensities of the glu capped SiNPs and quinine sulphate is about 34.58% with and excitation wavelength at 360nm.

4.8.2.4 Quantum yield for Lactose SiNPs in water
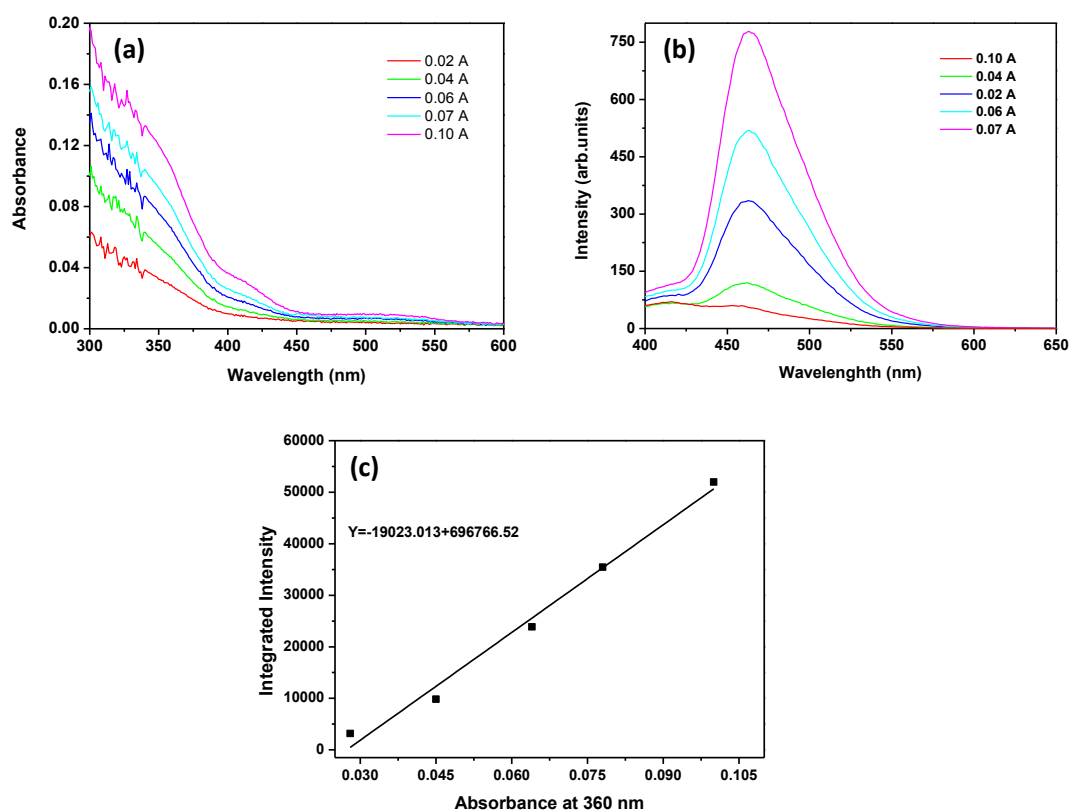
Figure 4.15: Quantum yield measurement of lactose capped SiNPs: (a) Absorption and (b) emission spectra obtained for different concentrations of lac capped SiNPs, (c) Scatter plot of integrated intensity (area under emission spectrum) against absorbance at 360 nm.

The gradient of quinine sulphate and lac capped SiNPs was obtained as 832456 and 696766.5 respectively (figure 3.12c) and (figure 4.15c). The refractive indexes of both solvents were known, thus the quantum yield of the lac capped SiNPs can be calculated as follows:

$$Q = 54.6\% \left(\frac{179663.7}{832456}\right) \times \left(\frac{1.33^2}{1.346^2}\right) = 44.62\%$$

The calculated quantum yield of lac capped SiNPs by comparing the integrated PL intensities of the lac capped SiNPs and quinine sulphate is about 11.55% with and excitation wavelength at 360 nm.

4.8.3 Photoinduced Electron Transfer (PET)

The increasing fluorescence QY in carbohydrate from gal capped SiNPs to lac capped SiNPs could be due to the Photoinduced Electron Transfer (PET) principle. PET often underlies the mechanism by which the 'switching' or 'sensing' effect occurs. Fluorescent signaling via the PET strategy is distinguished by its intrinsically supramolecular nature since distinct components perform each one of the necessary functions. The PET can be inhibited by conformational changes, local polarity modulation and hydrogen bonding. Such a suppression of the PET process means that the fluorescence is "switched on" again. Several researchers have reported the enhancement of the fluorescence due to protonation.[61-63]
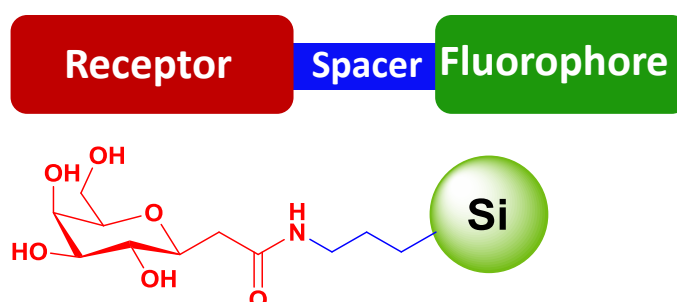
Figure 4.16: Schematic representation of the fluorophore – spacer – receptor format of PET system (top) and the analogous Gal receptor conjugation – spacer – SiQDs.

Figure 4.16 demonstrates the PET between the SiNP and carbohydrate moiety. In its 'off' state the excitation from fluorophore (SiQDs) components produces electron transfer from the receptor to the fluorophore. In its 'on' state the electron transfer is prohibited due to the arrival of the analyte at the receptor site. The prohibition of the electron transfer can possibly be understood with the help of Auger electron theory, suggested by Efros and Rosen *et. al.*[64] The Auger decay of multiexciton can lead to the ejection of a charge, a phenomenon known as Auger ionization. The fluorescence intensity or QY of the carbohydrate capped SiNPs increases perhaps due to the charging of the SiNPs core, in which the hot-electron trap[65] occurs due to the protective and non-conductive sugar molecules on the surface. In its "ON" state the electron does not eject from the SiQDs due to the hot-electron trap resulting in the increasing PL intensity and ultimately increases the QY of the nanoparticles. In its "OFF" state the fast nonradiative Auger recombination occurs that quenches the PL, which would correspond to weakly emitting states or week PL intensity.

4.8.4 pH effect

The pH effect in carbohydrate capped SiNPs was investigated by measuring photoluminescence (PL) at different pH conditions (from pH 1-14). It should be noted that pH effects are also one of the essential parameters in biological systems. For *in vivo* and *in vitro* studies, a photostable NP that is compatible with living cells would be potentially invaluable.[66] Thus, to utilize the semiconductor NPs efficiently and reliably in biomedical applications it is important to study the effect of pH on carbohydrate capped SiNPs emission characteristics. Figure 4.17 shows photoluminescence spectra of equal aliquots taken from a single preparation and dispersed in water, but using a series of different buffers to vary the pH. The various pH solutions were made by using pH tablets (4, 7 and 9) and values were set by adding stock solutions of 0.1M citric acid (19.2g/L) and 0.2M sodium citrate (28.4g/L). The pH of solutions was tested using pH electrode.
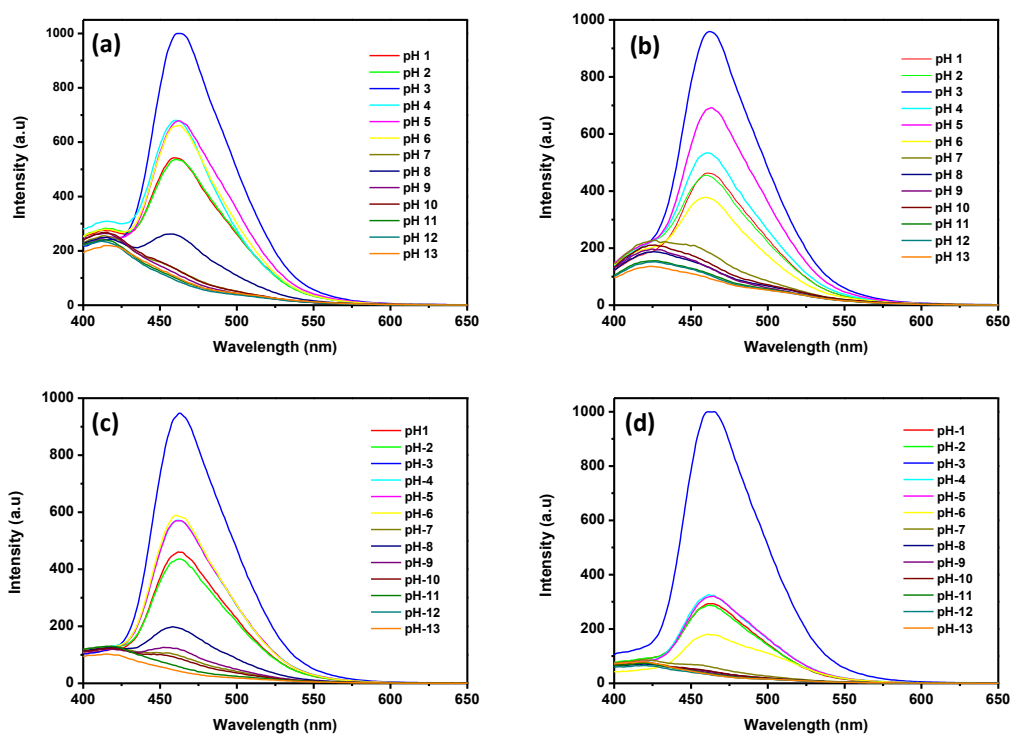
Figure 4.17: pH effect of carbohydrate capped SiNPs by emission using an excitation wavelength at 360 nm. (a) man capped SiNPs, (b) gal capped SiNPs, (c) glu capped SiNPs and (d) lac capped SiNPs.

In Figure 4.17 it is observed that all carbohydrate capped SiNPs show intense emission peak at pH-3. As the pH decreases the emission increases up to pH-3. Further decreasing the pH decreases the emission of carbohydrate capped SiNPs. At higher pH (8-13)

the emission decreases rapidly. As mentioned earlier, due to the bulky sugar molecules on the surface, steric hindrance is present which leaves some of the surface uncapped which is covered by amine functionality. As explained (see section 3.9.3) at low pH the amine group is protonated, and electron transfer between the amine moieties and the Si core is prohibited, yielding higher emission intensity. At higher pH protonation is either incomplete or absent, which allows involvement of the nitrogen lone pair in relaxation processes and yields a reduced emission. This phenomenon may perhaps be related to the presence of amine functionality on the surface of SiNPs due to the poor surface capping of sugar molecules which results in increasing and decreasing PL intensity by this pH effect nevertheless it still remains unproven based on the current data.

4.8.5 Photoluminescence (PL) Stability

For Silicon nanoparticles, a limiting factor is the insufficiency of PL stability for potential biological applications. To investigate the PL stability, time-dependent PL spectra were measured on all carbohydrate capped SiNPs in water (Figure 4.18) and Man SiNPs in dry state (Figure 4.19) by monitoring the PL emission using an excitation wavelength of 360nm
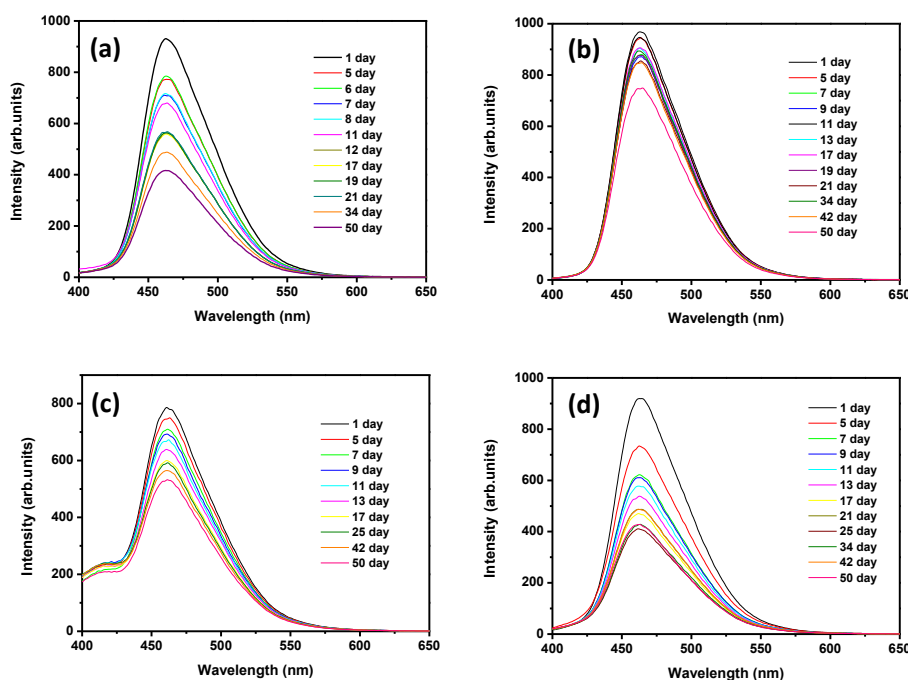
Figure 4.18: Ageing effect of carbohydrates capped SiNPs measured by PL using an excitation wavelength 360nm. (a) man capped SiNPs, (b) glu capped SiNPs, (c) gal capped SiNPs and (d) lac capped SiNPs in water.

It is observed that the sample remains stable for over a month if kept in the dark.[8] Figure 4.18, shows the PL decay of Man (a), glu (b), gal (c) and lac (d) capped SiNPs are moderately stable over a month. This gradual decreasing intensity indicates that the surface of SiNP undergo slow oxidation. Although the surface of SiNPs is highly capped with carbohydrate molecules but due to the bulky molecule on the surface steric hindrance is present, which leaves some areas uncapped. This allows some oxidation in water.

Carbohydrate capped SiNPs show blue-green luminescence in water and orange luminescence in the dry state. Figure 4.19 shows the stability of man capped SiNPs in dry state.
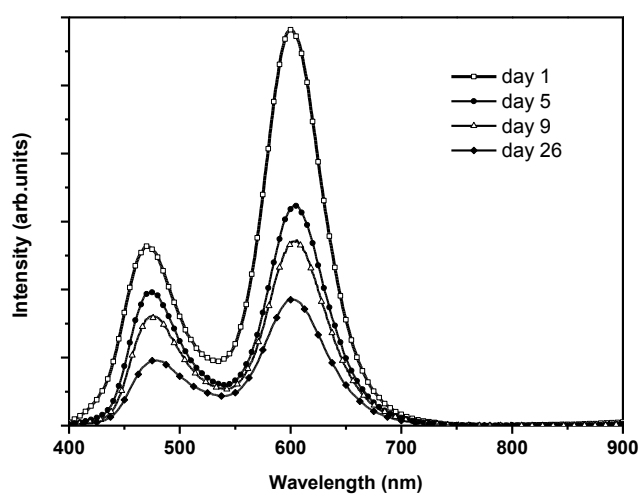
Figure 4.19: Ageing effect of Man capped SiNPs in the dry state measured by PL using an excitation wavelength 360 nm.

The sample was mounted on a glass cover slip and dried; this process was repeated several times until a thick film was formed. The sample was carefully dried under vacuum and fixed into the sample holder. The emission was monitored using an excitation wavelength of 360 nm. Figure 4.19 shows that the sample is moderately stable and with no sign of oxidation.

4.9 Biochemical Activity

As proof of principle the biochemical activity of carbohydrate capped SiNPs was tested with Con A. Assuming the SiNPs surface is functionalized by carbohydrate moieties, then the protein (Con A) would be expected to bind to the NPs and form an aggregate, which

would lead to loss of photoluminescence as well as formation of a precipitate after a certain time.
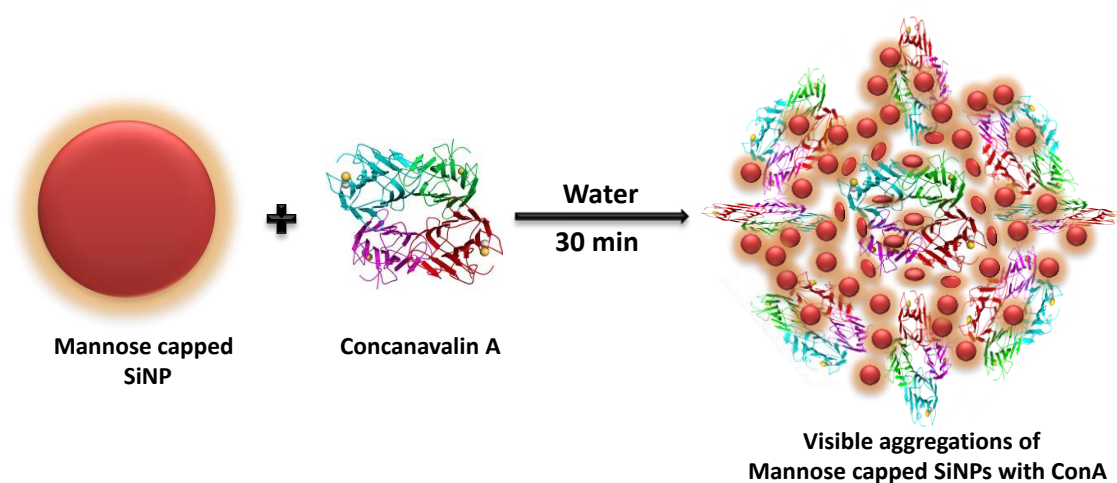
Figure 4.20: Graphical representation of agglutination of carbohydrate capped SiNPs by Con A tetramer in water.

Biochemical activity of man and gal capped SiNPs was tested using Con A (figure 4.20). Con A is a lectin, which has strong binding specificity toward mannose and weak binding affinity towards galactose. One ConA contain four mannose binding sites which can cross link to multiple mannose functionalized SiNPs, leading to the aggregation of the nanoparticles which results in the reduction of emission at 464 nm (Figure 4.21a,b). This aggregation can also be seen in TEM images (Figure 4.21c).
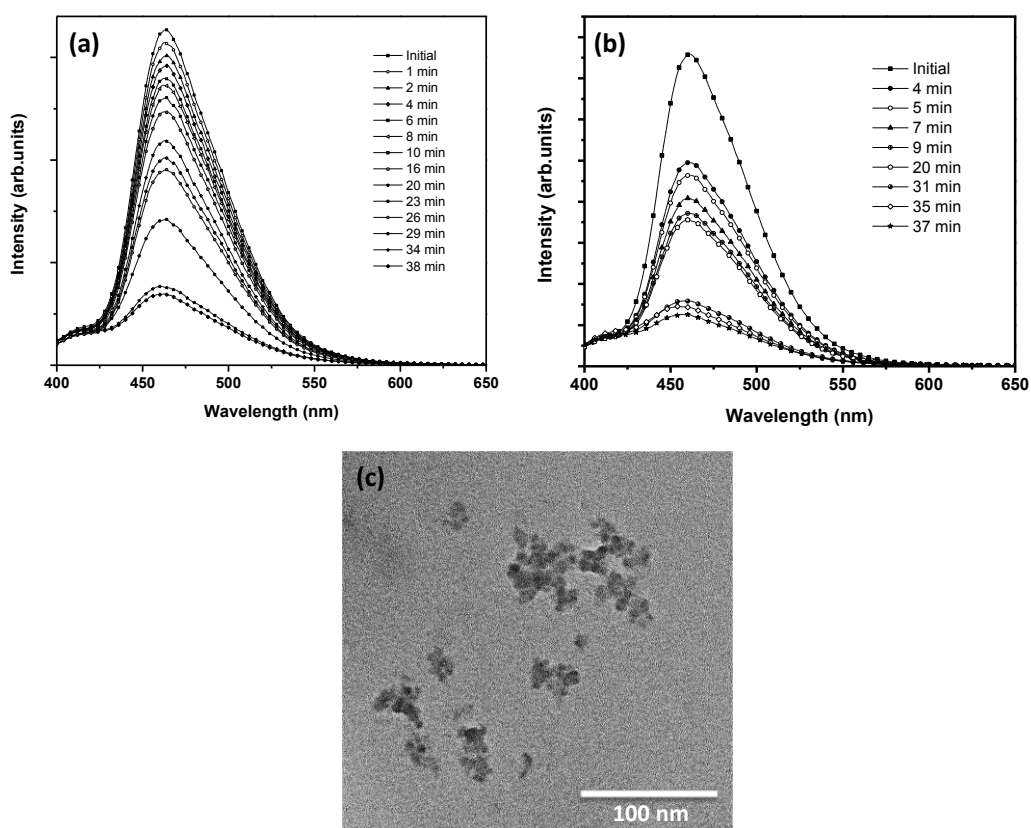
Figure 4.21 (a) Aggregations of man capped SiNPs and (b) gal capped SiNPs with Con A as monitored by PL spectroscopy. (c) TEM image of man capped SiNPs after addition of Con A.

Upon the addition of ConA to man (4.21a) and gal (4.21b) capped SiNPs, visible aggregates of particles were observed within a minute. This aggregation is associated with a significant reduction in the intensity of the luminescence peak at 464 nm (Figure 4.21a,b). The suspended aggregates gradually precipitated out of solution. After approximately 4 hrs all of the nanoparticle systems had completely precipitated, as shown by the gradual decreasing PL intensity with increasing time in Figure 4.21a,b. The man and gal capped SiNPs were also examined by TEM before and after ConA addition. Before ConA addition, the NPs were highly dispersed, (figure 4.1a), whereas large aggregates were formed after ConA addition (Figure 4.21c).
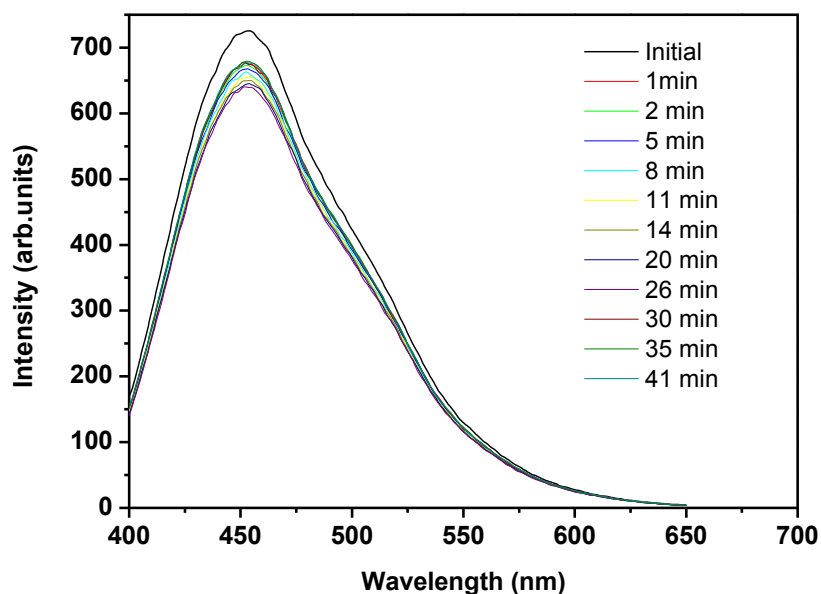
Figure 4.22: PL of amine terminated SiNPs upon addition of ConA with time

Amine terminated SiNPs was used as a control. In Figure 4.22, it is clearly seen that upon addition of ConA amine terminated SiNPs do not form any aggregation over time and therefore no loss in PL emission at 453 nm was observed.

4.10 Targeting Cancerous Cells

After functionalizing, characterizing and obeying the biochemical activity or interaction with Con A protein, it was time to test the effect of this multi functionalized carbohydrate capped SiNPs on the cells. Here as a proof of principle, only the influence of man capped SiNPs in MCF-7 cells was tested. Other carbohydrate capped SiNPs (gal, glu and lac) were tested on the cells including stability, toxicity etc. and this is briefly explained in chapter 5.

It is well known that mannose has a strong binding affinity towards lactin,[67] which is present on the surface of cells and is also well characterized with Escherichia coli system.[68,69] After successfully detecting lactin, we evaluated the effectiveness of Man-capped SiNPs in mammalian cell interaction and cancer cell detection. Antibodies can be used to detect particular antigens. However, some mutant cancer cells lack these markers. Also, antibodies can only bind to specific cell surface biomolecules. In contrast, carbohydrates can interact with a multitude of cells and impart information regarding carbohydrate receptors, therefore limiting the number of possible reagents.[70] MCF-7, a human breast cancer cell line

was chosen as the targeting cells by Man-capped SiNPs. In a non-cancerous cell line, galactoside binding galactines-4, -7, and -8 are absent. However, these galactines are present in the MCF-7 cancer cells.[71] This imaging experiment and cell culture was kindly performed by Dr Anja Muller from UEA (PHA). The MCF-7 cell line for this experiment was kindly supplied by Dr Yongping Bao from UEA (MED).

Fluorescence microscope images are shown in Figure 4.23. The control image of MCF-7 cells without incubation of SiNPs is shown in Figure 4.23a, bright fluorescence arises from the emission of man capped SiNPs shown in figure 4.23b.
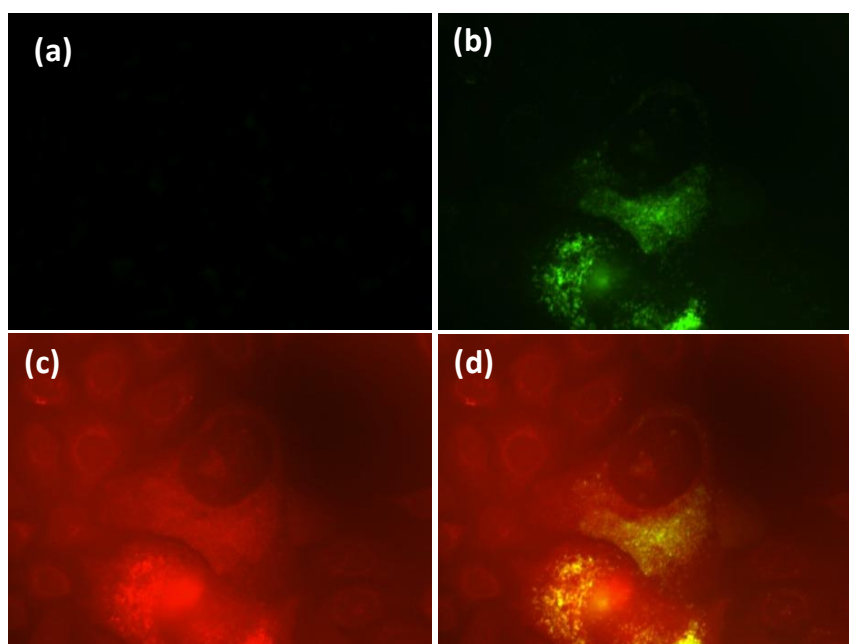
Figure 4.23: Fluorescence images inside living MCF-7 cancerous cells: (a) control; (b) fluorescence from Man-capped SiNPs inside the cells after 48 h incubation; (c) after 48 h Lysotracker stain; (d) merged images. Pictures were taken on live cells using a Leica fluorescence microscope.

In order to visualize the lysosomes, cells were stained with Lysotracker-Red, (see Figure 4.23c). The merged results are also shown in Figure 4.23d. The selective uptake and intracellular accumulation of man-capped SiNPs in MCF-7 cells is clearly observed and thus can lead to the further development of Man-capped SiNPs as a vehicle for targeted drug delivery.[72] Importantly, morphological damage to aqueous Man-capped SiNPs treated cells cannot be observed.

The strongly binding man-capped SiNPs are found to be internalized by the breast cancer cells. Although only one tumor cell line was used in this study, there is a possibility

that man-capped SiNPs may bind to other cancerous cell lines if there are similar receptors located on the surface of these cells. The research is still in progress using different types of tumor cells and testing them with man-capped SiNPs.

4.11 Crystallization of Carbohydrate capped SiNPs

Recently, there has been growing interest in assembling inorganic nanoparticles to exploit their collective properties and the possibility of using these properties in functional devices. Ensembles of nanoparticles can be used to improve the mechanical properties of composite materials; moreover they can display new electronic, magnetic and optical properties as a result of interactions between the excitons, magnetic moments or surface plasmons of individual nanoparticles.

Assembly is directed by the balance of attractive forces (such as covalent or hydrogen bonding, electrostatic attraction between oppositely charged ligands, depletion forces or dipole-dipole interactions) and repulsive forces (such as steric forces and electrostatic repulsion between ligands of like charge).[73] Self-organization of nanoparticles generates a variety of structures, including chains,[74-77] sheets,[78, 79] vesicles,[76, 80, 81] three-dimensional (3D) crystals[82-85] or more complex 3D architectures.[86]

Recently, the formation of 3D nanoparticle crystals with face-centered or body-centered cubic lattice structures was mediated by hybridizing complementary DNA molecules attached to the nanoparticle surface.[82, 83] The variation in DNA sequences or length of DNA linkers, and the absence or presence of a non-bonding single-base flexor, was used to tune interactions between the nanoparticle-DNA conjugates.

In a different strategy, crystals with a diamond-like structure were grown from oppositely charged gold and silver nanoparticles.[85] Crystallization of nanoparticles was achieved by screening electrostatic interactions; so that each nanoparticle was surrounded by a layer of counter-ions and the nanoparticles interacted by short-range potentials.

Here, we report the crystals or self-assembly of SiNPs into three-dimensional superlattice structures, using carbohydrate moieties which act as interparticle linkages. The formation of needle like crystal structures was observed in a nanoparticle based system. The characterization of these carbohydrate driven SiNPs crystals was carried out by using synchrotron FTIR, Scanning electron microscopy (SEM), EDX analysis and HRTEM images. Synchrotron FTIR microscopy as the main characterization technique was used to study the carbohydrate capped SiNPs crystals, due to the several advantages mentioned below.

142

4.11.1 SEM images of Carbohydrate capped SiNPs Crystals

After preparing the sample, SEM was used to visualize the shape and size of the crystals. Figure 4.24 shows the SEM images of glu capped SiNPs taken on to the carbon coated sample holder. The crystals were dropped onto the sample holder and coated with Gold (Au) as a reference for 5 minutes.
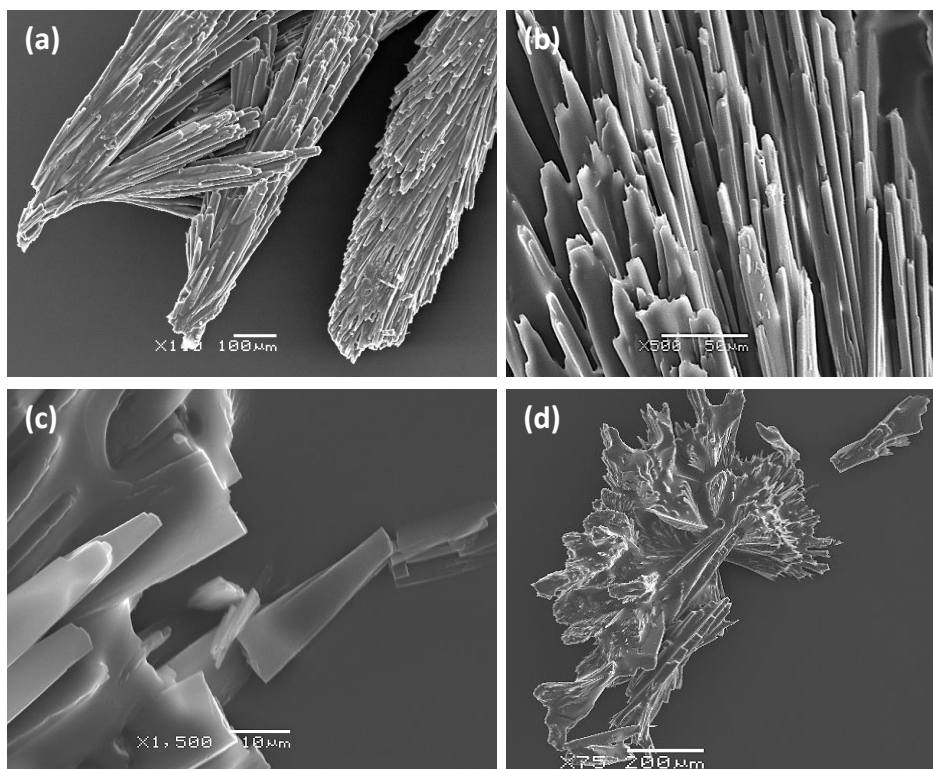
Figure 4.24: SEM images of (a) glucose, (b) galactose, (c) lactose and (d) mannose capped SiNPs crystals

The SEM images of glu, gal, lac and man capped SiNPs shown in figure 4.24, confirm the needle and sheet like crystal structure grown in methanol. The images also show the root of the crystals. The SEM obtained images showed that the gal, glu and man capped SiNPs crystals present a needle like structure whereas the lactose capped SiNPs crystals present a flat sheet or flat needle like structure.

4.11.2 HRTEM images of Carbohydrate capped SiNPs Crystals

The next point was to confirm whether the SiNPs act as a seed to self-assemble the crystal or act as an impurity. In order to confirm and understand the arrangement of SiNPs inside the crystals HRTEM imaging was further performed.

The HRTEM of carbohydrate capped SiNPs were acquired at Leeds University (Leeds, UK) in collaboration with Prof. Rik Brydson and group. Figure 4.22 shows the HRTEM image of glucose capped SiNPs crystals. The sample was placed on the grid and a drop of methanol was added to disperse the crystal.
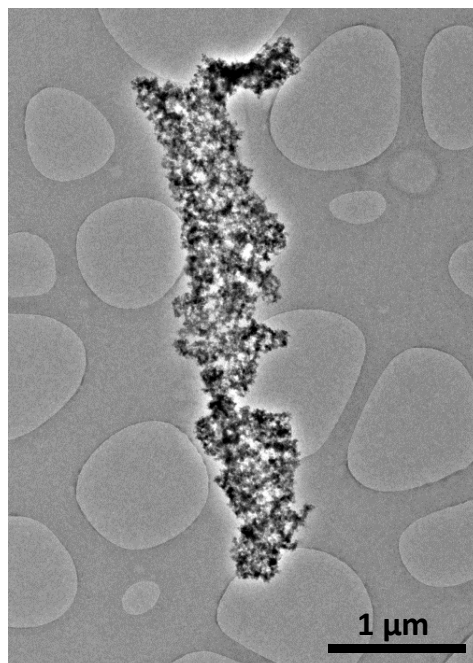
Figure 4.25: HRTEM image of glucose capped SINPs crystal.

In figure 4.25 the needle shaped glu capped SiNPs crystal shows the skeleton of the SiNPs arranged inside the crystal. These results are promising, however further study needs to be undertaken to find out the special arrangement of SiNPs inside the crystal. The HRTEM image found to be unsuccessful to provide this information. Hypothetically, if the SiNPs inside the crystal are arranged in 3D form then it is difficult to confirm the assemblies of SiNPs inside the crystal.

4.11.3 Elemental Analysis of Carbohydrate SiNPs Crystals

4.11.3.1 EDX Measurements

In order to confirm that the crystals are of the carbohydrate capped SiNPs and are not of the carbohydrates themselves, we performed EDX analysis. Figure 4.26 shows the EDX analysis of carbohydrate capped SiNPs crystals.
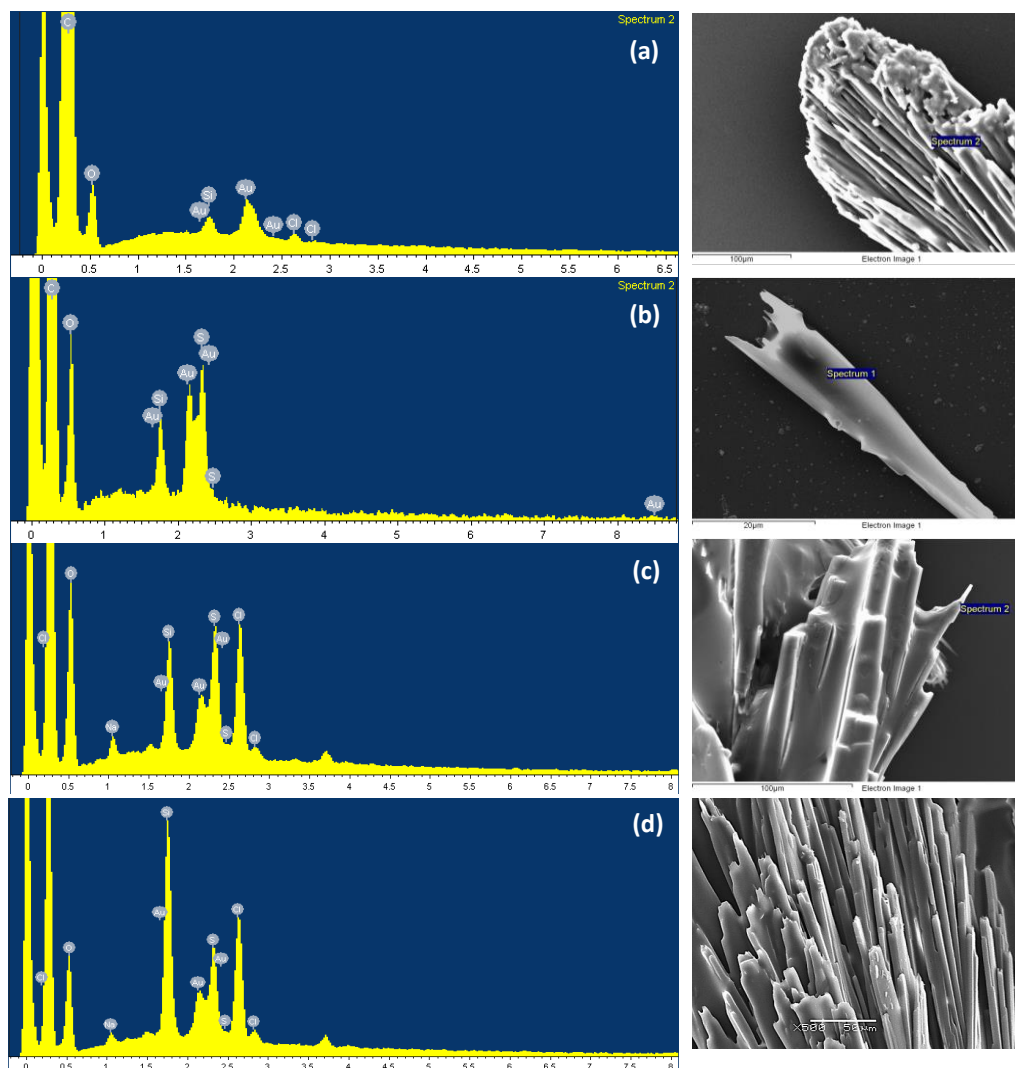
Figure 4.26: EDX analysis (left) and SEM images (right) of carbohydrate capped SiNP crystals. (a) glu capped SiNP, (b) lac capped SiNPs, (c) man capped SiNPs and (d) gal capped SiNPs.

In figure 4.26 the EDX graph (left) shows the silicon peak in reference to Au. The EDX analysis for all carbohydrate capped SiNPs crystals confirms that the crystals are not only from the starting material sugar but from the carbohydrate capped SiNPs.

4.11.3.2 Synchrotron FTIR Measurements

To confirm the bonding environment of these crystals, synchrotron FTIR microscopy measurement was carried out. The principle of FT-IR spectroscopy is to promote the excitation of molecular vibrations by submitting a sample to an infrared beam. The vibrational energy usually expressed as wave numbers is sensitive to the molecular composition of the atoms involved in the bond, nature of the bond, surrounding atoms, structure of the bond, etc. The technique is extensively used to characterize both organic and

145

inorganic samples. The principle of FTIR microscopy is to couple an FTIR spectrometer with a microscope. It enables on one hand to visualize the sample and to choose specifically the region for analysis and on the other hand to carry out two-dimensional acquisitions by raster scanning the sample. Infrared spectra are acquired at each pixel of 1D, 2D or 3D maps, and chemical maps can thus be derived. The principle of synchrotron FTIR microscopy is to use the synchrotron emission in the infrared domain as a source for FTIR microscopy. Compared to classical and normal FTIR sources, the synchrotron radiation brightness is far greater and enables the beam size to be reduced below 10 μm without a significant loss of photons. The usefulness of synchrotron (SR) FTIR micro spectroscopy derives from the fact that the IR source is 10-1000 times more intense than the conventional laboratory source.[87]

This equates to superior signal to noise ratios[88] in the resultant spectra, improving acquisition times and spatial resolution, both of which are important for analyzing the samples. Hence, by looking at all advantages of SR-FTIR spectroscopy, it's been chosen to study the carbohydrate capped SiNPs as it is a powerful characterizing technique for the location of chemical structure and physical heterogeneities in materials, as well as determinations of their association with localized inclusions.

The SR-FTIR experiments were carried out at Max-lab, Lund, Sweden. The crystals of carbohydrate capped SiNPs were grown in methanol at room-temperature (see chapter 2). The non-crystalline samples of carbohydrate capped SiNPs were freshly prepared and dried under reduced pressure. FTIR spectra of the corresponding acid sugar were also taken to compare with those of the functionalized carbohydrate SiNPs.

To characterize the bonding environment within the crystals, we performed the SR-FTIR measurements on acid functionalized sugar (starting material), non-crystalline sample (carbohydrate capped SINPs without forming crystals) and the crystals of carbohydrate capped SiNPs.

Figure 4.27 and 4.29 show the 2D and 3D images of SR-FTIR on the gal and man capped SiNP crystals respectively. Figure 4.28 and 4.30 shows the FTIR spectrum of gal and man capped SiNPs crystals. The sample was dried at room temperature and dropped on CaF_2 substrate.
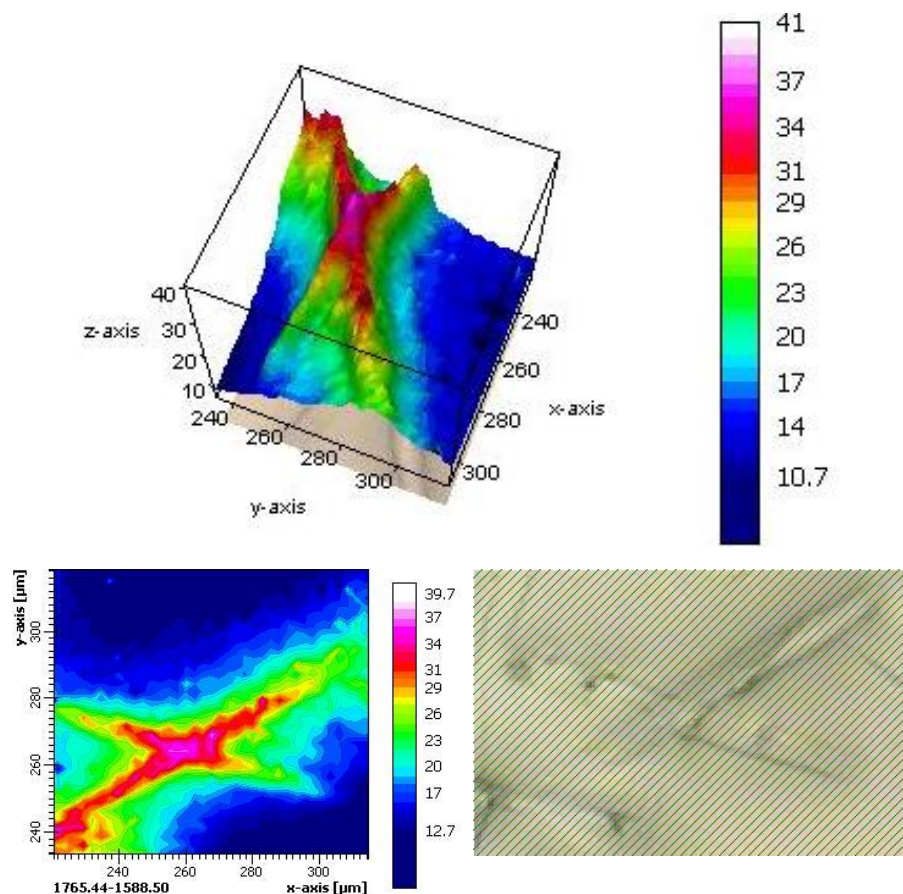
Figure 4.27: Mapping spectrum over an area of galactose capped SiNPs showing 2D and 3D spectrum. Red represents high intensity and blue represents low intensity along with video mapping image area. The 3D mapping area was selected from the amide bonding region from 1765 cm^{-1} to 1580 cm^{-1}.
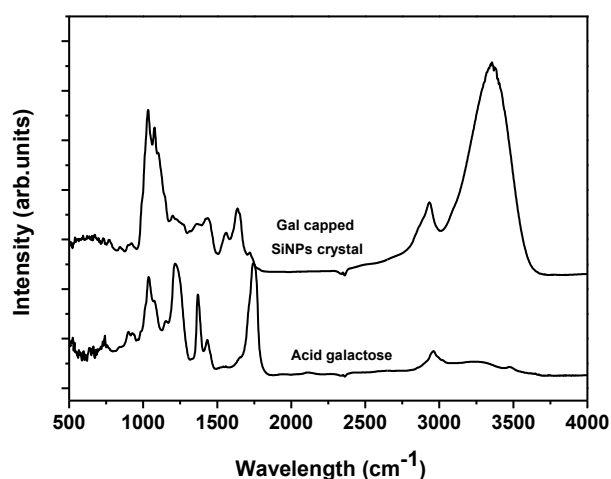
Figure 4.28: FTIR spectrum of gal capped SiNPs crystals and starting material acid galactose

Figure 4.29 show the 2D and 3D FTIR images of man capped SiNPs crystals.
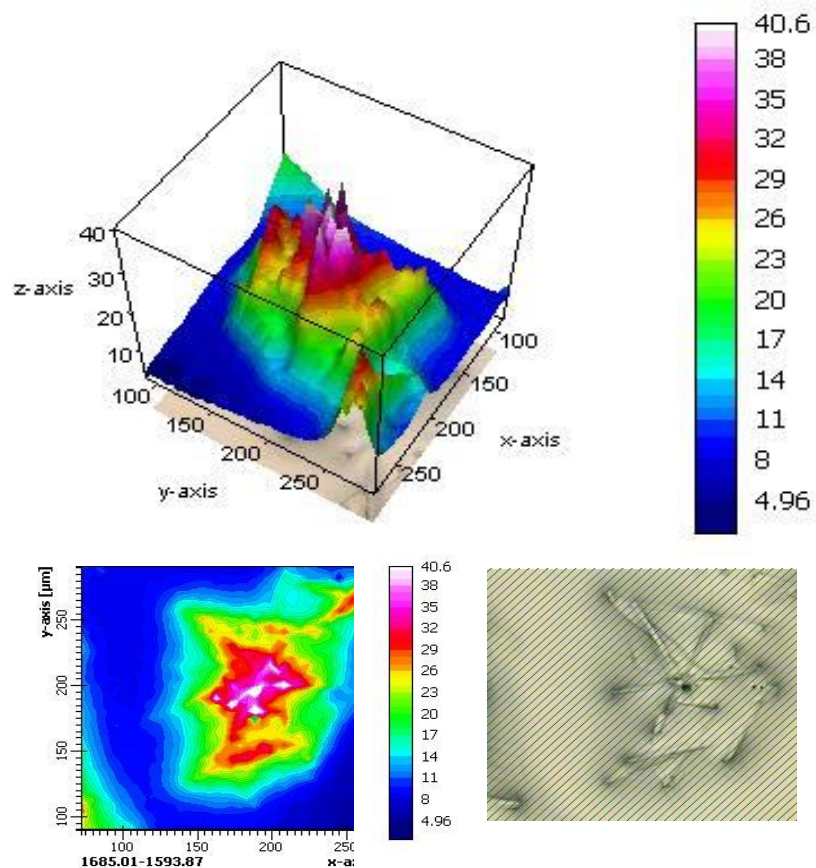
Figure 4.29: Mapping spectrum over an area of mannose capped SiNPs showing 2D and 3D spectrum. Red represents high intensity and blue represents low intensity along with video mapping image area. The 3D mapping area was selected from the amide bonding region from 1685 cm^{-1} - 1593 cm^{-1}.
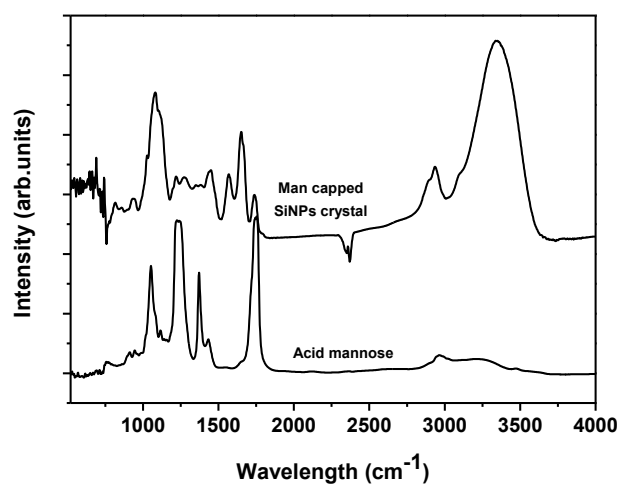
Figure 4.30: FTIR spectrum of man capped SiNPs crystals and starting material acid mannose

As mention above, the important characteristic of SR-FTIR microscopy is that it allows to map an interesting area of the sample and to perform the FTIR analysis on it. In

Figure 4.27 and 4.29 the crystals of gal and man capped SiNPs are clearly shown, the area of the crystals was mapped and analysis was performed. In order to confirm that the crystals are from the carbohydrate capped SiNPs and not from the starting material, the amide bonding region which appears from 1620 cm^{-1} to 1690 cm^{-1} region was integrated. After integrating the amide bonding region of 2D and 3D FTIR, it is clearly noticeable from higher intensity that the crystals are from the carbohydrate capped SiNPs.

Figure 4.28 and 4.30 show a typical FTIR spectrum of gal and man capped SiNPs crystals. The spectrum shows the feature around 3349 cm^{-1} characteristic of O-H bonding, 2929 cm^{-1} C-H bonding, 1651 cm^{-1} amide stretching, N-H stretching and C-N bending around 1560 cm^{-1}, Si-CH$_2$ symmetric bending and vibrational scissoring is at 1277 cm^{-1} and 1447 cm^{-1} respectively and feature at 1080 cm^{-1} is from C-OH, C-O, Si-O bonding. The amide bond at around 1634-1655 cm^{-1} is clearly visible in both FTIR spectra. The overall SR-FTIR spectrum confirms that the crystals are from the carbohydrate capped SiNPs and not from the carbohydrate itself.

Furthermore to confirm the bonding analysis, the 2D and 3D FTIR spectra on non-crystalline samples of carbohydrate capped SiNPs were acquired. The FTIR spectra on two different types of samples were performed. Firstly, the sample was dispersed in methanol and drop cast on the CaF$_2$ substrate. After drying, a thin layer of sample was formed on the substrate. A second sample was dried under vacuum and the powder was dropped on the CaF$_2$ substrate. The third sample was measured in combination of both thin layer as well as the dried sample.

4.11.3.2.1 Mannose capped SiNPs

The man capped SiNPs sample was dispersed in methanol (MeOH) and drop cast on Calcium fluoride (CaF$_2$) substrate. The substrate was placed at room temperature until the sample had dried out completely and later was introduced on the spectrometer. The area of interest was chosen and the region was mapped. Figure 4.28 represents 3D and 2D SR-FTIR spectra of man capped SiNPs, along with the image of the mapped area.
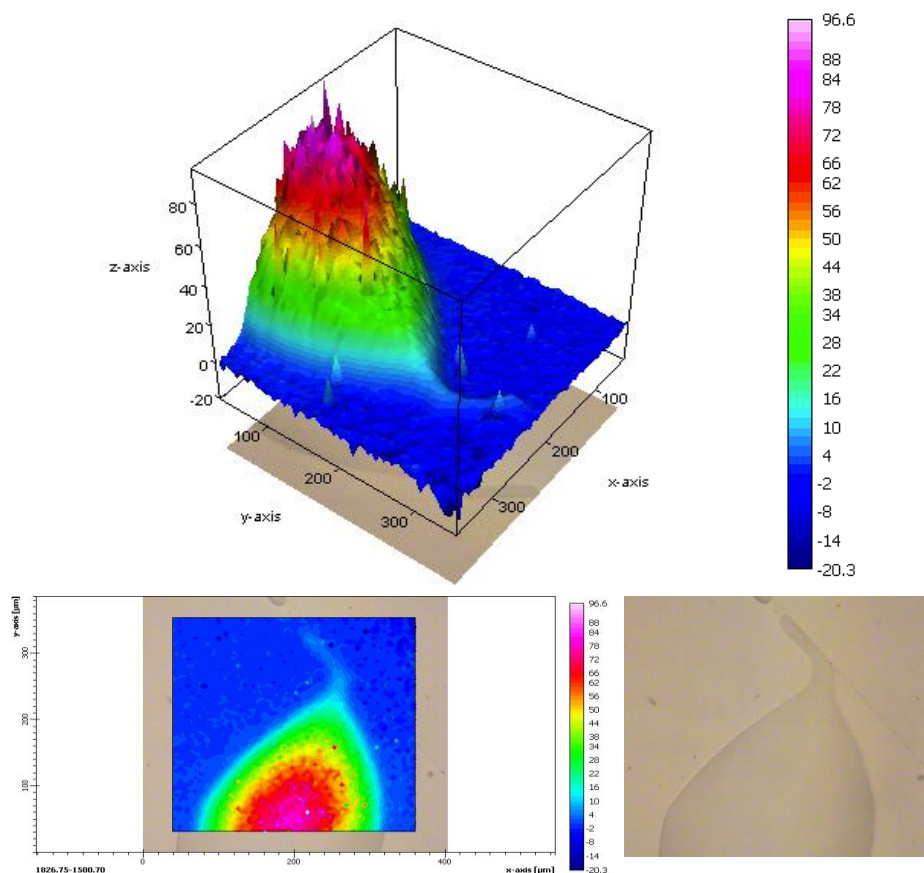
Figure 4.31: Mapping spectrum over an area of mannose capped SiNPs showing the distribution of Man capped SiNPs in 3D and 2D plot along with video image of the area mapped out of man capped SiNPs. The red represents high intensity, and blue represents low intensity.

The higher intensity map of 2D and 3D SR-FTIR spectra of man capped SiNPs was selected from 1826 cm^{-1}-1500 cm^{-1} as the feature from amide bonding. The overall bonding feature appears very sharp and clear compared with the conventional laboratory source.

4.11.3.2.2 Glucose capped SiNPs

The half of glucose capped SiNPs sample was dispersed in MeOH and drop cast on CaF$_2$ substrate, dried in vacuum at RT. The other half sample in the form of a dried powder was also dropped on the substrate and introduced in the scanning chamber. Interesting area was mapped as a combination of thin film and dried powder samples. Figure 4.29 shows the 3D, 2D and typical SR FTIR spectra of glucose capped SiNPs along with mapping image area.
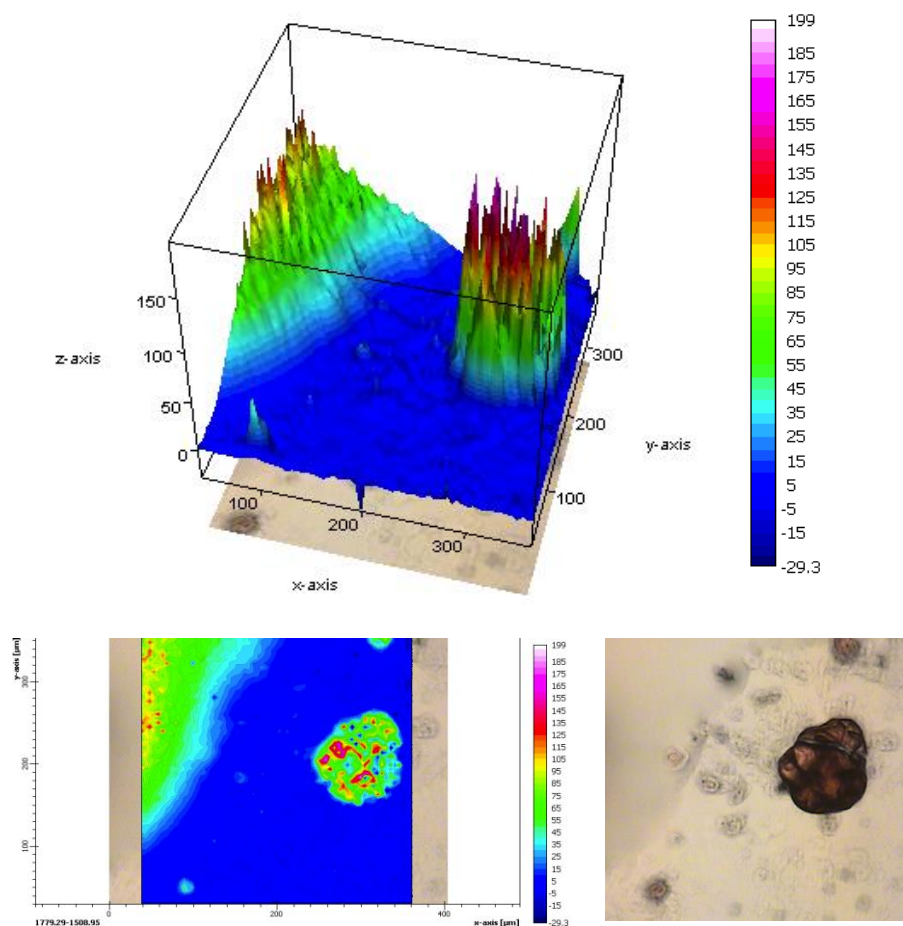
Figure 4.32: Mapping spectrum over an area of glucose capped SiNPs showing 3D and 2D mapping. Red represents high intensity and blue represents low intensity along with video mapping image area.

The amide bonding area for glu capped SiNPs was integrated from 1759-1509 cm^{-1}.

4.11.3.2.3 Lactose capped SiNPs

The dried powder of lactose capped SiNPs was dropped on CaF$_2$ substrate and the interesting area was mapped. Figure 4.33 shows the 3D and 2D images of lactose capped SiNPs. The amide bonding region was integrated from 1771-1490 cm^{-1}.
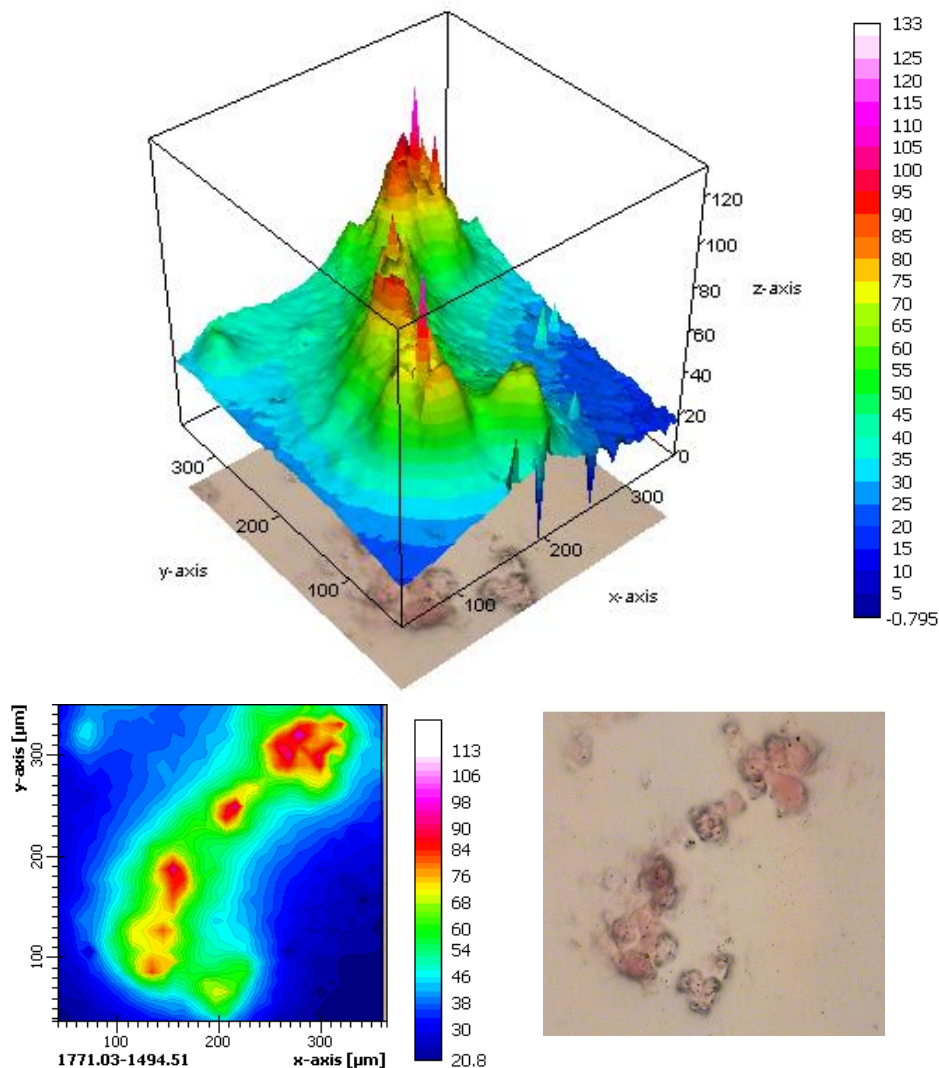
Figure 4.33: Mapping spectrum over an area of lactose capped SiNPs showing the distribution of lac capped SiNPs in 3D and 2D plot along with video image of the area mapped. The red represents high intensity, and blue represents low intensity.

All the obtained results for the crystal sample and non-crystalline sample showed no difference when the amide bonding region was integrated. This confirms that the crystals are from carbohydrate capped SiNPs and not from the carbohydrate alone.

The carbohydrate capped SiNPs crystals were accidentally noticed to be growing in methanol. Initially it was assumed that the crystals were forming due to the hydrogen bonding present in carbohydrate moiety, to confirm this phenomenon the crystals were grown with acetate (OAc) protected carbohydrate capped SiNPs (OAc-carbohydrate capped SiNPs) and it was noticed that the crystals grow even faster and much better than that of

unprotected carbohydrate capped SiNPs. This result indicates that the crystals are not completely driven by carbohydrate moiety, in which SiNPs act as an impurity, whereas the crystals are actually driven by overall carbohydrate capped SiNPs.

4.12 Conclusion

In conclusion, a simple method has been demonstrated to synthesize highly pure stable and brightly luminescent carbohydrate capped SiNPs through the utilization of amine-terminated SiNPs and by using carbodiimide-coupling reagent. The SiNPs capped with carbohydrate functionality show strong blue photoluminescence under UV excitation in water and strong orange photoluminescence in the solid state, with a high QY efficiency. These surface functionalized nanoparticles are stable against degradation over several weeks. The FTIR and NMR spectra obtained display the surface functionalization, confirming that the surface is effectively modified with carbohydrate moiety such as galactose, mannose, glucose and lactose. The EDX confirmed the makeup of the core shell of SiNPs as well as the overall chemical composition. The biochemical activity of highly pure gal and man capped SiNPs were tested with ConA. As an example, the SiNPs targeting MCF-7 has been investigated under the fluorescence microscope. The present work not only has implications in the area of surface functionalization of SiNPs but also has a broad potential to allow for study of various further applications, with considerable interest in both medicine and biology.

4.13 References

1.   Huang, X.; Neretina, S.; El-Sayed, M. A., Gold Nanorods: From Synthesis and Properties to Biological and Biomedical Applications. *Advanced Materials* **2009,** *21* (48), 4880-4910.

2.   Peer, D.; Karp, J. M.; Hong, S.; Farokhzad, O. C.; Margalit, R.; Langer, R., Nanocarriers as an emerging platform for cancer therapy. *Nat Nano* **2007,** *2* (12), 751-760.

3.   Ferrari, M., Cancer nanotechnology: opportunities and challenges. *Nat Rev Cancer* **2005,** *5* (3), 161-171.

4.   Pankhurst, Q. A.; Connolly, J.; Jones, S. K.; Dobson, J., Applications of magnetic nanoparticles in biomedicine. *Journal of Physics D: Applied Physics* **2003,** *36* (13), R167.

5.   Gabius, H.-J.; Siebert, H.-C.; André, S.; Jiménez-Barbero, J.; Rüdiger, H., Chemical Biology of the Sugar Code. *ChemBioChem* **2004,** *5* (6), 740-764.

6.   Hakomori, S., Glycosylation defining cancer malignancy: new wine in an old bottle. *Proceedings of the National Academy of Sciences of the United States of America* **2002,** *99* (16), 10231-10233.

7.   Dwek, R. A., Glycobiology:Toward Understanding the Function of Sugars. *Chemical Reviews* **1996,** *96* (2), 683-720.

8.   Babu, P.; Sinha, S.; Surolia, A., Sugar–Quantum Dot Conjugates for a Selective and Sensitive Detection of Lectins. *Bioconjugate Chemistry* **2006,** *18* (1), 146-151.

9.   Dam, T. K.; Brewer, C. F., Thermodynamic Studies of Lectin–Carbohydrate Interactions by Isothermal Titration Calorimetry. *Chemical Reviews* **2002,** *102* (2), 387-430.

10.   Ratner, D. M.; Adams, E. W.; Disney, M. D.; Seeberger, P. H., Tools for Glycomics: Mapping Interactions of Carbohydrates in Biological Systems. *ChemBioChem* **2004,** *5* (10), 1375-1383.

11.   Oh, E.; Lee, D.; Kim, Y.-P.; Cha, S. Y.; Oh, D.-B.; Kang, H. A.; Kim, J.; Kim, H.-S., Nanoparticle-Based Energy Transfer for Rapid and Simple Detection of Protein Glycosylation. *Angewandte Chemie International Edition* **2006,** *45* (47), 7959-7963.

12.   Lis, H.; Sharon, N., Lectins: Carbohydrate-Specific Proteins That Mediate Cellular Recognition. *Chemical Reviews* **1998,** *98* (2), 637-674.

13.   Lindhorst, T. K., *Essentials of carbohydrate chemistry and biochemistry*. Wiley-VCH: Weinheim, 2003.

14.   Lee, Y. C.; Lee, R. T., Carbohydrate-Protein Interactions: Basis of Glycobiology. *Accounts of Chemical Research* **1995,** *28* (8), 321-327.

15.   Mammen, M.; Choi, S.-K.; Whitesides, G. M., Polyvalent Interactions in Biological Systems: Implications for Design and Use of Multivalent Ligands and Inhibitors. *Angewandte Chemie International Edition* **1998,** *37* (20), 2754-2794.

16.   Lundquist, J. J.; Toone, E. J., The Cluster Glycoside Effect. *Chemical Reviews* **2002,** *102* (2), 555-578.

17.   Iqbal, S. S.; Mayo, M. W.; Bruno, J. G.; Bronk, B. V.; Batt, C. A.; Chambers, J. P., A review of molecular recognition technologies for detection of biological threat agents. *Biosensors and Bioelectronics* **2000,** *15* (11–12), 549-578.

18.   Huang, X.; Wang, Z., 1.10 - Strategies in Oligosaccharide Synthesis. In *Comprehensive Glycoscience*, Kamerling, H., Ed. Elsevier: Oxford, 2007; pp 379-413.

19.   Gupta, A. K.; Gupta, M., Synthesis and surface engineering of iron oxide nanoparticles for biomedical applications. *Biomaterials* **2005,** *26* (18), 3995-4021.

20.   Koh, I.; Wang, X.; Varughese, B.; Isaacs, L.; Ehrman, S. H.; English, D. S., Magnetic Iron Oxide Nanoparticles for Biorecognition: Evaluation of Surface Coverage and Activity. *The Journal of Physical Chemistry B* **2006,** *110* (4), 1553-1558.

21.   Lin, C.-C.; Yeh, Y.-C.; Yang, C.-Y.; Chen, C.-L.; Chen, G.-F.; Chen, C.-C.; Wu, Y.-C., Selective Binding of Mannose-Encapsulated Gold Nanoparticles to Type 1 Pili in Escherichia coli. *Journal of the American Chemical Society* **2002,** *124* (14), 3508-3509.

22.   Macher, B. A.; Galili, U., The Galα1,3Galβ1,4GlcNAc-R (α-Gal) epitope: A carbohydrate of unique evolution and clinical relevance. *Biochimica et Biophysica Acta (BBA) - General Subjects* **2008,** *1780* (2), 75-88.

23.   Horak, D.; Babic, M.; Jendelova, P.; Herynek, V.; Trchova, M.; Pientka, Z.; Pollert, E.; Hajek, M.; Sykova, E., d-Mannose-Modified Iron Oxide Nanoparticles for Stem Cell Labeling. *Bioconjugate Chemistry* **2007,** *18* (3), 635-644.

24.   Martínez-Ávila, O.; Hijazi, K.; Marradi, M.; Clavel, C.; Campion, C.; Kelly, C.; Penadés, S., Gold Manno-Glyconanoparticles: Multivalent Systems to Block HIV-1 gp120 Binding to the Lectin DC-SIGN. *Chemistry - A European Journal* **2009,** *15* (38), 9874-9888.

25.   Rojo, J.; Díaz, V.; de la Fuente, J. M.; Segura, I.; Barrientos, A. G.; Riese, H. H.; Bernad, A.; Penadés, S., Gold Glyconanoparticles as New Tools in Antiadhesive Therapy. *ChemBioChem* **2004,** *5* (3), 291-297.

26.   O'Farrell, N.; Houlton, A.; Horrocks, B. R., Silicon nanoparticles: applications in cell biology and medicine. *International Journal of Nanomedicine* **2006,** *1* (4), 451-472.

27.   Wang, Q.; Ni, H.; Pietzsch, A.; Hennies, F.; Bao, Y.; Chao, Y., Synthesis of water-dispersible photoluminescent silicon nanoparticles and their use in biological fluorescent imaging. *Journal of Nanoparticle Research* **2011,** *13* (1), 405-413.

28.   Sato, S.; Swihart, M. T., Propionic-Acid-Terminated Silicon Nanoparticles: Synthesis and Optical Characterization. *Chemistry of Materials* **2006,** *18* (17), 4083-4088.

29.   Belomoin, G.; Therrien, J.; Smith, A.; Rao, S.; Twesten, R.; Chaieb, S.; Nayfeh, M. H.; Wagner, L.; Mitas, L., Observation of a magic discrete family of ultrabright Si nanoparticles. *Applied Physics Letters* **2002,** *80* (5), 841-843.

30.   English, D. S.; Pell, L. E.; Yu, Z.; Barbara, P. F.; Korgel, B. A., Size Tunable Visible Luminescence from Individual Organic Monolayer Stabilized Silicon Nanocrystal Quantum Dots. *Nano Letters* **2002,** *2* (7), 681-685.

31.   Rogozhina, E. V.; Eckhoff, D. A.; Gratton, E.; Braun, P. V., Carboxyl functionalization of ultrasmall luminescent silicon nanoparticles through thermal hydrosilylation. *Journal of Materials Chemistry* **2006,** *16* (15), 1421-1430.

32.   Schuppler, S.; Friedman, S. L.; Marcus, M. A.; Adler, D. L.; Xie, Y. H.; Ross, F. M.; Chabal, Y. J.; Harris, T. D.; Brus, L. E.; Brown, W. L.; Chaban, E. E.; Szajowski, P. F.; Christman, S. B.; Citrin, P. H., Size, shape, and composition of luminescent species in oxidized Si nanocrystals and H-passivated porous Si. *Physical Review B* **1995,** *52* (7), 4910.

33.   Rogozhina, E.; Belomoin, G.; Smith, A.; Abuhassan, L.; Barry, N.; Akcakir, O.; Braun, P. V.; Nayfeh, M. H., Si--N linkage in ultrabright, ultrasmall Si nanoparticles. *Applied Physics Letters* **2001,** *78* (23), 3711-3713.

34.   Warner, J. H.; Hoshino, A.; Yamamoto, K.; Tilley, R. D., Water-soluble photoluminescent silicon quantum dots. *Angewandte Chemie-International Edition* **2005,** *44* (29), 4550-4554.

35.   Rosso-Vasic, M.; Spruijt, E.; van Lagen, B.; De Cola, L.; Zuilhof, H., Alkyl-Functionalized Oxide-Free Silicon Nanoparticles: Synthesis and Optical Properties. *Small* **2008,** *4* (10), 1835-1841.

36.   Mayne, A. H.; Bayliss, S. C.; Barr, P.; Tobin, M.; Buckberry, L. D., Biologically Interfaced Porous Silicon Devices. *physica status solidi (a)* **2000,** *182* (1), 505-513.

37.   Erogbogbo, F.; Yong, K.-T.; Roy, I.; Xu, G.; Prasad, P. N.; Swihart, M. T., Biocompatible Luminescent Silicon Quantum Dots for Imaging of Cancer Cells. *ACS Nano* **2008,** *2* (5), 873-878.

38.   Nilsson, J. R., How Cytotoxic is Zinc? A Study on Effects of Zinc on Cell Proliferation, Endocytosis, and Fine Structure of the Ciliate Tetrahymena. *Acta Protozool* **2003,** *42*, 19-29.

39.   Kirchner, C.; Liedl, T.; Kudera, S.; Pellegrino, T.; Muñoz Javier, A.; Gaub, H. E.; Stölzle, S.; Fertig, N.; Parak, W. J., Cytotoxicity of Colloidal CdSe and CdSe/ZnS Nanoparticles. *Nano Letters* **2004,** *5* (2), 331-338.

40.   Wang, Q.; Bao, Y.; Ahire, J.; Chao, Y., Co-encapsulation of Biodegradable Nanoparticles with Silicon Quantum Dots and Quercetin for Monitored Delivery. *Advanced Healthcare Materials* **2013,** *2*, 459-465.

41.   Miller, D. A. B., Silicon sees the light. *Nature* **1995,** *378*, 238.

42.   Alsharif, N. H.; Berger, C. E. M.; Varanasi, S. S.; Chao, Y.; Horrocks, B. R.; Datta, H. K., Alkyl-Capped Silicon Nanocrystals Lack Cytotoxicity and have Enhanced Intracellular Accumulation in Malignant Cells via Cholesterol-Dependent Endocytosis. *Small* **2009,** *5* (2), 221-228.

43.   Arya, H.; Kaul, Z.; Wadhwa, R.; Taira, K.; Hirano, T.; Kaul, S. C., Quantum dots in bio-imaging: Revolution by the small. *Biochemical and Biophysical Research Communications* **2005,** *329* (4), 1173-1177.

44.   Kramer, J. R.; Deming, T. J., Glycopolypeptides via Living Polymerization of Glycosylated-l-lysine N-Carboxyanhydrides. *Journal of the American Chemical Society* **2010,** *132* (42), 15068-15071.

45.   Taylor, C. M., Glycopeptides and glycoproteins: Focus on the glycosidic linkage. *Tetrahedron* **1998,** *54* (38), 11317-11362.

46.   Nakajima, N.; Ikada, Y., Mechanism of Amide Formation by Carbodiimide for Bioconjugation in Aqueous Media. *Bioconjugate Chemistry* **1995,** *6* (1), 123-130.

47.   Wang, Q.; Bao, Y.; Zhang, X.; Coxon, P. R.; Jayasooriya, U. A.; Chao, Y., Uptake and Toxicity Studies of Poly-Acrylic Acid Functionalized Silicon Nanoparticles in Cultured Mammalian Cells. *Advanced Healthcare Materials* **2012,** *1*, 189-198.

48.   Kumar, C. G.; Mamidyala, S. K.; Reddy, M. N.; Reddy, B. V. S., Silver glyconanoparticles functionalized with sugars of sweet sorghum syrup as an antimicrobial agent. *Process Biochem.* **2012,** *47* (10), 1488-1495.

49.	Earhart, C.; Jana, N. R.; Erathodiyil, N.; Ying, J. Y., Synthesis of Carbohydrate-Conjugated Nanoparticles and Quantum Dots. *Langmuir* **2008,** *24* (12), 6215-6219.

50.	Chao, Y.; Wang, Q.; Pietzsch, A.; Hennies, F.; Ni, H., Soft X-ray induced oxidation on acrylic acid grafted luminescent silicon quantum dots in ultrahigh vacuum. *Physica Status Solidi a-Applications and Materials Science* **2011,** *208* (10), 2424-2429.

51.	Wagner, C.; Riggs, W.; Davis, L.; Moulder, J., Handbook of X-ray photoelectron spectroscopy. In *Handbook of X-ray photoelectron spectroscopy*, Muilenberg, G. E., Ed. Perkin Elmer Corporation: Eden Prairie, Minnesota, 1997.

52.	*X-ray data booklet.* Lawrence Berkeley National Lab: Berkeley, 2001.

53.	Dementjev, A. P.; de Graaf, A.; van de Sanden, M. C. M.; Maslakov, K. I.; Naumkin, A. V.; Serov, A. A., X-Ray photoelectron spectroscopy reference data for identification of the C3N4 phase in carbon-nitrogen films. *Diamond and Related Materials* **2000,** *9* (11), 1904-1907.

54.	Jagst, E. Surface Functional Group Characterization Using Chemical Derivatization X-ray Photoelectron Spectroscopy (CD-XPS). Free University of Berlin, Berlin, 2010.

55.	Kerber, S. J.; Bruckner, J. J.; Wozniak, K.; Seal, S.; Hardcastle, S.; Barr, T. L., The nature of hydrogen in x-ray photoelectron spectroscopy: General patterns from hydroxides to hydrogen bonding. *Journal of Vacuum Science & Technology A: Vacuum, Surfaces, and Films* **1996,** *14* (3), 1314-1320.

56.	Dasog, M.; Yang, Z.; Regli, S.; Atkins, T. M.; Faramus, A.; Singh, M. P.; Muthuswamy, E.; Kauzlarich, S. M.; Tilley, R. D.; Veinot, J. G. C., Chemical Insight into the Origin of Red and Blue Photoluminescence Arising from Freestanding Silicon Nanocrystals. *ACS Nano* **2013,** *7* (3), 2676-2685.

57.	Chao, Y.; Krishnamurthy, S.; Montalti, M.; Lie, L. H.; Houlton, A.; Horrocks, B. R.; Kjeldgaard, L.; Dhanak, V. R.; Hunt, M. R. C.; Šiller, L., Reactions and luminescence in passivated Si nanocrystallites induced by vacuum ultraviolet and soft-x-ray photons. *Journal of Applied Physics* **2005,** *98* (4), -.

58.	Li, X.; He, Y.; Talukdar, S. S.; Swihart, M. T., Process for Preparing Macroscopic Quantities of Brightly Photoluminescent Silicon Nanoparticles with Emission Spanning the Visible Spectrum. *Langmuir* **2003,** *19* (20), 8490-8496.

59.	Xiong, H. M.; Wang, Z. D.; Xia, Y. Y., Polymerization Initiated by Inherent Free Radicals on Nanoparticle Surfaces: A Simple Method of Obtaining Ultrastable (ZnO)Polymer Core–Shell Nanoparticles with Strong Blue Fluorescence. *Advanced Materials* **2006,** *18* (6), 748-751.

60.	Ahire, J. H.; Wang, Q.; Coxon, P. R.; Malhotra, G.; Brydson, R.; Chen, R.; Chao, Y., Highly Luminescent and Nontoxic Amine-Capped Nanoparticles from Porous Silicon: Synthesis and Their Use in Biomedical Imaging. *ACS Applied Materials & Interfaces* **2012,** *4* (6), 3285-3292.

61.	Wasielewski, M. R., Photoinduced electron transfer in supramolecular systems for artificial photosynthesis. *Chemical Reviews* **1992,** *92* (3), 435-461.

62.	Morawetz, H., Fluorescence studies of polymer dynamics. *Journal of Luminescence* **1989,** *43* (2), 59-71.

63.	Shizuka, H.; Nakamura, M.; Morita, T., Intramolecular fluorescence quenching of phenylalkylamines. *The Journal of Physical Chemistry* **1979,** *83* (15), 2019-2024.

64.	Efros, A. L.; Rosen, M., Random Telegraph Signal in the Photoluminescence Intensity of a Single Quantum Dot. *Physical Review Letters* **1997,** *78* (6), 1110-1113.

65.   Galland, C.; Ghosh, Y.; Steinbrück, A.; Hollingsworth, J. A.; Htoon, H.; Klimov, V. I., Lifetime blinking in nonblinking nanocrystal quantum dots. *Nat Commun* **2012,** *3*, 908.

66.   Liu, Y.-S.; Sun, Y.; Vernier, P. T.; Liang, C.-H.; Chong, S. Y. C.; Gundersen, M. A., pH-Sensitive Photoluminescence of CdSe/ZnSe/ZnS Quantum Dots in Human Ovarian Cancer Cells. *The Journal of Physical Chemistry C* **2007,** *111* (7), 2872-2878.

67.   Jiang, X.; Housni, A.; Gody, G.; Boullanger, P.; Charreyre, M.-T. r. s.; Delair, T.; Narain, R., Synthesis of Biotinylated α-d-Mannoside or N-Acetyl β-d-Glucosaminoside Decorated Gold Nanoparticles: Study of Their Biomolecular Recognition with Con A and WGA Lectins. *Bioconjugate Chemistry* **2010,** *21* (3), 521-530.

68.   El-Boubbou, K.; Gruden, C.; Huang, X., Magnetic Glyco-nanoparticles: A Unique Tool for Rapid Pathogen Detection, Decontamination, and Strain Differentiation. *Journal of the American Chemical Society* **2007,** *129* (44), 13392-13393.

69.   El-Boubbou, K.; Zhu, D. C.; Vasileiou, C.; Borhan, B.; Prosperi, D.; Li, W.; Huang, X., Magnetic Glyco-Nanoparticles: A Tool To Detect, Differentiate, and Unlock the Glyco-Codes of Cancer via Magnetic Resonance Imaging. *Journal of the American Chemical Society* **2010,** *132* (12), 4490-4499.

70.   Wang, X.; Liu, L.-H.; Ramström, O.; Yan, M., Engineering Nanomaterial Surfaces for Biomedical Applications. *Experimental Biology and Medicine* **2009,** *234* (10), 1128-1139.

71.   Chandrasekaran, S.; Tanzer, M. L.; Giniger, M. S., Characterization of oligomannoside binding to the surface of murine melanoma cells. Potential relationship to oligomannoside-initiated cell spreading. *Journal of Biological Chemistry* **1994,** *269* (5), 3367-3373.

72.   Yamazaki, N.; Kojima, S.; Bovin, N. V.; André, S.; Gabius, S.; Gabius, H. J., Endogenous lectins as targets for drug delivery. *Advanced Drug Delivery Reviews* **2000,** *43* (2–3), 225-244.

73.   Bishop, K. J. M.; Wilmer, C. E.; Soh, S.; Grzybowski, B. A., Nanoscale Forces and Their Uses in Self-Assembly. *Small* **2009,** *5* (14), 1600-1630.

74.   Caswell, K. K.; Wilson, J. N.; Bunz, U. H. F.; Murphy, C. J., Preferential End-to-End Assembly of Gold Nanorods by Biotin–Streptavidin Connectors. *Journal of the American Chemical Society* **2003,** *125* (46), 13914-13915.

75.   Kang, Y.; Erickson, K. J.; Taton, T. A., Plasmonic Nanoparticle Chains via a Morphological, Sphere-to-String Transition. *Journal of the American Chemical Society* **2005,** *127* (40), 13800-13801.

76.   Nie, Z.; Fava, D.; Kumacheva, E.; Zou, S.; Walker, G. C.; Rubinstein, M., Self-assembly of metal-polymer analogues of amphiphilic triblock copolymers. *Nat Mater* **2007,** *6* (8), 609-614.

77.   DeVries, G. A.; Brunnbauer, M.; Hu, Y.; Jackson, A. M.; Long, B.; Neltner, B. T.; Uzun, O.; Wunsch, B. H.; Stellacci, F., Divalent Metal Nanoparticles. *Science* **2007,** *315* (5810), 358-361.

78.   Zhao, N.; Liu, K.; Greener, J.; Nie, Z.; Kumacheva, E., Close-Packed Superlattices of Side-by-Side Assembled Au-CdSe Nanorods. *Nano Letters* **2009,** *9* (8), 3077-3081.

79.   Tang, Z.; Zhang, Z.; Wang, Y.; Glotzer, S. C.; Kotov, N. A., Self-Assembly of CdTe Nanocrystals into Free-Floating Sheets. *Science* **2006,** *314* (5797), 274-278.

80.   Nikolic, M. S.; Olsson, C.; Salcher, A.; Kornowski, A.; Rank, A.; Schubert, R.; Frömsdorf, A.; Weller, H.; Förster, S., Micelle and Vesicle Formation of Amphiphilic Nanoparticles. *Angewandte Chemie International Edition* **2009,** *48* (15), 2752-2754.

81.   Park, S.; Lim, J.-H.; Chung, S.-W.; Mirkin, C. A., Self-Assembly of Mesoscopic Metal-Polymer Amphiphiles. *Science* **2004,** *303* (5656), 348-351.

82.   Park, S. Y.; Lytton-Jean, A. K. R.; Lee, B.; Weigand, S.; Schatz, G. C.; Mirkin, C. A., DNA-programmable nanoparticle crystallization. *Nature* **2008,** *451* (7178), 553-556.

83.   Nykypanchuk, D.; Maye, M. M.; van der Lelie, D.; Gang, O., DNA-guided crystallization of colloidal nanoparticles. *Nature* **2008,** *451* (7178), 549-552.

84.   Iacovella, C. R.; Glotzer, S. C., Complex Crystal Structures Formed by the Self-Assembly of Ditethered Nanospheres. *Nano Letters* **2009,** *9* (3), 1206-1211.

85.   Kalsin, A. M.; Fialkowski, M.; Paszewski, M.; Smoukov, S. K.; Bishop, K. J. M.; Grzybowski, B. A., Electrostatic Self-Assembly of Binary Nanoparticle Crystals with a Diamond-Like Lattice. *Science* **2006,** *312* (5772), 420-424.

86.   Sharma, J.; Chhabra, R.; Cheng, A.; Brownell, J.; Liu, Y.; Yan, H., Control of Self-Assembly of DNA Tubules Through Integration of Gold Nanoparticles. *Science* **2009,** *323* (5910), 112-116.

87.   Dumas, P.; Miller, L., The use of synchrotron infrared microspectroscopy in biological and biomedical investigations. *Vibrational Spectroscopy* **2003,** *32* (1), 3-21.

88.   Sham, T. K., *Ed. Chemical Applications of Synchrotron Radiation.* WorldScientific Publishing Co. Ltd: Singapore, 2002.

5 Carbohydrate Capped Silicon Nanoparticles for Selective Targeting of Cancer cells

5.1 Introduction and motivations

Each year, millions of people's lives worldwide are affected by a complex group of diseases known as cancer. For most cancer, chemotherapy has become an integral component of cancer treatment. Despite the last 30 years of effort on oncology drug discovery, conventional chemotherapeutic agents still exhibit poor specificity in reaching tumour tissue and are often restricted by dose-limiting toxicity. To overcome the limitation factor found in chemotherapy, targeted drug delivery and controlled drug release technology may provide a more efficient and less harmful solution. It is well known that each malignant cell type has a specific molecular signature that discriminates it from its healthy counterparts. Taking advantage of this molecular signature expressed by cancer cells, the availability of simple and fast methods to identify these unique cellular characteristics can greatly benefit cancer treatment and improve the clinical outcomes for patients. Presently the popular methods used in targeted cancer detection are biomarkers, including mutated DNA/RNA and overexpressed antigens. These methods are very time consuming to acquire, as it requires extensive prior knowledge of the presence of the specific markers. Moreover, tumour cells have high tendencies to mutate, which changes their antigenic modifications leading to negative results. An interesting alternative is to take advantage of the receptors present on the surface of cells as detection events.

Carbohydrates are attractive targets for receptor-mediated interaction and in particular glycoconjugates, which play important roles in cancer development and metastasis. All mammalian cells are covered with a dense layer of carbohydrates known as glycocalyx, in which carbohydrates are bound to proteins and lipids known as glycoproteins, proteoglycans and glycolipids. These naturally occurring glycoconjugates play an important role in the process of cell-cell interaction and cell-cell communications that is vital for physiological and pathological process.[1, 2] As one of the common cell-surface ligands, carbohydrates can direct the initiation of many medicinally important physiological processes where they are involved in a wide variety of events,[3-5] including inflammatory and immunological responses[6-8] tumour

metastasis,[9] cell-cell signalling,[10] apoptosis, adhesion,[11] bacterial and viral recognition,[11, 12] and anticoagulation.[13]

The biological roles of carbohydrates as signalling effectors and recognition markers are associated with specific molecular recognition in which proteins[14] or other carbohydrates[15] are involved. This characteristic led to the identification of tumours associated with carbohydrate molecules,[10, 16] and this has greatly improved the development of carbohydrate-based anticancer vaccine studies.[17] In comparison, the understanding of carbohydrate-binding properties of tumours is not as advanced. Cancer cells can interact with the extracellular matrix in their microenvironment through endogenous receptors binding with carbohydrates.[17, 18] These interactions vary, depending on the physiological state of the cells, as supported by the ground-breaking histological studies of tumour tissues.[19, 20] Therefore, the ability to characterize and distinguish carbohydrate binding profiles of a variety of cells can expedite both the mechanistic understanding of their role in disease development and the expansion of diagnostic and therapeutic tools.[21-23] As the differences among cancer cell subtypes and malignant vs normal cells can often be subtle, a suitable tool is needed to quantitatively analyse the fine characteristics in carbohydrate binding of various cell types.

When nanoparticles are functionalized with ligands such as antibodies, proteins or peptides, oligonucleotides or carbohydrates, they become excellent vehicles for biological applications at the cellular and molecular level. However, several features need to be fine-tuned including ligand density, particle diameter, surface charges, magnetic, electronic or optical properties, stability and targeting specificity.

Nanomaterials can serve as promising platforms for displaying carbohydrates for biological recognition. Due to the smaller sizes of NPs compared to their micrometer sized counterparts, NPs have much larger surface areas, which can enable higher capacity in receptor binding. In addition, multiple carbohydrate ligands can be immobilized onto one NP, which can potentially enhance the weak affinities of individual ligands to their binding partners.

SiNPs hold prominent interest in various fields of biomedical research including imaging, detection, sensing to drug delivery and new therapeutic uses.[24, 25] This is in addition to the electronic, magnetic and optical properties. Silicon nanoparticles (SiNPs) or Quantum dots have size dependent tuneable light emission, bright luminescence, stability against photobleaching compared to organic fluorescent dye molecules which makes them ideal tools for fluorescence imaging. All these properties have assisted

SiNPs as fluorescent cellular markers in a number of diagnostic and assay roles. Moreover when comparing with heavy metal and other types of semiconductor quantum dots, SiNPs exhibits low inherent toxicity.[26-29]

Herein, we explore the possibility of using glycoconjugated SiNPs to detect and outline various cell types on the basis of the more physiologically related carbohydrate-receptor interactions. We have focused on SiNPs functionalized with a carbohydrate that plays key roles in the molecular recognition processes rather than those where carbohydrates mainly function as NP stabilizing agents.[30-32] The information obtained on the physiologically relevant carbohydrate-receptor interaction can not only enhance our understanding of the roles carbohydrate plays in cancer but also guide the development of potential therapeutics such as agents against cancer adhesion.

5.2   Synthesis of Carbohydrate capped SiNPs

The carbohydrate capped SiNPs were synthesized from amine-terminated SiNPs as described in Chapter 4.[33] For instance the corresponding pyranosyl acid was reacted with EDC and *N*-hydroxysuccinimide (NHS) in the presence of DCM. After 2 hr the freshly prepared amine-terminated SiNPs were dissolved in water and added into the reaction mixture. The reaction was stirred for 24 hr at room temperature (Scheme 5.1).
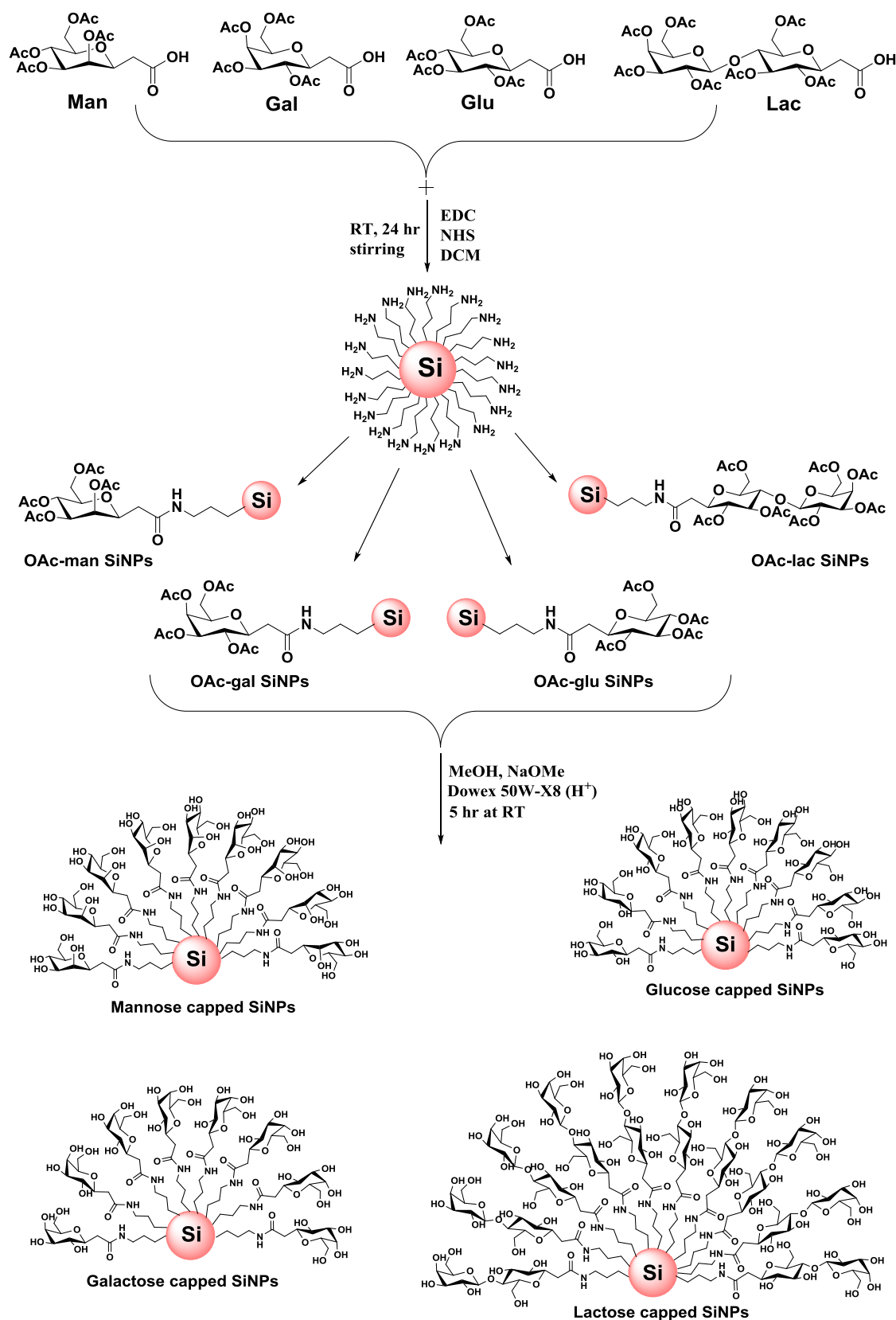
Scheme 5.1: Schematic representation of synthesis of carbohydrate capped SiNPs

The detailed procedure to synthesize carbohydrate capped SiNPs using EDC and NHS is briefly mentioned in the experimental section. The obtained carbohydrate capped SiNPs were characterized by several techniques discussed in Chapter 4.

5.3 Stability of Carbohydrate capped SiNPs in Biological Media

A significant challenge in application of nanoparticles in biomedical is to retain their stability in biologically-associated environments. The nanoparticles have to be hydrophilic and maintain a superior stability in biological media. For advanced biomedical applications of nanoparticles (e.g., in vivo diagnostics and therapy), additional requirements such as minimization of non-specific uptake by reticuloendothelial systems (RES) must be imposed in order to achieve long blood circulation time and high diagnostic or therapeutic efficiency.[34] For investigations of the *in vivo* effects of nanoparticles in the circulation and for measuring the effects of nanoparticles on different types of cells in vitro, nanoparticles have to be dispersed in physiological solutions. However, particles in solutions with physiological salt concentrations and pH values form micrometer-sized coarse agglomerates.[35-37] Coarse agglomerates of nanoparticles have been shown to exert different biological effects as compared to well-dispersed nanoparticles.[38-40] Moreover they induce toxicity to both *in vitro* and *in vivo* studies due to the aggregation. Therefore, it is important to investigate the effect of biological media on carbohydrate capped SiNPs.

In order to monitor the stability of carbohydrate capped SiNPs in biological medium, Dynamic Light Scattering (DLS) was used to monitor the variation of the average hydrodynamic size of the NPs in different media. For long-term stability test 0.1 mL solution of carbohydrate capped SiNPs was incubated in 1 mL of Dulbecco's Modified Eagle's Medium (DMEM) with 10% FBS, Roswell Park Memorial Institute (RPMI) medium with 10% FBS and Marc's Modified Ringers (MMR) as a function of time. The average hydrodynamic diameter was measured at four different time points 0, 6, 12 and 24 hours. Figure 5.1 and Table 5.1 show the stability of carbohydrate capped SiNPs by DLS in DMEM media for various time points such as 6hrs, 12hrs, and 24 hrs.

Table 5.1: Diameter of carbohydrate capped SiNPs by DLS in DMEM, RPMI and MMR media (± repeatability)

Carbohydrate capped SiNPs	DMEM media DLS Size (nm)			RPMI media DLS Size (nm)			MMR media DLS Size (nm)	
	6hr	12hr	24hr	6hr	12hr	24hr	Initial	24hr
Gal SiNPs	10 ± 1.0	10 ± 1.0	15 ± 1.5	10 ±1.0	10 ±1.0	16 ±1.0	37±3.0	58± 5.0
Man SiNPs	11± 1.0	13 ± 1.0	14 ± 1.0	11 ±1.0	15 ±2.0	20 ±1.0	20±1.5	43±3.0
Glu SiNPs	13± 1.0	13 ± 1.0	13 ± 1.0	14 ±1.0	16 ±1.0	16 ±1.0	15±1.5	72±5.0
Lac SiNPs	14± 1.5	14 ± 1.5	16 ± 1.0	14 ±1.0	15 ±1.0	15 ±1.0	38±4.0	43±5.0

The NPs dimension was monitored by DLS over time to evaluate the occurrence of cluster formation, through aggregation phenomena, which causes a shift of the particle size distribution (PSD) toward higher values.

Figure 5.1: Stability of (a) Gal, (b) man, (c) Glu and (d) Lac-capped SiNPs in DMEM media at various time points.

Figure 5.1 shows that there is some aggregation of carbohydrate capped SiNPs upon incubation with DMEM media. The gal capped SiNPs (figure5.1a) show a slight

broadening of the peak after 6 and 12 hrs but the peak position does not change. After 24 hrs the peak position shifts slightly but the overall results do not show any sign of aggregation in DMEM media. Besides gal capped SiNPs, the man, glu and lac capped SiNPs are also very stable in DMEM media.
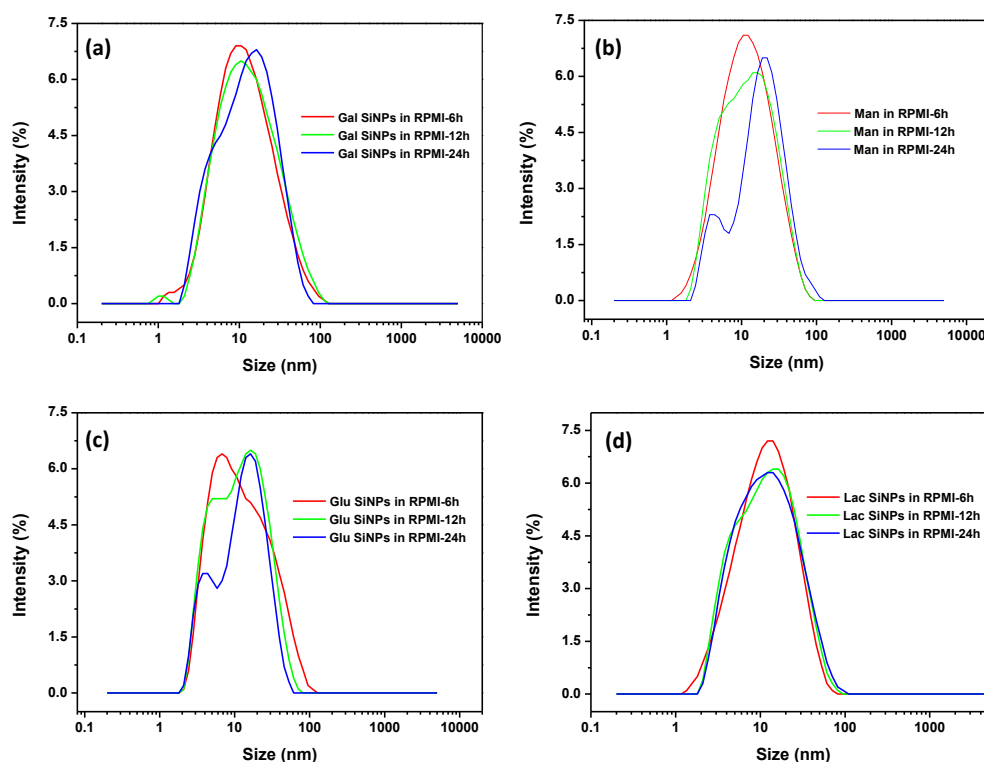
Figure 5.2: Stability of (a) Gal, (b) man, (c) Glu and (d) Lac-capped SiNPs in RPMI media at various time points.

The carbohydrate capped SiNPs were also incubated in RPMI media for various time points shown in figure 5.2. The gal capped SiNPs (figure 5.2a) did not show any aggregation for 6 and 12 hours but the peak position shifted slightly after 24 hr, which suggest that slight aggregation occurred. Similarly slight aggregation was observed in man capped SiNPs (figure 5.2b) after 24 hrs. The glu and lac-capped SiNPs were moderately stable and did not show any sign of aggregation.

Similar to the DMEM and RPMI biological media the carbohydrate capped SiNPs were also tested in MMR media, which was used to culture the *Xenopus* embryo. The NPs were incubated in MMR and the DLS spectra were obtained after adding the sample and after incubating for 24hrs. Figure 5.3 shows the DLS size distribution of carbohydrate capped SiNPs in MMR media.
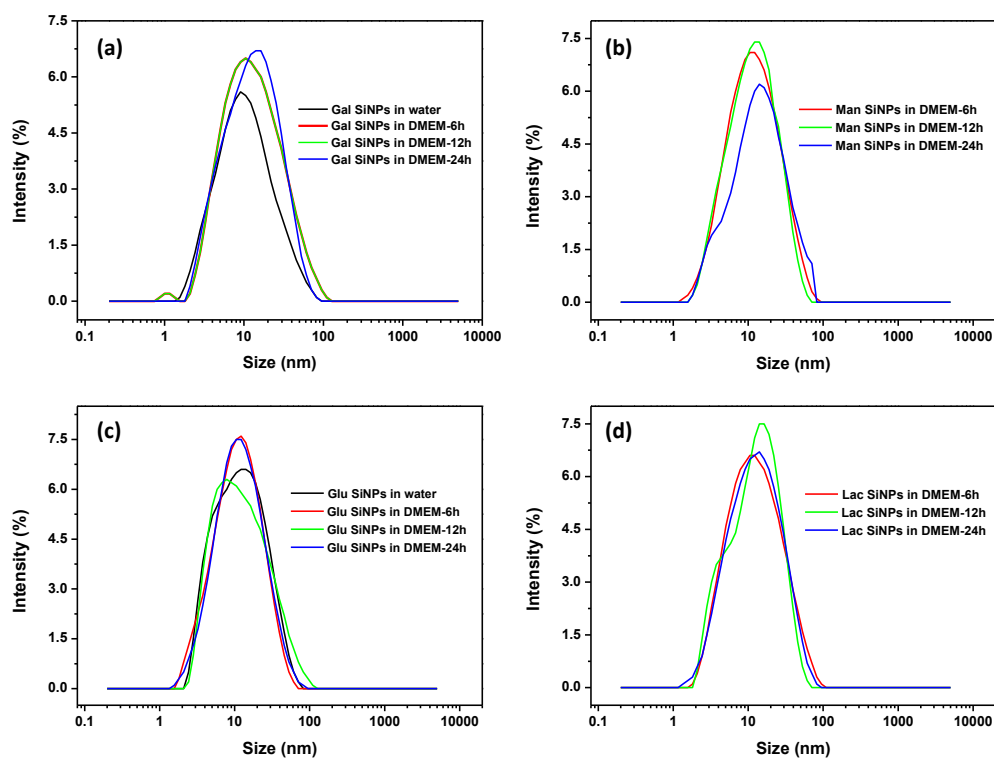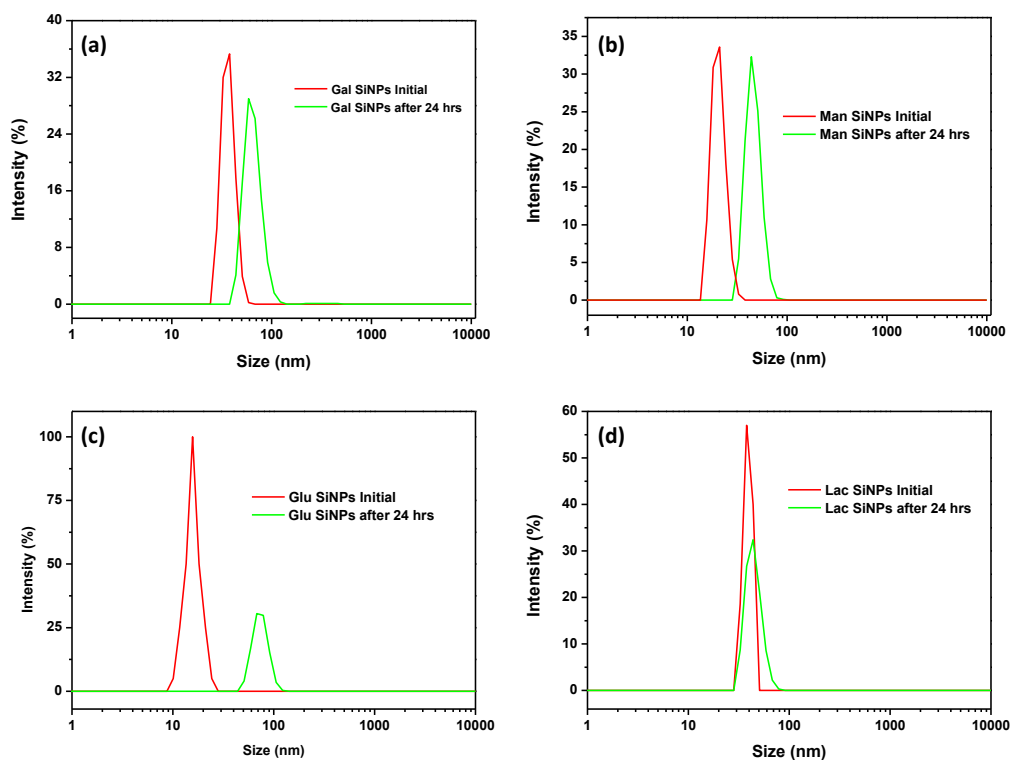
Figure 5.3: Stability of (a) Gal, (b) man, (c) Glu and (d) Lac-capped SiNPs in MMR media at various time points.

From figure 5.3 (table 5.1) it is clear that carbohydrate capped SiNPs show some extent of aggregation in MMR media. The size of gal capped SiNPs (figure 5.3a) increased in MMR immediately after the addition from around 11 nm to 37 nm (Table 5.1). After 24 hrs the overall diameter had increased up to 58 nm showing aggregation. Man capped SiNPs did not show any significant shift at the initial time point but the overall diameter increased slightly after 24 hrs. The glu capped SiNPs were stable after the addition but showed massive aggregation after 24 hrs. Similarly the lac capped SiNPs showed an increase in size after addition and some extent of aggregation after 24 hrs.

The overall DLS stability results demonstrate that the carbohydrate capped SiNPs are very stable in biological media like DMEM and RPMI. The main challenge of the NPs when developing for biological application or *in vivo* study is that they interact with body fluid and form an aggregation or a protein corona around the NPs, significantly reducing their selectivity towards the target as well as causing toxicity and

affecting the final therapeutic performance. This is the great advantage of carbohydrate capped SiNPs as they did not interact with the protein, which is contained in the DMEM and RPMI media, and were moderately stable. These stability results suggest that carbohydrate capped SiNPs can serve as an important platform to be used for *in vivo* study as well as for other biological applications.

On the other hand carbohydrate capped SiNPs exhibit aggregation in MMR media. This is possibly due to the basicity of MMR media that interferes with the surface charge of the carbohydrate capped NPs and forms the aggregates.

5.4 Cytotoxicity Assay of Carbohydrate capped SiNPs

5.4.1 *In vitro* Toxicity

The effect of carbohydrate capped SiNPs on the cytotoxicity of cells was determined by MTT assay. The toxicity was verified in both cancerous and non-cancerous cell lines. A549 (Human lung carcinoma), HHL-5 (human immortalized hepatocytes) and MDCK (Normal Kidney Epithelium cells) cells were plated in 200µL of complete culture medium containing 50, 300, 500, 700 and 1000 µg/mL concentrations of carbohydrate capped SiNPs in 96-well plates for 72 hours.
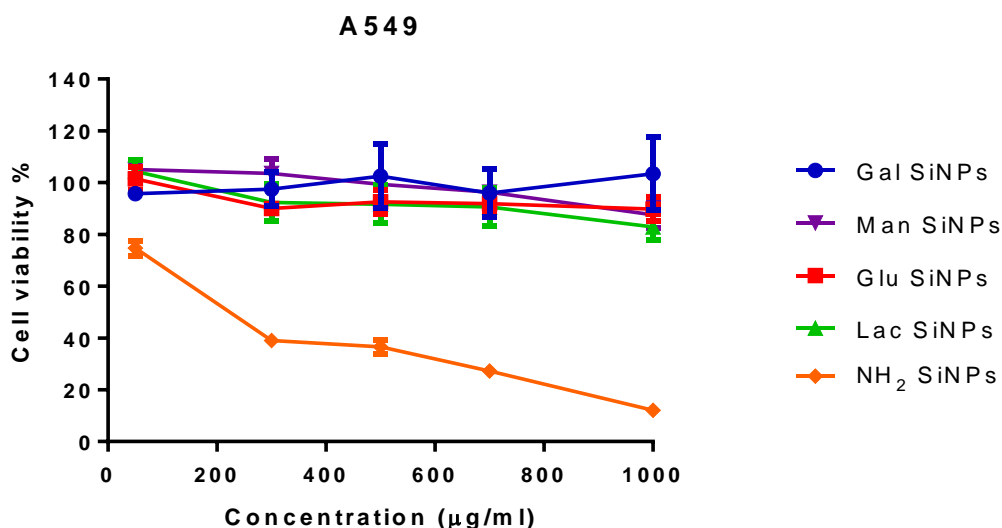

Figure 5.4: MTT graph of carbohydrate capped SiNPs in A549 cell lines at various concentrations
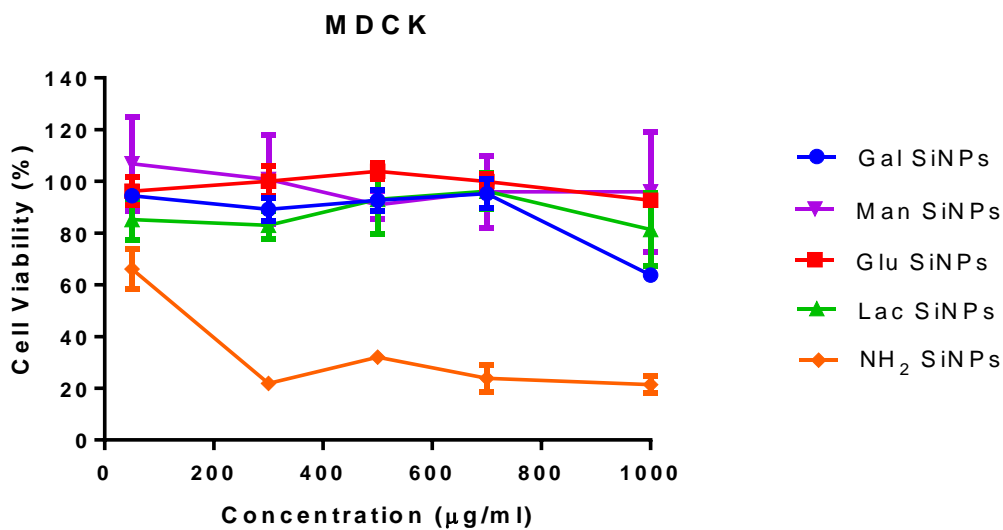
Figure 5.5: MTT graph of carbohydrate capped SiNPs in MDCK cell lines at various concentrations
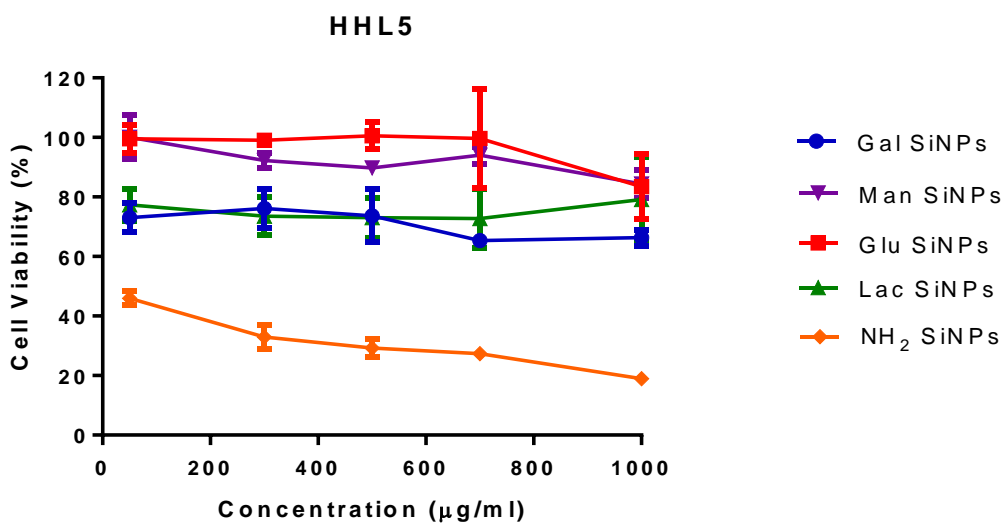

Figure 5.6: MTT graph of carbohydrate capped SiNPs in HHL5 cell lines at various concentrations

The results of the MTT assay, as a measure of metabolic competence of the cells for 72 hours exposure to carbohydrate capped SiNP, are shown in Figure 5.4, 5.5 and 5.6. As mentioned earlier the cell viability was verified in both cancerous and non-cancerous cell lines. Figure 5.4 shows the MTT data of carbohydrate capped SiNPs compared with amine-terminated SiNPs as a control in A549 (Lung cancer) cell line. It is observed that even at a higher particle concentration, i.e. 1000 µg/mL, all the cells could normally proliferate and maintain >95% of cell viability to that of the control cells during 72 hours culture. Whereas amine-terminated SiNPs induced toxicity above 200 µg/mL concentration, suggesting that the NPs are highly capped with carbohydrate moieties which make them non-toxic for cells. That amine-terminated SiNPs induce toxicity at 200µg/mL was confirmed by calculating IC_{50}, as shown in figure 5.7. This result suggests the lack of cytotoxic effects of carbohydrate SiNPs upon the cells. The carbohydrate capped SiNPs were also tested in normal cell lines i.e. HHL-5 and MDCK cell lines. Figure 5.5 shows the MTT data of carbohydrate capped SiNPs in MDCK cells. The cells maintained their viability throughout all concentrations compared to that of amine-terminated SiNPs suggesting that the carbohydrate capped SiNPs are non-toxic for normal cells as well. When the NPs were introduced to the HHL-5 cells (figure 5.6), the gal and lac-capped SiNPs showed some level of toxicity but less than amine-terminated SiNPs. Furthermore, as can be seen from Figures 5.4, 5.5 and 5.6, the proliferations of cells is not affected by increasing particle concentration (1000 µg/mL) in all of the cell cultures, which suggests the carbohydrate capped SiNPs did not cause any apparent harm to the viability of the different types of cells (HHL5, MDCK, A549) as well as for both normal and cancer cell lines.

The IC_{50} of amine-terminated SiNPs was calculated in HeLa cells by a research collaborator Dr. Nattika Saengkrit from Thailand. The stock solution of amine-terminated SiNPs was prepared by dissolving in water at conc. of 1mg/mL. The cells were then exposed to the amine-terminated SiNPs and incubated for 72 hours at 37°C. The MTT measurement was carried out using the standard procedure explained in chapter 2.

$IC_{50} = 0.29$ mg/ml
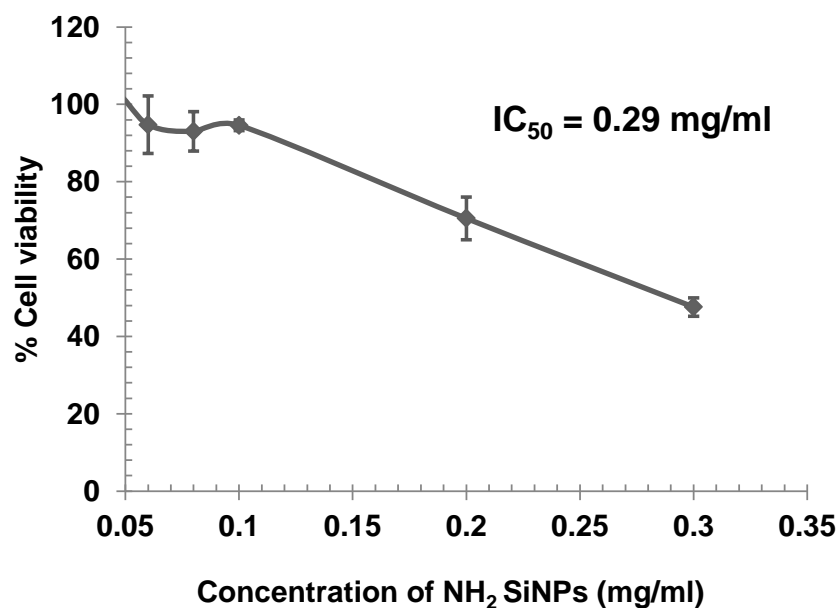
Figure 5.7: IC$_{50}$ of amine-terminated SiNPs in HeLa cells.

5.4.2 Toxicity by Cell Viability images

The cytotoxicity of carbohydrate capped SiNPs was assessed by their effect on cell morphology. The carbohydrate capped SiNPs were introduced into the A549, HHL5 and MDCK cells and incubated for 72 hours. The cells were observed under simple phase-contrast microscope shown in figure 5.8. The cell morphology was compared using control cells (without NPs). It is clearly observed that both cancerous and non-cancerous cells maintain the proliferation and did not show any cell damage or stress to the cells upon incubation with carbohydrate capped SiNPs. In contrast amine-terminated SiNPs were found to be toxic to cells resulting in cell death after 72 hours of incubation. The results strongly support the overall toxicity study and confirm that all carbohydrate capped SiNPs are highly non-toxic to both cancerous and non-cancerous cell lines from lowest to highest NP concentrations.
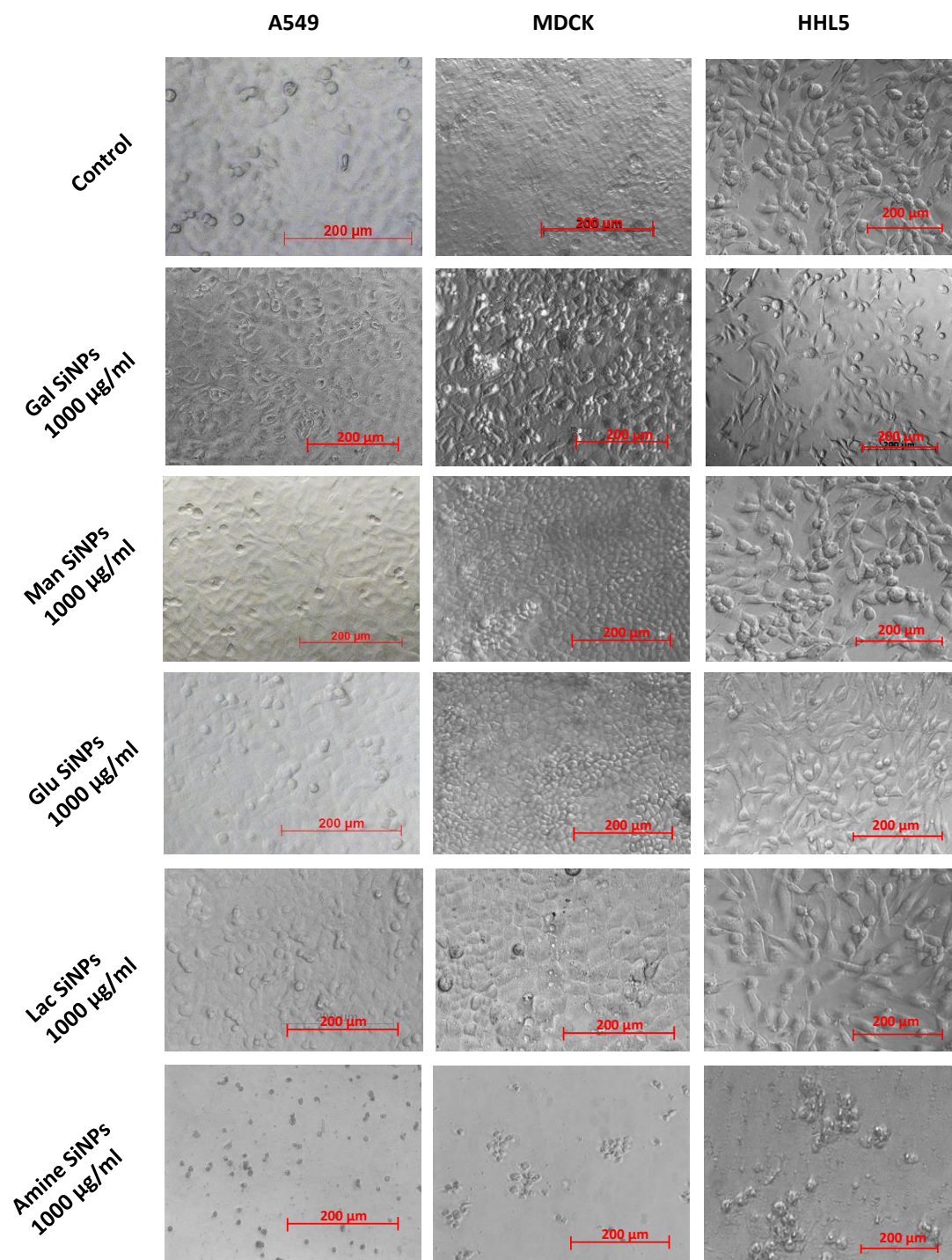
Figure 5.8: Effect of carbohydrate capped SiNPs on cell morphology in cancerous cell line A549 (Lung cancer) and non-cancerous cell lines MDCK (canine kidney) and HHL5 (human immortalized hepatocytes).

5.4.3 *In Vivo* Toxicity Assay

To study the interaction of nanomaterials with biological systems various *in vivo* biological models have been proposed. Although in widespread use, small animal models (rodents) are costly and labour intensive and furthermore raise important ethical issues and have generated resistance to life science research from the anti-vivisectionist lobby. All these issues and concerns can be relieved by using non-mammalian embryos for *in vivo* studies to probe the interaction between nanomaterials and tissues. Developmental biology offers powerful models to study the cell biological interaction with NPs. Embryos are particularly sensitive indicators of adverse biological effects on the organism. Moreover they provide a useful platform to study the mechanism of action of adverse effects resulting from exposure to NPs.[41, 42] For normal embryo development, highly coordinated cell-to-cell communications and molecular signaling are required; any perturbations by nanomaterials will disrupt orderly embryogenesis leading to abnormal development manifested as morphological malformations, behavioural changes and even embryo death.

As an experimental test system, *Xenopus laevis* offers several advantages: large numbers of embryos with each fecundation (thousands) with a very short early development time (3 days to reach tadpole), external development, close homology with human genes, aside from requiring much less material than small mammals for the assessment of nanomaterial–biological interactions and toxicity and less expensive husbandry/housing.

In this work we have used *Xenopus laevis* embryos as models for biodistribution studies of carbohydrate capped SiNPs. The carbohydrate capped SiNPs toxicity assay in *Xenopus* embryos was carried out by first year PhD student Carl Webster from Dr. Victoria Sherwood's group. Figure 5.9 shows the images of *X. laevis* embryos.

Control

Gal SiNPs 200 µg/mL

Man SiNPs 200 µg/mL

Glu SiNPs 200 µg/mL

Lac SiNPs 200 µg/mL

Amine SiNPs 200 µg/mL
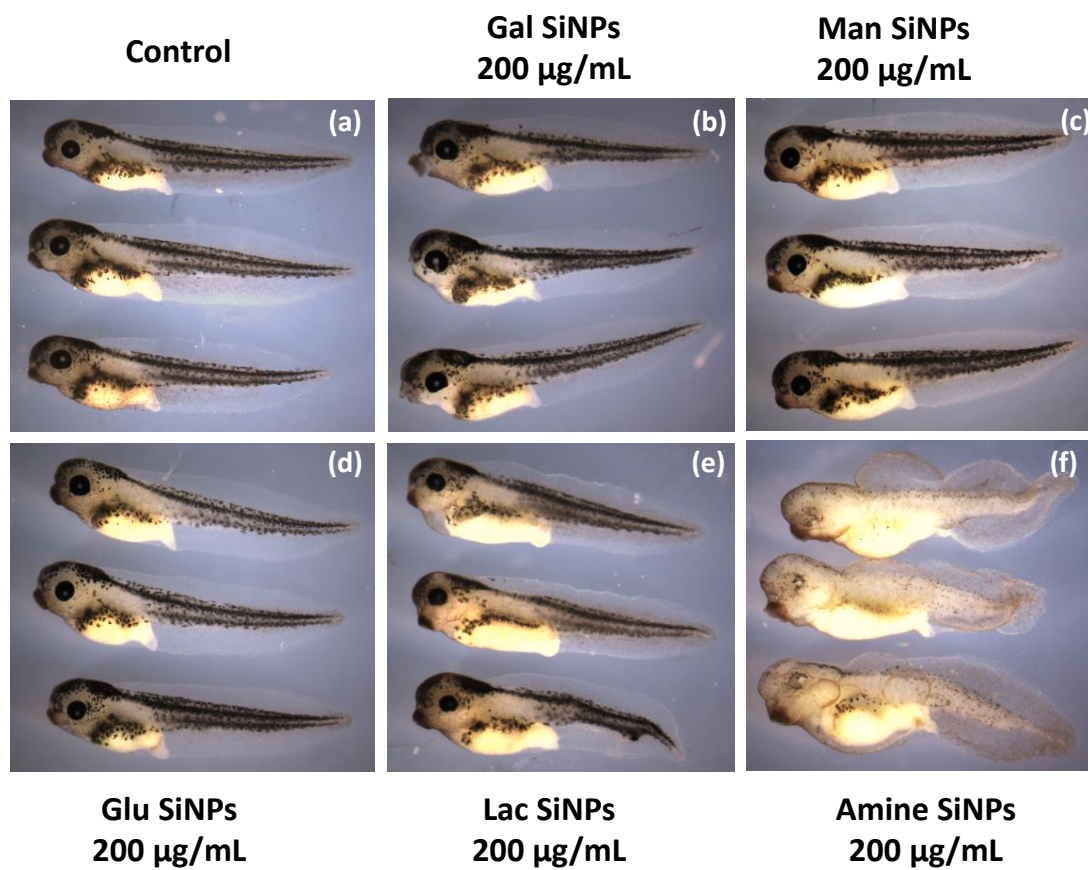
Figure 5.9: (b) - (f) representative range of Xenopus embryos exposed to a highest concentration of carbohydrate capped SiNPs 200µg/mL (a) control, (b) gal capped SiNPs, (c) Man capped SiNPs, (d) Glu capped SiNPs, (e) Lac capped SiNPs and (f) Amine-terminated SiNPs.
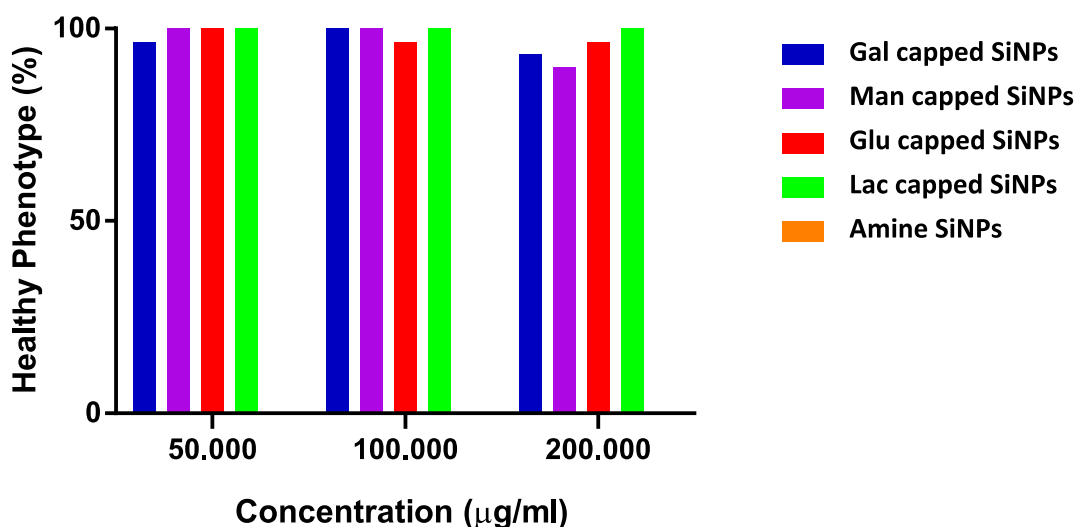
Figure 5.10: Graph representing the total Xenopus embryos at 200 μg/mL of conc. of NPs and classified as percentage of dead, having abnormalities or no abnormalities at stage 38.

In figure 5.9 the *Xenopus* embryos were exposed to a highest conc. of carbohydrate capped SiNPs and amine-terminated SiNPs at Nieuwkoop and Faber stage (NF ST) 15 and fixed at NF ST 38. The toxicity was compared using control *Xenopus* embryos (without NPs) shown in figure 5.9a. In total 30 embryos were assessed for each NP at highest conc. and classified as dead, having abnormalities, or no abnormalities, common malformations include stunted development, bent spine and tail, eye deformities, gut abnormalities, edema and blistering.

From figure 5.9 it is clearly observed that carbohydrate capped SiNPs show no or minimal toxicity to the *Xenopus* embryos at highest conc. Lac capped SiNPs showed to be slightly toxic as spotted by looking at tail deformities comparing to that of mannose (c) and glucose (d) capped SiNPs. Similarly gal capped SiNPs exposed embryos showed bent spine suggesting some toxicity. The experiment was carried out using various conc. such as 50, 100 and 200 μg/mL, nonetheless only highest conc. of *Xenopus* embryos images are shown in figure 5.9 as the lowest conc. did not show any morphological abnormalities in *Xenopus* embryos. Comparing to carbohydrate capped SiNPs, amine terminated SiNPs were shown to be highly toxic and resulted in the death of *Xenopus* embryos as shown in figure 5.9 and 5.10.

By studying both *in vitro* and *in vivo* toxicity it is clear that the carbohydrate capped SiNPs are non-toxic up to a certain extent and represent the potential for further biomedical application.

5.5 Cellular Uptake of Carbohydrate capped SiNPs Using Flow Cytometry

To clarify and demonstrate the relevance of the functionalization strategy on the NP-cell interaction, we performed cell uptake experiments using both cancerous and non-cancerous cell lines, all of which were done under the same conditions for all NPs. Flow cytometry was used to semi-quantitatively measure cellular uptake of the NPs. The instrument gave an accumulated intensity of the particles fluorescent in a number of cells (i.e. 10,000 cells). Therefore, the total fluorescence of particles in one cell is measured by this approach.[43] The carbohydrate capped SiNPs were introduced to cancerous cell lines like A549, MCF7, SK-Mel and normal non-cancerous cell lines including MDCK and HHL5.

A major hurdle for cancer treatment and early cancer detection is the identification of pertinent cellular signatures to allow the differentiation of normal cells from their cancerous counterparts. We envision that this can be achieved by analysis of the respective cellular characteristics toward carbohydrate binding.

This phenomenon was verified by evidence from the literature that MCF-7/Adr-res cells contain the cancer-specific galactoside binding galectins-4, -7, and -8, which are absent in non-cancer cell lines.[44] The Penades group also demonstrated that mouse melanoma cells are known to bind with lactose due to the presence of galectins on the surface.[45] It is also well known that liver cell hepatocytes contain the galactoside binding asialoglycoprotein receptor (ASGP-R) with galactose and galactosamine known to accumulate selectively in the liver via ASGP-R binding.[46] The evidences from the literature on overall glyco-nanoparticles specific binding to the specific cells are mentioned briefly in chapter-1.

Initially the uptake efficiency of carbohydrate capped SiNPs was measured at various time points in both cancerous and non-cancerous cell lines. Figure 5.11 and 5.12 show the uptake efficiency of carbohydrate capped SiNPs at conc. 200 µg/mL in A549, MCF7, SK-Mel, MDCK and HHL5 cells for 24, 48 and 72 hours.
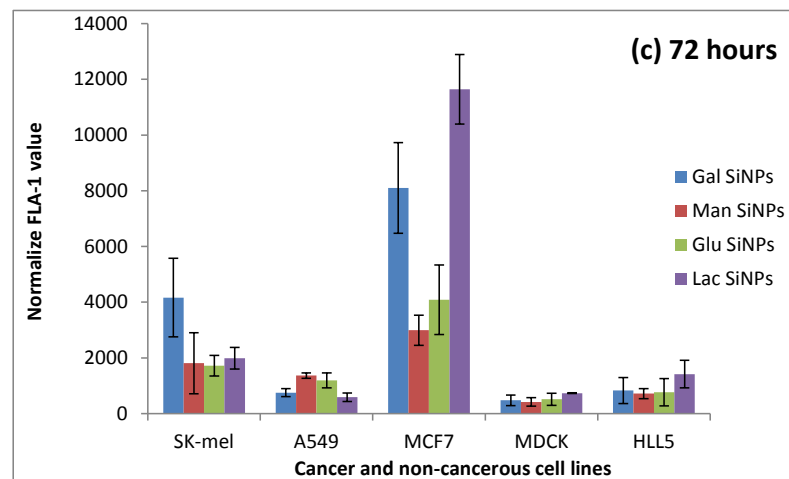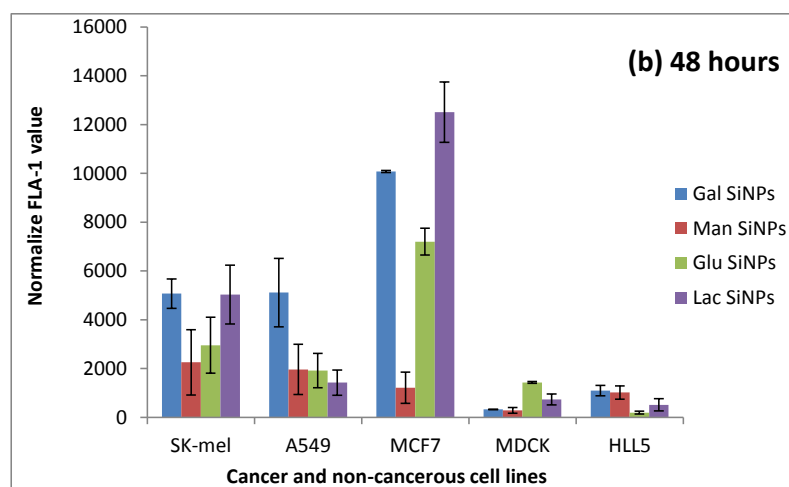
Figure 5.11: Uptake efficiency of carbohydrate capped SiNPs in cancer cells (A549, SK-Mel and MCF-7) and non-cancerous cells (MDCK, HHL5) at various incubation times (a) 24, (b) 48 and (c) 72 hrs. Collective results are normalized to untreated control cells, 24, 48 and 72 hours. Values are mean ± S.D of the results from three independent experiments.

From figure 5.11 it is observed that the carbohydrate capped SiNPs are successfully taken up by both cancer and non-cancer cell lines. It is clear that the uptake efficiency of cancer cells is assuredly more than that of the normal cells. The time dependent uptake efficiency of these NPs was also monitored at various time points 24 (figure 5.11a), 48 (figure 5.11 b) and 72 (figure 5.11 c) hours. The carbohydrate capped SiNPs were shown to be internalized within 24 hours, the uptake efficiency decreasing at 48 and 72 hours' time points (figure 5.12).
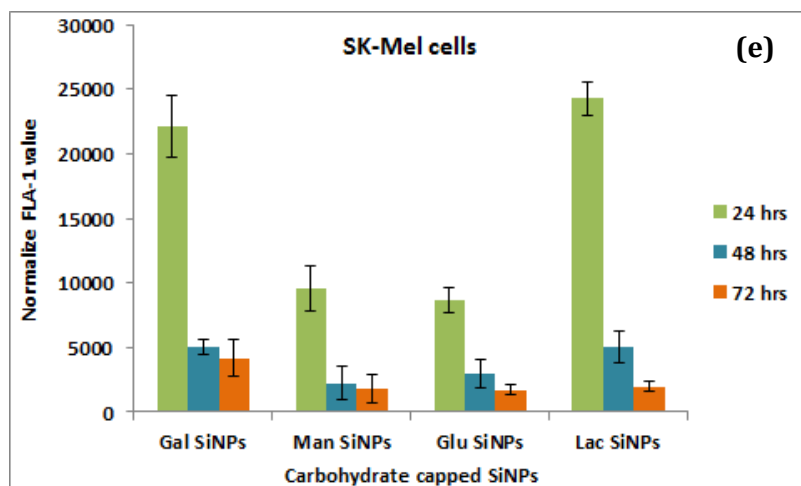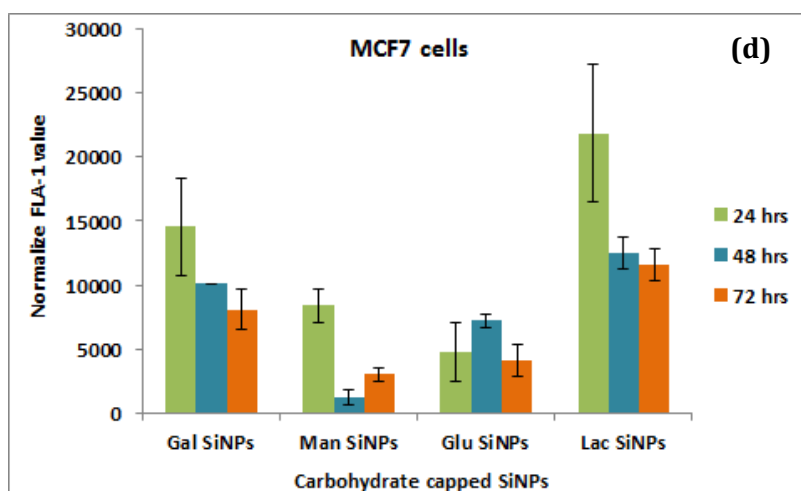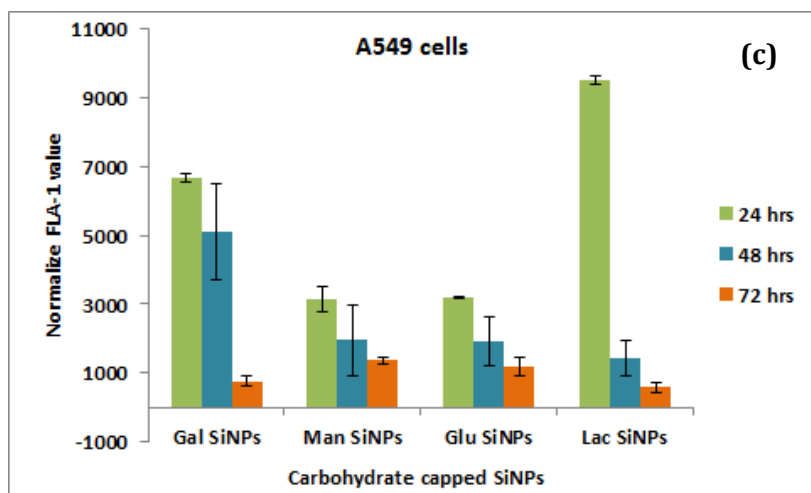
Figure 5.12: Time dependent uptake efficiency of carbohydrate capped SiNPs in cancer cells (A549, SK-Mel and MCF-7) and non-cancerous cells (MDCK, HHL5) at incubation time of 24, 48 and 72 hrs. Collective results are normalized to untreated control cells, 24, 48 and 72 hours. Values are mean ± S.D of the results from three independent experiments.

From figure 5.12 it is clear that all cells take up the carbohydrate capped SiNPs within 24 hrs, the overall uptake efficiency decreasing with increasing time. Based on flow cytometry response, it is observed that the binding of gal capped SiNPs and lac capped SiNPs in cancerous cells is higher, suggesting that these cell lines have active galactose and lactose receptors. SK-Mel cells were found to interact with gal and lac SiNPs more efficiently. This is of special interest since it is reported that melanoma cells bind to lactose, due to the presence of galactin on the surface.[45] Furthermore the brief time dependent uptake studies of carbohydrate capped SiNPs was performed in SK-Mel cells. The cells were exposed to the NPs at various time points and the results quantified by flow cytometry in figure 5.13.
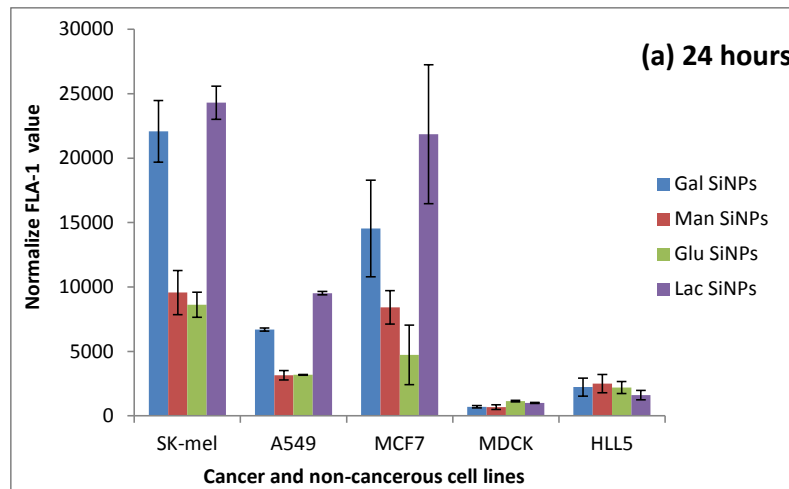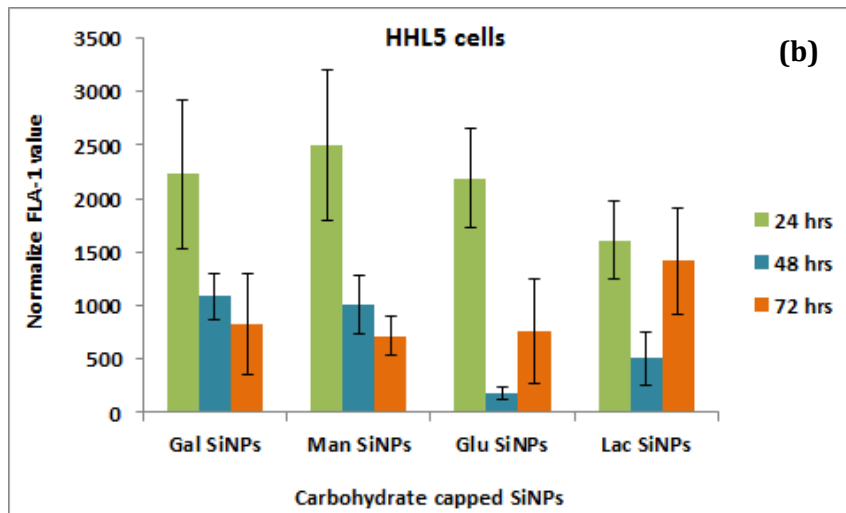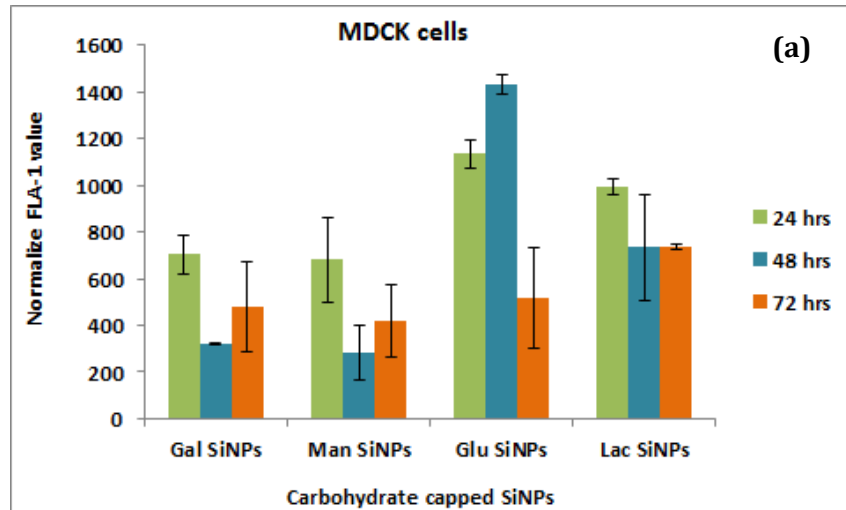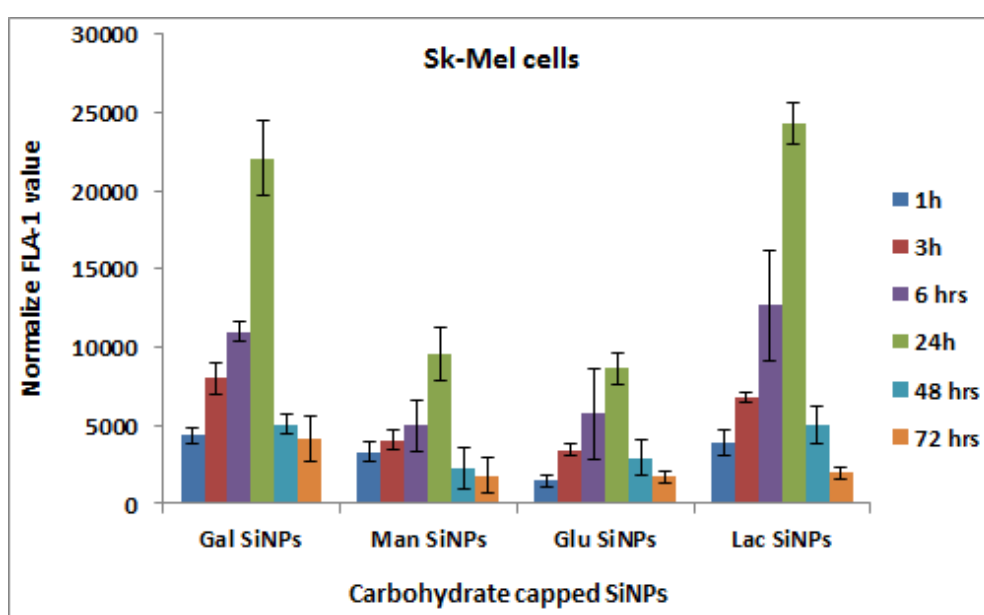

Figure 5.13: Time dependent uptake efficiency of carbohydrate capped SiNPs in SK-Mel cells at various incubation times of 1, 3, 6, 24, 48 and 72 hrs. Collective results are normalized to untreated control cells. Values are mean ± S.D of the results from three independent experiments.

Figure 5.13 clearly shows SK-Mel cells internalize the carbohydrate capped SiNPs within 24 hrs, which indicates that it is receptor mediate endocytosis.

To study further, the internalization mechanism of carbohydrate capped SiNPs was considered by incubating cells with all the NPs at 4°C and 37°C. Traditionally it has been proposed that diffusion and active transport of molecules across the cellular membrane are temperature dependent.[47] At low temperature transport activity is strongly reduced, thus uptake of molecules could be attributed to a non-specific diffusional entry into the cells.[48] Effects from low temperature may affect the binding of the ligand to specific cell receptors, the lateral mobility of the ligand-receptor complex,[49]

the formation of necks in the clathrin coated pits,[50] and/or the transport of endocytosed material from endosomes to lysosomes.[51] Endocytosis of ligands such as transferrin, cholera toxin or some viruses has been shown to be temperature dependent,[52-54] as the ligands are able to attach to cell membrane at low temperatures but are not internalized.

Based on the concept, carbohydrate capped SiNPs were incubated in SK-Mel cell line at different temperatures and data was obtained using flow cytometry analysis shown in figure 5.14.
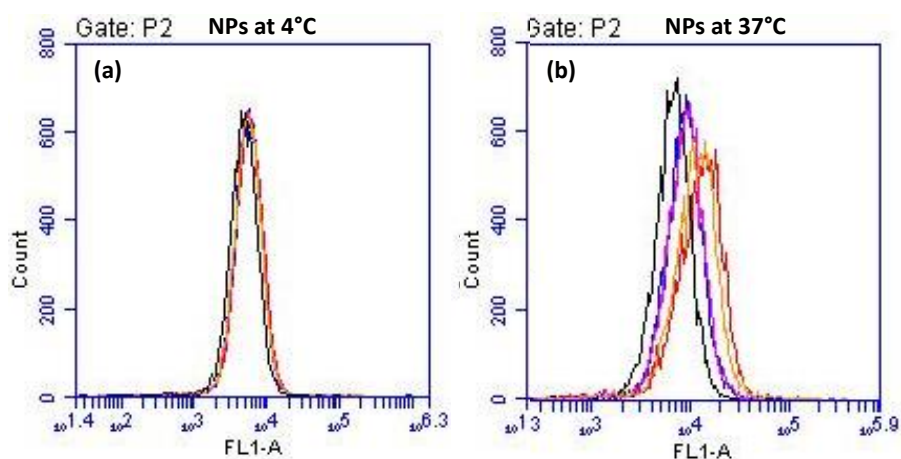
Figure 5.14: Uptake efficiency of carbohydrate capped SiNPs in SK-Mel cell line at (a) 4°C and (b) 37°C: Control-black, Gal-red, Man-blue, Glu-purple, Lac-orange at concentration of 200μg/mL.
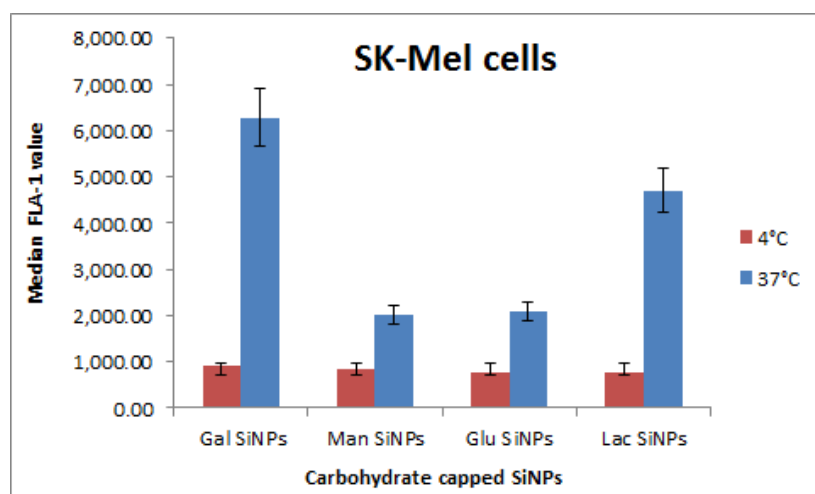
Figure 5.15: Uptake efficiency of carbohydrate capped SiNPs in SK-Mel cells at 4°C (Red) and 37°C (Blue) presented as a percentage of untreated control cells. Values are mean ± S.D of the results from three independent experiments.

From figure 5.14 and 5.15 it is clearly observed that the NPs kept at 4°C were not internalized in SK-Mel cells, while at 37°C all the carbohydrate capped SiNPs were internalized into the cells as confirmed by flow cytometry analysis. Therefore, the obtained results suggest that the cellular uptake of carbohydrate capped SiNPs is most likely energy-dependent.[55]

5.6   Cellular Uptake of Carbohydrate capped SiNPs Using Microscopy

In order to gain insights into how carbohydrate capped SiNPs internalize within the cells, a cellular uptake experiment was performed using fluorescence and confocal microscopy. Figure 5.16 and 5.17 show fluorescence images of HHL5 and A549 cells incubated with 150µg/mL Gal capped SiNPs for 24 hours. The cells were stained with actin staining (Texas Red®-X Phalloidin), DAPI was used to stain the nuclei. Figure 5.16 shows the fluorescence image of HHL5 cells incubated with gal capped SiNPs.

Figure 5.16: Fluorescence images of HHL5 cells incubated with gal capped SiNPs for 24 hours. (a) Control (without NPs) and (b) HHL5 cell with gal capped NPs. Red fluorescence from actin staining, blue from DAPI and green fluorescence from the Gal capped SiNPs.

Figure 5.16b shows HHL5 cells incubated for 24 hr with gal capped SiNPs. The results indicate that gal capped SiNPs did not accumulate within the cell and are in agreement with flow cytometry results.

Figure 5.17 shows the A549 cells incubated with gal capped SiNPs for 24 hours. The cells were stained with Phalloidin red and the nuclei stained with DAPI.
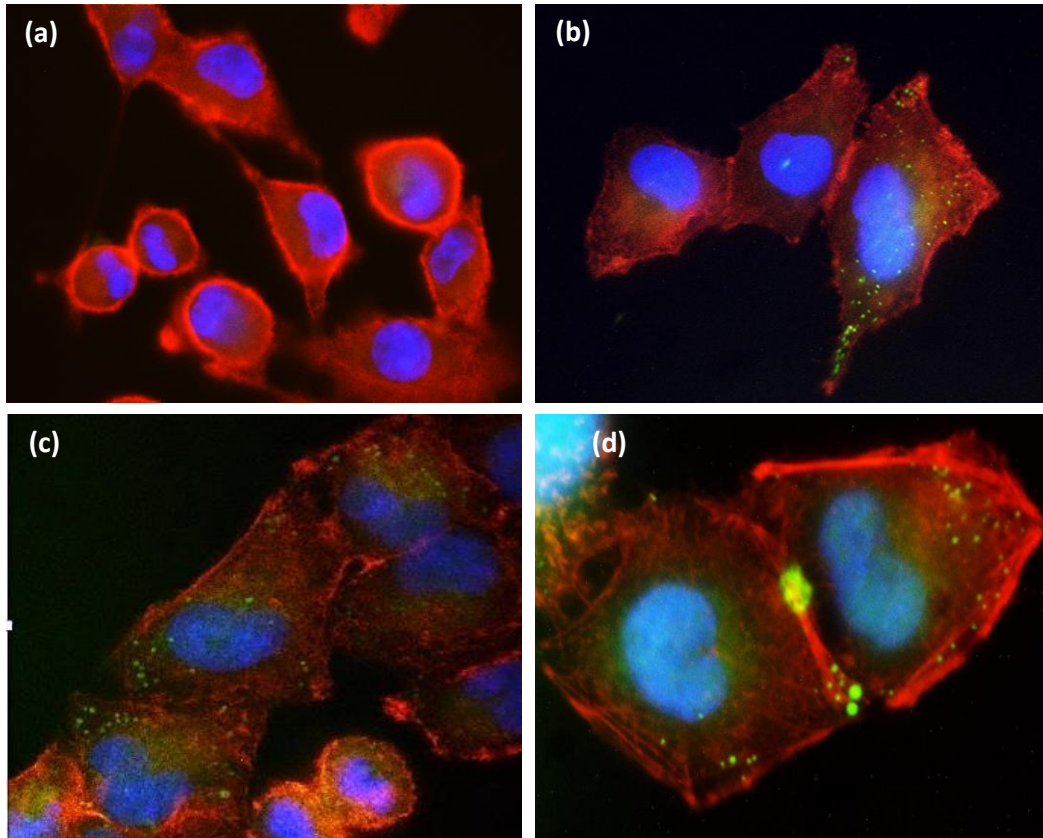
Figure 5.17: Fluorescence images of A549 cells incubated with gal capped SiNPs for 24 hours. (a) Control (without NPs) and (b), (c) and (d) A549 cell with gal capped SiNPs. Red fluorescence from actin staining, blue from DAPI and green fluorescence from the Gal capped SiNPs

In the case of A549 cells the gal capped SiNPs were found to be internalized within the cytoplasm, the green fluorescence is from gal capped SiNPs.
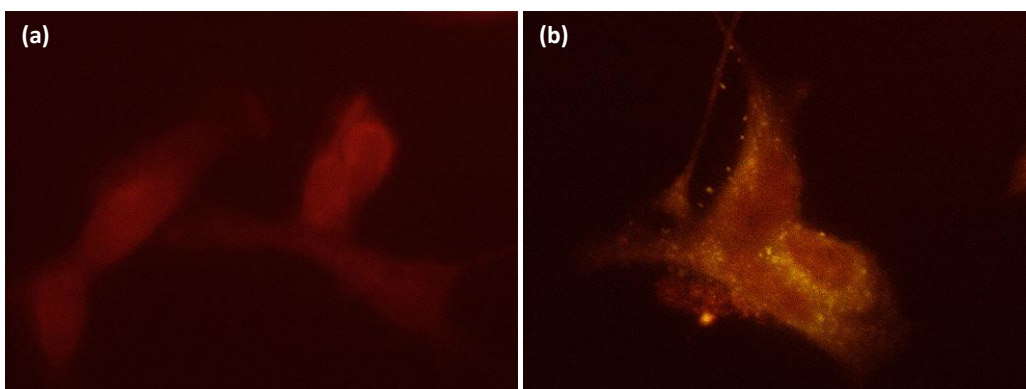
Figure 5.18: Fluorescence images of A549 cells incubated with gal capped SiNPs for 24 hours. (a) Control (cells without NPs) and (b) cells treated with NPs. Red fluorescence from LysoTracker-red and green fluorescence from the Gal capped SiNPs.

In order to visualize the lysosomes, cells were stained with Lysotracker-Red, see figure 5.18b. The selective uptake and intracellular accumulation of Gal-capped SiNPs in A549 cells is clearly observed and thus all these results can lead to the further development of carbohydrate capped SiNPs as a vehicle for targeted drug delivery.

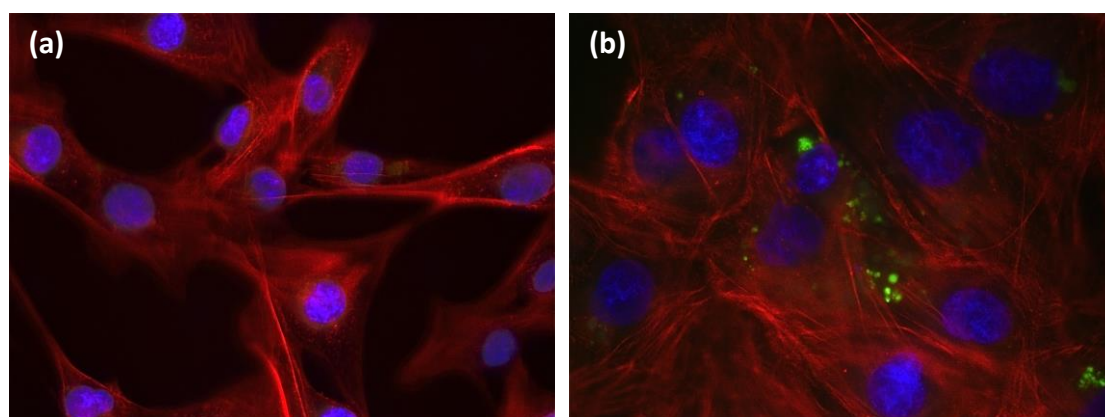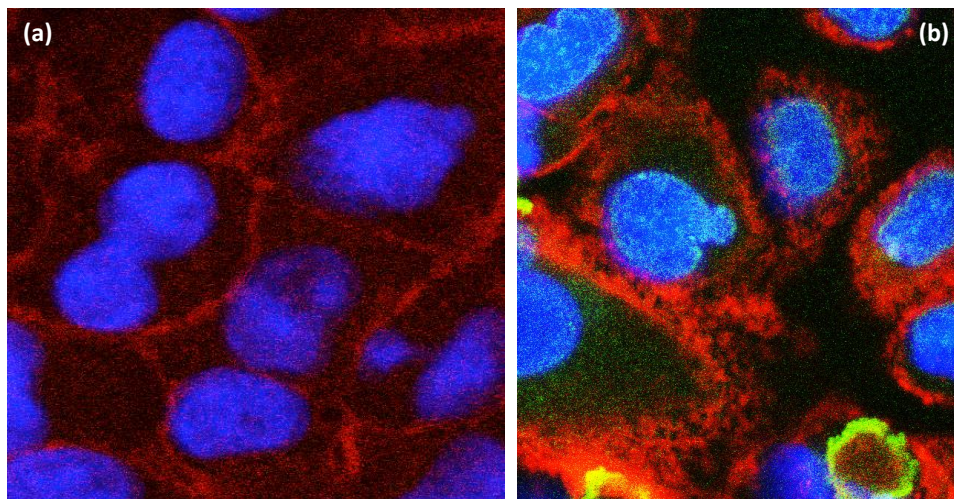**Figure 5.19: Fluorescence confocal images of A549 cells incubated with gal capped SiNPs for 24 hours. (a) Control (cells without NPs) and (b) A549 cell with NPs. Red fluorescence from Phalloidin red, blue from DAPI and green fluorescence from the Gal capped SiNPs**

Figure 5.19 shows the confocal images of A549 cells incubated with gal capped SiNPs for 24 hours. It is clearly observed that the gal capped SiNPs internalize within cytoplasm showing green fluorescence. Further study is ongoing to test other carbohydrate capped SiNPs in various cell lines including cancer and non-cancer cells.

5.7 Cellular Uptake Using Synchrotron FTIR Spectroscopy

To study the biological cells using infrared spectroscopy (IR) is nowadays an extensive and active area of research. Using synchrotron radiation (SR) IR microscopy gives a high spatial resolution and signal-to-noise ratio for cell study and has proven to be an ideal tool for investigating the biochemical composition of biological samples at the molecular scale. We tried to use this concept to investigate the surface functionalization of SiNPs inside the cells. The main aim of this study was to acquire and investigate the chemical bonding information of carbohydrate capped SiNPs inside the cells and confirm the uptake by cancerous cells using synchrotron FTIR. The MCF-7 (Human Breast cancer cell) were pre-incubated and stimulated with man capped SiNPs and fixed on the glass cover slip using paraformaldehyde (see chapter 2).

Figure 5.20 shows a typical FTIR spectrum from the region of MCF-7 cells stimulated with man capped SiNPs.
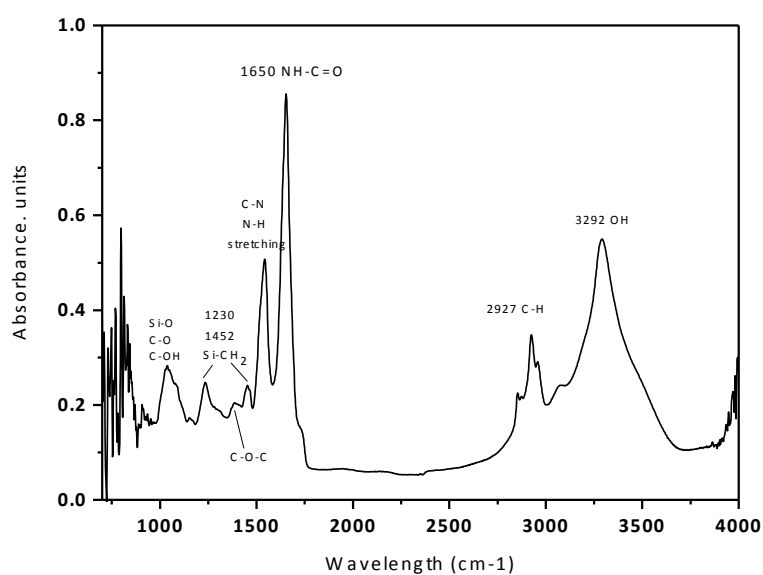
Figure 5.20: FTIR spectrum from MCF-7 cells stimulated with mannose capped SiNPs

The spectrum shows features around 3292 cm^{-1} from O-H bonding, 2927 cm^{-1} from C-H bonding, 1650 cm^{-1} from amide stretching, N-H stretching and C-N bending around 1542 cm^{-1}, Si-CH$_2$ symmetric bending and vibrational scissoring at 1230 cm^{-1} and 1452 cm^{-1} respectively and feature at 1039 cm^{-1} from C-OH, C-O, Si-O bonding. The features for C-C bonding also arise to related position to that of Si-C bonding at 1230 cm^{-1} and 1452 cm^{-1}.

Figure 5.21 shows the mapping 3D spectrum of MCF-7 cells, stimulated with man capped SiNPs.
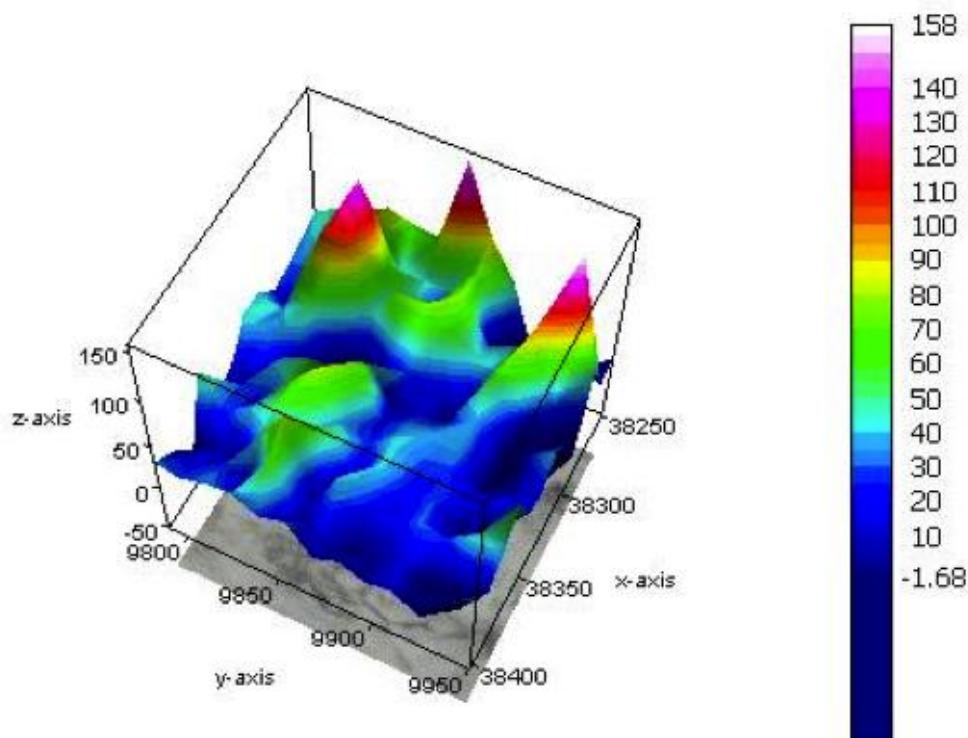
Figure 5.21: Mapping spectrum over an area of MCF-7 cells showing the distribution of man capped SiNPs. The red represents high intensity, blue represents low intensity.

The result showed the FTIR features for man capped SiNPs in MCF-7 cell line. Nevertheless it was difficult to distinguish the features from cells and sample as all cells contain carbohydrates and therefore they show exactly similar features in similar regions to that of the sample. In order to distinguish the features between the cells and the nanoparticles, further study needs to be undertaken to synthesize the carbohydrate capped SiNPs using a specific marker, which successfully appears in the blank region of FTIR *i.e.* from 1900 cm^{-1} to 2700cm^{-1}. This could be possible by using azide functionality or C=C / triple bond containing molecules.

5.8 Conclusion

The carbohydrate capped SiNPs prove to be very stable in biological media and this was confirmed by DLS measurements. The toxicity of carbohydrate capped SiNPs was tested both *in vitro* and *in vivo* (Xenopus embryo). The *in vitro* toxicity was tested by MTT assay in both cancer and non-cancer cell lines. The carbohydrate capped SiNPs were found to be non-toxic at highest concentration of 1000µg/mL. The *in vivo* toxicity of carbohydrate capped SiNPs was tested in *Xenopus Laevis* embryos; the SiNPs were

shown to be non-toxic for embryos up to a certain extent and no death or morphological damage was observed. The results were compared with amine-terminated SiNPs, which proved to be highly toxic and resulted in the death of embryos. The obtained results suggest that the SiNPs are highly capped with carbohydrate molecules, which make them stable as well as non-toxic for both *in vivo* and *in vitro* conditions.

The uptake efficiency of carbohydrate capped SiNPs was quantified by flow cytometry. The obtained results indicated that carbohydrate capped SiNPs internalize in the cell within 24 hours. The fluorescence uptake of carbohydrate capped SiNPs was quantified by both cancer and non-cancerous cell lines and the cancerous cell was shown to uptake more NPs than normal cell lines, which is important in terms of developing future targeted drug delivery systems. The uptake of carbohydrate capped SiNPs was visualized by fluorescence and confocal microscopy. The NPs showed quick accumulation inside cancer cells within cytoplasm.

Our understanding of cancer cell functions, such as endocytosis, cell-matrix and cell-cell communications, can be greatly enhanced by studying carbohydrate-receptor functions as a result of carbohydrate capped SiNP utilization. In addition, such studies can help further understanding of specificity and ligand optimization. In the future, this increasing knowledge base will enhance the applications of carbohydrate capped SiNPs for *in vivo* cancer detection.

5.9 References

1. Dwek, R. A., Glycobiology: Toward Understanding the Function of Sugars. *Chemical Reviews* **1996,** *96* (2), 683-720.

2. Varki, A., Biological roles of oligosaccharides: all of the theories are correct. *Glycobiology* **1993,** *3* (2), 97-130.

3. Werz, D. B.; Seeberger, P. H., Carbohydrates as the Next Frontier in Pharmaceutical Research. *Chemistry – A European Journal* **2005,** *11* (11), 3194-3206.

4. Raman, R.; Sasisekharan, V.; Sasisekharan, R., Structural Insights into Biological Roles of Protein-Glycosaminoglycan Interactions. *Chemistry & Biology* **2005,** *12* (3), 267-277.

5. Seeberger, P. H.; Werz, D. B., Synthesis and medical applications of oligosaccharides. *Nature* **2007,** *446* (7139), 1046-1051.

6. Simanek, E. E.; McGarvey, G. J.; Jablonowski, J. A.; Wong, C.-H., Selectin–Carbohydrate Interactions: From Natural Ligands to Designed Mimics. *Chemical Reviews* **1998,** *98* (2), 833-862.

7. Macher, B. A.; Galili, U., The Galα1,3Galβ1,4GlcNAc-R (α-Gal) epitope: A carbohydrate of unique evolution and clinical relevance. *Biochimica et Biophysica Acta (BBA) - General Subjects* **2008,** *1780* (2), 75-88.

8. Rabinovich, G. A.; Toscano, M. A., Turning 'sweet' on immunity: galectin-glycan interactions in immune tolerance and inflammation. *Nat Rev Immunol* **2009,** *9* (5), 338-352.

9. Nangia-Makker, P.; Conklin, J.; Hogan, V.; Raz, A., Carbohydrate-binding proteins in cancer, and their ligands as therapeutic agents. *Trends in Molecular Medicine* **2002,** *8* (4), 187-192.

10. Hakomori, S.-I.; Zhang, Y., Glycosphingolipid antigens and cancer therapy. *Chemistry & Biology* **1997,** *4* (2), 97-104.

11. Pieters, R. J., Maximising multivalency effects in protein-carbohydrate interactions. *Organic & Biomolecular Chemistry* **2009,** *7* (10), 2013-2025.

12. Lingwood, C. A., Oligosaccharide receptors for bacteria: a view to a kill. *Current Opinion in Chemical Biology* **1998,** *2* (6), 695-700.

13. Petitou, M.; van Boeckel, C. A. A., A Synthetic Antithrombin III Binding Pentasaccharide Is Now a Drug! What Comes Next? *Angewandte Chemie International Edition* **2004,** *43* (24), 3118-3133.

14. Lee, Y. C.; Lee, R. T., Carbohydrate-Protein Interactions: Basis of Glycobiology. *Accounts of Chemical Research* **1995,** *28* (8), 321-327.

15. Hakomori, S. I., Carbohydrate carbohydrate interaction as an initial step in cell recognition. *Pure Appl. Chem.* **1991,** *63*, 473.

16. Danishefsky, S. J.; Allen, J. R., From the Laboratory to the Clinic: A Retrospective on Fully Synthetic Carbohydrate-Based Anticancer Vaccines. *Angewandte Chemie International Edition* **2000,** *39* (5), 836-863.

17.　　Dai, Z.; Zhou, J.; Qiu, S.-J.; Liu, Y.-K.; Fan, J., Lectin-based glycoproteomics to explore and analyze hepatocellular carcinoma-related glycoprotein markers. *ELECTROPHORESIS* **2009,** *30* (17), 2957-2966.

18.　　Barthel, S. R.; Gavino, J. D.; Descheny, L.; Dimitroff, C. J., Targeting selectins and selectin ligands in inflammation and cancer. *Expert Opinion on Therapeutic Targets* **2007,** *11* (11), 1473-1491.

19.　　Kayser, K.; Heil, M.; Gabius, H. J., Is the Profile of Binding of a Panel of Neoglycoproteins Useful as a Diagnostic Marker in Human Lung Cancer? *Pathology - Research and Practice* **1989,** *184* (6), 621-629.

20.　　Kayser, K.; Bovin, N.; Zemlyanukhina, T.; Donaldo-Jacinto, S.; Koopmann, J.; Gabius, H.-J., Cell type-dependent alterations of binding of synthetic blood group antigen-related oligosaccharides in lung cancer. *Glycoconjugate J* **1994,** *11* (4), 339-344.

21.　　Rye, P. D.; Bovin, N. V., Selection of carbohydrate-binding cell phenotypes using oligosaccharide-coated magnetic particles. *Glycobiology* **1997,** *7* (2), 179-182.

22.　　Lerchen, H.-G.; Baumgarten, J.; Piel, N.; Kolb-Bachofen, V., Lectin-Mediated Drug Targeting: Discrimination of Carbohydrate-Mediated Cellular Uptake between Tumor and Liver Cells with Neoglycoconjugates Carrying Fucose Epitopes Regioselectively Modified in the 3-Position. *Angewandte Chemie International Edition* **1999,** *38* (24), 3680-3683.

23.　　Kim, E. Y. L.; Gronewold, C.; Chatterjee, A.; von der Lieth, C.-W.; Kliem, C.; Schmauser, B.; Wiessler, M.; Frei, E., Oligosaccharide Mimics Containing Galactose and Fucose Specifically Label Tumour Cell Surfaces and Inhibit Cell Adhesion to Fibronectin. *ChemBioChem* **2005,** *6* (2), 422-431.

24.　　Wang, Q.; Ni, H.; Pietzsch, A.; Hennies, F.; Bao, Y.; Chao, Y., Synthesis of water-dispersible photoluminescent silicon nanoparticles and their use in biological fluorescent imaging. *Journal of Nanoparticle Research* **2011,** *13* (1), 405-413.

25.　　O'Farrell, N.; Houlton, A.; Horrocks, B. R., Silicon nanoparticles: applications in cell biology and medicine. *International Journal of Nanomedicine* **2006,** *1* (4), 451-472.

26.　　Wang, Q.; Bao, Y.; Ahire, J.; Chao, Y., Co-encapsulation of Biodegradable Nanoparticles with Silicon Quantum Dots and Quercetin for Monitored Delivery. *Advanced Healthcare Materials* **2013,** *2*.

27.　　Kirchner, C.; Liedl, T.; Kudera, S.; Pellegrino, T.; Muñoz Javier, A.; Gaub, H. E.; Stölzle, S.; Fertig, N.; Parak, W. J., Cytotoxicity of Colloidal CdSe and CdSe/ZnS Nanoparticles. *Nano Letters* **2004,** *5* (2), 331-338.

28.　　Nilsson, J. R., How Cytotoxic is Zinc? A Study on Effects of Zinc on Cell Proliferation, Endocytosis, and Fine Structure of the Ciliate Tetrahymena. *Acta Protozool* **2003,** *42*, 19-29.

29.　　Mayne, A. H.; Bayliss, S. C.; Barr, P.; Tobin, M.; Buckberry, L. D., Biologically Interfaced Porous Silicon Devices. *physica status solidi (a)* **2000,** *182* (1), 505-513.

30.　　Chen, Y.; Ji, T.; Rosenzweig, Z., Synthesis of Glyconanospheres Containing Luminescent CdSe–ZnS Quantum Dots. *Nano Letters* **2003,** *3* (5), 581-584.

31.　　Moore, A.; Marecos, E.; Bogdanov, A.; Weissleder, R., Tumoral Distribution of Long-circulating Dextran-coated Iron Oxide Nanoparticles in a Rodent Model. *Radiology* **2000,** *214* (2), 568-574.

32.   Hu, Y.; Jiang, X.; Ding, Y.; Ge, H.; Yuan, Y.; Yang, C., Synthesis and characterization of chitosan–poly(acrylic acid) nanoparticles. *Biomaterials* **2002,** *23* (15), 3193-3201.

33.   Ahire, J. H.; Chambrier, I.; Mueller, A.; Bao, Y.; Chao, Y., Synthesis of d-Mannose Capped Silicon Nanoparticles and Their Interactions with MCF-7 Human Breast Cancerous Cells. *ACS Applied Materials & Interfaces* **2013,** *5* (15), 7384-7391.

34.   Moghimi, S. M.; Hunter, A. C.; Murray, J. C., *FASEB J* **2005,** *19*, 311-330.

35.   Murdock, R. C.; Braydich-Stolle, L.; Schrand, A. M.; Schlager, J. J.; Hussain, S. M., Characterization of Nanomaterial Dispersion in Solution Prior to *IN VITRO* Exposure Using Dynamic Light Scattering Technique. *Toxicological Sciences* **2008,** *101* (2), 239-253.

36.   Deguchi, S.; Yamazaki, T.; Mukai, S.-a.; Usami, R.; Horikoshi, K., Stabilization of C60 Nanoparticles by Protein Adsorption and Its Implications for Toxicity Studies. *Chemical Research in Toxicology* **2007,** *20* (6), 854-858.

37.   Buford, M.; Hamilton, R.; Holian, A., A comparison of dispersing media for various engineered carbon nanoparticles. *Particle and Fibre Toxicology* **2007,** *4* (1), 6.

38.   Wick, P.; Manser, P.; Limbach, L. K.; Dettlaff-Weglikowska, U.; Krumeich, F.; Roth, S.; Stark, W. J.; Bruinink, A., The degree and kind of agglomeration affect carbon nanotube cytotoxicity. *Toxicology Letters* **2007,** *168* (2), 121-131.

39.   Sager, T. M.; Porter, D. W.; Robinson, V. A.; Lindsley, W. G.; Schwegler-Berry, D. E.; Castranova, V., Improved method to disperse nanoparticles for in vitro and in vivo investigation of toxicity. *Nanotoxicology* **2007,** *1* (2), 118-129.

40.   Foucaud, L.; Wilson, M. R.; Brown, D. M.; Stone, V., Measurement of reactive species production by nanoparticles prepared in biologically relevant media. *Toxicology Letters* **2007,** *174* (1,Äì3), 1-9.

41.   Tseng, C.-L.; Peng, C.-L.; Huang, J.-Y.; Chen, J.-C.; Lin, F.-H., Gelatin nanoparticles as gene carriers for transgenic chicken applications. *Journal of Biomaterials Applications* **2013,** *27* (8), 1055-1065.

42.   Fako, V. E.; Furgeson, D. Y., Zebrafish as a correlative and predictive model for assessing biomaterial nanotoxicity. *Advanced Drug Delivery Reviews* **2009,** *61* (6), 478-486.

43.   dos Santos, T.; Varela, J.; Lynch, I.; Salvati, A.; Dawson, K. A., Quantitative Assessment of the Comparative Nanoparticle-Uptake Efficiency of a Range of Cell Lines. *Small* **2011,** *7* (23), 3341-3349.

44.   Chandrasekaran, S.; Tanzer, M. L.; Giniger, M. S., Characterization of oligomannoside binding to the surface of murine melanoma cells. Potential relationship to oligomannoside-initiated cell spreading. *Journal of Biological Chemistry* **1994,** *269* (5), 3367-3373.

45.   Rojo, J.; Díaz, V.; de la Fuente, J. M.; Segura, I.; Barrientos, A. G.; Riese, H. H.; Bernad, A.; Penadés, S., Gold Glyconanoparticles as New Tools in Antiadhesive Therapy. *ChemBioChem* **2004,** *5* (3), 291-297.

46.   Lee, R. T.; Myers, R. W.; Lee, Y. C., Further studies on the binding characteristics of rabbit liver galactose/N-acetylgalactosamine-specific lectin. *Biochemistry* **1982,** *21* (24), 6292-6298.

47.   Fricker, G., Biological Membranes and Drug Transport. In *Transporters as Drug Carriers*, Wiley-VCH Verlag GmbH & Co. KGaA: 2010.

48.   Pascual, I.; Berjón, A.; Lostao, M. P.; Barber, A., Transport of d-galactose by the gastrointestinal tract of the locust, Locusta migratoria. *Comparative Biochemistry and Physiology Part B: Biochemistry and Molecular Biology* **2006,** *143* (1), 20-26.

49.   Pastan, I.; Willingham, M., The Pathway of Endocytosis. In *Endocytosis*, Pastan, I.; Willingham, M., Eds. Springer US: 1985; pp 1-44.

50.   Willingham, M. C.; Pastan, I., Formation of receptosomes from plasma membrane coated pits during endocytosis: analysis by serial sections with improved membrane labeling and preservation techniques. *Proceedings of the National Academy of Sciences* **1983,** *80* (18), 5617-5621.

51.   Tjelle, T. E.; Brech, A.; Juvet, L. K.; Griffiths, G.; Berg, T., Isolation and characterization of early endosomes, late endosomes and terminal lysosomes: their role in protein degradation. *Journal of Cell Science* **1996,** *109* (12), 2905-2914.

52.   Mercer, J.; Schelhaas, M.; Helenius, A., Virus Entry by Endocytosis. *Annual Review of Biochemistry* **2010,** *79* (1), 803-833.

53.   Sofer, A.; Futerman, A. H., Cationic Amphiphilic Drugs Inhibit the Internalization of Cholera Toxin to the Golgi Apparatus and the Subsequent Elevation of Cyclic AMP. *Journal of Biological Chemistry* **1995,** *270* (20), 12117-12122.

54.   Harding, C.; Heuser, J.; Stahl, P., Receptor-mediated endocytosis of transferrin and recycling of the transferrin receptor in rat reticulocytes. *The Journal of cell biology* **1983,** *97* (2), 329-339.

55.   Silverstein, S. C.; Steinman, R. M.; Cohn, Z. A., Endocytosis. *Annual Review of Biochemistry* **1977,** *46* (1), 669-722.

6 Summary and Future Prospects

Nanotechnology is an emerging multidisciplinary science, which deals with the formation, investigation and manipulation of nano-objects (1-100 nm). Since the basis of many different physical processes can now be controlled up to the nanometer-scale, nanotechnology has a huge potential to revolutionize diverse fields of medicine and engineering.

In nanotechnology, research on semiconductor nanoclusters has been greatly focused on the properties of quantum dots (QDs); due to their unique size-range, characteristically on the boundary between quantum mechanics and Newtonian physics, the properties of nanoparticles differ from those of the bulk and of single atoms. Among semiconductor QDs, SiNPs in particular have additional advantages: exceptional optical and electronic properties such as size dependent-tunable light emission wavelengths, intense fluorescence, resistance against photobleaching and simultaneous excitation of multiple fluorescent colours. All these qualities make SiNPs in many respects superior over organic dyes and fluorescent proteins that are used for bioimaging purposes so far.

SiNPs can be synthesized from a variety of methods with different sizes and morphologies. By creating Si with nanoscale dimensions (SiNPs), it can be coaxed to emit visible light with relatively high efficiencies. The silicon surface can be well passivated, by synthesizing stable Si-C bonds. The methods to tailor silicon surfaces were developed on porous and planar Si and can also be applied for the functionalization of SiNPs surfaces. Such a coating of SiNPs could prevent surface oxidation. A high luminescence, well-developed surface passivation principles, and a low inherent toxicity of Si initiated the enthusiasm for the research in SiNPs.

The goals of the work described in this thesis are:

- The development and optimization of methods to synthesize stable and monodisperse SiNPs

- Photophysical characterization of synthesized NPs, also in terms of their functionalization

- Exploration of their possible applications, mostly in the area of biomedicine.

Chapter 1 describes the general properties of semiconductor quantum dots and SiNPs, in particular. The origin of SiNPs luminescence is described in detail, and an overview of published methods for the synthesis and functionalization of SiNPs is given, with a discussion of the advantages and drawbacks of each method. Moreover the possible biomedical applications as well as cytotoxicity studies of semiconductor NPs and SiNPs are also discussed.

Chapter 2 describes the origin and detailed methods used to synthesize porous SiNPs from electrochemical etching. It also explains the various apparatus and research techniques, including biological materials and cell lines, used in this thesis.

Chapter 3 describes the synthesis of stable and brightly luminescent amine-terminated SiNPs. The surface analysis of obtained amine-terminated SiNPs was confirmed by FTIR, NMR and XPS. The mean diameter of the crystal core of 4.6 nm was measured by transmission electron microscopy (TEM), which is in good agreement with the size obtained by dynamic light scattering (DLS).

The dry, amine-terminated product can be obtained from bulk silicon wafers in less than 4 h. This represents a significant improvement over similar routine procedures using porous silicon where times of >10 h are common. The emission quantum yield was found to be about 22%, which is the highest reported so far for silicon. The nanoparticles exhibited an exceptional stability over a wide pH range (4-14). They are resistant to aging over several weeks. The *in vitro* cellular uptake was monitored inside HepG2 cells, the amine-terminated SiNPs show quick accumulation in the cells confirmed by confocal microscopy. The amine-terminated SiNPs showed no significant cytotoxic effects toward HepG2 cells, as assessed with MTT assays.

Chapter 4 describes the first synthesis of SiNPs functionalized with carbohydrates. In this study, stable and brightly luminescent Galactose (Gal), Mannose (Man), Glucose (Glu) and Lactose (Lac) capped SiNPs were synthesized from amine terminated SiNPs and corresponding pyranoside acid. The surface functionalization was confirmed by FTIR, NMR, XPS and EDX studies. The mean diameter of the crystal core was 5.5 nm, as measured by TEM, while the hydrodynamic diameter obtained by DLS for Gal (11 nm), Man (15 nm), Glu (19 nm) and Lac (24 1.0 nm) capped SiNPs were measured in water. The quantum yield (QY) of photoluminescence emission found for gal, man, glu and lac capped SiNPs was about 16 %, 27%, 30% and 39% respectively. This is the highest QY reported so far for SiNPs. This phenomenon was successfully explained by photoinduced electron transfer (PET). The carbohydrate capped SiNPs

exhibited an exceptional stability over several weeks. Furthermore pH effect measurements demonstrated that the obtained SiNPs were highly stable in aqueous environments. The Man-capped SiNPs may prove to be valuable tools for further investigating within glycobiological, biomedical and material science fields. Experiments were carried out using Concanavalin A (ConA) as a target protein in order to prove the hypothesis. When Man functionalized SiNPs were treated with ConA, cross-linked aggregates were formed, as showed in TEM images as well as monitored by photoluminescence spectroscopy (PL). Man functionalized SiNPs can target cancerous cells. Visualization imaging of SiNPs in MCF-7 human breast cancer cells showed the fluorescence is distributed throughout the cytoplasm of these cells.

Chapter 5 explores the possibility of using carbohydrate capped SiNPs to target various types of cancerous cells using active receptor-mediated interaction. The stability of carbohydrate capped SiNPs in biological environment was confirmed by DLS analysis. The obtained data proved that the carbohydrate capped SiNPs do not form aggregation with proteins which are present in biological media and are highly stable. The toxicity of carbohydrate capped SiNPs was tested both *in vitro* and *in vivo* (Xenopus embryo). The *in vitro* toxicity was verified by MTT assay in both cancer and non-cancer cell lines. The carbohydrate capped SiNPs were found to be highly non-toxic up to the highest concentration of 1000 μg/mL. The *in vivo* toxicity of carbohydrate capped SiNPs was tested in *Xenopus Laevis* embryo. The SiNPs were found to be non-toxic for embryos up to a certain extent and no death or morphological damage was observed. The results were compared with control experiments of amine-terminated SiNPs which was used as the starting material in the synthesis of carbohydrate capped SiNPs. The obtained toxicity results in both *in vivo* and *in vitro* ascertained that the amine-terminated SiNPs are highly toxic and their presence led to cell (*in vitro*) and embryo (*in vivo*) death. The obtained results highlighted that SiNPs are functionalized with carbohydrate ligands which makes them non-toxic for *in vitro* and *in vivo* studies. Conversely amine-terminated SiNPs were shown to be poisons at similar concentration. The selective uptake efficiency of carbohydrate capped SiNPs in various cancerous and non-cancerous cell lines were quantified by flow cytometry analysis. The results indicated that carbohydrate capped SiNPs internalize in the cell within 24 hours of incubation. Moreover when compared with normal cells, the carbohydrate capped SiNPs were found to be accumulating more in cancerous cell than in the normal cells. In order to try and understand the internalization mechanism, cells were incubated with carbohydrate capped SiNPs at 4°C and 37°C. The obtained data showed that carbohydrate capped

SiNPs kept at 4°C were not internalized in SK-Mel cells, while at 37°C all the carbohydrate capped SiNPs were internalized into the cells as confirmed by flow cytometry analysis. This suggests that the cellular uptake is most likely energy-dependent or receptor mediated. The fluorescence uptake of carbohydrate capped SiNPs was visualized by fluorescence and confocal microscopy. The NPs show quick accumulation inside cancer cells within the cytoplasm.

6.1 Discussion and Future Prospects

The overall results described in the thesis provide a vision to understand the properties of SiNPs. The results also provide an excellent solution to synthesize stable and water soluble SiNPs, which show enormous possible applications in bioimaging as well in biomedical field. It is well known that SiNPs have a low intrinsic toxicity in various mammalian cell lines in contrast to Cd, for example. This is a huge advantage of SiNPs when considering their application in the biomedical field. While the number of NPs types continues to increase, studies to characterize their effects after exposure and to address their potential toxicity are few in comparison. In order to use SiNPs into clinical field, it is important to understand and uncover further toxicology study, like how multiple factors such as size, shape, composition, surface coverage, stability, concentration etc., influence the toxicity. The potential applications of SiNPs in biomedical field are: high-resolution cellular imaging, long-term *in vivo* cell tracking, tumour targeting, diagnostics, therapeutics etc. For all of these purposes it is significant to understand the biodegradation of SiNPs in the cellular environment and also important to study what cellular degradation SiNPs may induce. Moreover it is still unclear what happens with the NPs once they enter the body and how they influence various functions in cells and organism as a whole.

In order to understand and move forward, to explore the application of SiNPs more study needs to be undertaken. The research we have stated on various cell lines must be more systematic.

With respect to the synthesis of the SiNPs, it would be extremely useful to extend the method to allow for larger scale production of monodisperse SiNPs of a wide range of sizes (colours). Efforts also need to be directed towards, improving the purity of the final product by improving the method and reducing the use of toxic chemicals.

This would provide a wider range of applications, especially in bioimaging, where dyes emitting < 600 nm are problematic to use, since biomaterials could be

seriously damaged by the UV light needed for their excitation, and because auto-fluorescence is otherwise a nearly insurmountable problem. SiNPs with significantly higher emission wavelengths could also be used for deep-tissue imaging, as there would be much less interference (absorption) by the surrounding biomaterial.

The use of SiNPs for bioimaging should definitely be examined and extended to a wide variety of cell types, as each of them might display different toxicities. The influence of the functional groups attached to SiNPs should also be examined in detail, because this could also be a source of toxicity and not the SiNPs themselves.

In chapter 4 we have demonstrated an excellent method to synthesize carbohydrate capped SiNPs from amine-terminated SiNPs (in chapter 3). This opens a new door for various surface functionalizations on SiNPs using amine-terminated SiNPs as a precursor.

The purpose of synthesizing carbohydrate capped SiNPs is to selectively target various cancer cells. Our understanding of cancer cell functions, such as endocytosis, cell-matrix and cell-cell communications, can be greatly enhanced by studying carbohydrate-receptor functions as a result of carbohydrate capped SiNPs utilization. In addition, such studies can help further understanding of specificity and ligand optimization. However a systematic research needs to be undertaken to study the specific cancer cell with a similar pair of normal cells. To confirm that carbohydrate capped SiNPs can target specific cancer cell or can bind selectively to specific cancer, *in vivo* study needs to be performed. At present the literature reports the selectivity of glyco-conjugated NPs towards the detection of cancer and other types of diseases (chapter 5).

In terms of future prospective of using carbohydrate capped SiNPs for *in vivo* study to target a specific cancer and to eradicate the cancer, a drug delivery strategy needs to be developed. In our study we correspondingly design the drug delivery system to selectively target cancer and to eradicate the cancer. The modified drug delivery system shown in figure 6.1 represents a simple method to synthesize encapsulated carbohydrate functionalized SiNPs. In the course of my PhD, I synthesized the polymeric micelle, but unfortunately due to the time limitation couldn't proceed further. The carbohydrate with various surface conformations with both hydrophilic and hydrophobic ends was synthesized. The polymeric micelle was then formed by encapsulating drugs and SiNPs, using a double emulsion method, as illustrated in Figure 6.1. Specific surface conformation will provide potential to target different kind of

receptors in cancerous cells and SiNPs will help to monitor the capsule inside the *in vivo* system.
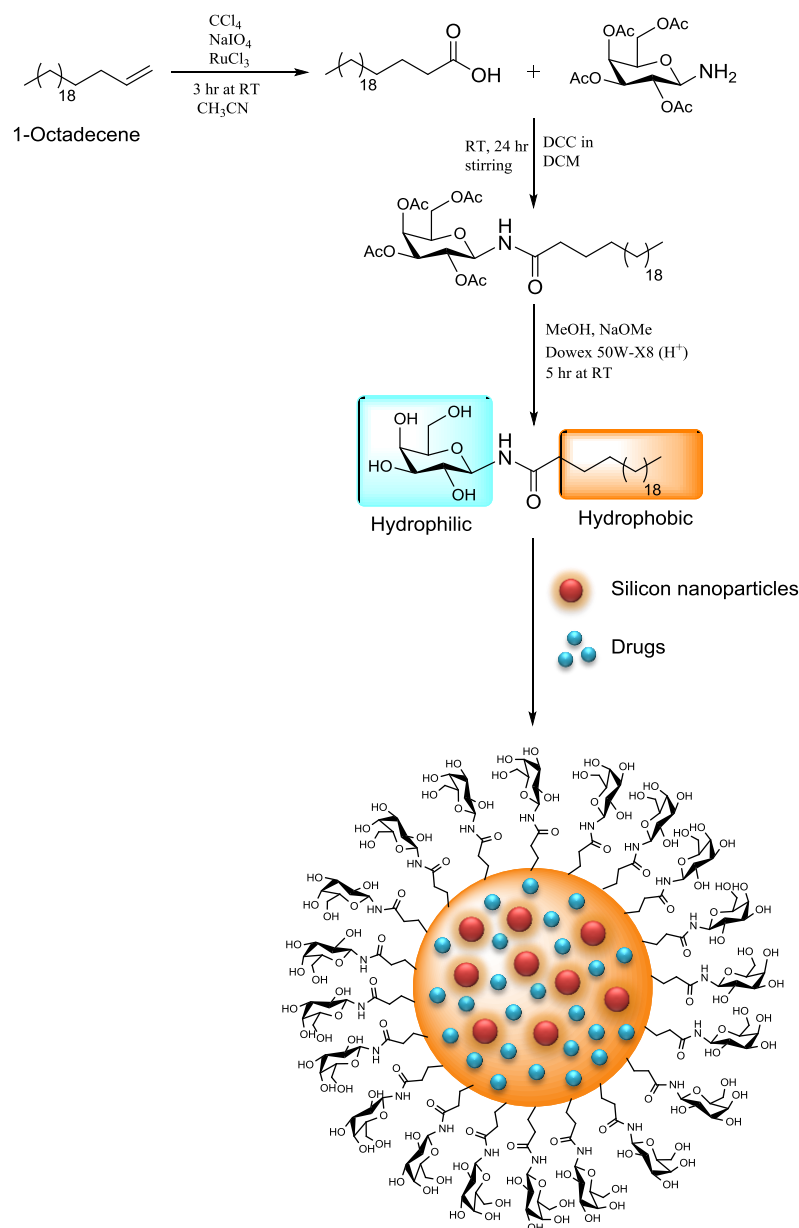

Figure 6.1: Schematic representation of SiNPs encapsulated mannose functionalized drug delivery system.

Further research is important in respect of developing and examining this micelle in both *in vitro* and *in vivo* systems. This will help to increase the understanding about selective targeting and delivering drugs to the cancer cells.

In chapter 4 we have highlighted the corresponding study of carbohydrate capped SiNPs mediated self-assemblies or crystals. The overall results confirm that the crystals are from carbohydrate capped SiNPs and not from the carbohydrate alone.

Moreover they also indicate that the crystals are not completely driven by carbohydrate moiety, where SiNPs act as an impurity. The crystals are actually driven by overall carbohydrate capped SiNPs, where SiNPs possibly act as seed and assemble into the crystal with the help of the carbohydrate moieties. Further study needs to be undertaken to resolve the crystals and to find out the special arrangement of SiNPs inside the crystals. Small Angle X-ray crystallography (SAXS) may help to resolve the question, as SAXS is capable of delivering structural information of macromolecules between 5 and 25 nm, of repeat distances in partially ordered systems.

In chapter 5 we attempted to monitor the carbohydrate capped SiNPs inside the cells. Due to the presence of similar bonding environment inside the cells, it was difficult to capture carbohydrate capped SiNPs inside the cells by SFTIR. Further study needs to be undertaken to synthesize the carbohydrate capped SiNPs using a specific marker, which successfully appears in the blank region of FTIR i.e. from 1900 cm-1 to 2700cm-1. This could be possible by using azide functionality or $C=C$ / triple bond containing molecules.

Furthermore in chapter 4 SiNPs are proven to be excellent energy donors (PET). There is a big opportunity in using them as pH sensor as well as application of this design principle to QDs would provide an opportunity for many more QD based probes, thereby taking advantage of their superior optical properties. Their high emission quantum yields would make them great candidates for many other energy transfer studies. In order to increase the energy transfer efficiency, other molecule should be considered as acceptors.

Elucidating some of the above mentioned problems would bring SiNPs closer to commercial applications, as there is a growing interest for their use in many different areas. Practical applications will not come without careful research, but the multidisciplinary nature of nanotechnology may accelerate these goals by combining the great minds of researchers in many different fields of science.